Picosecond studies of excited states in conjugated polymers

Hintschich, Susanne I.

Picosecond Studies of Excited States

in Conjugated Polymers

Susanne I. Hintschich

Department of Physics

University of Durham

A thesis submitted to the Faculty of Science at the University of Durham for the Degree of Doctor of Philosophy.

December 2006

Picosecond Studies of Excited States in Conjugated Polymers

by Susanne I. Hintschich

A thesis for the Degree of Doctor of Philosophy, submitted in 2006

Abstract

This thesis reports on the interplay between molecular structure and photophysics in light emitting conjugated polymers revealed by steady state and picosecond time-resolved fluorescence spectroscopy.

The fundamental excited state relaxation of a polyfluorene derivative is compared to that of two oligofluorenes using isolated molecules in dilute solution. Their long-time time-dependent spectral dynamics are monitored by means of picosecond streak camera and single photon counting techniques. Excited state relaxation in oligofluorenes is entirely conformational and depends on solvent viscosity. The intrachain photophysics of the polyfluorene is dominated by fast excitation migration with a slow conformational component. A rigid ladder-type polymer exhibits only migrational relaxation.

In analogy, the spectral dynamics of an alkoxy-substituted polyspirobifluorene are studied in dilute solution. Their qualitative dependence on solvent viscosity is elucidated by further femtosecond photobleaching measurements. Two excited states are proposed with the lower energy state involving strong spiroconjugation as confirmed by electronic structure calculations. Conversion between them occurs via conformational relaxation of the fluorene side groups. The sensitive reaction of these photophysics to the substitution pattern of the polymer suggests an easy chemical tunability of polyspirobifluorenes towards optimised charge carrier transport properties.

Finally, the formation of the beta phase in amorphous polydioctylfluorene is investigated as a function of spin coating fabrication in the solid state. It is suggested that it forms by condensation at colloidal sites, which arise from incomplete solvation in the master solution. A further room temperature phase exists in the absence of these nuclei. The excited state relaxation after energy transfer from amorphous to beta phase is monitored via time-resolved spectroscopy. Within the beta phase, exciton migration is restricted as confirmed by steady state anisotropy data. This evidence for exciton confinement is an important step towards the application of the beta phase as a polymer laser.

Declaration

All material contained in this thesis is original and is the result of my own work except where explicit reference is made to the work of others.

This thesis has not been submitted in whole or part for the award of a degree at this or any other university.

Acknowledgements

To start with, I'd just like to say a simple thank you to all the people who have made this work (and me sitting here in the middle of the night) possible.

First of all, thanks go to my supervisor, Prof. Andy Monkman, for his continuous support throughout the many years that I've been in Durham. His scientific inspirations and patience baby wise were just the things I needed to get to this stage. Not in the least, he made the OEM group such an enjoyable place to stay by choosing only the nicest people to work here. Hellos go to Hameed, Helen, Simon, Fran, CJ, Matti, DeChang, James, Naveed and especially to Fernando for his empathy with lasers and patience with students. I'm also sending big thanks to Hugh for his truly Portuguese hospitality.

Of greatest importance for the working of my experiment were of course Norman and Davy, whose helping hand was never far away. Thanks also to Norman for sharing his expertise as a grandpa.

The very first experiment of my PhD studies was growing a baby bump. Therefore, very warm thanks are bestowed to my parents and brother who took part in this in spite of living a thousand miles away. And, finally, I mustn't forget to thank little Hannah and big Carsten, for their plain existence, which gives me a home.

This work was generously funded by the Durham County Council in a OneNorthEast partnership project and by the University of Durham, who paid part of the nursery time.

That was the cheesy bit. Now, please feel free to read the scientific part of this work.

Index of figures and tables

1. Introduction

This thesis is a contribution in the field of light-emitting plastics, and here in particular light emitting conjugated polymers. In the past century, plastics have secured their place in our everyday life due to their mechanical properties, their cheap production and their function as electrical insulators. Compared to the above properties the ability of some polymers to conduct electricity and even emit fluorescence is rather young. Yet, the discovery of these materials, called conjugated polymers, was awarded the Nobel Prize in Chemistry in 2000. This progress was made possible by today's mature organic chemistry, whose versatility allows synthesising polymers for very specific applications, which increasingly advance into the domains of other materials classes such as semiconductors.

The year 1970 saw the beginning of intense research efforts into conjugated polymers with the discovery of electrical conduction in specific members of this family. Fifteen years on, the optimism was somewhat subdued by the fact that conducting polymers could still not quite compete with the properties of copper. Research now turned to the new field of polymer electrofluorescence, which experienced a dramatic boost by the initial findings of Sir Richard Friend *et al.* in 1990 with the demonstration of a reasonably efficient polymer light emitting diode (PLED) [1].

By now, many global companies have engaged industrial research in this field aiming at the replacement of LCD displays. The advantages of conjugated polymers are clear: As active emitters, they warrant a higher power efficiency and superior viewing angles. Thin film processing allows the construction of ultra-thin display panels. Device fabrication by ink-jet printing can compete up to the level of semi-disposable applications such as "electronic paper that fits into your pocket"[2]. Here, the mechanical flexibility and thin layer processing of conjugated polymers allows a completely new field of applications away from conventional TV displays: "The idea of a bendable, rollable, or floppy display panel is intuitively appealing."[3] Furthermore, unlike most of the competing technologies for display fabrication, which are based on glass substrates, conjugated polymers can be printed on lightweight, flexible, and robust plastic film substrates, potentially using a cost-effective roll-to-roll technology[3]. The synergy of all these features will result in unique new display and lighting devices with superior properties compared to all established technologies.

To put these ideas into practice, bendable driving circuits are being developed in the form of organic thin film transistors (OTFT). Implementing a suitable pair of electrodes, a display could even be

transparent, enabling applications in helmets or windows.

However, today the first TV-sized PLED display still awaits its introduction to the consumer market. Only few mass produced PLED applications have been accomplished so far, all of them on a small scale such as in car display panels or shavers. Some deficiencies of conjugated polymers still hinder the development: First, these materials are chemically soft and subject to degradation. Backbone oxidation was a widespread phenomenon in particular for blue emitters leading to colour instability and a reduced lifetime. Nevertheless, due to fundamental research in the last four years[4, 5], this effect could be understood resulting in the synthesis of more stable polymer derivatives[6]. Meanwhile, lifetimes in excess of 100.000 hours have been reported, which suffices for nearly any application[7]. Moreover, the aggregation of polymer chains gives rise to photophysics which can spoil an intrinsically sharp fluorescence spectrum and lead to dull display colours. This matter has been tackled by the attachment of sterically hindering side chains to the polymer backbones, which serve as spacers to inhibit interactions between the polymer chains. A further problem is the preferred generation of non-emitting triplet excitations in PLEDs. Harvesting these for emission is a current topic of research, which mainly focuses on the introduction of heavy metal dopants. However, difficulties still arise in creating blue emitting devices. This requires a host or matrix polymer which possesses enhanced charge injection and transport capabilities and simultaneously features a triplet exciton level higher than the blue emitting guest dopant in order to avoid energy transfer to the non-emitting host polymer level[8]. Conjugated polymers of high triplet energy, e.g. polycarbazoles, have been synthesised to aid the transfer of excitation energy in the latter case but a host polymer suitable for deep blue guest emission has not yet been presented. A fourth issue is the need to balance electron and hole transport in operating devices in order to minimise losses due to dark current. Most conjugated polymers favour the transport of holes. Strategies to compensate for the resulting imbalanced charge transport again involve the synthesis of more suitable materials, namely copolymers featuring electron transport moieties such oxadiazole[9].

Figure 1-1 – One of the first flexible PLEDs fabricated at Durham University using a Ni grid substrate (spacing of 150 μm). The active layer consists of a blue emitting polyfluorene. The size of the unit is 3 x 3 cm.

Figure 1-2 – In 2005 Samsung SDI presented its 40'' test PLED display with emphasis on blue emission. The Philips shaver model with monochrome PLED display is produced since 2002.

During their development, the lead of PLED research is melting in the competition with displays fabricated from small organic molecules (OLEDs) and field emission displays (FED or SED) made of carbon nanotubes. OLEDs, for example, can already be produced with a brightness and stability sufficient for televisions[10]. Thus, the future of fluorescent polymers is rather to be seen in large-scale lighting and disposable displays cheaply fabricated via ink-jet printing. Finally, organic luminescence is by no means limited to display and lighting applications but is increasingly employed in biological sensing including DNA identification. Here, compatibility requires novel water-soluble species, which currently experience a push in research activities[11].

Clearly, the synthesis of new materials remains a major route towards new and interesting developments. In fact, countless polymers are being synthesised aiming at different fields of application. Considering electroluminescence, during the last decade the family of polyfluorene derivatives have attracted particular research interest. Meanwhile, they have emerged as one of the most widely studied materials in this field due to an advantageous combination of properties. These include their availability in high purity and their good chemical stability compared to other conjugated polymers[12], the ease of chemical modification[12], the possibility of aligning polyfluorene chains to obtain polarised emission[13], the observation of amplified stimulated emission[14] and, not in the least, their blue emission colour, which makes them suitable host materials for red emitting dopants[15].

This thesis is an investigation into the fundamental photophysics of three polyfluorene derivatives. Although these materials have been synthesised with only modest chemical alterations, namely the substitution of different side groups, a wealth of significantly diverse photophysical phenomena is observed. On a molecular level, it is demonstrated that and how the details of chemical structure exert a strong influence on the photophysical behaviour of a conjugated polymer. Here, changes mainly arise from the pathways of excited state relaxation, which are modified as a result of the altered molecular geometry or solid state morphology. Via picosecond time-resolved spectroscopy and steady state techniques, the modification of these mechanisms is revealed in different categories including backbone conformational relaxation, side group relaxation and interchain exciton migration.

To begin with, one chapter is dedicated to the general theoretical background of conjugated polymers. In addition to this, the more specific theory content has been transferred to the subsequent chapters wherever this is required for the understanding of any particular work.

This is followed by a description and characterisation of the experimental techniques. In particular, the streak camera experiment, which was set up as a part of this work, and the time-correlated single photon counting (TCSPC) setup are illustrated in detail.

Following that, three chapters present three independent studies under the above outlined general agenda. The first of them is fundamental work on the conformational relaxation in conjugated polymers, which was triggered by the open questions of a previous publication by Dr. Dias *et al.*[16]. The study is carried out systematically using a prototypical polyfluorene derivative, PF2/6, and two oligofluorenes of different chain length. The spectral dynamics of these are investigated in dilute solutions with the aim to assess the weight of exciton migration for isolated polymer chains. As a further dimension, the range of solvents employed allows quantifying the effect of viscosity on the long-time conformational relaxation.

The second chapter focuses on the excited state processes in a polyspirobifluorene derivative. Spiro-substitution represents a novel and reliable way to avoid backbone oxidation[17, 18] but, in this particular case, it also entails very interesting photophysics caused by the alkoxy groups attached to the fluorene side group. Electronic structure calculations show that these amplify the participation of the conjugated side groups in the backbone excitation, which then modify the excited state behaviour via side group relaxation. The existence of two excited states is shown using a comparison of picosecond fluorescence spectroscopy and a time-resolved photobleaching experiment. Despite the fundamental character of this work, it provides direct input into the chemical optimisation of the charge transport in polyspirobifluorene derivatives.

Polydioctylfluorene (PFO) is considered the prototype of all present polyfluorene derivatives. Nevertheless, it exhibits a unique solid state morphology due to the competition of two room temperature solid state phases. Here, the lower energy beta phase traps excitations from the amorphous background phase. In combination with the previously observed amplified stimulated emission of the beta phase, PFO has the potential for an intrinsically dopes polymer laser. The prerequisites for this application are investigated in the third results chapter, focusing on the solid state. These include the control of beta phase formation during thin film fabrication, the question whether exciton migration is inhibited within the beta phase and an additional investigation into the effect of mirror quenching. The work mainly relies on room temperature steady state spectroscopy but is complemented by picosecond TCSPC and

temperature dependent measurements. The latter are particularly valuable for revealing the phase transitions of PFO below the temperature of nematic behaviour as well as the existence of a third phase, whose origin is not fully understood. Although this chapter leaves a number of questions unanswered, in particular concerning the sensitivity of beta phase formation, it sets the basis for further study towards the implementation of a polymer laser[19].

Finally, general conclusions summarise the results of all chapters.

2. Theory – The photophysics of conjugated polymers

2.1. The molecular structure of a conjugated polymer

2.1.1. The hybrid orbitals of the carbon atom

Conjugated polymers are organic macromolecules. They consist of tens to thousands of chemically linked repeat units, which form the polymer backbone and may be functionalised by the attachment of side groups. Carbon atoms, whose flexibility in chemical bonding is the basis of all organic chemistry, govern the chemical and physical properties of every conjugated polymer. The element carbon is characterised by four outer electrons, which are located in $2s^1$ and $2p^3$ orbitals. Due to the small energy gap between these orbitals, they can hybridise if required during bond formation. The arrangement into sp, sp^2 or sp^3 hybrid orbitals depends on the number and valence of the bond partners. Any unused electrons remain in the original p-orbitals.

The carbon atoms in conjugated polymers are sp^2-hybrids: These three orbitals overlap with those of hydrogen or other carbon atoms. Thereby strong σ-bonds are formed with a *bonding* σ-and an *anti-bonding* σ*-orbital, which arise from the linear combination of the partners' electron densities.

The remaining p_z-orbitals adopt an orientation orthogonal to the hybrid electrons. Commonly, they overlap sideways with a neighbouring p_z-state to form an additional weak π bond with a bonding π- and an anti-bonding π*-orbital. The simplest example of such a σ-π or double bond system with sp^2 hybrids is given by the ethene molecule shown in Figure 2-1. In a conjugated polymer, π-electrons are often part of the most delocalised bond. Hence, they are easy to excite, via a π-π*-transition, such that the ground (or *excited*) state of the molecule is often identified with them occupying the π-orbital (or *π*-orbital*).

Finally, the repeat units of a conjugated polymer may contain atoms that possess a valence different from four e.g. nitrogen. Such atoms contribute non-bonding or n-orbitals to the electron system. When excited, n-electrons are often accommodated in π*-orbitals (n-π*-transition).

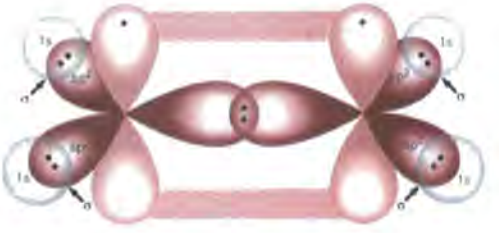

Figure 2-1 – The electron orbitals of the ethene molecule[158].

2.1.2. Conjugation

Several adjacent π-orbitals may overlap and generate a larger joint orbital where the electrons involved are highly *delocalised.* Then its spatial shape maps the distribution

of the contributing atoms above and below the molecule. Such delocalisation occurs in aromatic compounds, e.g. benzene, anthracene or fluorene, see Figure 2-2, which are often used as the building blocks of a conjugated polymer. A similar effect occurs in the aliphatic polyethylene $(CH)_n$, which is synthesised by the linking of many ethene units through an addition reaction. The molecule therefore exhibits alternating single (σ) and double (σ-π) bonds. This and the spatial periodicity arising from the shorter bond lengths of the double compared to the single bonds gives rise to the theoretical possibility of electron delocalisation along the entire polymer chain. This is termed *conjugation*; hence, polyethylene is a *conjugated polymer*. In general, a polymer chain is formed by linking many individual monomer units. If their chemical structure and the linking pattern exhibit alternating single and double bonds, one speaks of a conjugated polymer. Here, any incorporated aromatic units are viewed as consisting of three alternations[20]. As a consequence of conjugation, the molecular orbitals of several repeat units combine, i.e. they are delocalised, which leads to different photo-physical properties compared to the individual small molecules[21, 22]. In detail, delocalisation reduces the energy of ground and excited states, thus stabilising the molecule.

On a real polymer chain, conjugation is limited due to interruptions caused by saturated bonds in the system or a loss of planarity between adjacent repeat units. Both reduce the spatial overlap between the p_z-orbitals. Hence, the *effective conjugation length* is finite and may be further reduced in the presence of chemical or structural chain defects. In polyfluorene, the excited singlet state, S_1, typically extends over just four or five repeat units[22, 23].

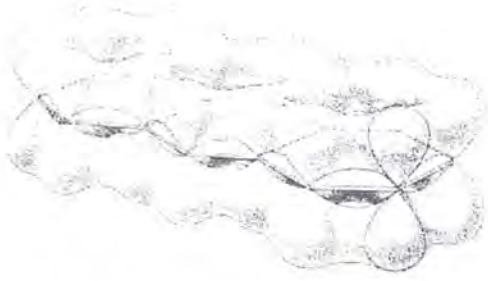

Figure 2-2 – Conjugation leads to the formation of the three-ring π-orbital in anthracene[20].

2.1.3. Excitons in a conjugated polymer

The nature of the excited states in a conjugated polymer was widely discussed some years ago. In 1980, Su, Schrieffer and Heeger[24] applied the conventional semiconductor *band model* to one-dimensional chains of polyethylene. By considering the periodicity of the polymer, they tried to describe conduction phenomena in organic materials. Their electronic structure was understood in terms of valence and conduction band in analogy to inorganic semiconductors. This model, however, proposes the existence of nearly free electrons in contradiction to the observed strong localisation of the excited state and its coupling to the vibrational modes of the molecule.

Therefore, in accordance with the excited state description in small molecules, an excitonic model is now preferred, which has been developed by Bässler and his research group[25-27]. An *exciton* is a Coulomb bound pair of electron and hole. In contrast to a geminate pair, these form a quantum mechanical unit involving the correlation of electron and hole spins.

The binding energy, E_B, of an excited electron-hole pair is the parameter which distinguishes between exciton and semiconductor model. While $E_B << 0.1$ eV suggests a free and wave-like electron as found in inorganic semiconductors, a value of several hundred millielectronvolts implies that an excited electron is strongly bound to its correlated hole, i.e. the existence of localised excitons. Recent experimental evidence clearly favours the latter model. As an example, photoluminescence studies with an applied electric field have directly demonstrated that a significant amount of Coulomb energy is needed to quench the fluorescence via dissociation of electron-hole pairs[28].

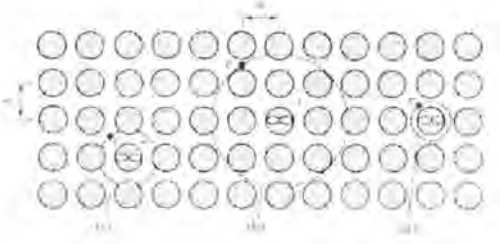

Figure 2-3 – The three types of exciton in an organic crystal[20]: (a) Frenkel, (b) Wannier-Mott and (c) charge-transfer exciton.

In the view of these facts, all work in this thesis assumes the excitonic model. In organic crystals, three types of excitons are distinguished according to their binding energy, as shown in Figure 2-3.

1) *Frenkel* excitons are tightly bound (E_B~1 eV) with electron and hole located on the same molecular unit[20]. Pronounced localization and zero dipole moment characterize a Frenkel exciton in addition to the emission of luminescence upon recombination.

2) *Charge-transfer* excitons are also strongly correlated but, here, electron or hole has transferred to an adjacent molecule causing a permanent dipole moment. The migration of electron and hole is independent of each other but they may recombine with the emission of delayed fluorescence similar to a geminate pair.

3) *Wannier-Mott* excitons show a large electron-hole separation of 40 to 100 Å[20]. Due to the rather low E_B of ~0.1 eV, the charge carriers migrate almost freely.

The excitons present in a conjugated polymer are intermediate between Frenkel and charge-transfer exciton with a binding energy of ~0.5 eV. They are usually located on one segment of a polymer chain but exhibit a more or less pronounced dipole moment, depending on the chemical build of the repeat units, which sometimes include groups of a distinct electron affinity (see chapter 5).

2.1.4. Polarons and geminate pairs

In a quantum-mechanical description, the Hamiltonian of the Coulomb interaction between the electron and hole of an exciton comprises two terms: a "classical" Coulomb energy and the exchange energy. The latter arises from the Pauli principle, which requires that the total (orbital and spin) wavefunction of the combined exciton state is antisymmetric. Thus, two fermions of the same spin cannot occupy the same orbital. For an exciton, the spins of electron and hole can combine in four ways, $\{\uparrow\downarrow\}$ (singlet state), $\{\uparrow\uparrow\}$, $\{\downarrow\downarrow\}$ and $1/\sqrt{2}(\{\downarrow\uparrow\}+\{\uparrow\downarrow\})$ (triplet states). While the exchange interaction is attractive for a singlet exciton, it is repulsive for a triplet exciton. As the classical Coulomb energy is the same in both cases, this gives rise to a higher triplet energy compared to the singlet as well as forcing electron and hole to occupy different orbitals in the triplet state.

When an exciton is given additional energy, e.g. thermal or electrical, the average electron-hole separation increases. Above a certain separation distance, the wavefunctions of electron and hole no longer overlap such that their exchange energy becomes negligible. However, the electron-hole pair may still be bound by Coulomb interaction. Such a state is termed a *geminate pair*. Its immediate recombination into an exciton is only prevented by the molecular nature of the polymer material: After a vertical electronic excitation in accordance with the Franck-Condon principle (see chapter 2.2.3.), the excited state relaxes. The geometry of the chromophore adjusts to minimise the excited state energy. In other words, the evaluation of the above Coulomb interaction is modified by changing the wavefunctions of electron and hole. As a result, any electronic excitation results in a local deformation of the molecular charge distribution, or *soliton*. Thus, any excited state – exciton, geminate pair or charged state – must be considered jointly with its associated soliton. The transfer of this soliton to another site, e.g. another molecule or molecular segment, requires an amount of energy. This amount corresponds to the difference of excited state energies of the two sites and is likely to be positive when the transfer originates from a relaxed molecular geometry. Therefore, a small energetic barrier must be overcome during formation and recombination of a geminate pair, as illustrated in Figure 2-4. In summary, geminate pair states are metastable and will eventually recombine

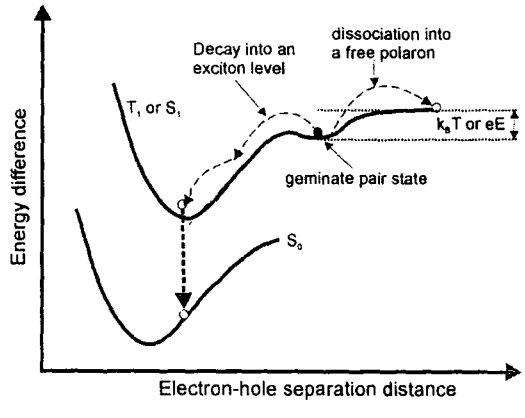

Figure 2-4 – Dependence of the excited state energy on the electron-hole separation with exciton (T=triplet and S=singlet), geminate pair and polaron states.

into an exciton. Alternatively, they might dissociate into separate charge carriers, e.g. if aided by an electric field, see Figure 2-4.

As such charged states are also associated with solitons. They cannot be considered as free charge carriers but are termed *polarons*. For polaron solitons, molecular deformations across ~ 20 repeat units[29] have been suggested.

2.2. Electronic transitions and spectroscopy

2.2.1. Photo-absorption and allowed transitions

Optical spectroscopy is an essential tool towards the understanding of the photophysics and excited states in a conjugated polymer. The necessary spectroscopic methods and terminology are introduced in this section.

In their application environment, PLEDs, excited states in conjugated polymers are generated via *electrical* excitation, i.e. injection and recombination of charge carriers. However, elementary information about these excited states is best gained via *optical excitation*, i.e. the absorption of radiation. This avoids the presence of charge carriers.

When electromagnetic radiation interacts with matter, transmission or absorption take place. The Beer Lambert Law describes the transmitted fraction of light in a material at a certain frequency, provided the intensity is low:

$$I(x) = I(0) \cdot \exp(-\alpha \cdot c \cdot x)$$

[Equation 2-1]

where I denotes the intensity of the (monochromatic) light, x the depth of the material, c the concentration of the absorber and α the frequency dependent absorption coefficient.

Each material has its characteristic absorption spectrum $\alpha(\lambda)$, where α may vary over orders of magnitude at different wavelengths. The product $A = \alpha c x$ describes the overall *absorbance* of an absorbing sample, $OD = log(e)*A$ is a common measure termed *optical density*. The absorbance is high where the energy of an incident photons coincides with a transition energy of the material. In small molecules, sharp absorption peaks appear at the corresponding wavelengths. Transitions in conjugated polymers typically extend over ~ 1 eV, usually in the visible (vis) to low energy UV range. A measure of the absorption strength from such broad absorption bands is obtained by integrating α over the frequency range of the transition[32]:

$$f = 6.25 \times 10^{-19} \cdot \int_{\nu_1}^{\nu_2} \alpha(\nu) d\nu \cdot \frac{mol}{m^2 s}$$

[Equation 2-2]

The *oscillator strength* f is a normalised, dimensionless quantity, which corresponds to the probability of the transition represented by the absorption band. This is used to compare the strength of different optical transitions. A value of $f = 1$ is related to a strong (*fully allowed*) and $f \rightarrow 0$

a very weak (*fully forbidden*) transition. The values of f are further classified in the framework of quantum mechanical calculations.

In a polyatomic molecule, a simplified Hamiltonian must be used to calculate probabilities of transitions. Essentially, this Hamiltonian is broken down into a set of *decoupled* sub-Hamiltonians representing the various factors which determine *f*, i.e. spin, parity, momentum properties and spatial shape of the involved orbitals. A general solution, i.e. a strong optical transition, is independently an eigenfunction of all sub-Hamiltonians. Separate transition probabilities p_i are found for spin (p_s), parity (p_p), momentum (p_m) and orbital symmetry (p_o). For a $\pi \rightarrow \pi^*$ transition in a polyatomic molecule these relate to *f* as follows:

$$f = p_s p_p p_m p_o f_a$$

[Equation 2-3]

where a fully allowed transition has the oscillator strength f_a. The probabilities p_i are summarised in *selection rules*:

Spin conservation. Spin changing optical transitions, e.g. from a singlet to a triplet state, are *spin forbidden*. Disturbances of the system due to heavy or paramagnetic atoms[20] may waive this rule. Here, *spin-orbit* coupling or *magnetic-spin* coupling entangles the sub-Hamiltonians of the system. Otherwise, transitions between states of different multiplicity are weaker by a factor of $p_s=10^{-5}$ compared to transitions between states of equal multiplicity[20].

Inversion of parity. Transition probabilities rise when wavefunctions of opposite parity are involved. Most molecules display some kind of symmetry. Wavefunctions of matching symmetry are termed gerade (g) and ungerade (u) if they change sign at the centre of symmetry. For the (g) orbital of benzene (and conjugated polymers) a transition to the (u)* state is *parity allowed.* Parity forbidden transitions such as g $\rightarrow$ g result in $p_p \sim 10^{-1}$. This rule can be waived due to symmetry-breaking vibrations of the system.

Conservation of momentum. The absorption of a photon results in no (elastic case) or only a small amount of momentum (inelastic case with phonon interaction) being added to the system. Transitions that involve large-scale changes in the angular or linear momentum are *momentum forbidden.*

Orbital overlap. For a spatially allowed transition, initial and final orbitals must simultaneously possess large amplitudes in the same region. For example, a good spatial overlap is given between the π and π^* orbitals of benzene as both orbitals lie in the same plane. When the areas of electron

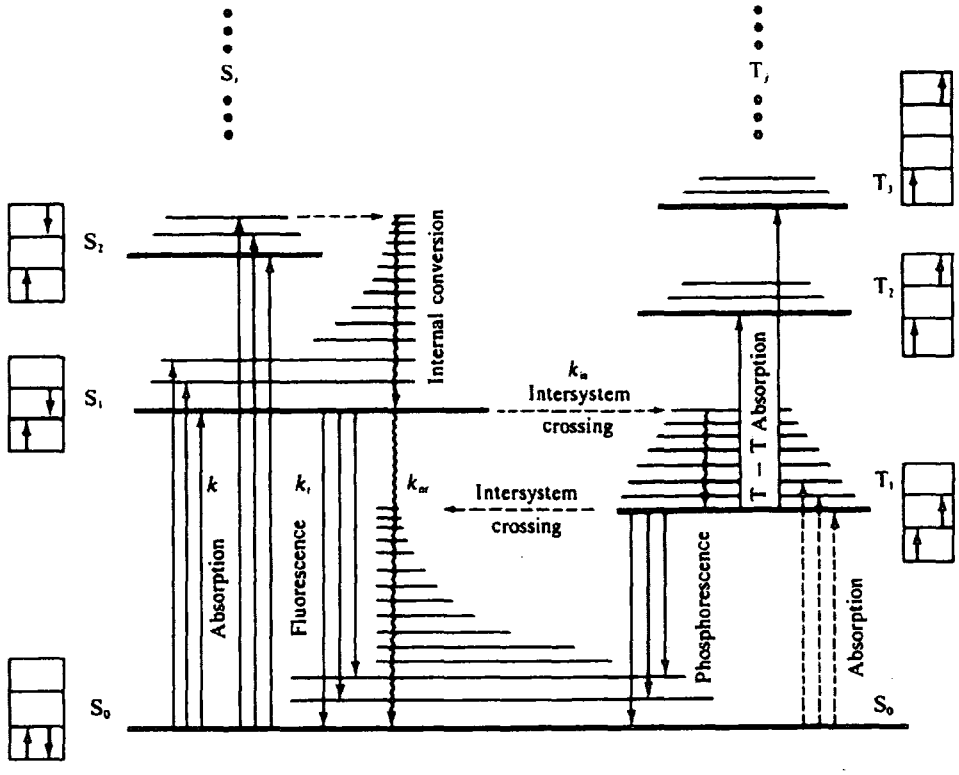

Figure 2-5 – The Jablonski diagram of a polyatomic molecule, taken from[20].

probability between initial and final state differ too much the transition is space or overlap forbidden. This is the case ($p_0 \sim 10^{-2}$) for a n $\rightarrow\pi^*$ transition as non-bonding n orbitals (e.g. of nitrogen) occupy a different plane than π^*.

2.2.2. The Jablonski diagram, vibrational coupling, intersystem crossing

At room temperature and without excitation energy, a molecule resides in the state of lowest energy, the ground state. As excitons exist in two multiplicities, this ground statecan exhibit either singlet (total spin of electron and hole equals 0) or triplet (total spin equals 1) character. As elaborated in section 2.1.4., the energy levels of singlet and triplet states differ by twice the exchange energy. This term is negative in the conjugated polymers studied here, such that the ground state is a singlet. In the *Jablonski diagram* of Figure 2-5, the ground state is denoted as S_0^0, with S for singlet, S_0 for the singlet electron configuration with the lowest energy (shown to the left of the diagram) and S_0^0 for the lowest vibrational level of the lowest state.

The energy of the lowest triplet state, T_1, is located below that of the first excited singlet, S_1, with a gap of typically 1 eV[34] for conjugated polymers. This gap can be tuned by the chemical structure of the chromophore[8]. As denoted to the right of the Jablonski diagram, the T_1 state involves

two unpaired electrons. This is caused by the Pauli principle, which requires an asymmetric orbital wavefunction for a two-fermion system with equal spins. Due to this electron configuration, all molecules with a triplet ground state are highly reactive and exhibit magnetic properties due to the unpaired spin. This situation is found for example in the paramagnetic ground state of oxygen, ^3O.

Now, attention is directed to the energetic sublevels of the ground and excited states. In this thesis, the term phonon will be used in context of conjugated polymers. In contrast to its meaning in crystal structures, where phonon refers to cooperative motions of the lattice, here it will be employed as a general term for any bond length vibrations, torsions or other motions of a polyatomic molecule. The energy levels of a polyatomic molecule couple to these modes. The quantised sublevels of vibrational energy that can be adopted by the molecule are illustrated in the Jablonski diagram, where each main state exhibits a number of overtones. While the energy separation between the main exciton levels lies in the UV or visible, the gap between the vibronic modes is usually found in the near infrared (IR). A typical separation of 180 meV is observed for the C-C stretch mode of conjugated polymers that contain benzene rings in their chromophores[33]. Other phonon modes, e.g. bond rotations, can be of lower energy, ~10 meV[23].

Electronic transitions between the states shown in Figure 2-5 are subject to the selection rules stated in the previous section 2.1. Thus, an optical excitation of a ground state polymer molecule, i.e. via the absorption of a photon, results in the formation of a higher excited singlet state. Transitions between states of different multiplicity are spin forbidden and triplet formation is inhibited during all natural absorption processes.

2.2.3. Photo-excitation, and the Franck-Condon principle

The different electronic states of a molecule are characterised by different potential energy curves and equilibrium bond lengths, as shown in Figure 2-6, for a diatomic molecule. Therefore, electronic excitation results in a change of the molecular charge distribution, which disturbs the equilibrium of Coulomb forces and causes the molecule to relax towards a new conformation. In general, equilibrium bond lengths increase when a molecule is excited.

The interaction of a photon with a chromophore (or electroactive part of a molecule) occurs on a time scale of 10^{-15}s [32]. The time required for the above vibrational relaxation state is comparably long, e.g. 10^{-13} s [32,35], such that the molecule can be considered rigid during the absorption process[32], which is a concept known as the *Franck-Condon-Principle*.

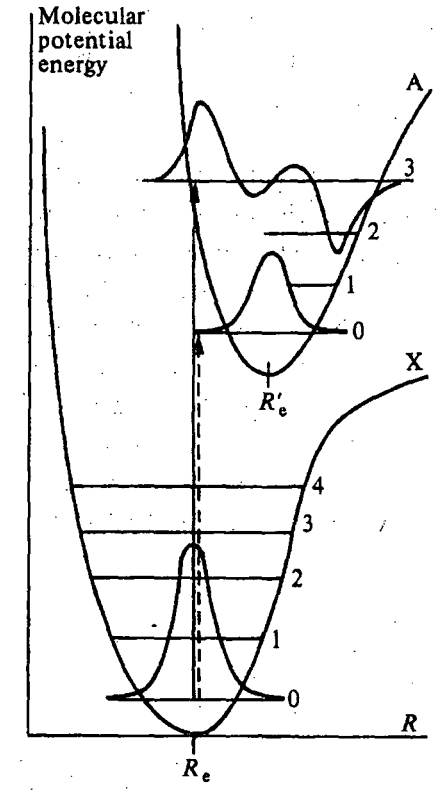

Figure 2-6 – Illustration of the Franck-Condon-Principle for a diatomic molecule, with R_e (equilibrium bond length), X (ground state) and A (excited state). Vibrational sub-levels and their wavefunctions are indicated (taken from P.W. Atkins, Molecular Quantum Mechanics, 1983).

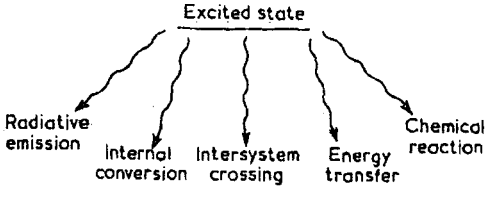

Figure 2-7 – Different pathways for the deactivation of an excited state in a conjugated polymer (taken from C. H. J. Wells, Introduction to molecular photochemistry (Chapman and Hall, London, 1972).

This causes electronic transitions to occur between different vibronic levels in both absorption and emission, which gives the corresponding spectra their mode structure. The absorption strength is highest between the states S_0^0 and S_n^k, where k is the vibrational level of S_n which has the highest spatial overlap with the S_0^0 wavefunction. Hence, higher vibrational states may be favoured. Excess vibrational energy then dissipates into thermal motion of the environment (*vibrational cooling*) and the molecule relaxes to the S_n^0 state within 10^{-12} s after the transition[36]. This as well as further processes of excited state relaxation lead to the localisation of the excitation on a particular (low energy) part of the chromophore, which usually consists of several repeat units. Thus, an exciton is formed. The mechanisms, such as conformational relaxation and exciton migration, are described in detail in chapter 4.

2.2.4. Excited state deactivation

Singlet excitons in conjugated polymers exhibit lifetimes between 10^{-10} and 10^{-9} seconds[37]. The return of an excited chromophore to its stable ground state can be accomplished via the emission of a photon.

Radiative transitions between states of equal multiplicity are termed *fluorescence (F)*. The spin forbidden transitions are termed *phosphorescence (Ph)*. Considering the Franck-Condon-principle, *F* and *Ph* generate states in higher vibronic levels of

S_0, which then relax to S_0^0. As a result, the typical fluorescence and phosphorescence spectra of a conjugated polymer consist of several vibronical modes. The energy difference between these modes corresponds to the energy gap between the vibronic sublevels, see Figure 2-8.

The nature of the transitions involved causes the mirror symmetry between the absorption and the fluorescence emission spectra, as illustrated in the Jablonski diagram. The energy difference between their 0-0 modes, i.e. $S_1^0 \leftrightarrow S_0^0$, is termed the *Stokes shift*. It is caused by the conformational relaxation of the molecule upon excitation.

Radiationless transitions. Other deactivation processes compete with *F* and *Ph*: *Internal conversion (IC)* describes radiationless transitions between states of equal multiplicity. *Intersystem crossing (ISC)* refers to those between states of different multiplicity. IC and ISC are both favoured where comparably small energy gaps need to be bridged as here phonons are

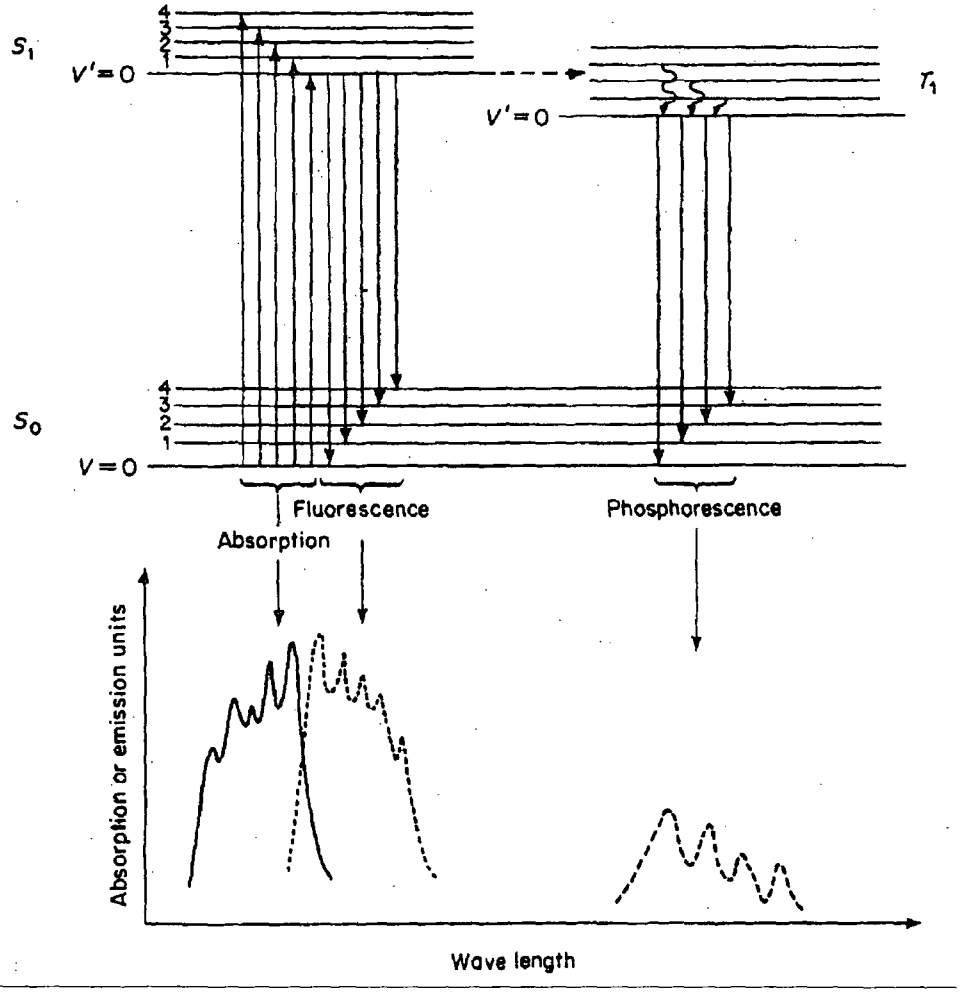

Figure 2-8 – Electronic transitions and typical spectra of absorption, fluorescence and phosphorescence. Inter-system crossing takes place between S_1^0 and T_1^n due to the small energy gap. Taken from E. F. H. Brittain, W. O. George, and C. H. J. Wells, Introduction to molecular spectroscopy; theory and experiment, Academic Press, 1970.

emitted instead of photons. Such conditions are given between adjacent S or T levels of high n. Therefore, the deactivation $S_n \rightarrow S_1$ and $T_n \rightarrow T_1$ occurs almost exclusively via internal conversion in less than a picosecond[38]. The remaining step is then accomplished by the emission of fluorescence, $S_1 \rightarrow S_0$, or phosphorescence, $T_1 \rightarrow S_0$.

Under photo-excitation, ISC represents the only way to populate the triplet manifold via $S_1^0 \rightarrow T_n^k$, as illustrated in Figure 2-8. This process is slow as it requires a spin flip of either electron or hole. The presence of heavy or paramagnetic atoms such as sulphur or oxygen, respectively, increases the ISC rate by an enhancement of spin-orbit coupling. This mixes the respective sub-Hamiltonians and partly waives the spin conservation rule, see above. Therefore, conjugated polymers such as polythiophenes exhibit ISC yields of up to 50 % in solution[39] in contrast to a limit of 3 % in polyfluorenes.

After vibrational relaxation to the lowest triplet state T_1^0, another spin flip is needed for the return to the ground state. This results in typical *long-lived* triplet lifetimes between 10^{-3} and 1 second in a conjugated polymer[40, 41]. The final step is often accomplished via ISC or bimolecular annihilation. However, phosphorescence, $T_1^0 \rightarrow S_0^k$, is not entirely forbidden although its observation may require an extremely sensitive detector[40, 41].

2.2.5. Inhomogeneous broadening and disorder

Exciton-phonon coupling and excited state relaxation depend on the chemical structure of the conjugated polymer. Different materials exhibit different degrees of flexibility, which allow the polymer chains to adopt a characteristic range of conformations. Structural disorder is present in all conjugated polymers and the random variation of conformations translates into energetic disorder, as is further elaborated in chapter 4. In that sense, each exciton is unique with respect to the geometry (or *conformation*) of the molecule it resides on. The ensemble of all chromophores is hence described by a Gaussian density of states (DOS) instead of the sharp energy levels shown in Figure 2-5.

In conjunction with the Franck-Condon-Principle conformational disorder results in the emission of an ensemble fluorescence or phosphorescence spectrum consisting of vibronic modes. The relative intensity of these modes is described by the Huang-Rhys parameter, S, which is described in detail in chapter 4. A large 0-0 mode is an indication that ground and excited states exhibit similar equilibrium conformations.

Due to disorder, the vibronic modes assume a Gaussian shape (*inhomogeneous broadening*) which is broadened in comparison to the intrinsic Lorentzian linewidth that is derived from the finite excited state lifetime (*homogeneous broadening*). The degree of disorder and

inhomogeneous broadening is activated by temperature and influenced by the frictional and Coulomb interactions of the chromophore with its environment.

2.3. Energy transfer

The interaction between chromophores can alter the intrinsic photophysics observed for an isolated exciton, which was described in the previous chapter. This results in differences between the fluorescence properties of polymer solutions and solid state films, which are both affected by quenching processes due to dopants, impurities or chain defects – but to different extents. To explain these and other effects, this chapter introduces concepts for the transport of energy in a conjugated polymer.

2.3.1. Reabsorption

An excited chromophore D (for *donor*, D* denoting its excited state) is deactivated via the emission of a photon of energy $h \cdot \nu_{photon}$, being the photon frequency:

$$D^* \rightarrow D + h \cdot \nu_{photon}$$

On its journey out of the polymer sample it may be absorbed at an *acceptor* chromophore, A:

$$A + h \cdot \nu_{photon} \rightarrow A^*$$

This occurs on the condition that A has an excitable frequency at ν_{photon}, i.e. a nonzero value of α. Therefore, for reabsorption to occur, the emission spectrum of D must overlap sufficiently with the absorption spectrum of A.

If D and A are of the same species, the strongest overlap commonly occurs between the 0-0 modes of the above spectra. The effect is most pronounced when the average path of light in a sample is long, i.e. in polymer films with thicknesses of several hundred nanometers or highly concentrated solutions. Then, reabsorption decreases the emission of a polymer sample out of the 0-0 mode[42] and can also cause a considerable extension of the fluorescence lifetime.

2.3.2. Förster resonance energy transfer

Förster or *resonant energy transfer* again involves a donor chromophore D and an acceptor A, whose emission (D) and absorption (A) spectra overlap. However, here energy is transferred via a direct electromagnetic interaction of donor and acceptor, as shown in Figure 2-9:

$$D^* + A \rightarrow D + A^*$$

Unlike reabsorption, the intermediate step of photon emission does not happen. Therefore, Förster transfer does not alter the shape of the donor fluorescence spectrum but the intensity of all vibronic modes is equally decreased.

This requires an interaction between the dipole moments of donor and acceptor

orbitals. As published by Förster[36] in 1959[#], this process is not coherent as it involves a coupling of the vibronic levels of the acceptor state, A, to the excited donor state, D*. When the energy of D* coincides with a transition energy of A both are in resonance and energy is transferred. The subsequent relaxation of A* to its S_0^0 level renders the transfer process *irreversible*. The following rate equation is derived for the *very weak coupling limit*[36], which applies to conjugated polymers:

$$K_{D\to A} = \frac{1}{\tau_D}\frac{1}{R^6}\left(\frac{\kappa^2 \cdot 8.8\cdot 10^{23}}{n_0^4}\int\frac{F_D(\lambda)\delta_A(\lambda)}{\lambda^4}d\lambda\right)$$

[Equation 2-4]

τ_D is the donor lifetime in absence of the acceptor, R the spatial separation between donor and acceptor, and n_0 the refractive index of the medium. Essentially, the integral evaluates the overlap between the normalised emission spectrum of D and the absorption spectrum of A. κ is a factor describing the orientation of the dipoles of D and A with respect to each other. For an ensemble of randomly oriented dipoles, κ is 2/3.

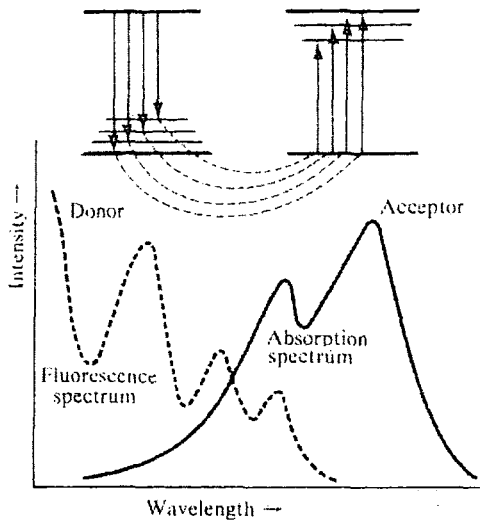

Figure 2-9 – Illustration of resonance energy transfer from a donor to an acceptor state[20].

For Förster transfer to occur, the *overlap integral* must be nonzero. Unlike reabsorption, resonant energy transfer does not make use of a mobile energy carrier, i.e. a photon. Therefore, a minimum distance must be kept between donor and acceptor. Upon rewriting [Equation 2-4 one can define the *Förster radius* R_F as the distance where the transfer rate equilibrates the total decay rate of the donor:

$$K_{D\to A} = \frac{1}{\tau_D}\frac{{R_F}^6}{R^6}$$

$${R_F}^6 = \frac{\kappa^2 \cdot 8.8\cdot 10^{23}}{n_0^4}\int\frac{F_D(\lambda)\delta_A(\lambda)}{\lambda^4}d\lambda$$

[Equation 2-5]

Experimentally, it is more convenient to observe the characteristic radius, $\overline{R_0}$. At this distance the energy transfer rate equals the total rate of decay of D*:

[#] Förster first published this description 1948 in „Zwischenmolekulare Energiewanderung und Fluoreszenz", Annalen der Physik 2(1-2): 55-75

$$K_{D\to A} = \frac{1}{\tau}\left(\frac{\overline{R_0}}{R}\right)^6 = \frac{1}{\tau_D}\left(\frac{R_F}{R}\right)^6$$

[Equation 2-6]

The conversion is done via $\tau = \Phi_F \tau_D$, where Φ_F denotes the natural fluorescence quantum yield of D. In conjugated polymers, $\overline{R_0}$ can reach up to 50 Å[43], which is sufficient to allow intermolecular transfer.

2.3.3. Exciton migration

An exciton consists of an excited electron located near its correlated hole, which reside on a segment of polymer chain and cause a local molecular distortion. Due to this localisation it is considered as a pseudo-particle.

Hence, if an exciton transfers from a donor chromophore (or site) on a conjugated polymer to an accepting site of the same species, this transfer can effectively be seen as exciton migration. In general, excitons spatially migrate driven by the energy gradient within the distribution of excited state energies, i.e. towards sites of locally minimised energy. Thus, energy is transported through the polymer material. The theoretical framework is explained in detail in chapter 5. Commonly, one distinguishes between intramolecular (along a single polymer chain) and intermolecular (between chains) exciton migration. The former occurs in isolated molecules, which are present in dilute solutions. Here, the mechanism is one-dimensional and, thus, less efficient than the latter, multidimensional, type, which dominates exciton migration in closely packed solid state films.

Depending on the precise experimental conditions, exciton migration can be a rapid process that covers large distances of up to 100 nm[26]. Therefore, it very often precedes or activates a further, secondary transfer process, of either Förster or Dexter type, by bringing a suitable donor excitation into the vicinity of an acceptor site.

2.3.4. Dexter transfer

In the above Förster mechanism any transitions involving a triplet exciton are spin forbidden, such as *triplet-triplet transfer*:

$$D^*(T_n^0) + A(S_0^0) \rightarrow D(S_0^0) + A^*(T_m^k)$$

Also, due to the weak dipole-dipole interaction, the triplet absorption and, hence, the overlap integral of [Equation 2-4 are vanishingly small. Still, triplet excitons are able to migrate via a slower mechanism called *Dexter transfer*, which requires only the conservation of the total spin of D and A. In short, Dexter transfer involves the exchange of electrons between D and A.

When a donor D and an acceptor site A are very close such that their orbitals overlap, an electron at D has a nonzero probability to appear on site A. The typical donor-acceptor distances for *electron exchange* range between 10 and 15 Å.

The theory of electron exchange transfer was developed by Dexter[44], who calculated the rate of triplet-triplet energy transfer as:

$$k_{D\to A} = \frac{2\pi}{\hbar}|\beta_{D\to A}|^2 \int F_D(E)F_A(E)dE$$

[Equation 2-7]

where $k_{D\to A}$ represents the exchange energy interaction between donor and acceptor. Here, the overlap integral is not evaluated from the fluorescence but from the normalised phosphorescence spectrum of the donor, $F_D(E)$.

Dexter transfer is less probable for singlet excitons because $k_{D\to A}$ is low compared to the Förster transfer rate for large spatial separations of D and A. On the other hand, electron exchange transfer is the preferred mechanism for triplet excitons. Their large radiative lifetime (slower than their $k_{D\to A}$) theoretically enables transfer sequences resembling the hopping migration of singlets.

2.3.5. Trapping and quenching

The migration of a singlet or triplet exciton is terminated when they reach a local minimum of site energy that (during their lifetime) cannot be overcome by thermal activation. These minima exist within the intrinsic local density of exciton states but can also arise from chemical or morphological chain defects, which are present in every polymer sample. In the latter case, one speaks of energetic *traps*. As an example, chemical degradation such as oxidation of individual repeat units leads to the formation of keto defects[4, 5], in particular at unsealed surfaces of thin films. In addition to these defects, a certain level of impurities, e.g. metal ions, always remains inside the material after synthesis and can also trap excitations. The presence of many trap sites reduces the average mobility of excitons.

Most defects primarily interact with singlet excitons via Förster transfer. The interactive radius of triplet excitons is limited by Dexter transfer. For the latter, exceptions arise in the presence of heavy or paramagnetic atoms such as oxygen, which introduce spin-orbit coupling and waive the spin forbiddance of the Förster transfer reaction. Therefore, dissolved oxygen needs to be removed from a solution sample (*degassing*) prior to excitation. Otherwise, dynamic trapping will take effect after typically 1 μs, rate limited by the diffusion of oxygen to polymer molecules.

Excitons trapped at defects or impurities tend to decay non-radiatively via internal conversion, i.e. they are *quenched*. Thus, excitation energy is captured and lost for fluorescence. If luminescence is emitted from a trap it will be red-shifted with respect to the host luminescence due to its low site energy. Note that the emission from a chemically different chromophore (compared to the polymer host) will exhibit a different spectrum. In the case of oxidation or *keto* defects, green luminescence is emitted with a low quantum yield, which leads to a colour instability of the polymer sample[4, 5].

2.3.6. Doping in polymer light emitting diodes (PLEDs)

In contrast to the above unwanted traps, one can deliberately introduce acceptor sites. In this case, the donor sites of the conjugated polymer are termed *host* and the imbedded acceptor *dopant* sites are termed *guest*. For such *doping* one chooses a guest material with an absorption spectrum that overlaps well with the host emission. This ensures that energy transfer, i.e. mostly Förster type, efficiently competes with the other deactivation channels of the polymer, including fluorescence. The dopant concentration is adjusted to provide an average host-guest distance smaller than the Förster radius.

Then, the dopant, which should exhibit a high luminescence quantum yield, emits at the expense of the host fluorescence. This is important for the application of conjugated polymers in light emitting diodes (PLEDs). A secondary goal in PLED development is also the tuning of the emission spectrum to obtain an output colour suitable for the RGB system. However, blue-emitting PLEDs are unlikely to be created via doping due to the red-shift involved in the energy transfer [45, 46].

As mentioned above, the electrical excitation applied in PLEDs creates a majority of triplet excitons, which mainly decay non-radiatively. To overcome the spin forbiddance of phosphorescence and also harness triplet states for luminescence, many dopants are heavy atom complexes involving platinum and iridium.

Apart from their improvement to PLEDs, doping is a useful tool for investigating energy transfer processes. With their help[47], it has become clear that often not the donor-acceptor interaction but the preceding exciton migration poses the rate limiting step of energy transfer.

2.3.7. Bimolecular annihilation

Above discussed were the *unimolecular* excited state processes of conjugated polymers. Their rates depend linearly on the concentration of excitons, [X]. In contrast to this, *bimolecular annihilation* processes depend on $[X]^2$ and accelerate rapidly at high excitation doses.

Triplet-triplet annihilation (TTA). High triplet densities lead to TTA. In electroluminescence devices, these are reached due to the favoured the formation of triplet excitons. However, also in photo-excited polymer samples, triplets may accumulate due to their long triplet lifetime. TTA involves the collision of two triplet excitons[48]:

$$T_1 + T_1 \Rightarrow \begin{Bmatrix} \frac{8}{9}(S_0 + T_n) \\ \frac{1}{9}(S_0 + S_n) \end{Bmatrix} \qquad \textit{[Equation 2-8]}$$

Commonly, this is an intrachain process as Dexter transfer requires an exciton separation of below 15 Å. Via TTA, one ground state exciton and one highly excited triplet or singlet are formed, the latter in a ratio of 8:1. Note, while the above equation gives only the final states, also intermediate quadrupole states are involved.

TTA is an important triplet quenching mechanism in both polymer solutions[49] and solid state films. Additionally, it is the source of solid-state *delayed fluorescence (DF)*[31] in many conjugated polymers: Singlet excitons can be formed via TTA, which may, in turn, emit fluorescence. Thus, the fluorescence lifetime is extended, e.g. in polyfluorenes up to the microsecond range[31]. TTA is distinguished from the other mechanism of delayed fluorescence, geminate pair recombination, via its quadratic excitation dose dependency.

Singlet-triplet annihilation (STA). Triplet excitons can quench the singlet state via *singlet-triplet annihilation (STA)*[50], in particular in electro-luminescence devices where the triplet density is high. As here, singlets are already a minority and triplets do not contribute to the luminescence, there have been attempts to dope polymer LEDs with triplet quenchers to inhibit STA and, thus, to increase the electroluminescence quantum yield[50, 51]. STA requires a Förster transfer process:

$$S_1 + T_1 \Rightarrow S_0 + T_n \qquad \textit{[Equation 2-9]}$$
$$T_n \Rightarrow T_1 + heat$$

Via a spin-allowed transfer reaction the singlet passes its energy to the triplet, raising it from T_1 to an upper triplet state. For that purpose, singlet fluorescence and triplet-triplet absorption must overlap. As a reverse transfer, triplet energy might also be given to the singlet state but this includes a transition from T_1 to S_0 and is spin forbidden.

Singlet-singlet annihilation (SSA). In analogy to STA, singlet-singlet annihilation involves the Förster transfer between two excited singlet excitons. Thereby, one returns to the ground state and the other is raised to an upper singlet state:

$$S_1 + S_1 \Rightarrow S_0 + S_n \qquad \textit{[Equation 2-10]}$$
$$S_n \Rightarrow S_1 + heat$$

The occurs when the singlet concentration is very high such that the collision of two singlet excitons becomes probable, i.e. they approach each other closer than their Förster radius. SSA leads to a reduced singlet lifetime and a non-linear excitation dose dependency. It is frequently observed in solid state conjugated polymers.

2.3.8. Loss of polarisation

Considering optical excitation via a linearly polarised laser, only those chromophores of an ensemble can be excited, which exhibit an electrical dipole moment parallel to that of the photon, i.e. the electrical polarisation of the beam. If this is directly followed by a radiative decay to the ground state without any intermediate processes, the emitted photon is polarised at a fixed angle to the excitation photon[52].

However, as elaborated above, excitations in a conjugated polymer can undergo a variety of processes before eventually decaying to the ground state. Most of them, in particular structural relaxation and excitation migration, gradually reduce the correlation between an exciton and its initial state, with respect to both initial

energy and dipole moment. This entails time-dependent changes of the fluorescence spectrum. While the former manifests itself in spectral dynamics, the latter results in a time-dependent decrease of the correlation between excitation and emission polarisation. Starting from linearly polarised photo-excitation, the emission will eventually be randomly polarised. A measure of this loss of polarisation memory is the fluorescence anisotropy, r,[52] see also chapter 5:

$$r(t) = \frac{I_{\parallel}(t) - I_{\perp}(t)}{I_{\parallel}(t) + 2 \cdot I_{\perp}(t)}$$

[Equation 2-11]

where, $I_{\parallel}$ and $I_{\perp}$ represent the intensities of the fluorescence emitted at parallel and perpendicular polarisation, respectively, compared to the excitation beam. Effectively, the time-dependence of r is observed as a decay of the initial polarisation, $I_{\parallel}$, and a build-up of the orthogonally polarised fluorescence, $I_{\perp}$, on the same time scale, which depends on the underlying excited state relaxation. This happens in addition to the intrinsic radiative decay in a conjugated polymer. Therefore, any experiment which aims to measure the overall time-resolved fluorescence needs to account for the anisotropy decay. This is always the case when a the detected signal is proportional to the total fluorescence intensity, $I_T = I_{\parallel} + 2 \cdot I_{\perp}$. As shown in chapter 3, this can be accomplished by detecting a signal that is polarised at *magic angle* or 54.7° to the excitation beam.

2.4. Interchain interactions

2.4.1. Solution versus thin films

In small organic molecules and conjugated polymers, the nature and decay of excited states differ significantly between dilute solution and the solid state. This is caused by the different levels of intermolecular interaction.

In solution, each solute molecule adopts an independent equilibrium conformation. For polymer chains, the interaction with the surrounding solvent molecules leads to an equilibration of the twist angles between repeat units and the bond lengths, see also chapter 4. As an example, the polyfluorene PF2/6 is known to adopt a helical structure[53].

Compared to the molecular conformation, the persistence length of a polymer chain is a "macroscopic" quantity. It describes the distance over which the macromolecule does not bend backwards on itself. The persistence length depends on the chemical build and rigidity of the backbone and can be large[53]. Coiling is associated with interchain interactions between different molecular segments. These are aggravated by poor solvation, which forces the solute into a mode condensed shape.

The intermolecular interactions between different molecules are ideally random. The solute molecules diffuse freely depending on the viscosity of the solvent and on the steric hindrance posed by the molecular volume, which is determined by the molecular weight and the bulkiness of any

side groups. The rate of diffusion and the polymer concentration govern the number of contacts between molecules and, with it, any bimolecular processes[51].

The driving force of intermolecular interactions for any molecular solute is the variation of electron density across the molecule, i.e. electrostatic forces arising from microscopic dipole moments. Such forces can be promoted by certain molecular shapes, e.g. the disc shape of anthracene. Also, any side chains are of importance due to their prominent position at the outside of a molecule. In this context, particularly bulky side chains or macromolecules are also affected by steric interactions, e.g. entanglement.

To summarise the above, interchain interactions are negligible in a dilute solution of a non-polar conjugated polymer in a reasonably good solvent. Therefore, the interchain migration of excitons is inhibited in such systems. Thus, the importance of non-radiative paths is decreased by reducing the effective radius of traps and quenching sites.

While photoluminescence quantum yields (PLQY) of 90 % may be reached in dilute solution, this value is decreased to less than 30 % in thin films. This is caused by the much closer packing of polymer chains in the latter. Although residual solvent may be present in the solid state, depending on solvent viscosity, film thickness and sample treatment, its contribution to the spacing of polymer chains is negligible. This, in turn stimulates interchain interactions during film deposition when the molecules try to reach an equilibrium position, which may lead to aggregation, see below, and subsequent luminescence quenching.

Also other thin film processing can induce a microscopic arrangement up to crystalline ordering[54, 55]. These processes require an increased mobility of molecules or molecular segments, which is facilitated by

a) an exposure to solvent vapour. The presence of additional solvent spacers reduces both steric and electrostatic interactions.

b) heating above the glass transition temperature, T_G, of the polymer (*annealing*). For amorphous materials such as polymers, T_G describes the temperature above which the relative molecular mobility becomes thermally activated.

Generally, the close packing and frequent interchain contacts in the solid state cause a high efficiency of energy transport via resonant transfer and electron exchange. Therefore, excitons exhibit a high interchain mobility in the solid state, resulting in a high interaction radius of every quenching site. The conjunction of aggregation and migration increases the importance of non-radiative excited state decay, thus reducing the PLQY. From another point of view, deliberately introduced dopant sites are much more efficient in the solid state.

One can avoid interchain migration by isolating the molecules, i.e. by imbedding the polymer chains into matrix molecules which serve as spacers. Such a setup is

useful for investigating the properties of static individual molecules as in REF [56]. However, it cannot be employed in PLED application as intermolecular energy transport is a fundamental function of any light emitting diode.

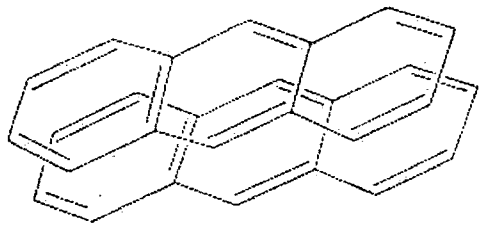

Figure 2-10 – The sandwich type dimer of anthracene[20].

2.4.2. Aggregation

Two classes of intermolecular interactions are distinguished, depending on whether they occur between molecules in their ground or excited state. Interactions between molecules in their ground state are termed *aggregation*. Conjugated segments of different polymer chains (or of one coiled chain) in close proximity may interact as described in the previous section. As a result, weak physical or even chemical bonds are formed that did not exist in either of the original chromophores. Such processes are promoted by a high concentration of molecules (in solution) but also by certain molecular charge distributions or shapes, e.g. for anthracene (see Figure 2-10).

An aggregate exhibits electron orbitals combined of those of its constituents. Polymer chains experience a break of intrachain conjugation at aggregated segments, which is caused by the electron density drawn off their backbones. Dimer formation is a special case of aggregation of two identical molecules (or in the case of polymers, repeat units), as illustrated in Figure 2-10.

The absorption and emission spectra of an aggregated species resemble those of its constituents albeit with a red-shift and considerable additional broadening[20, 57]. Aggregate emission can give a major contribution to the total emission of a polymer sample but the broad spectra are not desired in PLED application.

2.4.3. Excimer formation

The term *excimer* refers to an interaction of a ground state molecule with one in the *excited* state. Therefore, its ground state is repulsive, i.e. dissociative, such that no absorption spectrum can be attributed to the new species. In contrast to aggregates, excimers are not detectable with absorption spectroscopy. An excimer formed between chemically different molecules or repeat units is called *exciplex*.

Due to the radiative transition to the repulsive ground state, illustrated in Figure 2-11, excimer emission is red-shifted and exhibits a characteristic Gaussian shape without vibronic modes[20, 58]. Thermal energy is required during emission to overcome the potential barrier that has led

to excimer association. Therefore, the emission quantum yield increases with rising temperature.

Both, aggregates and excimers act as structural traps and emit with a low quantum yield at the expense of the host (polymer) fluorescence, thereby reducing the overall emission.

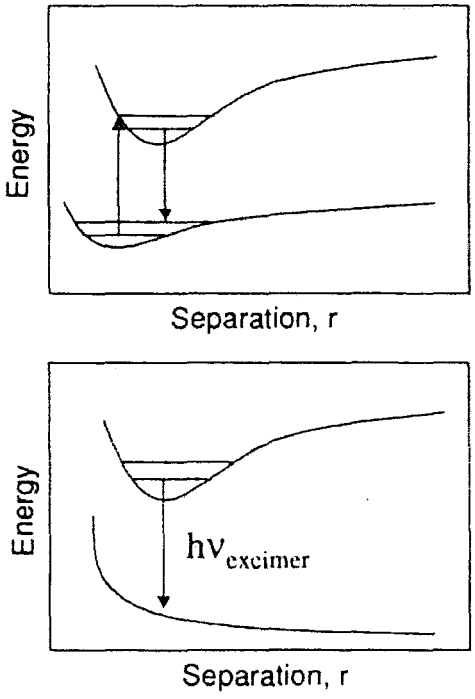

Figure 2-11 – Illustration of the difference between aggregate and excimer emission. Taken from I. D. W. Samuel, G. Rumbles, and R. H. Friend, Primary Photoexcitations in Conjugated Polymers (World Scientific) 1997.

3. Experimental techniques

3.1. Sample fabrication and characterisation

3.1.1. Materials

The conjugated polymers and oligomers studied here vary for each chapter; hence they will be introduced separately. In general, these materials emitted fluorescence in the blue.

3.1.2. Fabrication

The fabrication and type of samples was varied and will be introduced in the corresponding chapters. Briefly, two types of samples were studied, solutions and thin films. For solution samples, a range of nonpolar organic solvents was used. Depending on the solute material, stirring and heating was occasionally necessary and will be indicated. Thin films of conjugated polymers were fabricated under clean room conditions by spin-coating a highly concentrated (5 to 20 mg per mg solvent) master solution of the material onto cleaned quartz or sapphire discs of 10 mm diameter, and occasionally onto other substrates. Sapphire discs were used for low temperature measurements to achieve a better thermal contact. The thickness of the films was determined with a thin film analyser (FilmMetrics F20-UV). This device was calibrated after each switch-on, using a silicon test substrate with a defined layer of silicon oxide on top. The film thickness depended on the concentration of the master solution, the viscosity of the solvent and the rate of rotation. A typical film of polyfluorene spun from a 5 mg/mg toluene solution at 2500 rpm for 60 s would be 50 nm thick. Further data are shown in chapter 5.

3.1.3. Steady state characterisation

Absorption spectra of all samples were obtained using a commercial PERKIN-ELMER double-beam spectrometer. Steady state excitation and emission spectra were recorded with either of two similar Jobin-Yvon spectrofluorimeters (FLUOROMAX 3 and FLUOROLOG) prior to each time-resolved experiment. Thus, spectral anomalies arising from an impure solvent or aggregation of the solute molecules etc. were excluded. The quantum yield measurements presented in chapter 5 were carried out using an integrating sphere method in combination with the FLUOROMAX fluorimeter.

Both spectrofluorimeters and the integrating sphere were calibrated by Dr. L.-O. Pålsson using a tungsten calibration lamp (Ocean optics, NIST standard).

3.2. Source of photo- excitation

3.2.1. Laser specifications

Following initial characterisation, the samples were studied by time-resolved measurements, which are explained in detail below. The photo-excitation for these experiments was achieved by a mode-locked Ti:Sapphire laser (Mira 900,

Coherent) with an output pulse width of less than 2 ps and a repetition rate of 76.3 MHz. The output wavelength was tunable between 700 and 1000 nm with a maximum output power of ~ 2 W at 800 nm.

3.2.2. Frequency doubling

The main absorption bands of the common conjugated polymers and oligomers are located between the green visible (550 nm) and the near UV range (350 nm). Hence, for photo-excitation, the output frequency of the Ti:sapphire laser had to be doubled, using the birefringence of a beta barium borate (BBO) crystal. The efficiency of second harmonic generation varied with the input wavelength depending on the properties of the BBO crystal (Castech, type 1[59]). Typically 10 % power conversion was achieved by adjusting the orientation of the crystal with respect to the beam as appropriate for the wavelength used. The overall output power reached a maximum of 120 mW at λ_{out}=400 nm, which corresponds to a dose of 1.6 nJ per pulse.

3.2.3. Excitation and collection

In front of the sample, the final polarisation of the laser beam was brought to vertical using a Berek polarisation compensator.

A very low excitation power of maximal 20 mW arrived at the sample (0.26 nJ per pulse). When using a solution sample, the beam was collimated in front of the sample down to a path diameter of the order of 0.1 mm, corresponding to an excitation density of maximal 26 nJ/mm^2. Still, no signs indicating a saturation of long-lived species, e.g. triplet states, were observed. Emission was collected perpendicular to the excitation path through an aperture of 2.5 mm in diameter.

For a thin film sample, a slightly varied excitation geometry was used, see Figure 3-2 below. Otherwise, the 90-degree or L-shaped geometry used for solutions would have resulted in both, comparably poor collection efficiency and a distortion of the emission decay resulting from the path differences between different positions on the sample. Moreover, to avoid specular reflection of the excitation beam into the monochromator, the sample had to be turned out of the 45° position, worsening the above deficiencies. A nearly zero-degree geometry provides optimal collection efficiency and a minimal path difference from the sample surface whilst simultaneously getting rid of specular reflections. In order to avoid damage of the thin film samples as well as annihilation processes, the excitation spot size was regulated down to ~3 mm using an iris, corresponding to an excitation density of 0.03 nJ/mm^2 per pulse.

A standard setup of two lenses was used to collect and focus the sample emission onto the entrance slit of an Acton Spectra Pro 2300i double subtractive monochromator.

3.2.4. Magic angle detection

Vertically polarized laser light is used to excite the solution and film samples in the

presented experiments. Due to the rotation of emitting molecules or excitation migration along a polymer chain, depolarization of the emission takes place after excitation (anisotropy decay[52]). Simplified, the emission component polarized parallel to the excitation beam I_V (vertical) shows a faster apparent decay due to the depolarization component, which adds to radiative decay and excitation quenching. In analogy, the component polarized perpendicular to the laser I_H (horizontal) will show a build in due to excitations converting from vertical polarisation. One can make use of such measurements to study the physical processes causing depolarisation. However, the presented experiments focus on time dependent intensity measurements. It is therefore desirable to detect a signal proportional to the total fluorescence intensity, namely $I_T=I_H+2I_V$ [52], as otherwise the fluorescence decay dynamics will be distorted.

In addition to anisotropy decay, the monochromating device and in particular its gratings contribute to this distortion by transmitting I_H and I_V to different degrees. Hence, the effectively transmitted signal is some linear combination of I_H and I_V, which is characteristic for the monochromator and can be quantified by its (wavelength dependent) G-factor[52]. Whilst, when recording anisotropy decays it is necessary to correct for the G-factor, it suffices for the measurements shown here to collect fluorescence at a polarisation angle of $\alpha=54.7°$ to the vertical excitation beam. Then, the detected intensity is proportional to I_T:

$$\begin{aligned}&\cos^2\alpha\cdot I_V+\sin^2\alpha\cdot I_H\\&=0.333\cdot I_V+0.667\cdot I_H\\&=0.333\cdot I_T\end{aligned}$$

[Equation 3-1]

For this property, $\alpha=54.7°$ is also called the "magic angle". The phenomenon arises from the fact that the intensity transmitted by a polariser (here: a Glan-Thompson polariser) depends on the $\cos^2$ of its angle to the incident polarisation.

The observed fluorescence decay is then free of components from depolarisation.

3.3. Time Correlated Single Photon Counting (TCSPC)

3.3.1. One sample – two experiments

The majority of results presented in this thesis were obtained from two experiments; time correlated single photon counting (TCSPC) and streak camera measurements. As shown in Figure 3-2, a combined setup was used by attaching the two detectors to different exits of the monochromator. Via flip mirror, they could be used alternatively to measure the time-resolved fluorescence of the sample. TCSPC and streak camera experiments could thus be carried out on the same sample without changes in excitation and collection conditions. Only the monochromator setup had to be slightly changed. For streak camera measurements, a dispersed emission spectrum was coupled

out by replacing the first grating of the double monochromator with a mirror. For TCSPC, double subtractive monochromation was used, making use of the dispersion compensation and high spectral resolution of the Acton device.

The strength of this combined setup lies in the complementary techniques: On one hand, the time-resolved emission spectra obtained via streak camera give an overview of any spectral dynamics. On the other, TCSPC is able to study these dynamics in detail by collecting emission decays at appropriate points in the spectrum, determined from the streak camera data. The superior signal-to noise ratio makes the TCSPC data suitable for re-convolution analysis.

This combined experiment was designed by Prof. A.P. Monkman and set up by Prof. Monkman and Dr. Fernando B. Dias. The TCSPC component, laser and optical path were maintained and optimised by Dr. Dias.

3.3.2. Detection for TCSPC

For TCSPC, the spectral resolution of the monochromator was ~ 4 nm as determined from the spectral width of a scattered laser signal. The monochromated sample emission was detected by a highly sensitive micro-channel plate (MCP, Hamamatsu). The device covered a time range of 3.333 ns. The time increment could be chosen as Δt = 0.815 or 3.26 ps via a software interface. Δt corresponds to the minimum time resolution of the system, which could achieved by a deconvolution of the signal from the response of the system to a scattered laser pulse.

3.3.3. Mode of function

For single photon counting, a trigger diode (excited by the laser at 76.3 MHz) is connected to the MCP. At the same rate, the sample is excited by the laser. Its emission is fed to the MCP. An emission photon detected by the MCP gives the "START" signal. A capacitor attached to the MCP is being charged at a known rate. The next trigger of the diode following detection sets a "STOP" to the charging process, as shown in Figure 3-3. Any constant offset between detection and trigger was compensated for electronically. The voltage at the capacitor is then related to the charging time, t_{char}. This, in turn, is related the time of photon detection after sample excitation, t_{photon}, via:

$$t_{photon} = T - t_{char} \qquad [Equation\ 3\text{-}2]$$

with T being the temporal spacing of the excitation pulses, i.e. 13.1 ns. The temporal resolution of this technique is limited by the accuracy of detecting the capacitor voltage. Thus, an incident photon is associated with its time of arrival, t_{photon}, and a detection

Figure 3-1 - Photograph of the laboratory with TCSPC and streak camera set up.

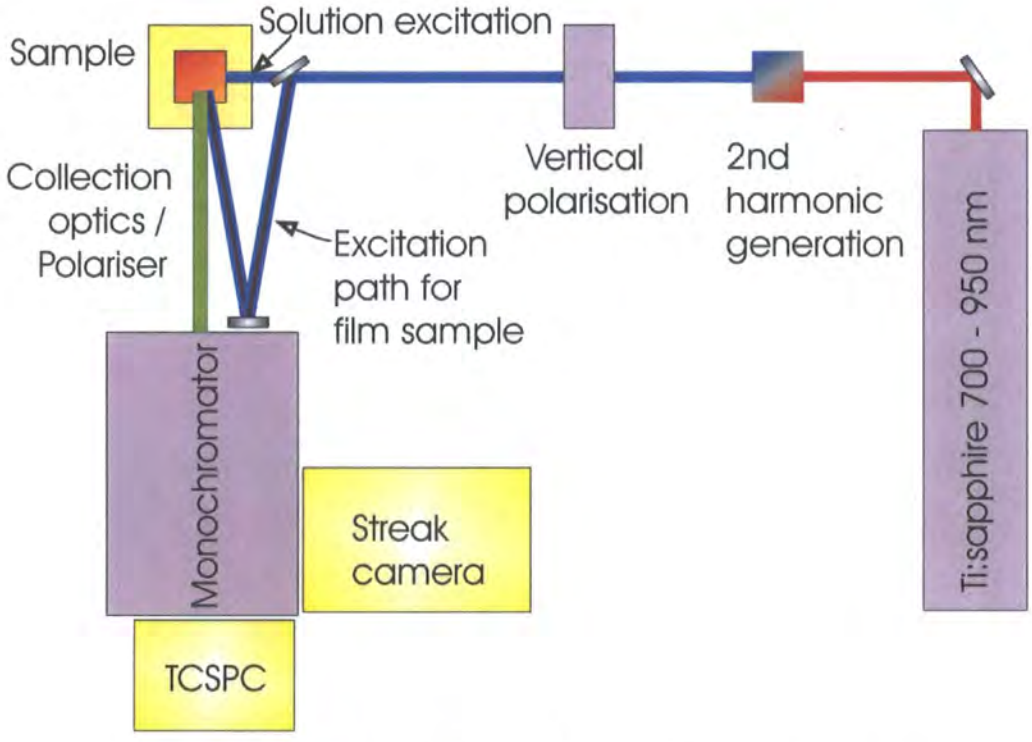

Figure 3-2 - Schematic of the combined TCSPC and streak camera setup.

channel within the detection window of 3.333 ns. Depending on the requirements of the experiment, this window could be divided into either 1024 or 4096 detection channels of a width of 3.26 or 0.815 ps, respectively.

During a photon counting experiment, many photons are detected in the above way and the detection events for each detection channel are counted. Thus, for a large number of repetitions, one obtains a histogram of the emission decay, similar to the one shown in Figure 3-4. However, this histogram is only valid if no more than a single emission photon hits the detector between two adjacent excitation pulses. This is due to the MCP, which needs to recharge itself after detection and is "blind" to a second photon during a certain time window. Thus, multiple exposures do not

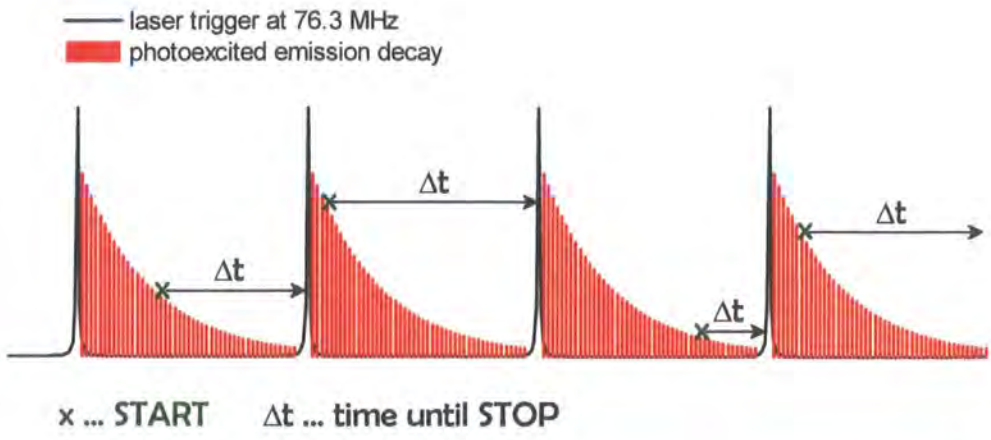

Figure 3-3 - Schematic of the reverse TCSPC principle[60]. The red bars represent the detection channels with their corresponding probability of detecting an emission photon.

contribute to the histogram and invalidate the underlying Poisson statistics. Overexposure commonly results in distorting the observed decay kinetics. Hence, care must be taken when adjusting the signal intensity. As an example, at the given excitation rate of 76.3 MHz the rate of incident photons was kept below 0.1 MHz, corresponding to only a 1000^{th} of excitation events resulting in a detected emission photon. Note that conventional single photon counting experiments operate using the excitation trigger as a START and the detection event as the STOP. Hence, the majority of activity does not result in counts. As the here used reverse mode is only active when counts are actually made it is far more efficient. Besides, the system would otherwise not be able to respond to the very high laser repetition rate.

Furthermore, this rate of 76.3 MHz corresponds to photo-excitation every 13.1 ns. Long-lived excitations like triplet excitons, with a lifetime between milliseconds and seconds, will therefore build up inside the sample via inter-system crossing. Singlet-triplet annihilation can be the result. This is excluded when using the low excitation pulse doses given above.

3.3.4. Alignment, wavelength calibration and time response

The entrance slit of the MCP attached to the monochromator exit was oriented vertically. Thus, horizontal alignment of the path of sample emission was necessary to achieve perpendicular in-coupling into the detector. After alignment, the horizontal positions of sample holder and collection optics were left unaltered, valid for both, TCSPC and streak camera measurements. Only changes between solution and film samples, or the use of a cryostat, required new alignment. Vertical alignment of the emission path was ensured by keeping all components at the same height.

A NIST standard calibration lamp was used for spectral calibration of the monochromator.

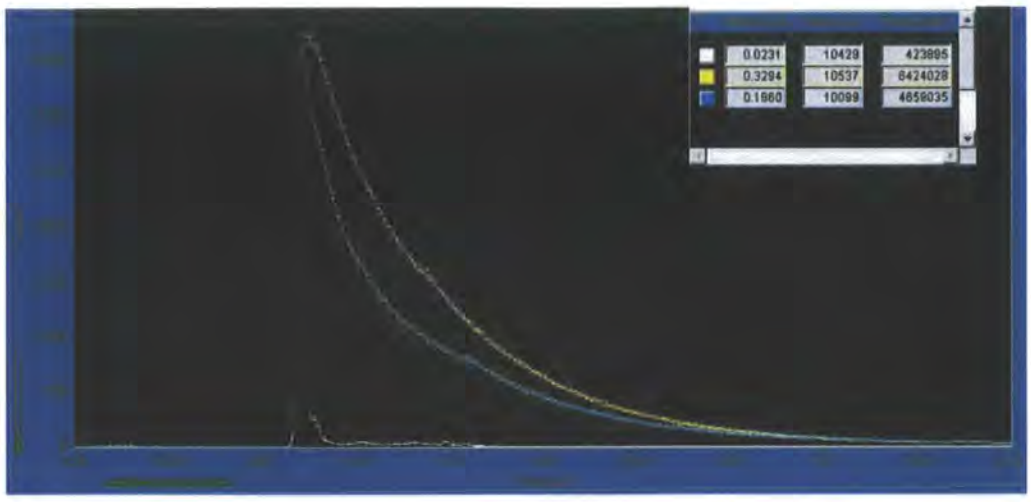

Figure 3-4 - Screenshot of the TCSPC software with two collected decay curves (blue, yellow) and the corresponding scatter reference (white). The insert window shows corresponding curve parameters.

The temporal response of the system was determined using a scatter solution (ludox dissolved in water), placed in the aligned solution sample holder, and detecting the TCSPC trace of the scattered laser beam as illustrated in Figure 3-5. From this time profile, typically an FWHM of 25 ps was determined. Any deviation (increase) from this value indicated a misalignment of the second harmonic generating crystal, the laser beam or the collection optics.

When studying thin film samples by TCSPC, a scatter sample representing the different optical geometry was used, commonly the reflection from a blank substrate or the sample itself, yielding a FWHM of 30 ps of the laser profile. The slight increase with respect to solution samples is attributed to the different excitation geometry as well as the slightly increased area for emission collection, see above.

3.3.5. Data acquisition

A typical TCSPC experiment comprised at least two measurements: First, a scatter profile of the laser from an appropriate scatter reference (see above) was recorded. Then, the sample was placed in the same position as the reference, the monochromator collection wavelength was moved to the desired point in the emission spectrum and collection of the emission decay was started. The time of collection was adjusted as appropriate to the emissivity of the sample at the collection wavelength: For data analysis, typically 10^4 (at the maximum of the decay curve) had to be accumulated. For samples exhibiting extremely weak emission (10^2 photons per second or less), occasionally only 2000 counts at the decay peak could be acquired.

By adjusting an electronic delay, the decay peak was shifted to the ~ 0.6 ns position of the 3.333 ns window covered by the MCP; thus, information on background counts could be obtained. These background

counts increase linearly with accumulation time; hence, a range of signal-to-noise ratios from 10^2 to 10^3 was observed for the samples used. These comparably high values were required for re-convolution analysis, see below.

Finally, most samples exhibit wavelength dependent fluorescence decays. As the object of this work was to study the underlying spectral dynamics in various systems, fluorescence decays were commonly collected at more than one wavelength. A typical TCSPC experiment comprised 2 or 3 decay curves plus the corresponding scatter reference.

3.3.6. Data analysis

As mentioned above, the response function of the setup ranged from 25 to 30 ps. Using a procedure called re-convolution fitting one can extract further information from the experimental data, down to a time scale comparable to the channel width, i.e. 1 or 4 ps. Re-convolution fitting was accomplished using either George Striker's program[16] (running in LINUX) or the "Globals" program[61] (running in WINDOWS). Both used similar procedures, only differing in the available algorithms, and gave comparable output. With the input of an emission decay and its corresponding excitation time profile, the program fits the decay using a sum of exponentials convolved with the excitation profile. The output comprises the fit parameters (amplitudes and time constants) of the exponentials used as well as a measure of the quality of the fit (χ^2 and normalised residuals, see Figure 3-7).

The number of exponentials is defined by the user. If an amplitude appears to be insignificant, it can be reduced. If the quality of the fit is not satisfactory it may be increased.

3.3.7. Issues for data interpretation

General. Using re-convolution fitting, one can extract more information from the decay curve on a short time scale, which would otherwise not be accessible from the raw data. The output sum of exponentials represents the decay curve for instant system response – but a priori no more than that. One must be aware that physical meaning can only be interpreted into the number of exponentials, their amplitudes and time constants if additional knowledge exists. Such knowledge may be obtained from series of measurements varying a sample parameter such as the solution concentration, the solvent viscosity or polarity, the chromophore size within a series of oligomer emitters, the substrate of a thin film or the composition of a thin film structure. Dependences of the amplitudes or decay constants on that parameter may then reveal underlying physical (or chemical) processes.

Non-exponential decays. Even if series of measurements were taken and consistent dependencies were obtained, no multiexponential fit can physically

represent systems with non-exponential contributions to the decay. In these cases one will face problems with fitting, have to increase the number of exponentials and observe varying numbers of exponentials even if the signal-to-noise ratio is sufficient to give a good fit. This is a major drawback of the analysing software. To deal with the problem, one needs to agree on a consistent analysis for the whole series of measurements, i.e. focus on relative experiments within the series. To do this, a concept of the underlying decay processes is helpful as well as varying further sample parameters. Recently, the Globals program also offers user-defined decay kinetics, albeit these were not used for the presented work.

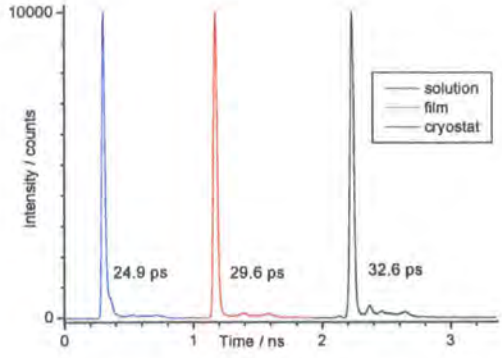

Figure 3-5 - Profiles of scatter samples with their corresponding pulse width: Ludox solution, thin film (wider pulse), thin film placed in a nitrogen cryostat (showing unwanted reflections of the excitation beam).

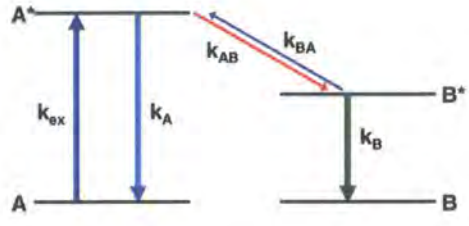

Figure 3-6 - Schematic of a photo-physical system of two species, A and B, including radiative excitation of A, radiative decay of A and B, transfer between A and B.

Invalid scatter reference. For the fitting procedure to yield valid results, the time profile of scattered light obtained from the scatter reference, which is used for re-convolution, must represent the true time profile with which the sample is photo-excited.

Any component not directly related to sample emission, e.g. a stray reflection from a substrate, invalidates the convolution. In this context, problems were encountered when using a cryostat to study solutions or thin films at low temperature. This was done in some cases, using a JANIS liquid nitrogen cryostat, whose inner and outer windows gave rise to reflections visible in the scatter reference signal as shown in Figure 3-5. Although with careful alignment and repetitive measurements these problems could finally be excluded, in doubt, the analysis of the short-lived decay components was left aside, comparing only the long-time decay kinetics without re-convolution fitting.

3.3.8. Global analysis

In the case of global analysis, multiple decay curves are fitted using the same time constants as shown in Figure 3-7. As an example, the method can be applied to a series of TCSPC decays taken at different points in the fluorescence spectrum of a

sample, with a common scatter reference profile for re-convolution.

In particular, systems exhibiting a finite number of 2 to 4 characteristic time constants are best analysed globally, e.g. with a radiative decay of species A, a transfer rate from species A to B and the radiative decay of species B as illustrated in Figure 3-6. Depending on the emission spectra of species A and B, the amplitudes of the different components will vary with the TCSPC collection wavelength. The optimal points for collection, e.g. those particularly dominated by a certain component, can be determined via streak camera (see below).

For photo-physical systems with unknown spectral dynamics, one must ensure that global analysis is valid in order to avoid a distortion of the output decay parameters (time constants) which may arise from the constraints imposed by global fitting. The validity of the global method can be verified by analysing a representative number of decay curves with individual re-convolution fitting, as introduced above. If the same set of time constants is found for each decay curve then global fitting can be applied. Poor global fitting is indicated by a poor χ^2, residual exponential components, interdependences of the fit parameters (amplitudes), an excessive number of exponentials and several insignificant amplitudes within the set of decay curves. Then, one needs to revise the method of analysis, e.g. return to individual fitting.

Well-behaved systems for global analysis are, for example, oligofluorene solutions undergoing excitation relaxation, which is discussed in detail in chapter 4.

3.3.9. Reconstructed time-resolved spectra

Emission decays recorded at more than one wavelength contain information about spectral dynamics. This information can be visualized by reconstructing time dependent spectra from the decay curves. However, a large number of collection wavelengths are necessary to obtain an acceptable spectral resolution. Then, a common time zero of all decay curves must be identified and the curves need to be scaled to reflect the actual emission spectrum[52]. Normalisation can be achieved by relating the total time-integral of a decay curve (minus its background) to the corresponding intensity value in the known steady state emission spectrum. Alternatively, one can normalise each decay curve by its accumulation time and scale the set using the spectral response of the TCSPC system, if known.

If one is only interested in relative changes of the time-dependent emission spectra, the latter correction for the sensitivity of the detector to different wavelengths is not needed.

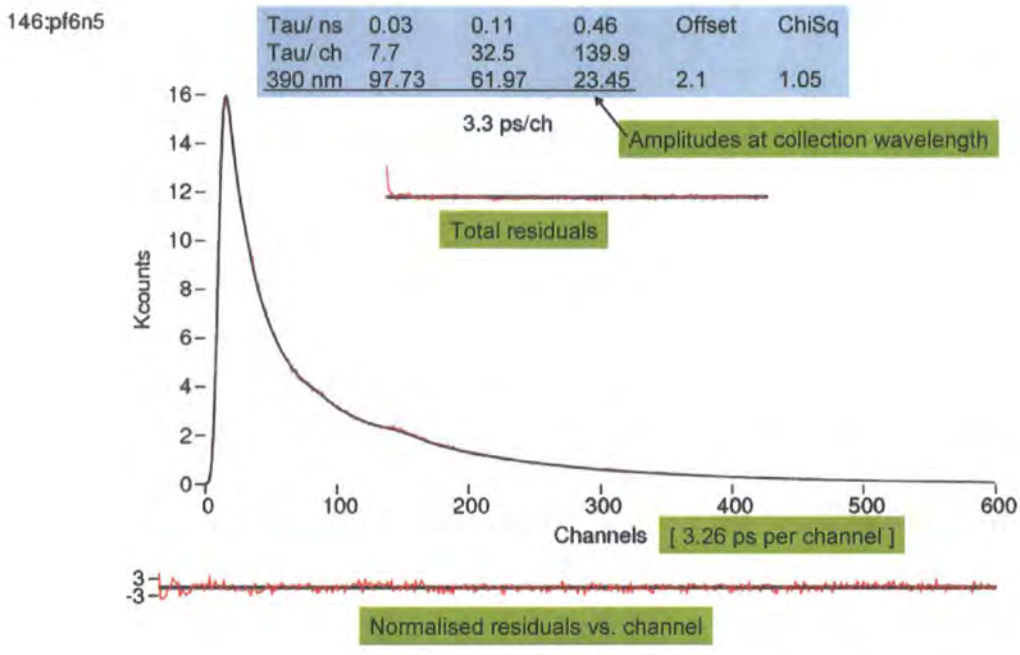

Figure 3-7 - Result of the re-convolution analysis of a single TCSPC decay curve using George Striker's program "sandbox" (sample: a decalin solution of pentafluorene). The decay times and amplitudes are given in the inset.

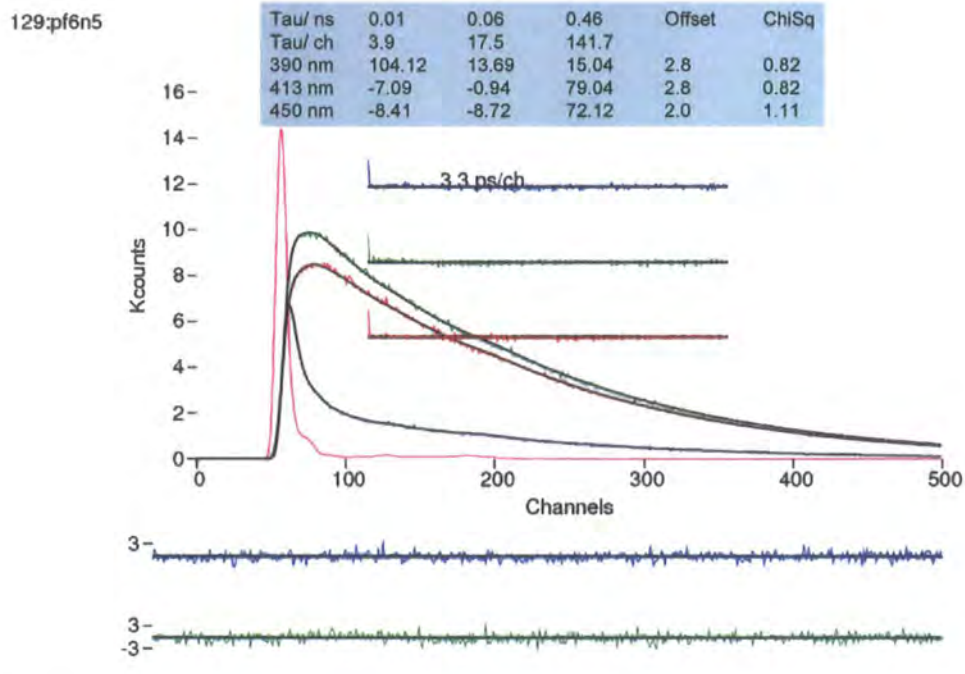

Figure 3-8 - Similar to the previous figure, global analysis of 3 decay curves obtained from a toluene solution of pentafluorene. The scatter reference is shown in pink. The blue inset gives the fit amplitudes corresponding to the collection wavelengths (blue: 390 nm, green: 413 nm, red: 450 nm), negative values correspond to an exponential build-up.

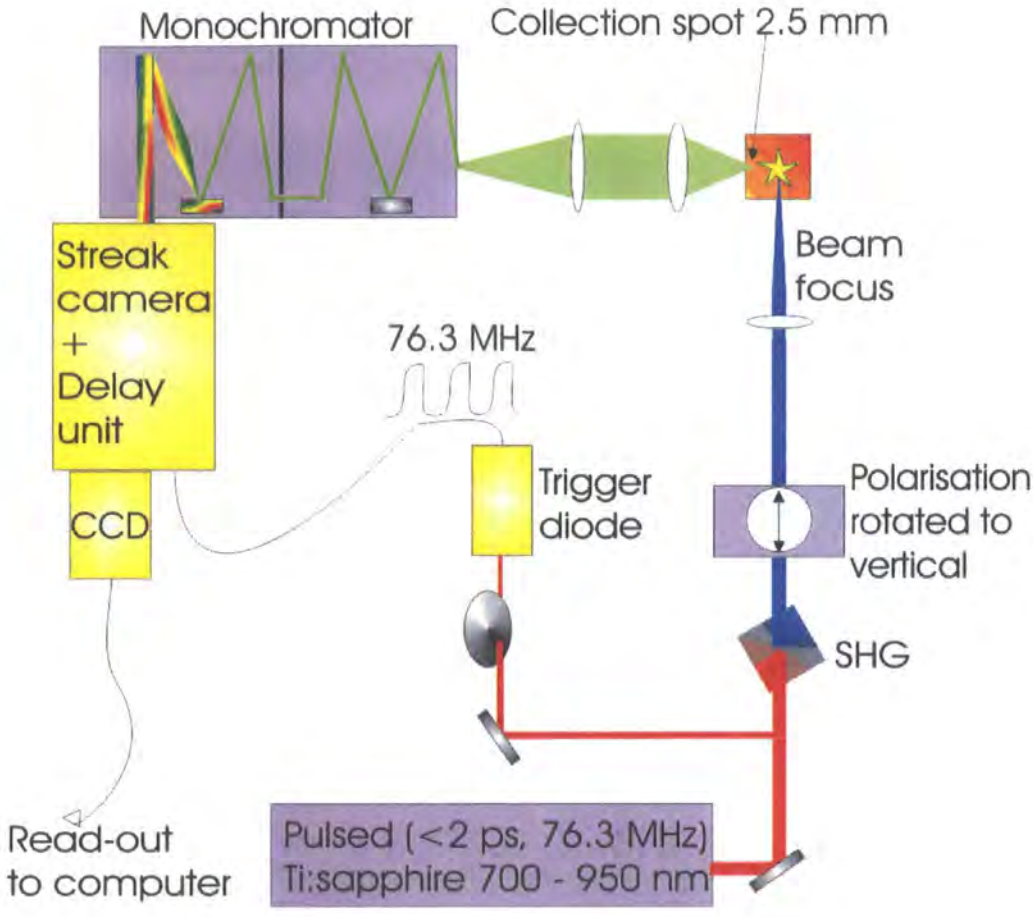

Figure 3-9 - Schematic of the streak camera experiment.

3.4. Streak Camera

3.4.1. Mode of function

Although spectral dynamics can in principle be monitored via TCSPC, they are best observed using time-resolved spectroscopy. In particular, acceptable spectral resolution is obtained more quickly. The experiment presented here uses a Hamamatsu streak camera detector (C5680). A detailed setup is shown in

Figure 3-9:

The dispersed emission spectrum of a sample is fed to the horizontal entrance slit of the detector. Input optics collect the light and, with correct focusing, form an image of the slit on the photocathode of the streak tube, which has a sensitive area of 0.15 x 5.33 mm^2. The photocathode converts the incident spectral image consisting of photons into an electron image. These electrons are then accelerated by electrodes and pass a pair of deflecting plates generating a deflecting electric field. The plates are driven by a high-speed sweep voltage, such that the electrons of the image experience a deflection dependent on the time at which they pass the plates, spreading the dispersed spectrum on a vertical time axis. In order to synchronise the timing of the sweep with the rate of

arriving electrons (e.g. 76.3 MHz), a separate "delay unit" (Hamamatsu, C6878) accepts a trigger signal from a high-speed pin-diode, which is exposed to a diverted fraction of the laser beam used for photo-excitation of the sample.

Thus, the electron image of the sample emission is swept across an MCP detector, which magnifies the signal electronically and converts the electrons back into light using a phosphor screen. Finally, a digital CCD camera (Hamamatsu, C4742-95-12NRB) reads out an image of the phosphor screen, similar to that shown in Figure 3-10. This image (1280 x 1024 pixels) has a vertical time axis and a horizontal wavelength axis. For the presented measurements, only an image of 640 x 512 pixels was read out, averaging over 2x2 pixels of the original image. Via software, vertical (decay curves) or horizontal (time-resolved spectra) profiles can be read out from this image.

Note. For Figure 3-10 and all subsequent streak camera images, different colours code the different intensity values detected

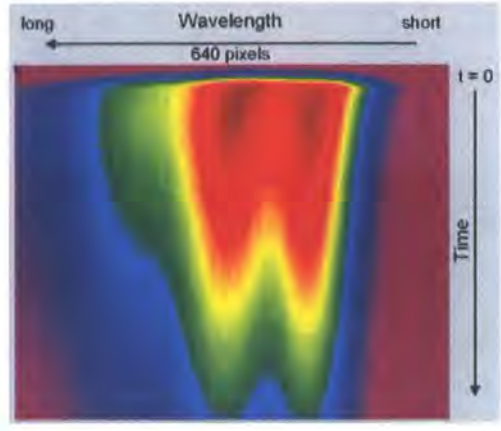

Figure 3-10 - Raw image as detected by the CCD camera. Vertical size: 512 pixels.

at each pixel. Black and red are used for maximum, blue or dark blue for minimum intensity. The spectral (horizontal) axis will be indicated if necessary. The time (vertical) axis can be obtained from Table 3-1.

3.4.2. Alignment

In contrast to the TCSPC detector, the entrance slit and sensitive cathode area of the streak camera are oriented horizontally. Hence, despite the horizontal alignment of the sample and collection optics carried out for the TCSPC experiment is valid for streak camera measurements, a further vertical fine alignment of the collection optics must be done in order to project the incoming emission spectrum precisely onto the 150 microns wide photocathode. Such alignment was frequently necessary, after each re-alignment of the tunable laser beam, and was done using the streak camera in "focus mode", i.e. with switched-off deflection. In contrast to the above

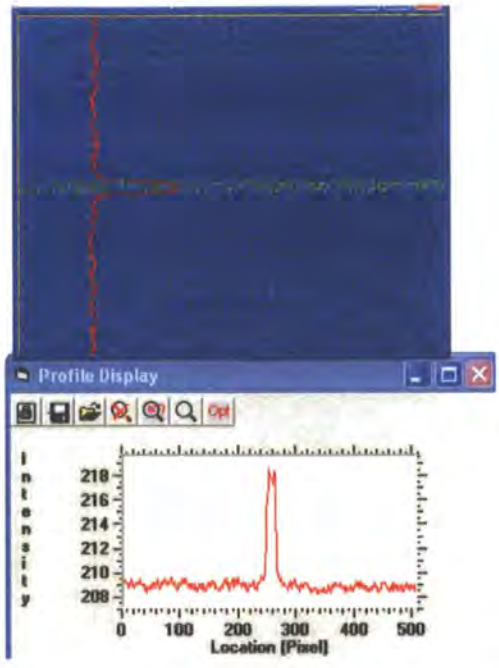

Figure 3-11 - Streak camera image in focus mode (no deflection), shutters closed, high MCP gain. The image reveals the sensitive photocathode area (green, centre) from which thermal electrons are emitted and magnified depending on the MCP gain. The surrounding blue area indicates the noise level of CCD detection, which varies depending on exposure time. The red line is a vertical profile of the image (horizontal width 640 pixels).

Figure 3-12 - As previous figure. Streak camera image in focus mode at high MCP gain. Shutters are open to detect the dispersed emission spectrum of an MeLPPP solution (greenish-yellow line). Compared to the grey horizontal line, the spectrum is detected with a slight tilt but still projected onto the photocathode area (blue) to its full horizontal extent.

described deflection called "operate mode".

Focus mode produces a static image of the sensitive area of the photocathode, see Figure 3-11 on which any sample signal appears as a horizontal line.

Visible from Figure 3-12 is a slight tilt of this line, resulting from imperfect attachment of the streak camera to the monochromator, after the camera had been moved to its final laboratory. Within the scope of mechanical fine adjustment, this tilt was minimised such that the sampleemission was fully displayed along the full horizontal width of the sensitive area. The remaining gradient, in operate mode visible as a wavelength dependent time zero, is corrected for via software (curvature and shading correction), see below.

3.4.3. Time resolution

The time resolution of the streak camera system is determined in operate mode, from a vertical profile of an image of scattered laser light, see Figure 3-13 and Figure 3-14. This can be obtained using a scatter reference sample as for TCSPC but also from an emissive sample, provided that (Raman or Rayleigh) scatter and emission spectrum are spectrally well separated. Extreme caution must be taken to prevent overexposure of the streak camera with intense scatter signals so as to avoid damage of the MCP.

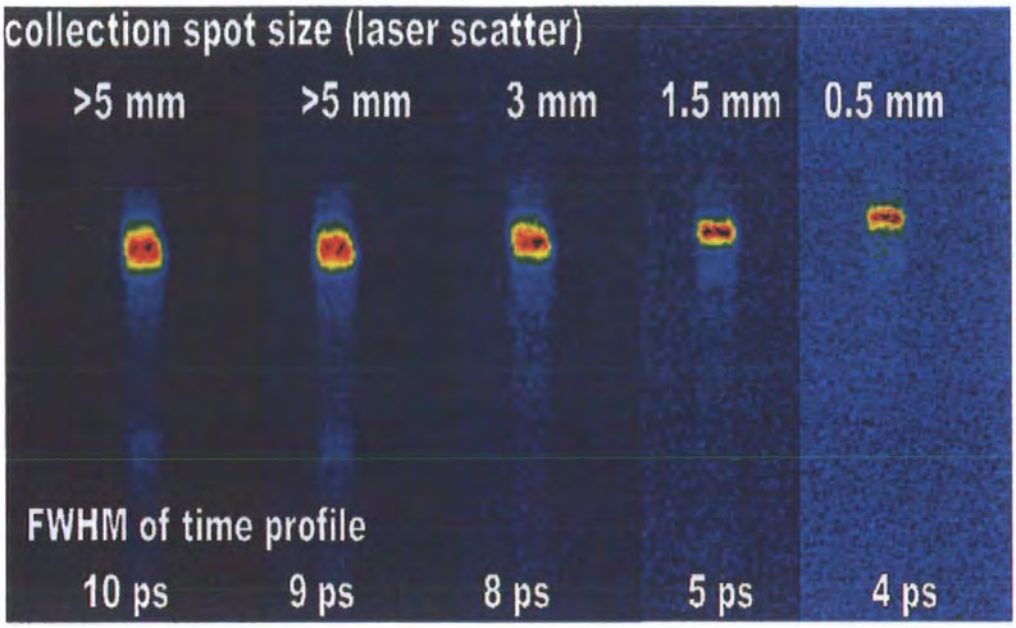

Figure 3-13 - Five streak camera images of the scattered excitation beam in operate mode, time range 1. All from the same reference sample. When the size of the collection spot (on the sample) is increased, the collected intensity increases (the background noise level decreases) but the time resolution of the image decreases. Spot size commonly used: 2.5 mm for solution, 3 mm for film samples. All pulses are 4 nm wide.

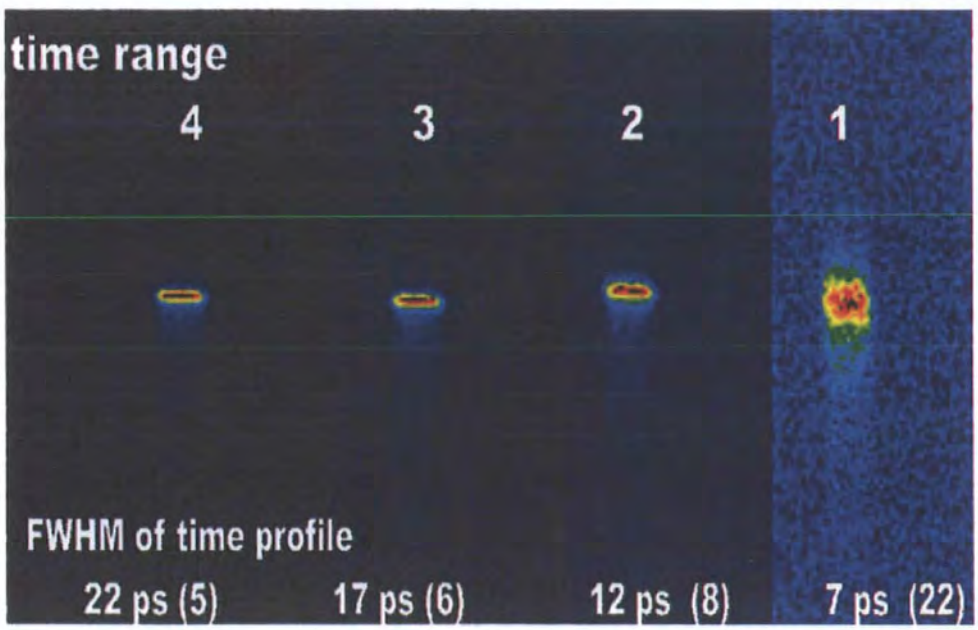

Figure 3-14 - Four streak camera images of the scattered excitation beam in operate mode. The full width at half maximum of their vertical profiles (not shown) is given in picoseconds and pixels (see brackets). All images from the same reference sample under typical measurement conditions (streak entrance slit 30um, collection spot 2.5 mm). All pulses are 4 nm wide. The background noise reflects the changing peak height with time range.

Time range	Time window covered, ΔT	Time per pixel, *dt* (average)	Time resolution, Δt, under average conditions	Dynamic range $\Delta T / \Delta t$	Determined by
1	158.8 ps (DR: 25)	0.31 ps	< 7 ps (ideal: 3.5 ps) (22 pixels)	< 30	Δt_1 and Δt_3
2	788.9 ps	1.54 ps	< 12 ps (8 pixels)	< 80	Δt_1, Δt_2 and Δt_3
3	1512.5 ps	2.95 ps	< 17 ps (6 pixels)	< 100	Δt_2 and Δt_3
4	2189.6 ps	4.28 ps	< 23 ps (5 pixels)	< 100	Δt_2 and Δt_3

Table 3-1 – Time resolution characteristics of the four streak camera time ranges.

The ideal time resolution of the streak camera is determined by three components[62]:

$$\Delta t \propto \Delta t_1 \cdot \Delta t_2 \cdot \Delta t_3$$

[Equation 3-3]

Δt_1 is the spatial spread of the laser beam. Δt_1 depends on the size of the spot from which sample emission is collected as illustrated in Figure 3-13. On the basis of these measurements, the fixed solution sample holder was built with a spot size of 2.5 mm. Δt_1 also depends on the width of the horizontal entrance slit of the streak camera[62], which was generally chosen to be 30 μm as recommended by the camera manual. Both of the above choices reflect a compromise between required signal intensity and optimal time resolution.

Δt_2 represents the spatial resolution of the system, particularly the CCD camera pixels, and its relation to the deflection speed, i.e. the time per pixel in the final CCD image. The operating mode offered a choice of four deflection sweep speeds, corresponding to "time ranges", whose characteristics are presented in detail in Table 3-1 and Figure 3-14. Finally, Δt_3 is a component intrinsic to the streak tube, related to the deflection electric field. For the above ideal Δt to be reached, the trigger diode used to synchronise deflection sweep and excitation rate must be aligned and exposed to optimal intensity. Thus, shape and jitter of the trigger profile can be adjusted to achieve optimal reaction of the receiving "delay unit". This step is crucial for obtaining good time resolution and was repeated after each switch-on of the streak camera and after tuning the laser.

The time resolution commonly obtained with the system in time range 1 was ~6.5 ps at 400 nm, which is larger than the optimal value (3.5 ps) mainly due to the large collection spot size.

3.4.4. Wavelength calibration, spectral resolution and coverage

The (horizontal) pixel-to-wavelength calibration was obtained using a NIST standard lamp. As for TCSPC, the spectral resolution, $\Delta\lambda$, varied with the monochromator slit widths, as shown in Figure 3-15. Typically, $\Delta\lambda$ was 4 nm, determined from the horizontal width of lines in the emission spectrum of the above calibration lamp. Also the excitation pulse is detected with this spectral width as demonstrated in Figure 3-15. Using a grating of 150 g/mm in the monochromator sufficed to cover the fluorescence spectra of most samples with a single image of 117.9 nm in width. In addition, an excitation scatter signal could often be simultaneously displayed as a direct measure of the time resolution of that particular image, see above. The latter procedure was useful when dealing with adverse experimental conditions such as an unstable excitation laser or trigger diode.

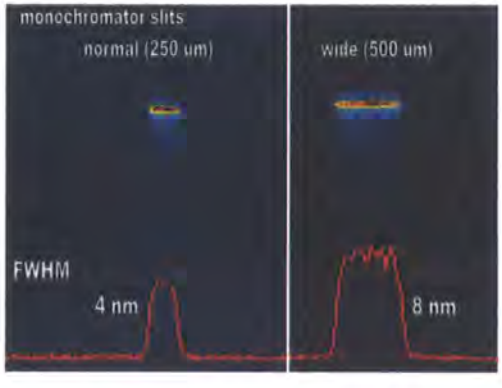

Figure 3-15 - Crude measure of the spectral resolution. Two streak camera images of the scattered excitation beam in operate mode, time range 2, from the same reference sample. For commonly used monochromator slit widths (entrance and interior, simultaneously), a resolution of 4 nm is observed. Both pulses are 12 ps wide.

The resulting jitter of the trigger signal artificially broadened the time resolution depending on the exposure and accumulation time (see next section) of the measurement, such that Δt had to be determined separately for each image in these cases.

3.4.5. Synchroscan and locking

For the presented measurements, the camera was used in "synchroscan", i.e. accumulating a large number of sweeps on the CCD chip before reading out the image to the computer. Synchroscan mode is practically achieved by sweeping the deflected beam first down (creating the desired image) and back up (creating an image with reversed time direction) in cycles synchronised with the trigger rate. The ellipticity of the cycles is reflected in the nonlinearity of the time axis of each image. As the time window actually viewed by the CCD detector does not comprise the entire cycle, a certain delay parameter must be specified via software to select a time window displaying the emission decay. This parameter is processed by the delay unit into a voltage, which could change with the unit warming up, resulting in a vertical shift of the image. Within limits, the voltage could be locked to warrant the

congruency of subsequently accumulated images over a longer period of time.

3.4.6. Image acquisition

For a better efficiency and signal-to-noise ratio, images could be accumulated on the CCD chip for a specified time (exposure time, between 20 ms and 10 s) before read-out. The exposure time depended on the intensity of the sample signal: First, overexposure had to be avoided. Second, a certain intensity value (350-400) at signal maximum was necessary to obtain an acceptable signal-to-noise ratio. If this value could not be reached by increasing excitation intensity, opening slits (within limits) or increasing the accumulation time, an additional gain could be applied to the MCP, which increased the signal in linear steps but also amplified the noise. Hence, MCP gain was mainly used for very weakly emitting, e.g. biological, samples as shown below.

By integrating (several hundred) of these accumulated images on the computer, the signal-to-noise ratio could be further increased provided that the individual images fulfilled the above intensity criterion, as otherwise read-out noise would dominate the accumulated image. Considering the upper and lower intensity limits, the dynamic range of intensities detectable in a single accumulated experiment was restricted to a factor of ~$2x10^2$, for a typical sample as shown in Figure 3-16.

An option for extremely weakly emitting samples was "photon counting acquisition" (PC). Here, maximal MCP gain was used and the signal intensity adjusted (reduced) to meet the requirements of single photon counting statistics, see TCSPC experiment. However, PC was not applicable to the strongly emitting samples used here.

3.4.7. Corrections

Each final image underwent background subtraction using a dark image recorded under conditions identical to the image acquisition. This image could either be separately recorded for each measurement or pre-stored.

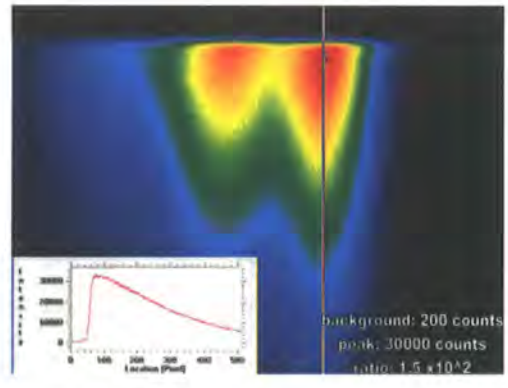

Figure 3-16 - Intensity dynamic range for a typical measurement, without integrating over several pixels. From the corrected streak camera image (operate mode, time range 2) a vertical profile (decay curve along the vertical line) is taken and displayed in the inset. Its signal-to-noise ration is calculated to the right. Sample: Polyfluorene dissolved in decalin. The image covers the spectral range from 373 nm (right) to 491 nm (left), the profile is placed at ~ 420 nm.

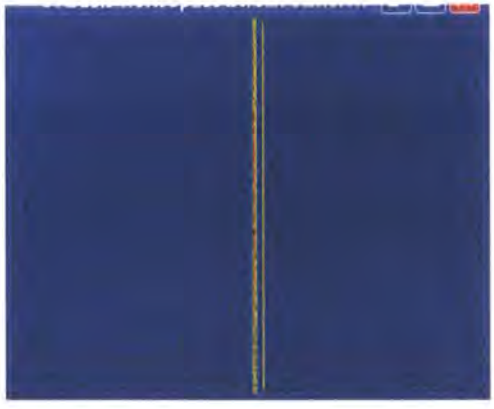

Figure 3-17 - Streak camera image of an emission line of the continuously emitting calibration lamp, in operate mode. No vertical curvature is observed. The white line is a guide to the eye.

When operating the streak camera in synchroscan mode, the electron deflection is not horizontally flat but has an elliptic shape, causing the time-zero-line, i.e. the onset of the emission signal in operate mode, of an image to be curved to a degree depending on the time range.

Additionally, also due to the slight tilt of the emission spectrum with respect to the horizontal axis shown above, the time-zero-line was a function of horizontal CCD pixel, i.e. wavelength. Therefore, a horizontal (wavelength) curvature correction was applied to each image. Figure 3-18 illustrates how a user- defined parabolic curve reflecting the observed time-zero line was used by the software to perform a matrix operation on the image, I(x,y) (x-horizontal, y-vertical pixel). Unfortunately, this method can only process integer x and y values, which created steps in the time-zero-line of the image, see Figure 3-18.

The input curvature correction curves were defined once for each time range, using images of the scattered laser beam in three different x-positions on the CCD detector by moving the centre wavelength of the monochromator. Vertical curvature correction was not necessary, as shown by the perfectly vertical emission lines of the wavelength calibration lamp in operate mode, as shown in Figure 3-17.

Furthermore, a "shading" correction could be applied: The image of a tungsten lamp (emitting continuous light with a known spectrum) was recorded in operate mode using high accumulation to obtain a very good signal-to-noise-ratio. Ideally, this image should display a constant intensity for constant wavelength (x) and a horizontal intensity profile identical to the spectrum of the lamp L(x). Deviations from this ideal image are detected in the image of Figure 3-19, S(x,y), which arise due to inhomogeneities in the illumination of the various detectors used in the streak camera and, mainly, due to the wavelength-dependent sensitivity of monochromator grating and CCD. These are also present each measured image, I(x,y), and can now be corrected for via:

$$I_{SHAD}(x,y) = \frac{I(x,y) \cdot K \cdot L(x)}{S(x,y)}$$

[Equation 3-4]

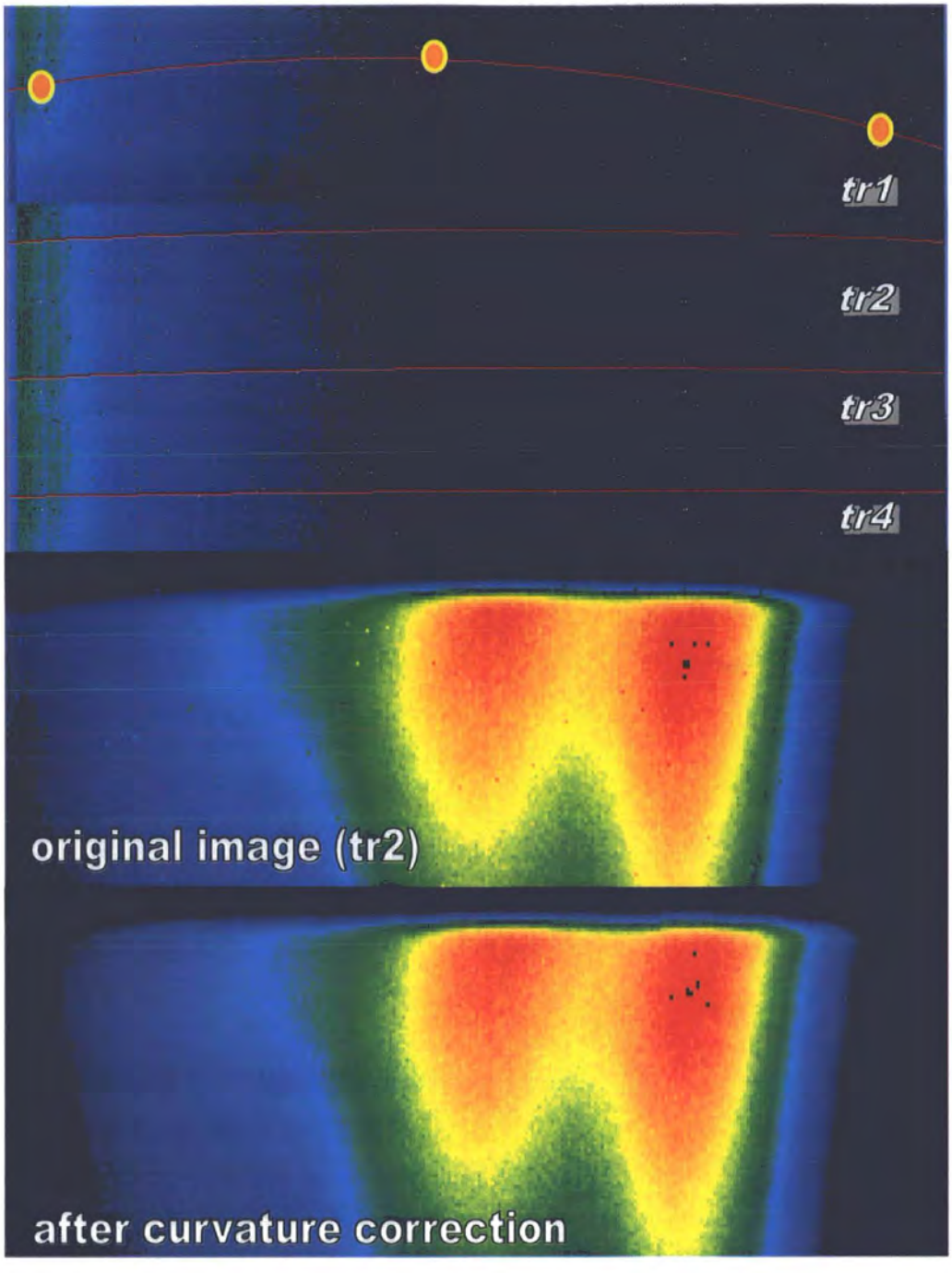

Figure 3-18 - Top: Curvature correction curves (red lines) reflecting the horizontal curvature of the streak camera images in each time range. Each curve is a polynomial generated from three horizontally shifted excitation pulses (orange/yellow). Bottom: An image of time range 2 is curvature corrected. The correction algorithm generates steps in the corrected image, mainly visible in its time-zero line (onset of the emission).

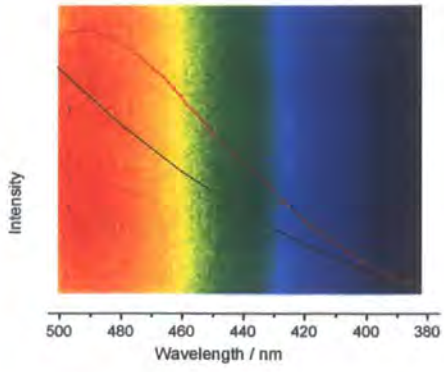

Figure 3-19 - The streak camera image of a tungsten lamp in operate mode (with a horizontal profile, red curve) superimposed on its specified emission spectrum (black graph). The wavelength scale applies to both curves and the image.

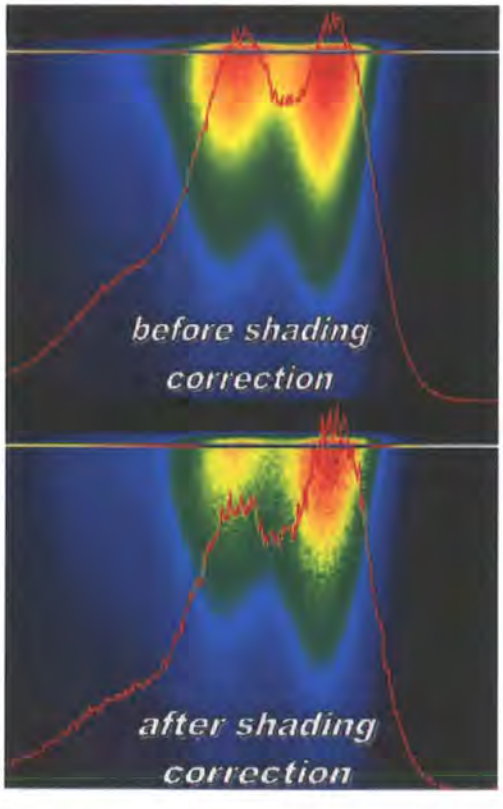

Figure 3-20 - Shading correction is applied to a streak camera image (time range 2). Spectral profiles (red curves) are taken along the horizontal lines across the overall emission peak. These are typical time-zero spectra. The signal-to-noise ratio decreases due to the correction procedure. Sample: PFO in decalin solution.

Naturally, this operation increases the noise level of the image dependent on the noise of S(x,y), which is illustrated in Figure 3-20. K is an arbitrary constant used to scale the corrected image.

Finally, defect pixels can sporadically form on the CCD camera due to degradation. The streak camera software offers a possibility to mask them, once identified, automatically for each recorded image.

3.4.8. General steps for data analysis

A recorded and corrected image was analysed by exporting horizontal (spectral) and vertical (decay) profiles. To do this, a rectangular region of interest within the image was specified and averaged vertically (for spectra) or horizontally (for decays), as indicated in Figure 3-21. For time-resolved spectra, the width of these regions was commonly chosen similar to the applying time-resolution. The time-zero spectrum was identified as the horizontal profile with the highest peak intensity.

Note that decay kinetics were only analysed to validate TCSPC data, which were otherwise superior in their signal-to-noise ratio. Nevertheless, streak camera emission decays could in principle be analysed in the same way as TCSPC data (via re-convolution fitting) provided that a valid scatter profile was available. Otherwise, the very short lived decay components could not be evaluated.

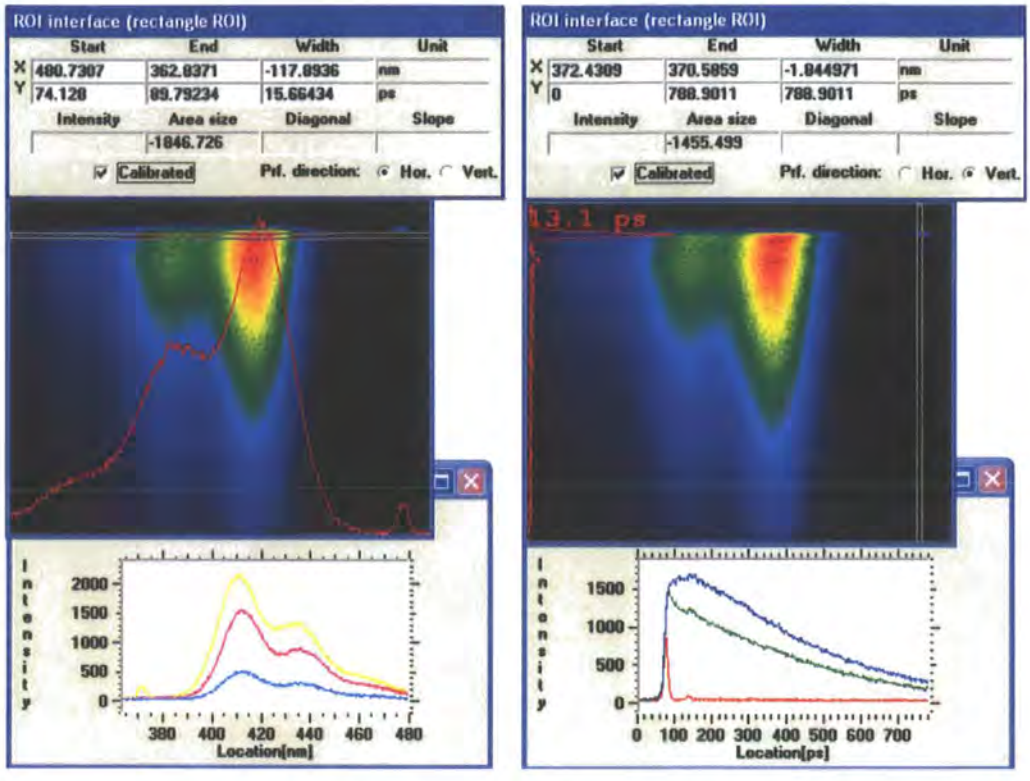

Figure 3-21 - The corrected image of the previous figure is analysed by taking 3 horizontal (left) and 3 vertical (right) profiles. The region of interest (rectangle ROI) for one profile of each direction is indicated by a rectangle in the image and characterized by the values in the top insets, X corresponding to spectral position, Y to time position. Note, both sample emission and excitation pulse are recorded. The width of the latter is 13 ps. Horizontal profiles integrate over 15 ps. The onset (time zero) of the image is determined from the horizontal profile with the highest intensity (as shown, left, yellow spectrum).

Time-resolved spectra, however, provided a complementary dimension to the TCSPC measurements. Depending on the spectral shape, a number of spectral parameters (peak energy, position and FWHM of the first vibronic, ratio of first and second vibronic) could be extracted, e.g. via peak fitting, which were then displayed as a function of time. In this context, TCSPC can monitor a red shift but its dynamics are only then correctly reproduced by re-convolution fitting when no other significant spectral changes take place simultaneously, e.g. a broadening or narrowing of the spectrum. With time-resolved spectra, one is able to separate changes in different spectral parameters. Additionally, the sensitivity to subtle spectral changes such as the slight narrowing without accompanying red-shift observed for the excited state relaxation of polyfluorene (see chapter 4) is much higher than for TCSPC due to the higher spectral resolution.

3.4.9. Limitations

The limitations of the streak camera experiment lie in its restricted dynamic range in intensity and time. The setup

presented here is tailored to monitoring the time-resolved fluorescence characteristics of conjugated polymers and oligomers, whose excited state lifetimes commonly range between a few hundred picoseconds and 1 nanosecond.

However, already dynamical components below 10 ps (many excited state relaxation processes) or above 1.5 ns (found for the fluorescence of many small organic molecules or biological samples) cannot be resolved or require special data treatment. Already for the case of the polyspirobifluorene investigated in chapter 5, long-lived decay times of 2 nanoseconds excited at a rate of 76.3 MHz (every 13.1 ns) resulted in a residual signal of 0.5 - 1 percent of the time zero signal, which was still manageable by an additional background subtraction. Samples exhibiting longer-lived components as could not be analysed in terms of decay kinetics. Also, the fluorescence spectra of common conjugated polymers conveniently fit into a streak camera image when using a 150 g/mm grating in the monochromator (width 117.9 nm). Many other chromophores emit wider spectra making it necessary to record several images at different centre wavelengths from which a composite image was generated.

All of the above limitations were practically experienced when studying the fluorescence of the "marker" molecule dansyl attached to the protein α-chymotrypsin[63]. Although this project initiated by Prof. Samir K. Pal (of the Bose Centre for Basic Science in Kolkata) is not directly related to the conjugated polymers and oligomers studied in this thesis, it provides an insight into excited state relaxation, from a biological point of view, and shows the general applicability of the streak camera system in time-resolved spectroscopy.

As a brief summary, the relaxation and decay of the marker fluorescence was monitored with α-chymotrypsin in different environmental conditions: The intact and the denatured protein were dissolved in bulk solvent (water) but also enclosed in reverse micelles. It was found that the excited state of dansyl relaxes much faster than the time resolution of the streak camera images when aided by the conformational arrangement of the intact protein. Thus, only the long-lived tail of the relaxation could be detected. Simultaneously, the decay of the dansyl fluorescence continued beyond the 2.1 ns covered by time range 4, such that it could not be analysed quantitatively. The marker fluorescence from the denatured protein is much broader, relaxes more slowly and decays more rapidly as shown in the figures. Hence, its photo-physics are better suited for monitoring via streak camera. In all cases, the time-resolved fluorescence spectra of dansyl, such as those shown in Figure 3-22, had to be obtained from composite images due to the broad emission spectra. Obvious are the difficulties faced when joining the 3 or 4 separate streak camera images (taken under identical conditions) due to insufficient shading correction at the borders. Best

results were obtained when averaging 2 corrected images across their overlapping regions. From each spectrum, the centre of gravity was calculated using an EXCEL routine, which was then used to evaluate the dynamic red-shift and, hence, the excited state relaxation.

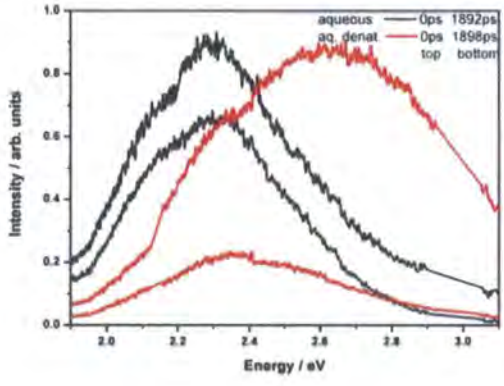

Figure 3-22 - Spectral profiles of dansyl labeled α-chymotrypsin in aqueous solution at 0 and 1900 ps after excitation. Black: Intact protein. Red: Denatured protein.

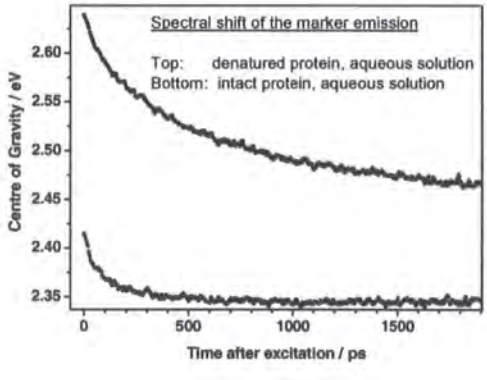

Figure 3-23 - Dynamic red shift of the fluorescence spectra of the previous figure.

In summary, no excited state lifetime could be extracted, only long-lived relaxation processes were detectable and the emission spectra show breaks. Nevertheless, the shape of the marker fluorescence spectra and the dynamics of the spectral red-shift sufficed to distinguish between intact and denatured α-chymotrypsin molecules. Hence, these measurements show the limits of the streak camera system.

However, the strength of the experiment is the instant visualisation of spectral dynamics, which allows one to quickly evaluate a sample and tell the necessity for further measurements, e.g. determine optimal collection wavelengths for TCSPC. By obtaining a sufficient signal-to-noise ratio and applying the above image corrections, the dynamics of spectral parameters can be detected with an accuracy that is not so easily obtained with TCSPC.

4. Conformational relaxation of conjugated Polyfluorene-type materials

4.1. Background

In conjugated materials, many photophysical (and photochemical) processes are linked to structural dynamics due to some degree of electron-phonon coupling. The electronic excitation of a chromophore – be it part of a long conjugated chain or a small fluorescent molecule – is governed by the Franck-Condon principle: The actual transition of a molecule from its ground to the excited state, e.g. from S_0^0 to S_1^n, occurs immediately. Concomitant changes in the electronic charge distribution of a chromophore are not equilibrated instantaneously: The molecular geometry (or conformation) adjusts on a finite time scale dependent on the phonon modes involved. This optimisation is called conformational relaxation and manifests itself in spectral dynamics such as a red shift of the fluorescence spectrum, the Stokes shift. The emphasis of this chapter is on the conformational relaxation of conjugated polymers and their oligomers. In the following, an introduction will be given as to what is known about this mechanism and the other types of excitation relaxation which may compete with it. This includes an excursion to small molecules, where a lot of experience exists with conformational processes on a photochemical and -physical basis. Next, the focus is set on the excited state relaxation in conjugated polymers and, finally, the advantages of conjugated oligomers for this study are elucidated.

4.1.1. Small Molecules

Conformational relaxation and the dynamic influence of the medium on photo-physical properties are experimentally well studied phenomena for solutions of small fluorescent dye molecules like Coumarin, DCM or auramine.[64] Typical relaxation times span a wide range from tens of femtoseconds up to 100 picoseconds. Therefore, this field has received growing attention with the availability of femtosecond experimental techniques.[64, 65] However, extracting the pure conformational dynamics from experimental data is not a trivial task as other relaxation mechanisms compete with it and need to be disentangled.[64]

Solvation. The above measurements are commonly carried out on solution samples, which naturally allow more conformational degrees of freedom compared to the solid state. However, the medium surrounding the chromophore dynamically reacts to changes in the dipole moment of the chromophore, especially if the medium is a polar solvent.[64] Such intermolecular relaxation due to electrostatic interactions between solvent and solute is called solvation. If solvent and excited chromophore are polar, a dynamic solvatochromic red-shift is observed in the emission spectrum. For cases of pure solvation, the corresponding spectral relaxation time is a characteristic of the solvent and is the same for a variety of

solutes. This presents one possible strategy to identify solvation components.

Vibrational cooling. Additionally, in the femtosecond region, a further process called vibrational cooling is active,[64] which transfers excess vibrational energy from the fluorophore to the surrounding medium, bringing the excited molecule for example from an S_1^n to the S_1^0, the lowest singlet excited state. Vibrational cooling entails spectral changes such as a red-shift but also characteristic spectral narrowing.[66]

Specific solute-solvent interactions need to be accounted for, if solute and solvent are not chemically inert.

Interactions between types of relaxation. All of the above processes may be present in addition to conformational relaxation. They compete and interact depending on the chemical and physical properties of solvent and chromophore, e.g. polarity, viscosity, bond structures and molecular size.[64] This can lead to a complex overall relaxation pattern, which is commonly quantified in terms of the dynamic spectral red-shift

$$C(t) = \frac{E(t) - E(t=\infty)}{E(t=0) - E(t=\infty)}$$

[Equation 4-1]

where E represents the energy of the emission peak or its first mode and t refers to the time after excitation. The time dependence of C(t) shows how the solute-solvent system reaches its equilibrium (see Figure 4-1) and may be fitted with a decay law representing the underlying relaxation mechanisms in order to obtain time constant(s) for these mechanisms.

As shown above, disentangling the various overlapping time constants is a major task in assessing these spectral dynamics. In well-behaved cases, one process may dominate the other.[64] If conformational relaxation is dominant, the observed relaxation time(s) varies depending on the original molecular motion, e.g. a rotation of a functional group, alterations of bond lengths[67] or molecular torsion,[64, 68, 69] which in small molecules may even entail a switch between trans and cis isomers[66].

On the other hand, solvation may prevail, for example in the dye DCM, which forms a charge-transfer state upon excitation,[64] whose large dipole moment induces a pronounced reaction of a (polar) solvent resulting in a large dynamic red-shift of the DCM emission. The invariant relaxation times are used to identify such cases. Later on, this strategy will be applied to this study of polyfluorene-type molecules, where toluene is a commonly used solvent. Due to the prevailing availability of solvation data for polar solvents, benzene is the solvent closest to toluene whose relaxation is published: The solvation of Coumarin 153 in benzene has been measured with time constants of 230 fs and 2 ps,[70] which will be

similar to those of toluene on account of its similar physical and chemical properties.[70] The upper limit of 2 ps will be compared to the experimental relaxation times exhibited by polyfluorene in order to help identify the mechanisms governing the relaxation in this material.

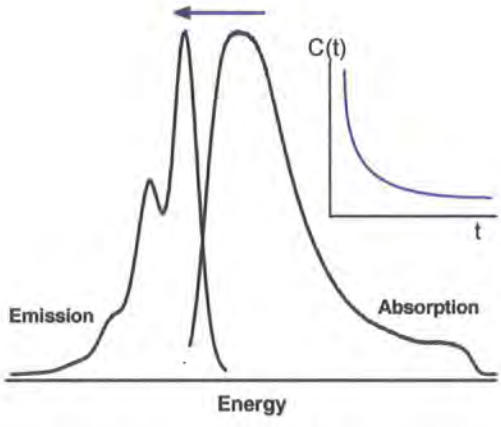

Figure 4-1 – All excited state relaxation processes are observed as a dynamic red-shift of the emission spectrum.

4.1.2. Conjugated polymers

Classification of processes. A priori, all of the aforementioned relaxation processes can also occur in an extended conjugated chain:

1) In conjugated polymers, vibrational cooling to the S_1^0 state is supposedly the first step after excitation and associated with a time scale below 100 fs.[35]

2) Solvation, i.e. the reorganisation of solvent molecules around the excited chromophore, will naturally occur on the same time scale as for small molecules. However, as both, the common organic (aromatic) solvents and the solute polymer exhibit little polarity[70, 71], the effect of solvational spectral changes is expected to be less significant than for small polar fluorophores in polar solvents.

3) The presence of conformational relaxation in conjugated polymers is intrinsically anchored to their strong electron-phonon coupling. Its significance is fundamental, extending from the formation of excitons and polarons[23] to the explanation of spectral shapes and quantum yields. Conformational dynamics have only recently received growing attention, in particular there have been theoretical and simulation studies. These findings will be summarised below. A comprehensive experimental study, however, is still lacking. This study partly tries to close this gap.

4) Additionally, the extent of a polymer chain enables the migration of excitations as a form of excited state relaxation, which competes with conformational relaxation. The extensive theoretical and experimental findings from this field are also further discussed.

5) Occasionally, very broad emission spectra are observed, which are further red-shifted. These are associated with the presence of new species such as oxidation defects[4, 5], charge transfer states[52], excimers[72] or aggregates[57], which then emit instead of the original polymer molecules, comparable to dopant molecules[47]. For this study, such extrinsic species were excluded by careful choice of materials and sample preparation. To the limits of detection their

absence was ensured via emission spectroscopy.

This study is only concerned with the intrinsic relaxation of excitations in pure conjugated polymers and oligomers. The disorder of these materials is a main driving force.

Molecular conformations. Primarily, all conjugated polymers exhibit a certain degree of structural disorder. Although materials like polyfluorene exhibit a long macroscopic persistence (> 50 nm)[53], they exhibit a large variety of microscopic structure. Depending on the chemical configuration of the repeat units this may arise from rapidly fluctuating wormlike twists of the chain[73] to more rigid breaks and kinks[74, 75] of the molecular structure.

The fluctuating contribution is driven by phonon activity, i.e. the vibrations and torsions of bonds and bond systems. The most widely known example of this is the C-C bond stretch common to all polyfluorene type materials, which causes the energy gap between the fluorescence modes of ~ 180 meV. Compared to this, the energy of torsional modes is small and cannot be resolved by common fluorescence spectroscopy. However, as was shown by Karabunarliev *et al.*[68, 69] and Tretiak *et al.*[23, 78], molecular torsions are a major factor in generating disorder.

Always, ground and excited state have their energetic minimum in a certain conformation, e.g. at a certain angle between the repeat units (dihedral angle)[76, 77] as indicated in Figure 4-2. For some fluorescent conjugated materials, including poly-phenylenevinylenes (PPVs) and poly-paraphenylenes (PPPs), this is a planar conformation. However, the chemically related polyfluorenes (PF) exhibit twist angles of 36° [12, 78]. Often it is a particular chemical substitution of side chains, which are primarily used to enhance solubility, that may influence conformational species by inducing energy barriers for bond rotation or favouring a certain dihedral angle between the repeat units, as found in oligothiophenes[76].

Disorder. Irrespective of the precise type, any molecular motion changes the conformation of a chromophore, such that each polymer or oligomer molecule of a sample "looks" different even if their chemical build is identical. The conformation has an effect on local interactions such as molecule-solvent, intramolecular and nearest neighbour intermolecular interactions. These, in turn, can have an effect on the electronic properties of a chromophore, e.g. its energy, lifetime, dipole moment etc..

Locally, an individual, equilibrated chromophore optimises its electronic energy by adjusting its conformation. Deviations from optimum are caused by thermal activation, i.e. the excitation of phonons by transfer of thermal energy from neighbouring solvent molecules or chromophores. Ideally, the *local* distribution of energies, P(E), is of the type

$P(E) \sim \exp[-E/k_BT]$, i.e. a Boltzmann distribution.

However, due to interactions of the chromophore with the local environment other than heat exchange, equilibration may be restricted such that the absolute energetic minimum cannot be reached. Considering a large ensemble of chromophores, it exhibits a random variation of local environments. Here, a much wider *global* energy distribution than the ideal Boltzmann distribution is generated, which is of Gaussian shape. This effect is called *inhomogeneous broadening*.

Thus, two effects are associated with molecular motions: First, global inhomogeneous broadening and, second, local deviations of molecular conformations from their optimum.

The chemical structure of a material determines the flexibility of the molecules and, hence, the impact of molecular motions and inhomogeneous broadening. The "softness" of the chemical bonds involved in molecular deformation, i.e. the energy of the vibrational and torsional modes, is compared to the thermal energy available to excite such motions. As an example, an intrinsic reduction of the torsional degrees of freedom occurs in "ladder-type" poly-paraphenylenes (LPPPs)[33, 79]. Here, bridge bonds between the repeat units essentially inhibit torsional motions as they are stiff at room temperature. These molecules are forced into a planar conformation.

Inhomogeneous broadening is decreased in the ground and excited state of these materials, which is reflected in the narrow vibronic modes of the absorption and emission spectra, respectively. An example of high conformational flexibility are the highly disordered PPVs[73], which exhibit broad and structureless absorption and emission spectra at room temperature, i.e. a high degree of inhomogeneous broadening.

Conformational relaxation. In summary, a wide distribution of conformations translates directly into a wide global distribution of excited state energies. This duality between conformational and energetic disorder[80] acts as the driving force to reorganise the global density of states distribution (DOS) in the form of conformational or migrational relaxation.

The principle of conformational relaxation is already contained in the concept of the polaron, which implies that a charged polymer chain will always experience a deformation of its residual charge distribution. Similarly, a neutral excited state, such as an exciton, represents a change in the occupied molecular orbitals, which entails a reaction of the molecular geometry. Figure 4-2 illustrates the underlying mechanism: An electronic transition from S_0^0 to S_n^n occurs under the Franck-Condon principle, i.e. the molecular geometry is "frozen", followed by vibronic cooling.

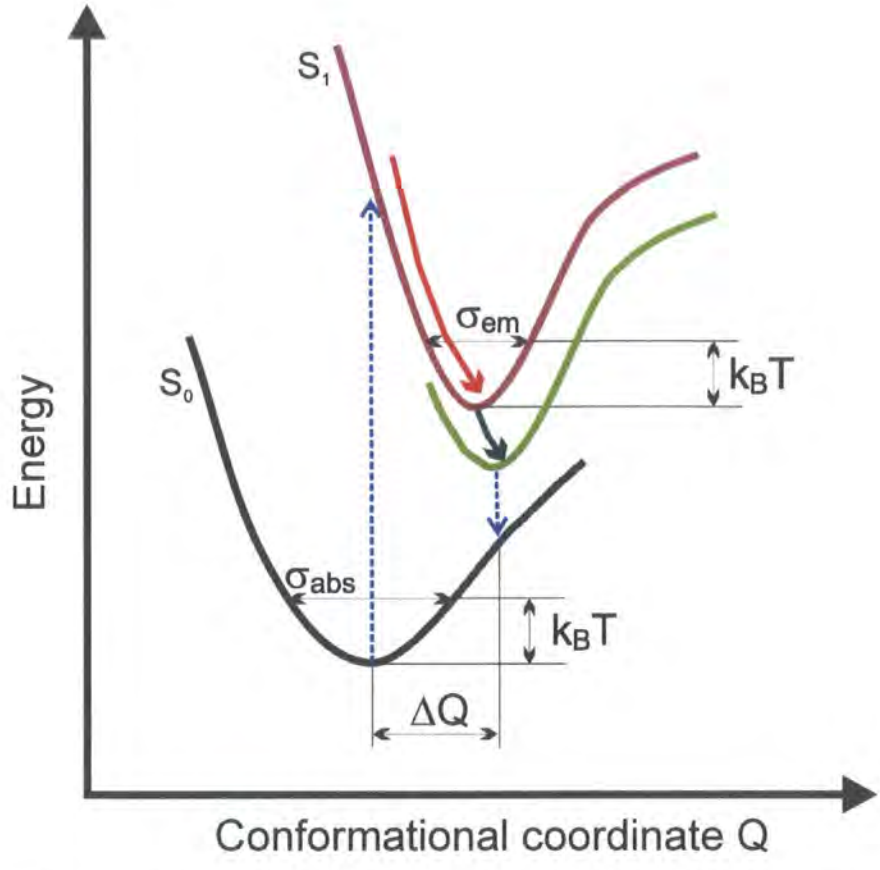

Figure 4-2 – Illustration of the excited state processes in an isolated chromophore. Note, the potential curves are given as functions of conformation, not vibrational energy. Photoexcitation (long blue arrow) follows the Franck-Condon principle. After that, excess structural energy is dissipated (red) and slower molecular relaxation (green) further increases the geometry difference between ground and excited state. The width of the ground and excited state distribution of excited state energies (DOS) is governed by the steepness of the potential curves with respect to the temperature.

However, as the wavefunction of a molecule is different between ground and excited state, the spatial charge distribution changes upon excitation, resulting in unbalanced molecular forces. These forces are visualised in Figure 4-2 in terms of ground and excited state potentials which differ in their equilibrium molecular conformation. Here, the conformational coordinate Q may for example represent a characteristic bond length of the molecule. After excitation, the bond is "elongated" from its new equilibrium length and possesses excess vibrational energy. The molecule vibrates. By frictional coupling to the "bath", excess energy is dissipated while, at the same time, the new (excited state) equilibrium is adopted and bond length adjustment takes place. Naturally, a larger molecule is an ensemble of several of these oscillators. Altogether, the relaxation of these oscillators results in a change of the molecular conformation. The chromophore adopts the geometry of the lowest possible energy. Spectroscopically, this decrease of energy corresponds to a dynamic red-shift,

e.g. of the fluorescence spectrum. In the steady state, a red-shift between absorption and emission spectrum is observed, the *Stokes shift*.

Note that not only vibrational but also other types of structural energy are gained and dissipated during and after excitation. However, larger scale molecular relaxation will couple to different, softer phonon modes, such as torsions, which require a longer time scale to equilibrate[78]. In Figure 4-2 this is visualised as a shift of the excited state potential curve after vibrational relaxation and bond length adjustment.

After an electronic transition, the individual molecules do not only adopt new conformations but also their ensemble disorder is changed at a fixed temperature. In all common conjugated polymers, the inhomogeneous broadening is reduced in the excited state, which is observed as a break in the ideal mirror symmetry between absorption and emission spectra. As an example, the room temperature absorption spectra of polyfluorene reflects a wide DOS, its emission spectrum is red-shifted and well-resolved, at room temperature showing vibronic modes spaced by 180 meV, which are associated with a C=C bond stretching mode[33], see also Figure 4-5 below. The underlying mechanism was studied by Sluch *et al.*[77] for a PPV type polymer, who concluded a steeper potential energy surface and stronger electron-phonon coupling in the excited state, see Figure 4-2.

For a transition from ground to excited state, the same thermal activation energy does no longer suffice to sustain the previous elongation from equilibrium for each individual molecule[77]. Therefore, at a given temperature, the global deviation from optimum, i.e. the inhomogeneous broadening, must decrease in the excited state. The global DOS becomes narrower.

Naturally, at low temperature the mirror symmetry between absorption and emission spectrum can be restored by withdrawing the thermal energy necessary for the inhomogeneous broadening of ground and excited state. Accordingly, Stokes shifts between absorption and emission decrease at low temperature[22]. In cases of highly disordered materials such as PPV, resolved fluorescence modes are only observed at low temperature. Consistent with theoretical prediction[69], experimentally observed Stokes shifts are particularly pronounced for these highly twisted molecules. In contrast to this, the ladder-type poly-para-phenylene MeLPPP exhibits mirror symmetric and well resolved spectra at room temperature, with an extremely low Stokes shift[79]. This is caused by the chemically confined conformation of ground and excited state, which leaves little scope for structural relaxation in the intrinsically narrow DOS.

In summary, both spectral red-shift and narrowing are the spectroscopic characteristics of conformational relaxation. Depending on the time scale of this relaxation with respect to the excited state lifetime, the decay to the ground state

occurs from a more or less relaxed geometry. In the fluorescence spectra, this manifests itself as a change in the relative heights of the vibronic modes. In short, the larger the difference between ground and excited state conformation is, the higher the overlap between the orbitals of S_1^0 and the S_0^n of higher n. – The Franck-Condon principle also applies to the emission process. In simple systems such as crystals, this effect is quantitatively described by the Huang-Rhys factor, *S*. In the case that excess energy is stored in a harmonic oscillator system, i.e. for vibrational relaxation, *S* can be written as[81]

$$S = \frac{2\pi^2 M\nu}{h} \cdot (\Delta Q)^2 \qquad \textit{[Equation 4-2]}$$

with M as the reduced mass and ν the frequency. ΔQ represents the separation between the equilibrium positions of the ground and excited state oscillators or, in general, the relaxational shift along some kind of configuration coordinate. In practice, *S* can be obtained from emission spectra using

$$S = I_{mode} / I_{0\leftarrow 0} \qquad \textit{[Equation 4-3]}$$

to obtain a measure of the nuclear displacements involved in structural reorganisation. I_{mode} is the intensity of the fluorescence mode associated with the vibration and $I_{0\leftarrow 0}$ is the intensity of the 0-0 vibronic mode, the vibrational origin. In the case of identical ground and excited state wavefunctions, i.e. zero displacement, *S* would be zero.

This chapter mainly evaluates the characteristics of conformational relaxation – spectral red-shift, narrowing and decrease of S – and their dynamics. As to the underlying molecular processes, an overview of the corresponding literature is given in the following. In line with the work of Sluch *et al.*[77], on excited state planarisation of PPV type materials, Karabunarliev *et al.* [68] calculated minimised energy configurations for the excited and the ground state wave functions of para-phenylene oligomers. Here, the modes active in electron-phonon coupling were revealed to be librational (torsional) modes, which stiffen upon excitation rendering the average molecule more planar than in the ground state. Thus, while the ground state allows flexibility between neighbouring repeat units in terms of averaged higher torsional angles[73, 82], the excited state at the same temperature will be relatively rigid, often favouring the planar conformation. This ties in with the reduced inhomogeneous broadening of the excited state DOS as elaborated above.

The concept of effective conjugation length. From another perspective, conformational disorder may be described by a distribution of effective conjugation lengths. Here, the conjugation along a polymer chain suffers partial breaks at structural or chemical defects of the polymer chain. In detail, these could be sharp kinks, defects in hybridisation that arise during synthesis but also oxidation (keto) defects. In general, the conjugation

along a macromolecule requires a strong coupling of the orbitals of neighbouring atoms. For this to occur, the planarity between repeat units is essential. Any deviation results in a reduced coupling. Thus, a highly twisted molecule is divided into many conjugated segments of varying length, which serve as chromophores or exciton sites. As above, a long effective conjugation along a chain segment corresponds to a low excited state energy, which translates into energetic disorder. However, with respect to the actual complex adjustment of bond lengths and nuclear displacements, which takes place in order to optimise the energy of the final (lowest) excited state S_1^0 [52], a single disorder parameter is a very simplified description. This was shown in an excited state simulation study by Tretiak *et al.* [23], which revealed in detail the nuclear motions that dominate the electron-phonon coupling in a PPV. These range from high frequency C=C stretch modes (ν_{mode} = 1700 cm^{-1}) and quinoidal ring motions (ν_{mode} = 1300 cm^{-1}) to low frequency torsional modes and chain stretching (ν_{mode} = 100 cm^{-1}) [23]. To each of these modes one can assign a vibrational reorganisation energy E_{rel} via the Huang-Rhys relations above. The study thus emphasised how vibrational, torsional and other low energy conformational relaxation are expressions of the same phenomenon, excited state relaxation – just on different energy scales. Despite such detailed knowledge, little experience exists with respect to the time scales, in which the twisted geometry relaxes into a more planar configuration in the excited state. A simulation study on PPV by Franco *et al.* [78] showed that high energy fluctuations due to bond alternation occur within 20 fs whereas low energy torsional modes between neighbouring repeat units happen on the 1 ps scale. Plausibly, energy, time and spatial scale of conformational relaxation are intrinsically linked. However, while the above values give a dynamical classification for similar processes in other conjugated polymers, they were obtained for a molecule in vacuum, i.e. without considering a medium that certainly influences the structural dynamics e.g. via solute-solvent interactions. As an example, one expects that steric hindrance due to bulky side chains or in highly viscous solvents would slow down the relaxation dynamics. This gap is covered in the present study by an experimental investigation of the relaxation dynamics with particular focus on the viscosity dependence of the relaxation constants found.

Exciton self-localisation. Having elaborated why and how conformational relaxation occurs, attention is now turned to the importance of this process for the photophysics of a conjugated molecule. As a side effect, this energetic stabilisation proceeds in the direction of a more localised excitation; this is termed *self-localisation*. The initial photo-excitation is delocalised across the entire chromophore (or conjugated chain segment). However, conformational rearrangement is not

equally distributed over the extent of this initial excitation. Instead, due to the inhomogenity present in the initial excited state wavefunction, certain parts of the chromophore relax further and faster than others, which binds or centres the excitation at this particular part due to its locally lower energy. This decreases the delocalisation down to a localisation length or exciton size, which is characteristic for the material [78]. A shallow structural trap is thus generated by the excitation itself. Such self-localisation gradually transforms the initially delocalised excitation into an actual exciton – a metastable, localised, tightly bound electron-hole pair. Due to its enhanced stability, the emission of this relaxed exciton also exhibits a higher quantum yield than that of the unrelaxed state[23]. Note that self-localisation is naturally not relevant to short chromophores, whose size inhibits a complete delocalisation and renders the excitation rather concentrated right from the beginning.

Exciton migration. Conformational relaxation competes with other excited state processes, whose weight depends on the medium surrounding the chromophore. As an example, the lack of experimental knowledge about conformational relaxation in extended conjugated molecules is founded in the original desire to improve polymer light emitting diodes, which are based on the solid state. Here, a molecule is restricted in its conformational response due to the close packing of molecules. Further, the interchain interactions prevailing in the solid state increase the importance of excitation migration as a relaxation mechanism. A large number of publications exist on this second major process leading to energetic relaxation in pure conjugated polymers in the solid state. Its theoretical framework was established by Bässler and co-workers[27] and in the time-dependent experiments in solid state by Richert *et al.*[83] and Meskers *et al.*[26]. Here, energy transfer is associated with the exciton "hopping" motion between localized energetic sites. The probability, i.e. rate k_{ij}, for a certain "jump" depends on the distance (r_{ij}) between the two sites involved (i and j) as well as their energy levels (e_i, e_j)[83]:

$$k_{ij} = A(r_{ij}) \exp\left(-\frac{e_j - e_i}{k_B T}\right), \quad e_j \geq e_i$$

$$k_{ij} = A(r_{ij}), \quad e_j \leq e_i$$

[Equation 4-4]

Thus, like conformational relaxation, migration is also (indirectly) driven by the structural disorder[80], which generates the inhomogeneously broadened DOS in which the excitons can migrate. If initially created at random energy within this DOS, excitons will preferentially migrate to sites of lower energy, i.e. to the tail states of the DOS, according to the second equation. Such down-hill migration is naturally associated with a shift of the average emission energy. The time-dependent density of accepting tail states crucially depends on the ambient temperature. For every finite temperature, energetic relaxation terminates once

thermally assisted jumps (corresponding to the first equation) become equally probable compared to non-assisted jumps to lower energy sites. After this relaxation time no further energetic relaxation is expected.

The final emission spectrum is red-shifted and well resolved, provided that no extrinsic species have formed as described above. Only as a special case, when site-selective excitation is applied with an excitation energy below a certain "localisation energy", excitons are on average forced to thermally assisted jumps (uphill migration) and then a slight broadening of the emission spectrum is observed[26].

Summary. The effects of conformational relaxation and exciton migration are similar: Considering a wide DOS, i.e. a large torsional disorder, significant conformational relaxation towards a more ordered structure is expected. Equally, a wide DOS allows a larger shift of the average excited state energy within the DOS. On the other hand, little migration to low energy sites is possible in a very narrow and sharp DOS. From a conformational perspective, this refers to an already defined and relaxed state permitting little rearrangement. However, the two processes diverge considerably from a conceptual point of view: While migration occurs within an existing static DOS, conformational relaxation dynamically changes the DOS, leading to self-localization.

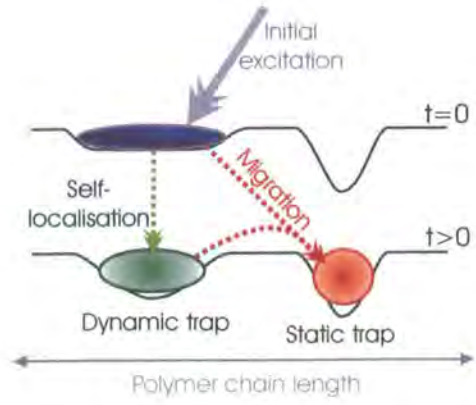

Figure 4-3 – Illustration of the different functions of conformational relaxation and exciton migration within the excited state DOS of a conjugated polymer. The dips represent chromophores along the polymer chain and the depth their energy.

The difference between self localization and migration can be a significant one with respect to the main application of conjugated polymers in electroluminescent devices. In pure polymer devices[1], excitation migration is the motor of mechanisms such as quenching at oxidation defects[4, 5], at the electrodes of a device or due to bimolecular annihilation of singlet and/or triplet excitons[84, 85]. All of these phenomena are detrimental to device performance. On the other hand, the migration of single excitons can be harnessed by deliberately doping polymers with acceptor molecules[86] to open a more efficient radiative decay channel and, in the case of heavy metal dopants, ideally to employ both singlet and triplet excitons for emission[87]. Thus, the degree of migration determines the fate of an excitation and ultimately governs device performance.

On the other hand, self-localisation, i.e. immobility, of an exciton will render it less subject to the influence of quenching sites. Similarly, with suppressed exciton annihilation, which is controlled by exciton diffusion, it may be possible to achieve excitation densities suitable for lasing[88]. To exploit these advantages and prevent exciton migration, a fast and efficient conformational relaxation is highly desirable for pristine polymer diodes. Today's conjugated materials commonly exhibit excitations with high mobility in the solid state, considering that their excitation energy is efficiently transferred to various dopants[89, 90]. To my knowledge, there has been no demonstration of a certain light-emitting conjugated polymer that self-localises via conformational reorganisation. The specific synthesis of a suitable material, however, requires an understanding of the reorganisation processes on a molecular level. In particular, it is necessary to distinguish conformational changes and migration as competing types of relaxation. Since the break of the mirror symmetry between steady state absorption and emission spectra could be explained by either of them, plain spectral changes are not sufficient for a distinction, but spectral dynamics need to be investigated in order to quantify their individual effects in terms of red-shifts and time scales. For a number of conjugated polymers, this has been done from the perspective of migration[26, 79, 91], mostly focusing on the solid state, where exciton migration prevails. This resulted in a migration dominated picture of the excited state relaxation. This study chooses to investigate the specific effects of conformational relaxation, which have previously been neglected, in order to estimate their relative importance.

4.1.3. Feasibility of an experimental study

Oligo- and polyfluorenes. In order to observe pure conformational relaxation, one needs to exclude the competing relaxation mechanisms listed in the previous sections. Exciton migration can be partly ruled out by investigating isolated molecules, i.e. using dilute solutions, in order to suppress any interchain interactions, which may promote migration[92]. The residual intrachain migration[80] is excluded entirely[35] when only the chemical building blocks of long conjugated polymers are looked at, i.e. small model compounds.

The emission and excitation spectra of hexyl-substituted oligofluorenes, which are shown later on in Figure 4-7, shift to the red as the chain length is increased. This shift arises from the increasing extent of the excited state wavefunction with chain length. While for excitation, it reflects the initial delocalisation and approaches a final value at a molecule length of up to 10 repeat units[22, 93, 94], emission converges at a lower value of 4 repeat units[78] due to self-localisation.

For this study, fluorene oligomers consisting of 3 and 5 fluorene repeat units,

respectively, were chosen. Due to their size, the molecules may only accommodate a single excited state, inhibiting exciton migration. Without the interference of excitation migration but still retaining the basic molecular structure of the polymer of interest, oligofluorenes therefore provide access to the conformational relaxation of polyfluorene. As will be shown below, any spectral changes due to solvation can also be excluded although this requires experimental proof.

In its various forms, the polymer of interest, polyfluorene, is one of the most studied conjugated polymers to date[26, 85] exhibiting bright blue fluorescence in devices[95] and interesting structural properties including beta phase formation[96]. Additionally, polyfluorene chains can be aligned to emit polarised light, making it an interesting material for device applications[13] and, hence, for fundamental research.

Polyfluorene consists of biphenyl units bridged by a non-conjugated carbon atom, which renders the repeat unit relatively rigid and planar. A variety of side chains can be attached to this carbon atom, enabling good solubility in aromatic solvents. Other organic liquids such as methylcyclohexane (MCH) or the family of alkanes are rather poor solvents, promoting aggregation of the long polymer chains. Due to the decreased probability of intermolecular interactions in solution, such effects are reduced for oligofluorenes. In turn, a better solubility allows more flexibility in the choice of solvents, which influence conformational dynamics. Thus, the dependence of relaxation time constants on solvent viscosity and temperature can be studied without side effects like aggregation.

In addition, the two different oligomers (tri- and pentafluorene) offer a possibility to vary the excited state energy[22], in a controlled way to investigate dependences of the relaxation behaviour on molecular size. Thus, one gains insight into the mechanism governing the structural changes and shines new light on the dynamics of the process.

Precursor study and reference material. A translation of the oligomer findings to isolated polyfluorene-type polymers requires a comparison of experimental data. Therefore, measurements on poly[9,9-di(ethylhexyl)fluorene] (PF2/6) molecules must be taken under identical experimental conditions. These can then be used to estimate the relative importance of intrachain exciton migration versus conformational relaxation for the polymer. In this context, Dias *et al.*[16] observed a solvent and temperature dependence of the excited state relaxation of PF2/6, which led to the conclusion that the relaxation dynamics are caused by conformational processes, namely chain planarisation via torsional adjustment. However, doubts remained as to the presence of exciton migration. In addition, the observed temperature dependence was analysed without addressing temperature dependent changes of the solvent properties, which

also affect the relaxation dynamics. The Arrhenius behaviour derived from the temperature dependence thus reflects a mixture of solute and solvent properties and their interactions. In particular, the solvent viscosity η (empirically) exhibits thermally activated behaviour via

$$\eta(T) = \eta_0 \cdot \exp\left(\frac{E_A}{k_B T}\right)$$

[Equation 4-5]

E_A and k_B being the activation energy and Boltzmann constant, respectively. Although these problems might have occurred, the above experimental data provide valuable information to validate the present oligomer and PF2/6 results because experimental setup and analysis are essentially the same. Also, PF2/6 was obtained from the same provider[12].

[Note: The main improvement to the single photon counting setup of Dias et al.[16] is an enhanced time resolution of 4 ps. However, the relaxation processes observable by both systems are the same, considering that compared to expectations from simulation (20 femtosecond to picosecond range[78]) still only a restricted time window in the tail of the relaxation can be monitored.]

An additional means to check the consistency of my measurements is looking at a ladder-type polymer with inhibited torsional relaxation such as MeLPPP. Here, conformational dynamics are restricted to high energy vibrational relaxation in the subpicosecond region. As will be illustrated later on, the Stokes shifts expected, e.g. from steady state spectroscopy, are so small that the non-existent picosecond spectral dynamics of MeLPPP can be used as a reference for the resolution of my experimental setup.

4.2. Materials and Methods

4.2.1. Materials

The chemical structures of all materials used are given in Figure 4-4. 9,9-dihexylfluorene as well as monodisperse tri- and penta[9,9-dihexylfluorene] (trifluorene and pentafluorene, respectively) were synthesized as described in the literature[97] by Dr. Mustafa Tavasli. The oligofluorenes were synthesized with a pyridine unit at one end of the chain, as shown in Figure 4-4, for further application as ligands in Iridium complexes. Nevertheless, no effect of this single pyridine unit on fluorescence decays, emission and excitation spectra of the oligofluorenes was detectable compared to published oligofluorene data[22], see Figure 4-7.

Poly[9,9-di(ethylhexyl)-fluorene] (PF2/6) was synthesised by the group of Prof. U. Scherf via Yamamoto coupling[98] with an average molecular weight corresponding to approximately 60 repeat units per chain. As polyfluorenes can be synthesized with up to 1000 repeat units, this is comparably short but prevents the molecule from coiling back on itself[53].

Although a certain level of oxidation defects is always present in polyfluorene type materials, their emission[4, 5] was not detectable via fluorescence spectroscopy in solution. A comparison of the noise level to the peak of oligofluorene or polyfluorene emission gives a limit of well below 1 % of oligofluorene molecules with an oxidation defect. For polyfluorene, the limit is even lower since the efficiency of oxidation quenching thrives mainly on exciton migration[5].

The methyl substituted poly(para-phenylene) (MeLPPP) was also synthesised by the group of Prof. Scherf[99]. As PF2/6, this conjugated polymer exhibited no detectable signs of degradation or aggregation and was only studied in "good" solvents. Its steady state spectra of Figure 4-18 are in agreement with the literature[99].

4.2.2. Sample preparation

Solutions. In order to investigate the influence of the solvent on the time-dependent spectral relaxation, the oligofluorenes were dissolved in toluene, n-pentane, n-heptane, n-octane, n-nonane or n-hexadecane (all 95%, from ROMIL) and decalin (Riedel-deHaen). PF2/6 and MeLPPP were dissolved in either toluene or decalin to warrant good solubility. All solvents were fresh, spectroscopy grade and used as supplied. They were chosen for reasons of chemical stability and reproducibility of a sample. No specific solvent-solute interactions are known. Solution concentrations were typically kept at 10^{-5} wt. /wt. to avoid intermolecular interactions such as aggregate formation.

Solvent viscosity. The above solvents are non-polar and their viscosity η is the main parameter of interest with an influence on conformational relaxation. Especially the homologous family of alkanes offers the possibility to vary solvent viscosity without changing other properties (e.g. polarity) too much. Viscosity data as obtained from the literature[71, 100, 101] are shown in Table 4-1.

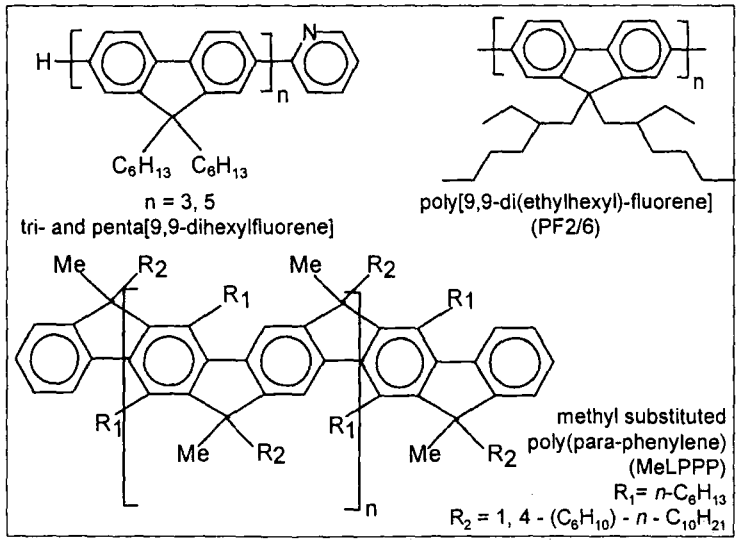

Figure 4-4 – The chemical structures of the materials investigated in this chapter.

Solvent	Viscosity η in cP at 20 °C	Boiling point in °C	Dielectric constant (20 °C)	Polarity
n-pentane	0.24	36	1.84	
n-hexane	0.33	69	1.88	0.000
n-heptane	0.41	98	1.9	0.000
n-octane	0.54	125	2.0	
n-nonane	0.71	151	2.0	
n-hexadecane	3.34	287		
toluene	0.59	110	2.38	0.017
MCH	0.7	101	2.02	0.000
decalin	3.55	185	2.15	0.11

Table 4-1 – Properties of the solvents used in this chapter taken from various online sources. MCH – methylcyclohexane. The polarity of the solvents is given in terms of the Lippert function.

Most measurements in this chapter are therefore carried out on alkane solutions of oligofluorenes in order to benefit from their combined advantages.

Additionally, using a JANIS liquid nitrogen cryostat, a decalin solution of pentafluorene was cooled down to study the temperature dependence of conformational relaxation. The analysis of the experimental data required the temperature dependent viscosity of decalin. This was obtained via extrapolation of published η(T) data[71, 102] assuming thermally activated behaviour. The freezing point of decalin is at 233 K. During the measurement the decalin solution was cooled from room temperature down to 240 K. In the proximity of a phase transition point, the simple assumption of $\eta(T) \sim \exp(E_A/k_BT)$ is questionable. Other approaches (double Arrhenius, Williams-Landel-Ferry or Vogel-Tammann-Fulcher models) are more suitable. However, the use of any of these models would not be based on experimental data. Also, the estimated η(T) data will not be used for quantitative analysis. The Arrhenius extrapolation is therefore justified as an approximation.

Thin films. Finally, as all PLEDs are based on the solid state, PF2/6 thin films are investigated. These were fabricated from a master solution of 10 mg PF2/6 per mg toluene, which was spin coated onto spectrosil (quartz) discs of 1 cm diameter at 2500 rpm. Film thicknesses of approximately 50 nm were measured using a reflective ellipsometry device.

4.2.3. Methods

Photo-excitation. The above solution samples or appropriate references (Rayleigh scatter solutions, e.g. ludox) were studied in

Quartz fluorescence cuvettes of 10 x 10 mm path length.

Excitation in the main absorption band – between 365 and 380 nm (oligofluorenes and PF2/6) or at 435 nm (MeLPPP) – was accomplished by a vertically polarised, frequency doubled Ti:Sapphire laser with an output pulse width of less than 2 ps and a repetition rate of 76.3 MHz, the power not exceeding 5 nW for a spot size below 1 mm^2. On one hand, low excitation power delays sample degradation. On the other, it ensures single excitation of the multi-chromophore polymers, preventing bimolecular annihilation.

TCSPC. Perpendicular to the excitation path, the sample emission (from a 2 mm excitation path) was collected and passed through a polariser set at magic angle to the vertical and a monochromator (Acton Spectra Pro 2300i), with 4 nm spectral resolution. As introduced in chapter 3, time-correlated single photon counting (TCSPC) is used to detect time-resolved fluorescence decays with a system response of 25 ps. Deconvolution of a scatter reference signal from the fluorescence decay curve yields an overall time resolution of approximately 4 ps, only limited by the detection channel width of 3.26 ps. This technique is suitable when a high signal-to-noise ratio is required but has the disadvantage that only one emission wavelength can be monitored at a time. Time-resolved spectra can be reconstructed from this method[52] but for an acceptable spectral resolution this requires a large number of individual measurements at varying wavelengths.

Streak camera. Picosecond emission spectroscopy via a streak camera setup is a complementary experiment. Here, the first grating of the double subtractive monochromator used for TCSPC is replaced by a mirror. A flip mirror directs the dispersed sample emission to the entrance optics of the streak camera. (Otherwise, all experimental conditions are identical to TCSPC.) A time-resolved spectral image can be read out from the camera via computer. From each measured image, a background image (obtained under identical conditions) is subtracted. Finally, all images are corrected for curvature, shading and spectral response using the streak camera software, see chapter 3. Spectra at fixed points in time are then read out as profiles integrating over a specified image section. The overall time-resolution of the system is determined during each measurement from the FWHM of the Rayleigh or Raman scattered excitation beam from the sample directly in the measured image. Time range 2 (typically 13 ps) or 1 (typically 7 ps) were used for this chapter.

Prior to each time-resolved measurement, steady state excitation and emission spectra were recorded (using a Jobin-Yvon FLUOROLOG spectro-fluorimeter) in order to avoid effects like aggregation or degradation by comparison with known

spectral data[22], and to double check the sample concentration.

4.3. Results - Oligofluorenes

4.3.1. Steady state spectra

The measurements on alkane solutions of oligofluorenes will provide the basis for all conclusions about the conformational relaxation in polyfluorene. To start with, steady state spectroscopy is used to characterise the samples: Figure 4-8 shows the excitation and emission spectra of tri- and pentafluorene in pentane and hexadecane (spectra from heptane and nonane solution lie between these extremes), which demonstrate that:

a) Excitation spectra are independent of the emission wavelength monitored so that only one type of chromophore is active, which excludes the presence of aggregation.

b) Emission spectra are independent of the excitation wavelength (within the range used) so that the excitation used in the time-resolved experiments (365 to 380 nm) lies well above the localisation energy. In conjugated polymers, the latter term describes the excitation threshold which is needed to populate the exciton density of states (DOS) sufficiently for exciton migration to occur. Commonly, the localisation energy is found as the peak position of the 0-0 fluorescence mode[26].

[Note: Although migration is not expected in the above oligofluorenes, the excitation and emission spectra of Figure 4-5 and Figure 4-6 give evidence for some other disorder driven process which populates states of higher energy than the excitation. The author found this behaviour in a variety of conjugated polymers, e.g. polyfluorenes and MeLPPP, and oligofluorenes - in the solid state as well as in solution. These measurements were done using standard equipment and are repeatable beyond doubt. It remains unclear how this "up-conversion" *of excitation energy works except that it is somehow related to the redistribution of energy, which occurs at excitation above the localisation limit.]*

c) A slight solvatochromism is observed for both excitation and emission. Going from pentane to hexadecane, they red-shift by 17 meV. For TCSPC measurements, this has been corrected for by adjusting the collection wavelengths to the same relative position in the spectrum for each sample.

d) The relative importance of the first (0-0) fluorescence mode is decreased for the trimer. This is a general trend for oligomers[22] linked to the decrease of Huang-Rhys factor with chain length. Polyfluorene exhibits an even more pronounced first mode, see Figure 4-24. This may be interpreted as increasing restrictions of movement at a larger molecular size due to the larger molecule-

solvent interface. This, in turn, implies that the importance of conformational relaxation decreases with chain length.

e) In addition, Stokes shifts can be estimated from Figure 4-7 by taking the difference between excitation and emission maxima. This rather crude estimate yields values above 300 meV independent of oligomer and solvent. However, to be exact, the Stokes shift is the difference between the 0-0 excitation and emission modes, which for the excitation spectra is not the same as the overall peak since the 0-0 mode is hidden by inhomogeneous broadening. This is clearly shown by the emission spectra of Figure 4-5, which are independent of the excitation energy. Sample dependent changes in Stokes shift may therefore be hidden as well. Of the actual shift of 300 meV only the magnitude has a physical meaning.

In summary, the spectral characterisation yields no abnormalities. The steady state spectra of oligofluorenes shift to the red with increasing molecular size. As shown in section 4.1.3, evidence can be drawn from this to safely exclude exciton migration in tri-and pentafluorene. Any Stokes shift observed in these materials must hence arise from solvation and/or conformational relaxation.

For the following time-resolved measurements, note that both oligofluorenes are photo-excited with the same photon energy (365 to 380 nm) regardless of any steady state spectral shift. Comparing this to Figure 4-5, pentafluorene will carry more excess energy directly after excitation than trifluorene. Nevertheless, at 1 ps after excitation this will have been released by vibronic cooling so that for our measurements both oligomers may be treated as being at a comparable vibrational "temperature".

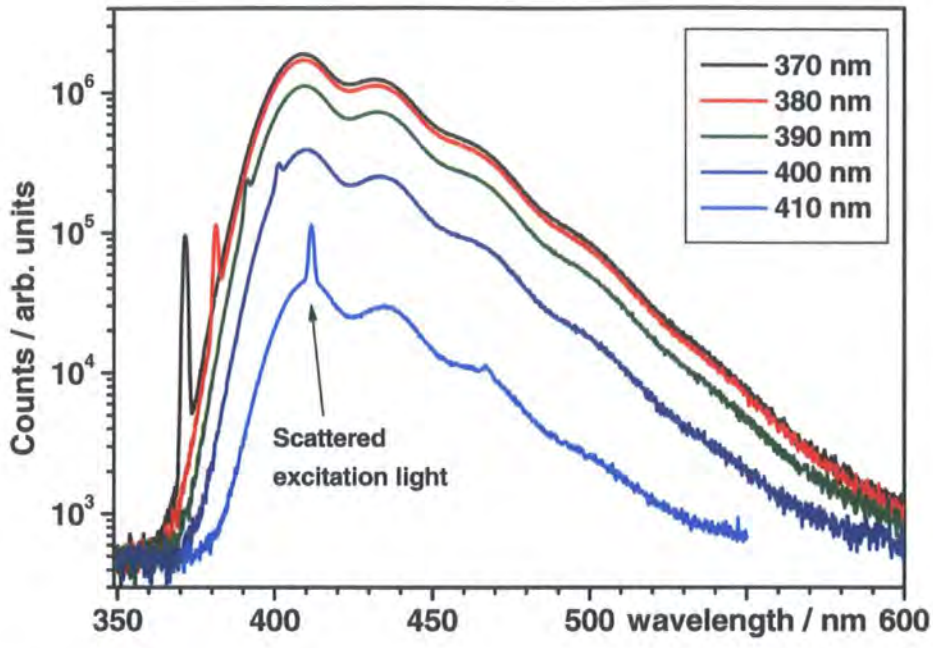

Figure 4-5 – Photoluminescence spectra of a 10^{-5} wt./wt. pentafluorene/hexadecane solution. The spectral shape is constant for all excitation wavelengths (see legend) up to the localisation point near the peak of the 0-0 emission mode.

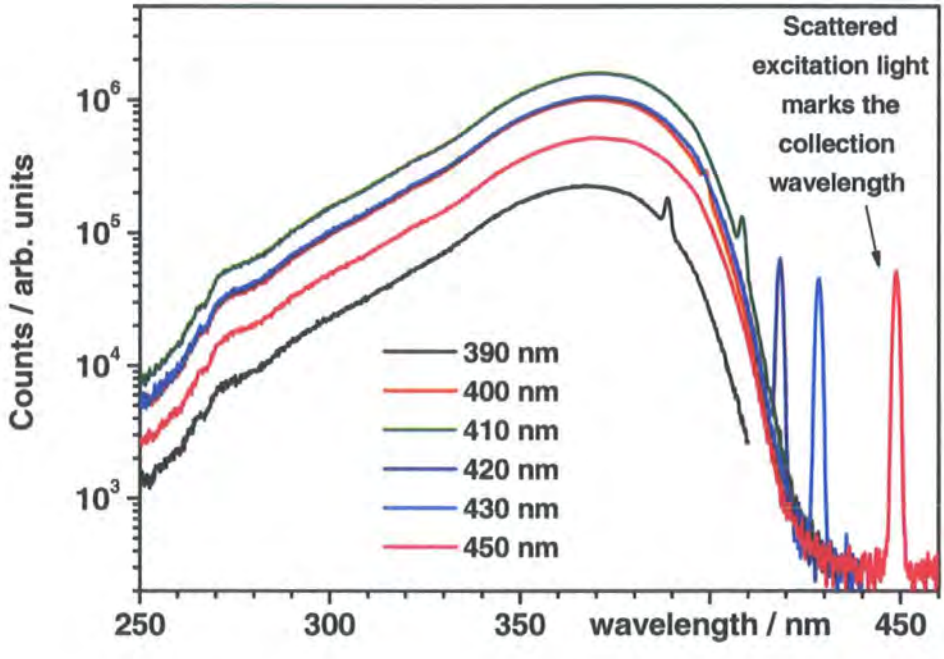

Figure 4-6 – Photoexcitation spectra corresponding to Figure 4-5 showing independence of collection wavelength (see legend) and "up-conversion" (see text).

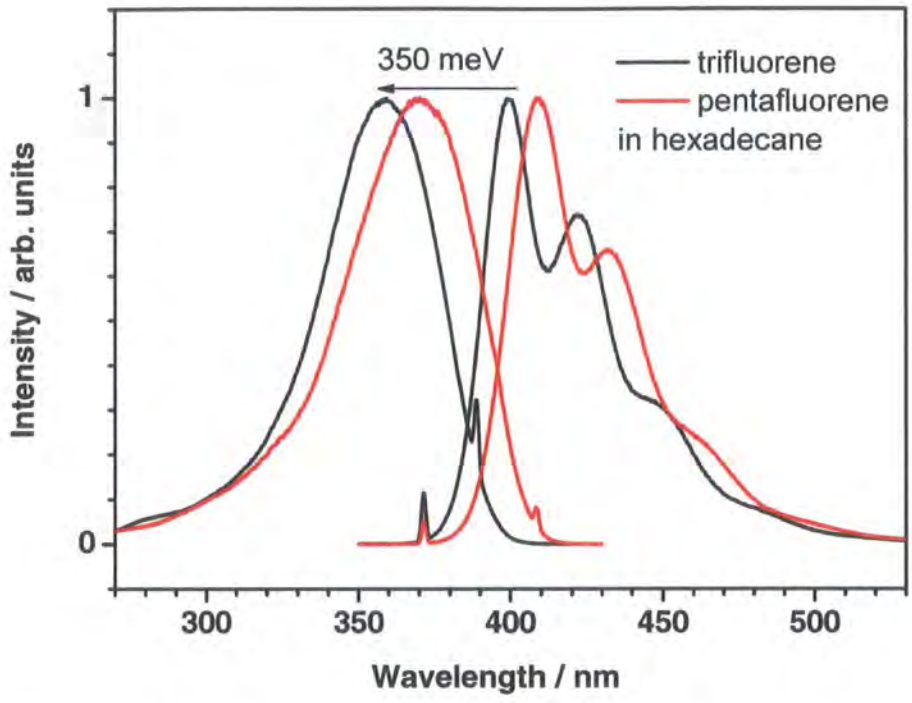

Figure 4-7 – A comparison of the steady state excitation and emission spectra of the trifluorene and pentafluorene dissolved in hexadecane at 10^{-5} wt./wt.. The Stokes shift is an estimate from the relative peak positions of the spectra.

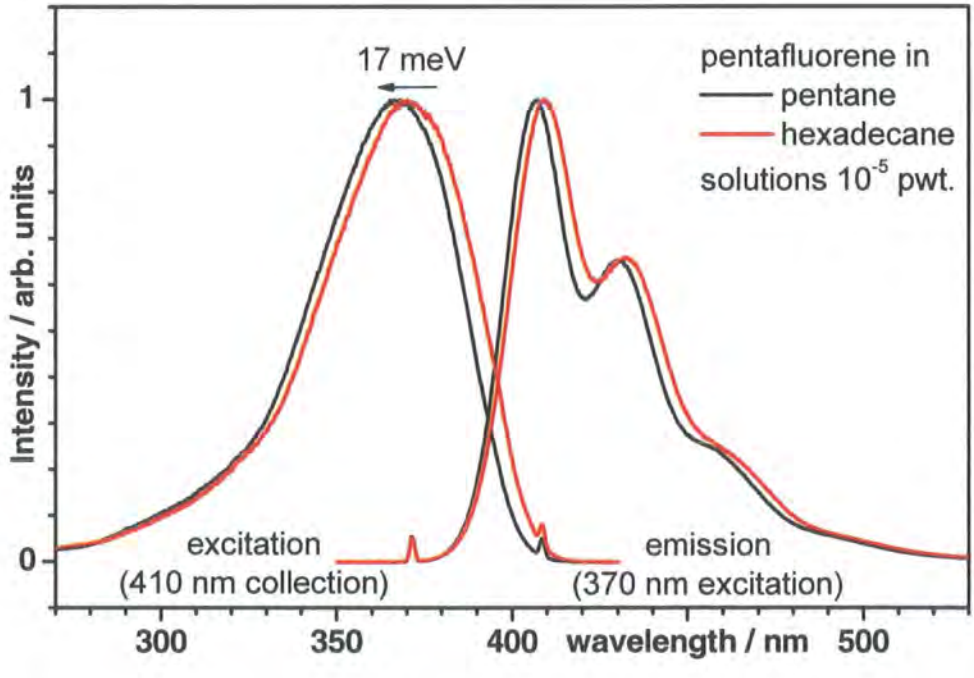

Figure 4-8 - A comparison of the steady state excitation and emission spectra of pentafluorene dissolved in pentane or hexadecane at 10^{-5} wt./wt.. The spectral shift due to solvatochromism is indicated.

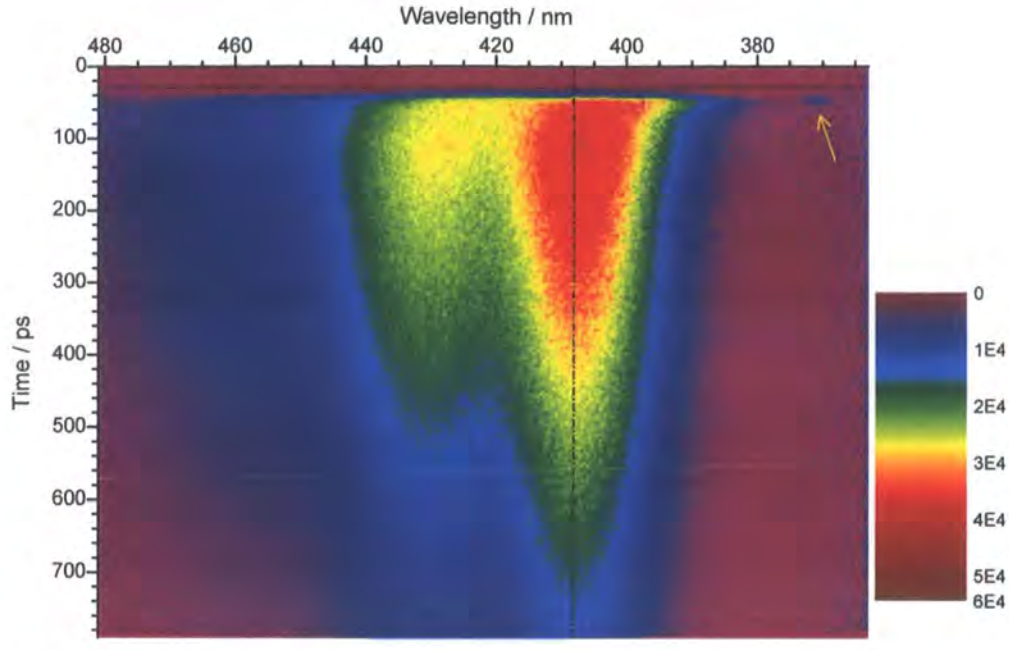

Figure 4-9 – Streak camera image recorded from pentafluorene in heptane at 10^{-5} wt./wt.. The colours code the signal intensity in counts.

4.3.2. Streak camera measurements

Figure 4-9 shows a streak camera image of the time-resolved emission from a heptane solution of pentafluorene. The image has been corrected for background, shading, curvature etc.. Areas of high emission intensity are shown in yellow/red while low intensity is coded in dark blue. Time evolves from top to bottom covering 788.9 ps in total (time range 2). The Raman scattered excitation pulse (blue) in the upper right corner gives a time resolution of the measurement of 13.9 ps (FWHM). Already visible by eye is a red-shift of the pentamer fluorescence occurring within the first 100 ps after excitation.

From this image, a series of horizontal profiles (each integrating over a 14 ps window) was taken. Figure 4-10 shows the initial (0 to 14 ps after excitation) and final (630 to 644 ps) emission spectra. The red-shift within the time window amounts to 20 meV, which seems small, compared to the visible shift from Figure 4-10 – most of the latter disappears when averaging over 14 ps. Clearly, the time resolution does not suffice to follow the changes adequately. Repeating the experiment in time range 1 (resolution 7 ps) does not solve this problem, which is expected considering that time constants of 1 ps were estimated from molecular dynamics simulation[78] for torsional modes of polyfluorene. The time scale is no proof of conformational relaxation in oligofluorenes. This requires dependences on solvent and molecular size.

A highly viscous solvent, albeit outside the alkane range, is decalin. Streak camera measurements similar to the above were carried out on a decalin solution of trifluorene with a time resolution of 13.2 ps.

Averaged spectra are shown in Figure 4-10 revealing a red-shift comparable to pentafluorene in heptane. Additionally, the vibronic modes of the final spectrum are better resolved than at t=0. Albeit weaker, this is also observed for pentafluorene. Both, red-shift and mode narrowing are expected when relaxation of the fluorophores takes place: The streak camera measurements monitor a smooth transition of high into low energy states, both types showing their own distinct emission spectra. A look at the time-dependent spectra also shows that the ratio between the first and second fluorescence mode increases with time, i.e. the Huang-Rhys factor, S, of the spectra decreases. However, S is not trivial to quantify due to the overlap of first and second vibronic. A decrease of S notifies a decreasing disorder, which is also expressed by mode narrowing. Therefore, it shall suffice to quantify red-shift and narrowing only.

A quantitative analysis of the spectral evolution is provided in Figure 4-12. As demonstrated in Figure 4-11, the high energy side of the 0-0 vibronical mode of each time-resolved spectrum was fitted to a Gaussian, to obtain quantitative values for the peak energy and width of the first vibronic mode, which were then plotted versus time in Figure 4-12. For both, tri- and pentafluorene, the red-shift of the centre energy and the narrowing of the first vibronic occur simultaneously and then saturate after 100 to 300 ps. Qualitatively, the relaxation dynamics are very similar for trifluorene in decalin and pentafluorene in

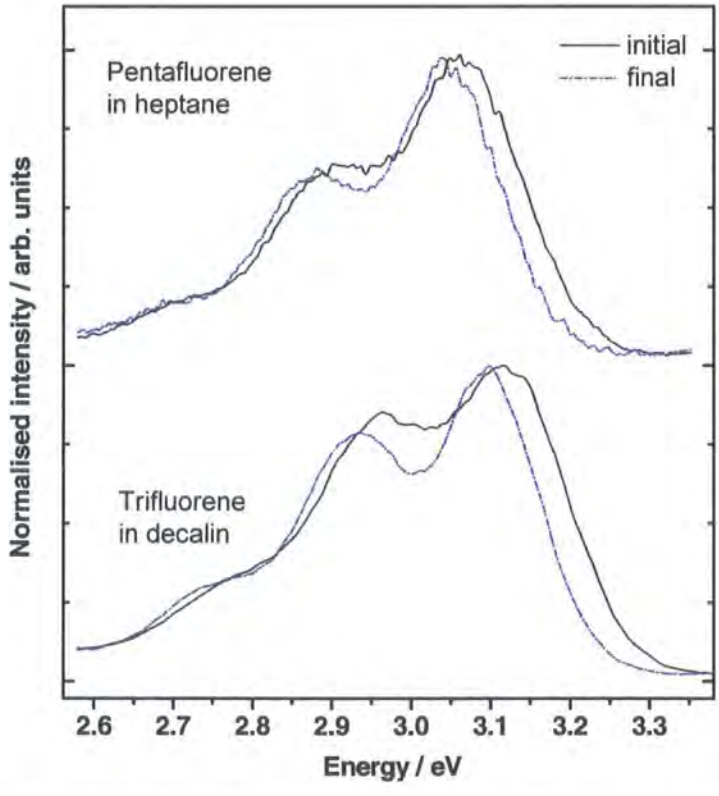

Figure 4-10 – Initial and final emission spectra of oligofluorene/alkane solutions at 10^{-5} wt/wt, see text.

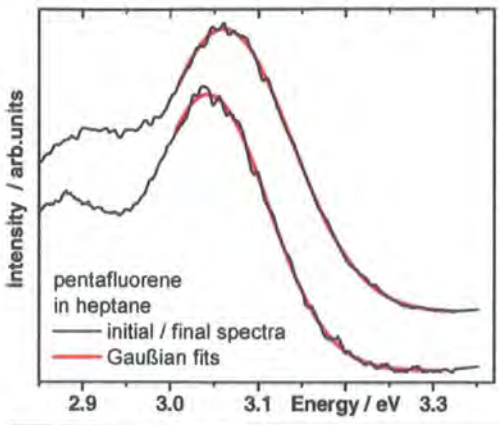

Data: n5in7_initial		Model: Gauss	
Equation: y=y0 + (A/(w*sqrt(PI/2)))*exp(-2*((x-xc)/w)^2)			
y0	0.03262	±0.00137	
xc	3.06052	±0.00021	
w	0.1545	±0.00053	Chi^2/DoF = 0.00007
A	0.18102	±0.00075	R^2= 0.99946

Data: n5in7_final		Model: Gauss	
Equation: y=y0 + (A/(w*sqrt(PI/2)))*exp(-2*((x-xc)/w)^2)			
y0	0.03992	±0.00191	
xc	3.04225	±0.00038	
w	0.13584	±0.00082	Chi^2/DoF = 0.00018
A	0.1551	±0.0011	R^2= 0.99864

Figure 4-11 – Analysis of the streak camera spectra using Gaußian fits to the 0-0 fluorescence modes, with parameters shown in the bottom panel. Top/bottom curve and data correspond to the initial/final spectrum of pentafluorene in heptane.

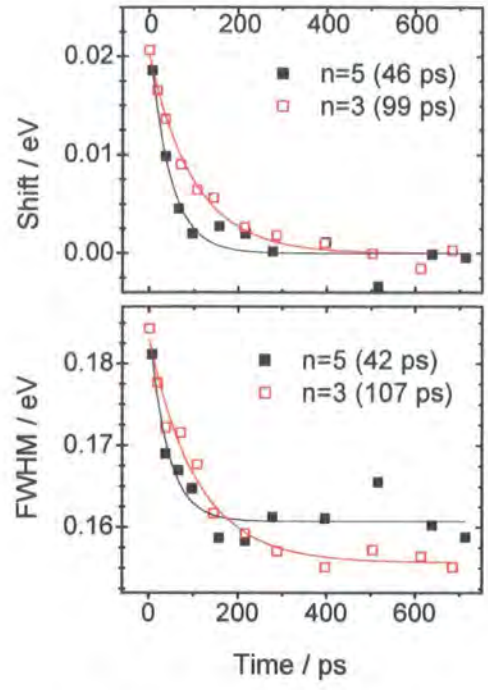

Figure 4-12 – Spectral dynamics of pentafluorene in heptane (n=5) and trifluorene in decalin (n=3) obtained from the 0-0 fluorescence mode via the procedure of Figure 4-11. The lines are mono-exponential fits to the data with time constants shown in brackets.

octane, confirming that both are governed by a similar relaxation mechanism.

Note from Figure 4-12 that for oligofluorenes, no further spectral changes are expected after 600 ps. Comparing the total Stokes shift of 20 meV after 7 ps (~ time resolution of time range 1) to the hundreds of meV expected from steady state spectra, the streak camera apparently fails to detect a large part of the short-time relaxation processes. Absolute values of shifts and narrowing therefore have little meaning. Note that the absolute peak position of both, pentafluorene in heptane and trifluorene in decalin solution, converges at 408 and 401 nm, which deviates by less than 0.5 nm from steady state spectra recorded using the Fluorolog spectrometer (not shown).

Now, the dynamics of the observable long-lived relaxation tail in different materials may be compared: To guide the eye and roughly estimate the relaxation kinetics, both red-shift and narrowing have been fitted using monoexponential decay curves with time constants ~ 45 ps (pentafluorene in octane) and ~100 ps (trifluorene in

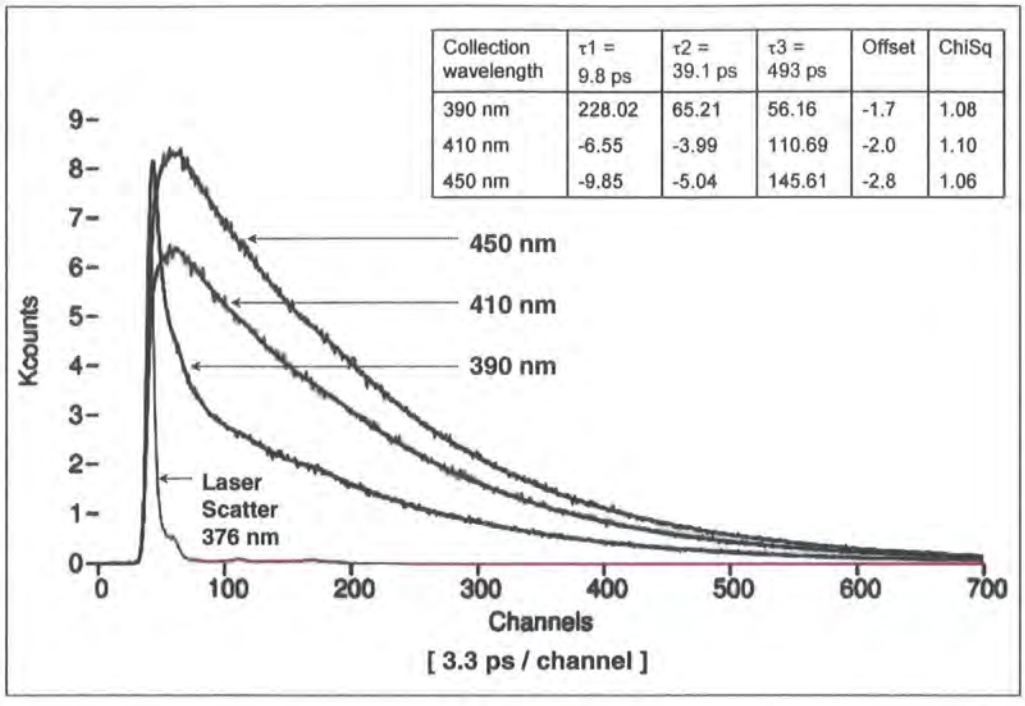

Figure 4-13 – Global analysis of a TCSPC experiment on pentafluorene in 10^{-5} wt./wt. heptane solution. The collection wavelengths are indicated as well as the scatter reference used for deconvolution. The inset table gives the fit amplitudes and exponential time constants, see text.

decalin). As has been shown previously for PF2/6[16], the slower relaxation of trifluorene may arise from the higher viscosity of decalin compared to octane. Therefore, the next section aims to reveal the relaxation dynamics in greater detail by obtaining data from tri- and pentafluorene in a variety of solvents.

4.3.3. TCSPC measurements

Time-resolved single photon counting (TCSPC) provides a superior signal-to-noise ratio and, after re-convolution fitting, a better time resolution of 4 ps. TCSPC is, hence, better suited to obtain quantitative kinetical details than streak camera experiments. However, with TCSPC one cannot monitor directly the shift and narrowing associated with excited state relaxation. Instead, one obtains the relaxation kinetics from wavelength dependent fluorescence decays. Figure 4-13 shows TCSPC data obtained from pentafluorene in heptane solution. To tie in with the spectral changes observed above, collection wavelengths were set to 390 nm (3.18 eV, blue edge of the fluorescence spectrum), 410 nm (3.02 eV, peak of the 0-0 vibronic) and 450 nm (2.76 eV, in the red tail). Global analysis as introduced in chapter 3 was successfully performed on this dataset although it required a sum of three exponentials. Nevertheless, each component is justified, contributing a significant amplitude at each of the collection wavelengths. All fit parameters are shown in the table inset in Figure 4-13.

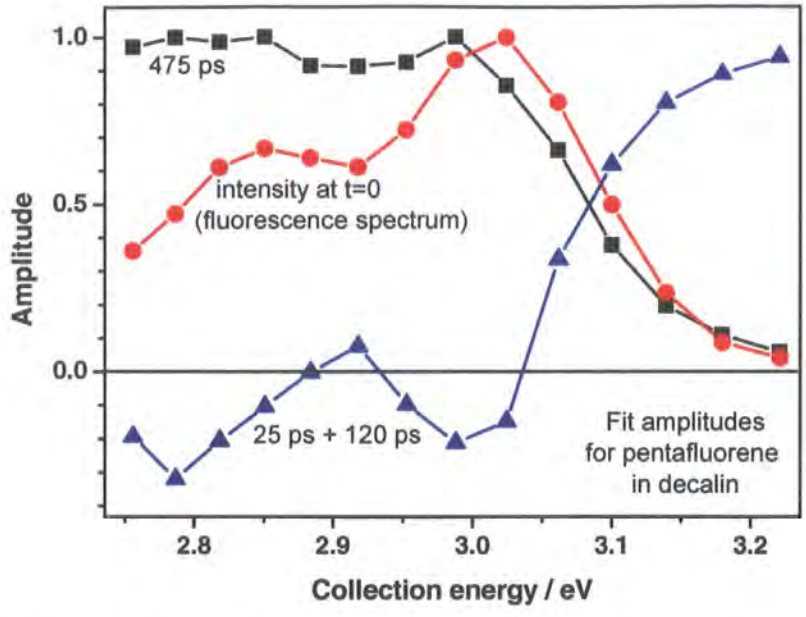

Figure 4-14 – Normalised fit amplitudes of a TCSPC experiment on pentafluorene 10^{-5} wt./wt. in decalin solution. Blue triangles represent the decay/rise components, black squares the overall decay. These are contrasted to the normalised initial fluorescence spectrum (red circles).

Here, positive amplitudes correspond to decay and negative ones to a build-up.

Common for all collection wavelengths, a long-lived decay time (τ_3) of 490 ps is found: In this context, singlet excitons in polyfluorene commonly exhibit a lifetime of 350 ps[103]. For the smaller oligomer, a longer lifetime is expected[22]. Thus, the 490 ps reflect the lifetime of the singlet excited state in pentafluorene. The remaining two components are shorter lived (τ_1 = 10 ps and τ_2 = 40 ps). τ_1 and τ_2 constitute the difference between the three analysed decay curves: Both appear as a fast decay on the blue edge of the emission spectrum but as rise times in the red tail. This is consistent with the red-shift observed via streak-camera. τ_1 and τ_2 will therefore be referred to as relaxation times. In Figure 4-12, exponential kinetics of 45 ps have been estimated, corresponding to τ_2 = 40 ps. However, a biexponential fit in Figure 4-12 is not meaningful as τ_1 = 10 ps would yield an insignificant amplitude in the slower time resolution of the streak camera.

In another, analogous TCSPC experiment on a decalin solution of pentafluorene, a larger number of more closely spaced collection wavelengths was used (see Figure 4-14). The results were analysed globally using randomly mixed sets of three decay curves each. Again, three exponential components were identified: A decay time (singlet lifetime) of τ_3 = 480 ps was observed for all wavelengths. The additional amplitudes corresponding to τ_1 =25 ps and τ_2 = 120 ps were found to be a continuous function of the collection wavelength, as shown in Figure 4-14, i.e. starting with positive values in the blue edge of the emission, crossing zero near the peak of the 0-0 vibronic mode and then

becoming negative. This pattern, albeit weaker, repeats itself for the other vibronic modes and validates the observance of a red-shift of the emission spectrum on the time scale of τ_1 and τ_2. Comparing the quantitative values to the streak camera data, it is safe to conclude that TCSPC can follow the dynamics of conformational relaxation by measuring τ_1 and τ_2.

Now, dependencies of the above relaxation constants on the properties of the molecule and the surrounding medium will be investigated. TCSPC experiments as above were carried out on pentafluorene and trifluorene in a variety of solvents ranging from pentane to hexadecane, which have been chosen because the family of alkanes offers the possibility of varying viscosity without changing the chemical properties, e.g. the polarity, of the solvent too much. Decalin and toluene were used for comparison outside the alkane family.

Global analysis of these measurements yields bi- or triexponential decay behaviour for all of the samples following the described pattern: Independent of viscosity, the fluorescence decays exhibit an overall decay constant τ_3 of 490 ps (for pentafluorene) and a larger singlet lifetime of 600 ps for trifluorene, as expected for an even shorter molecule. One or two additional fast components reflect the relaxational shift appearing as a steep decay of the high energy emission but as a rise time at lower energy. Note, in contrast to τ_3 it is not attempted to interpret physical meaning into τ_1 or τ_2 in order to distinguish between the different relaxation constants. Instead, they merely provide a measure to compare the time scale of the relaxation kinetics in different samples.

sample	wavelength	tau1	tau2	tau3	A1	A2	A3
trimer	385	**8.1**		**659**	0.532		0.467
in	400				0.011		0.989
pentane	440				-0.161		1
trimer	385	**17**		**637**	0.612		0.388
in	400				0.029		0.971
heptane	440				-0.062		1
pentamer	390	**9.5**	**39**	**494**	0.655	0.185	0.16
in	410				-0.066	-0.032	1
heptane	450				-0.074	-0.031	1
pentamer	390	**15**	**65**	**496**	0.652	0.191	0.157
in	400				0.279	0.252	0.469
nonane	450				-0.031	-0.077	1
pentamer	390	**38** +/- 6	**174** +/- 13	**496** +/- 5	0.482	0.61	0.952
in	400				0.236	0.303	0.994
hexadecane	450				-0.028	-0.161	1

Table 4-2 – Results of TCSPC measurements on oligofluorenes in alkane solvents with time constants and corresponding amplitudes obtained via global reconvolution fitting.

Generally, two components were required to fit the data of slowly relaxing samples, whereas one component sufficiently described samples exhibiting fast relaxation. Apparently, this must be ascribed to the limited time resolution. Therefore, one may propose that the relaxation kinetics are essentially non-exponential and that the TCSPC measurements are unable to follow rates faster than 4 ps so that for samples showing fast relaxation less exponential components suffice to reproduce the decay curve within the experimental errors.

Table 4-2 gives the experimental data for a selection of samples and also includes the amplitudes associated with each exponential component. The errors for the time constants ranged between 1 and 10 %, as indicated, depending on the signal-to noise ratio of the raw TCSPC data (which depends on the collection (integration) time of the measurement and the intensity of the sample emission). Sufficient reproducibility is always ensured.

4.3.4. Relaxation constants vs. viscosity

Figure 4-15 shows the dependence of the TCSPC relaxation constant(s) on solvent and material:

First, the attention is turned to trifluorene. Note that always the longest observable relaxation times, i.e. τ_2, are compared with each other. Nevertheless, the corresponding shorter components, τ_1, are shown as well if they are detectable. For completion, τ_1 and τ_2 should be shown in the context of their relative amplitudes. However, since these depend on the relation between the time resolution and τ_1 or τ_2, they often bear little physical meaning and are, hence, left out.

In Figure 4-15, solvent viscosity is varied by dissolving trifluorene in different alkanes: In general, an increase in viscosity (from 0.24 cP for pentane to 3.34 cP for hexadecane) results in a remarkable increase of the long relaxation time τ_2 (from 8 ps to 93 ps, respectively). Such behaviour is expected for a relaxation process depending either on molecular motions of the solvent (solvation) or on motions of the solute with frictional coupling to solvent molecules (conformational relaxation).

In agreement with the above, a similar dependency is observed for pentafluorene, going from 15 ps in pentane to 174 ps in highly viscous hexadecane. For the pentamer, however, relaxation times are between 10 and 50 % larger than for the trimer.

Note that solvents of the alkane family are not the most common used to dissolve fluorene based materials. A different type of solvent, e.g. aromatics, may attach differently to the solute and therefore changes its relaxation behaviour. In short, there may be other parameters than viscosity that govern the relaxation dynamics. In order to explore the potential influence of the aliphatic alkane solvents, the above findings were cross-checked

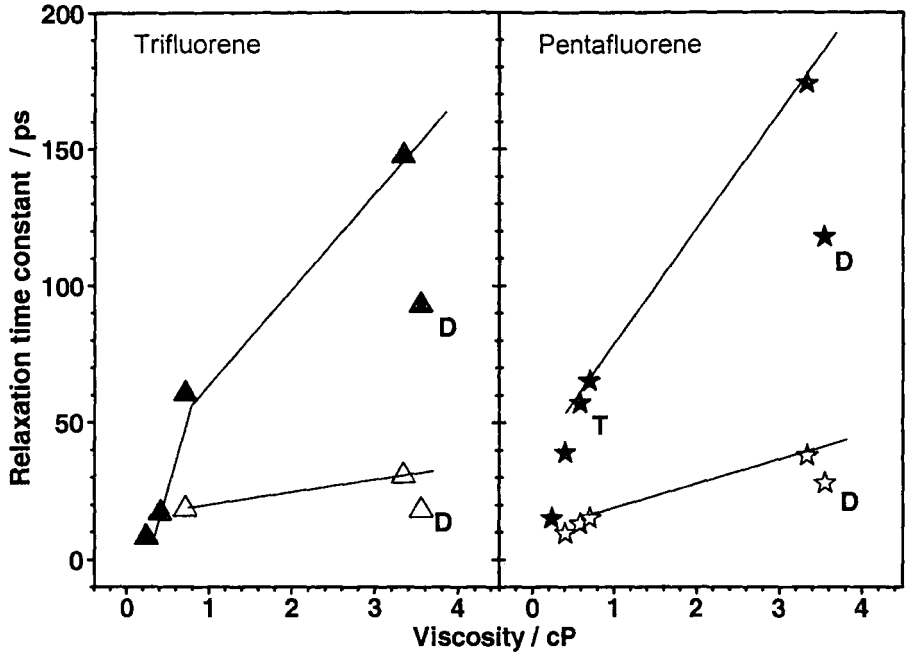

Figure 4-15 – Relaxation times of trifluorene and pentafluorene in alkane solvents, as a function of solvent viscosity. Hollow symbols represent the shorter time constant, if two relaxation times were observed. D – decalin. T – toluene.

using toluene (0.59 cP) as well as the highly viscous decalin (3.55 cP at room temperature) as solvents for both tri- and pentafluorene. If the observed relaxation constants exclusively depend on the viscosity of the solvent, then the τ_1 and τ_2 in toluene will fit in between heptane and nonane, while the constants for decalin will be comparable to those observed with hexadecane. As shown in Figure 4-15, the relaxation constants observed for a toluene solution of pentafluorene indeed agree with the alkane measurements.

However, decalin solutions exhibit relaxation times about 30 % below the expected value, for both penta- and trifluorene. Several origins can be responsible for this:

a) Specific interactions between decalin and the oligofluorene, which are very unlikely considering the chemical structure and experience from other non-polar solvents.

b) For alkanes, the slope of the τ_2 dependency on viscosity decreases towards hexadecane. Similarly, it may decrease for high viscosity aromatics. However, aliphatic and aromatic solvents may cause different slopes due to different interactions with the solute: According to the common rule "Like dissolves like" alkanes will preferably dissolve the side chains but aromatics to the backbone.

c) The general decrease of the slope towards high viscosity may reflect problems with dissolving the oligomers. In fact, the shorter alkanes are better solvents

than hexadecane. However, decalin is a better solvent than hexadecane contradictory to its faster relaxation time.

d) In addition to the viscosity, which reflects the bulk friction between solvent molecules, also microscopic properties such as the volume of the molecule may determine the relaxation dynamics. Thus, the steric hindrance of solute motion is considered as well as the rigidity of the solvent cage. This phenomenon is known from protein solvation, where the bulk water properties have little relevance to water molecules in the vicinity of the protein. Since an aromatic molecule is more compact than an aliphatic one of the same weight ($M_{W\ decalin}$= 138 g/mol is even smaller than $M_{W\ hexadecane}$= 226 g/mol), it poses less hindrance to solute motion thus enabling faster relaxation times.

4.3.5. Temperature dependent experiments

It remains to confirm that decalin acts as a regular solvent for pentafluorene by utilizing the temperature dependence of viscosity. Figure 4-16 shows the variation of relaxation constants with decreasing solution temperature: Indeed, τ_1 and τ_2 increase continuously towards lower temperature, i.e. for higher viscosity. The lowest temperature used was 240 K, which is close to the freezing point of decalin (233 K). Here, the extremely slow conformational relaxation of pentafluorene (τ_2 = 300 ps) becomes comparable to the excited state lifetime (490 ps), which implies that in the solid state this type of relaxation will be frozen. Note that the emission spectra (monitored via streak camera) did not show any sign of

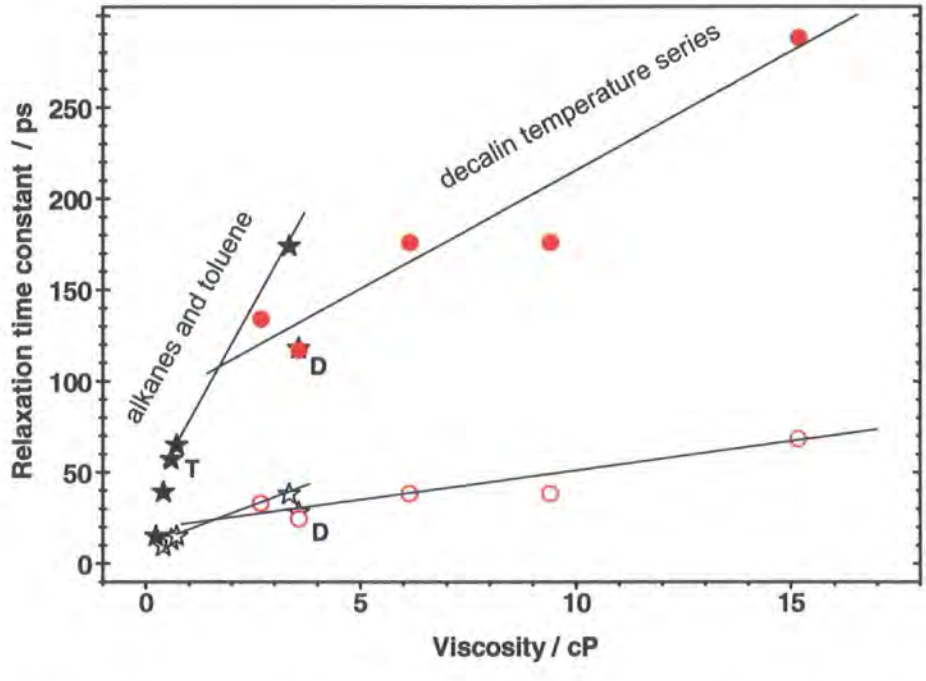

Figure 4-16 – Relaxation times of pentafluorene in alkane solvents as in Figure 4-16 are compared to those in decalin solution at various temperatures, see text. The solid lines are guides to the eye. T – toluene, D – decalin.

aggregation of the pentafluorene molecules and the room temperature relaxation constants were unchanged after re-heating to 293 K. In summary, decalin behaves well as a solvent.

In the work by Dias *et al.*[16], a similar experiment was carried out on PF2/6 using decalin and methylcyclohexane as solvents. Here, the temperature dependence of relaxation constants was analysed in terms of a thermally activated behaviour of an underlying conformational relaxation. However, my own results demonstrate the key role of the solvent viscosity for the long-time energetic relaxation of conjugated oligofluorenes. The apparent break between hexadecane and decalin also indicates that factors other than the viscosity of the solvent affect the relaxation process, especially at high viscosity. It is therefore not possible to neglect the temperature dependence of solvent properties in a quantitative analysis as shown by the unphysical high activation energy for torsional relaxation of 100 meV, found by Dias *et al.*[16]. Steady state spectroscopy would certainly resolve an energy spacing of this order. The 100 cm^{-1} (12.4 meV) for torsional modes found by Franco *et al.*[78] are more realistic.

It must be noted that using a nitrogen cryostat in the streak camera/ TCSPC experiment introduced problems associated with scattered light from the inner cryostat windows. This can distort the scatter reference and crucially influence the exponential components of a decay analysis. Careful alignment and repetitive measurements were therefore essential to obtain the above decalin TCSPC data. Less sensitive were the temperature dependent spectra recorded via streak camera as no deconvolution is used here. In order to validate the consistency of the temperature dependent measurements, a heptane solution of pentafluorene was monitored by streak camera at 290 and 190 K under otherwise identical conditions (not shown). When extracting initial and final emission spectra in analogy to Figure 4-10, one can observe an increase in quantum yield. Additionally, the width of the equilibrated DOS is decreased at low temperature. Both effects are expected. Hence, the experimental setup with inserted cryostat can be used to obtain sensible experimental results.

4.3.6. Picture of conformational relaxation in oligofluorenes

To summarise the above, the spectral dynamics of oligofluorene solutions are characterised by a red-shift of the emission and a simultaneous narrowing of the vibronic modes as expected for excited state relaxation. These dynamics are observed with picosecond time resolution. However, they only account for a fraction (~10 %) of the overall steady state Stokes shift and narrowing between excitation and emission spectra. This fraction is higher for better experimental time resolution and slower spectral changes – apparently, only long-lived relaxation components can be detected.

The time scales of the above changes are consistent between streak camera and TCSPC measurements. It is found that the relaxation of trifluorene happens significantly faster than that of pentafluorene.

As previously observed by Dias *et al.* on PF2/6[16], also in oligofluorenes the relaxation (both, shift and narrowing) slows down as the solvent viscosity increases. A comparison between aliphatic and aromatic solvents indicates that factors other than viscosity have an influence as well, e.g. the volume of the solvent molecules. Consistently, slower relaxation is also observed at lower temperature. How much of the latter dependency is caused by the increase of viscosity at low temperature must be further investigated. In total, relaxation times span from the resolution limit (4 ps) up to the order of the singlet lifetime (300 ps), depending on solvent-solute system and temperature.

Excitation migration is ruled out for the above oligomers. Thus, the observed spectral evolution is entirely caused by conformational processes if solvation effects can be excluded: The molecular rearrangement of a solute always entails a reaction of the solvent, i.e. local solvent relaxation. The time scales expected for the latter slightly overlap with the observed relaxation constants and can extend up to a few picoseconds[64, 66, 70]. However, spectral narrowing is not intrinsic to conventional solvation but rather arises from an average dissipation of excess energy from an ensemble of fluorophores[66], as will be discussed below. Moreover, when comparing trimer and pentamer, a solvent interacts with the same local environment, i.e. hexyl side chains, for both oligomers. Therefore, similar relaxation constants are expected for a purely solvent controlled process. The persistent increase of relaxation time (between 10 and 50 %) for the longer oligomer can thus not be explained by solvent relaxation alone. Naturally, solvent molecules will react to solute rearrangements, but their relaxation does not determine the rate of the spectral changes observed.

Slower relaxation in pentafluorene is rather caused by the increase of the volume and steric hindrance of the rearranging molecule. Additionally, the more delocalised exciton wavefunction of the pentamer compared to the trimer reduces the driving force for reorganisation, as suggested by bond length calculations[67]. Furthermore, the Huang-Rhys factors in steady state absorption spectra decrease for longer chains[22], which gives evidence of a decreased energetic disorder and, again, less driving force. Thus, for various reasons, the balance between conformational energy gain and the hindering frictional forces is not profitable for reorganising more than 4 repeat units, as shown by self-localisation simulations[78].

What do the relaxation dynamics tell about the actual molecular rearrangement on the picosecond scale? One implication of the slower conformational relaxation of the pentamer is that more than three repeat

units must be involved in the observed long-time conformational rearrangement.

Apparent from steady state spectra of Figure 4-17, the fluorene monomer also exhibits a large Stokes shift. Since the fluorophore only consists of a single repeat unit, no long-time relaxation is expected. Unfortunately, monofluorene needs to be excited deep in the UV, outside the range of the laser source. Hence, the absence of a long-lived (picosecond) relaxation component could not be confirmed. It is, however, expected that the fluorene Stokes shift arises either from solvation or from subpicosecond relaxation of a single repeat unit: On one hand, there is an abundance of studies on small dye molecules giving evidence of large shifts for polar solvation[64, 70]. On the other hand, fluorene, its derivatives and the solvents used here are *nonpolar*. Subpicosecond solvational shifts will therefore not dominate the spectral changes. Instead, simulation studies on PPV and polyfluorene suggest that upon excitation the bonds within the repeat unit are deformed to give the phenyl rings a more quinoid geometry[67, 78].

Thus, considering the Stokes shift of fluorene, one should distinguish between picosecond relaxation involving several repeat units and subpicosecond monomer-type relaxation, which causes a large Stokes shift but eludes experimental detection in this study. One can draw a parallel to the simulations of Franco *et al.*[78] on polyfluorene in vacuum, who distinguished between 20 fs dynamics for bond stretching

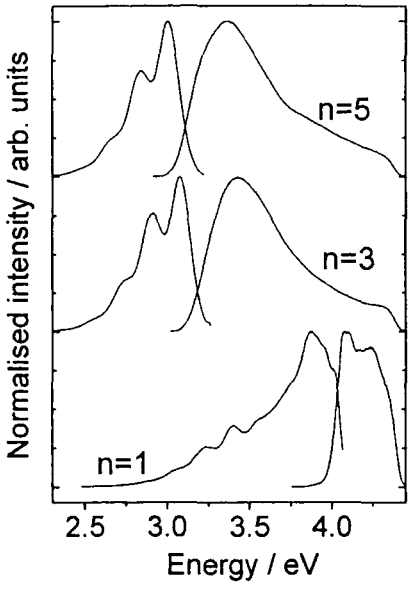

Figure 4-17 – Steady state photoluminescence and –excitation spectra of penta-, tri- and monofluorene (from top).

and a 1 ps time scale for the torsional rearrangement. In conclusion, picosecond time-resolved spectroscopy has revealed the torsional relaxation times for tri- and pentafluorene.

4.4. Results – Polyfluorene

4.4.1. Steady state spectra

Following the same pattern as for the oligomers, one can now approach the excited state relaxation of polyfluorene. As a basis, Figure 4-18 shows again the steady state excitation and emission spectra of poly[9,9-di(ethylhexyl)-fluorene] (PF2/6) and the ladder-type polymer used as a reference, MeLPPP. The PF2/6 spectra resemble that of pentafluorene, only red-shifted and, as expected, with a higher weight of the first vibronic mode or a lower

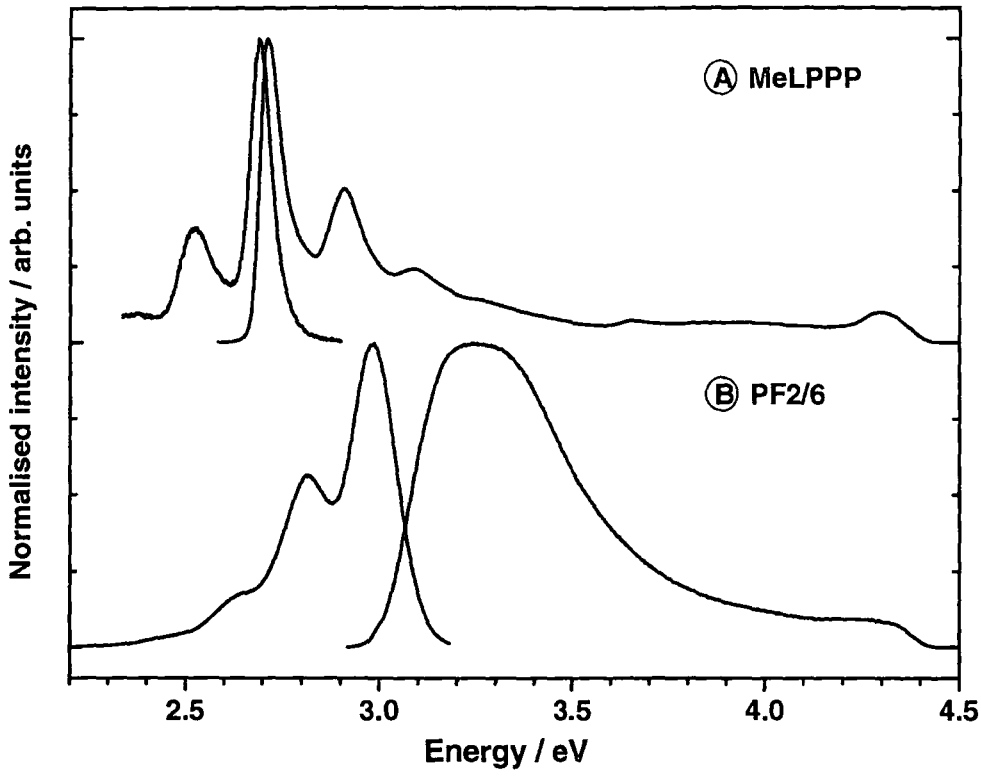

Figure 4-18 – Steady state excitation and emission spectra of MeLPPP and PF2/6 in toluene solution, at 10^{-5} wt./wt.. The Stokes shift of MeLPPP is extremely small compared to PF2/6.

Huang-Rhys factor. The Stokes shift is comparable to that of tri-and pentafluorene, hundreds of meV. According to their molecular weight, the PF2/6 chains consist of approx. 60 repeat units. Hence, exciton migration opens up another route for excited state relaxation apart from conformational changes and solvation.

The MeLPPP spectra on the other hand clearly show the high microscopic order of the MeLPPP molecule: The Stokes shift is exceptionally low as is the Huang-Rhys factor, indicative of the very small difference between ground and excited state geometry.

In analogy to the oligofluorenes, the above and other steady state spectra served to exclude aggregation and excessive solvatochromism. Again, streak camera and TCSPC measurements will be used to characterise the excited state relaxation of PF2/6 and MeLPPP on the picosecond time scale.

4.4.2. Streak camera measurements

Figure 4-19Figure 4-20 present a corrected streak camera image to illustrate the spectral dynamics of PF2/6 in decalin and toluene solution, at room temperature. The time resolution given by the vertical width of the scatter pulse is ~13 ps, for both images. Similar to the excited state relaxation in oligofluorenes, a red-shift of the emission occurs after excitation. Also the dynamics of this shift are familiar: Whereas in toluene, equilibrium is reached

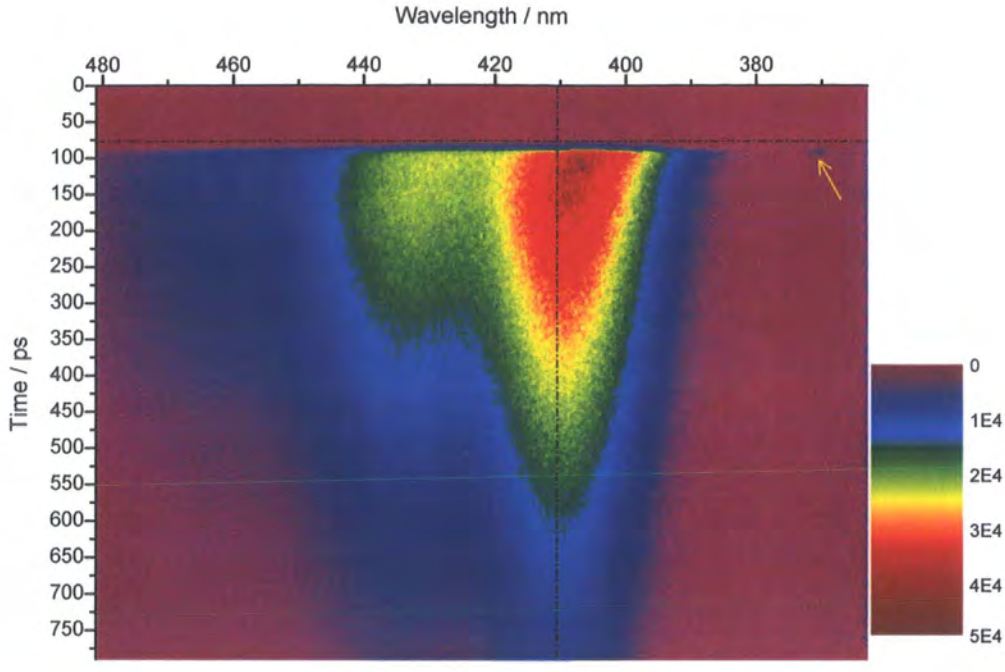

Figure 4-19 – Corrected streak camera image of the fluorescence of PF2/6 in a 10^{-5} wt./wt. decalin solution. The colour code represents the intensity values in counts per pixel. The arrow indicates the scattered excitation beam. The dashed lines are vertical and horizontal guides to the eye to help estimate spectral dynamics.

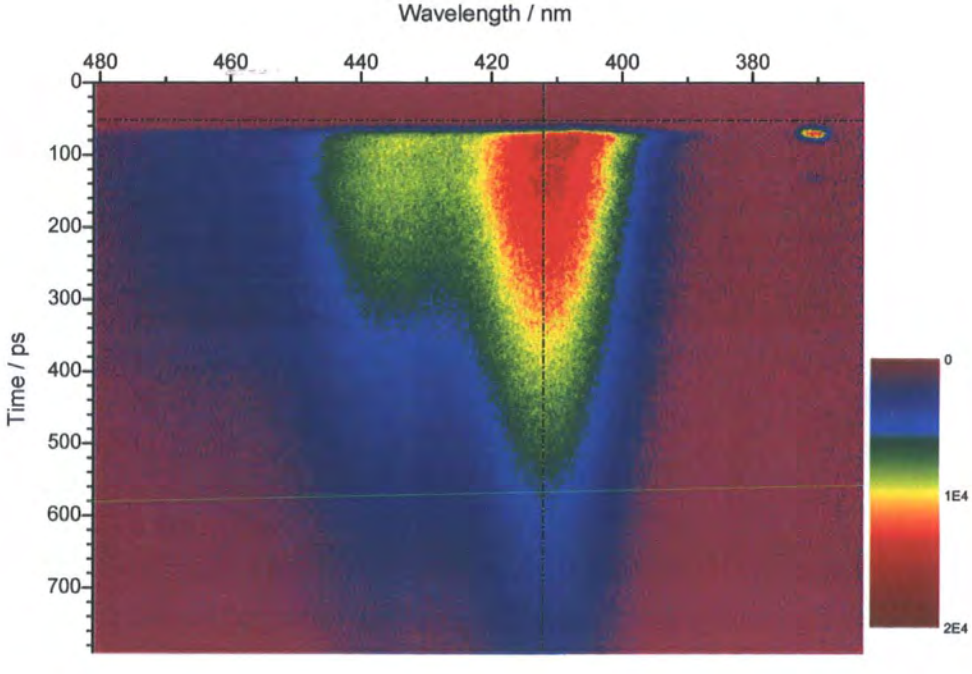

Figure 4-20 – In analogy to Figure 4-19 a streak camera image of the fluorescence of PF2/6 in dilute toluene solution.

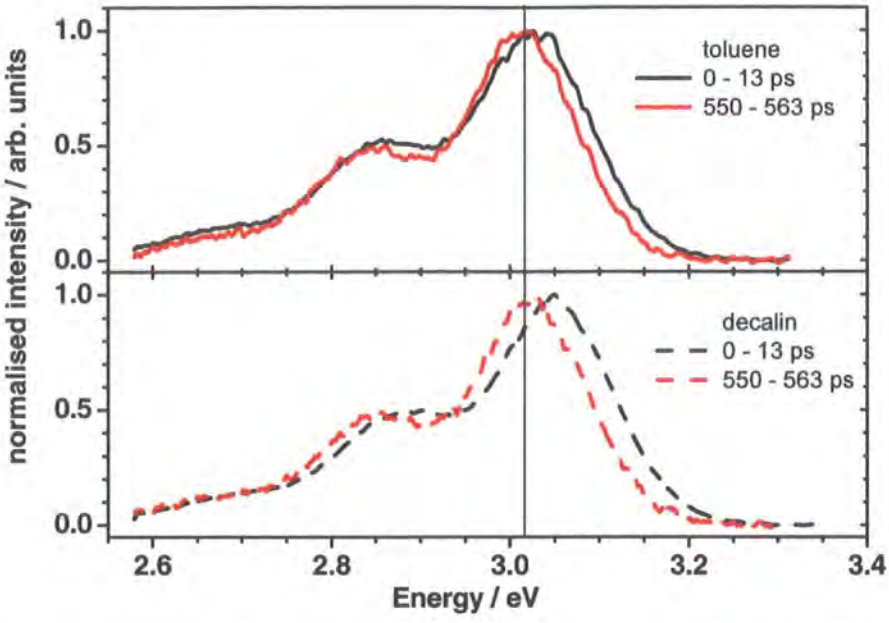

Figure 4-21 – Time-resolved spectra obtained from Figure 4-19 and Figure 4-20 for PF2/6 in toluene and decalin solution. Black line – initial, redline – final spectrum of the time range 2 streak camera image.

after 100 ps, a significantly larger time of ~300 ps is required for PF2/6 in decalin. Due to its slowness compared to the time resolution, the decalin shift appears much larger.

The PF2/6 spectra are now analysed more accurately by taking horizontal profiles (time-resolved spectra). Figure 4-21 gives the initial (0-13 ps) and final (550 - 563 ps) spectra obtained from PF2/6 in toluene and decalin solution Although a red-shift is visible, it is significantly less pronounced than in the shorter molecules. A mode narrowing is also present but barely visible; one needs to compare the sides of the 0-0 modes or the dip (between first and second mode) between initial and final spectrum. To obtain quantitative measures, the high energy sides of the 0-0 modes of the PF2/6 spectra (from the presented images and matching time range 1 (7 ps) images) were again fitted to Gaussian curves. Figure 4-22 provides the corresponding fit parameters, peak energy and FWHM as a function of time. The spectral red shift evolves very similarly compared to the oligomers, i.e. it levels off at long times and can be fitted with an exponential decay (time constants: 28 ps for toluene and 62 ps for decalin). As expected from the studies of Dias *et al.*[16], relaxation in a high viscosity solvent is slower. Spectral narrowing is observed but since the effect is halved (compared to oligofluorenes) the noise contribution to the plot is significant. However, the time dependence of spectral narrowing differs qualitatively from the oligofluorenes: While for tri- and pentamer all spectral changes roughly obey the same exponential decay law, in PF2/6 the decrease of spectral width continues beyond the monitored time span

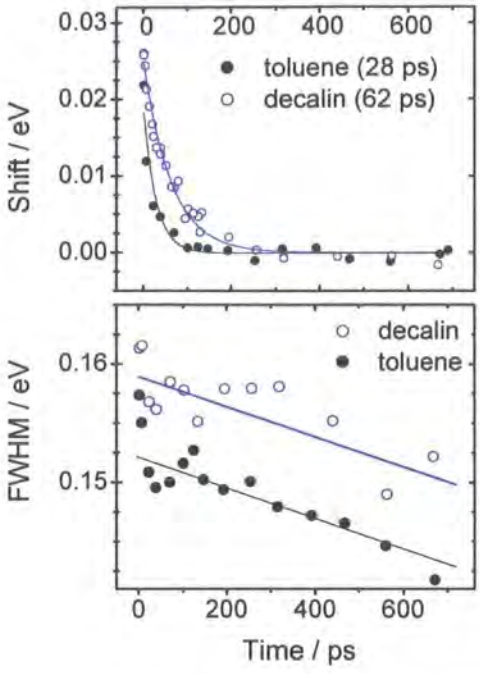

Figure 4-22 – Shift and width dynamics of the 0-0 fluorescence mode of PF2/6 in toluene and decalin solution obtained from Gaussian fits of time-resolved streak camera spectra (time ranges 1 and 2). The lines are mono-exponential fits (top) or guides to the eye (bottom).

and does not track the behaviour found for the corresponding red-shift. This is the case for PF2/6 in decalin and toluene solution alike and manifests a fundamental difference to the relaxation dynamics found for oligofluorenes. Indeed, the underlying relaxation mechanism – conformational changes in short molecules and additional exciton migration in the polymer – justify such differences. These results will be further discussed later on, jointly with TCSPC data on PF2/6.

To consider streak camera measurements for the moment, Figure 4-23 shows an analogous measurement for a dilute solution of MeLPPP in decalin. An attempt to analyse this image using the same Gaussian fitting procedure as above failed because apparently in this material the inhomogeneous broadening is so low that it does not dominate the shape of the DOS. Instead, the shape of the vibronic modes reflects a mixture of Lorentzian and Gaussian line shapes, representing homogeneous and inhomogeneous broadening, respectively. This doubles the number of free fitting parameters. Therefore, this method is no longer comparable to the one used before for PF2/6.

Nevertheless, one can still resort to a visual analysis, i.e. to comparing the normalised time-resolved spectra. Initial and final spectral profiles for MeLPPP in decalin are shown in Figure 4-24. Both are identical apart from a high energy component visible in each of the initial spectrum's modes. This component is not related to solvation or conformational relaxation as it decays in the same time for toluene and decalin and disappears after about 25 ps. The remaining parts of the spectrum are unchanged throughout this evolution and stay constant until the end. Subtracting the final from the initial spectrum (both normalised) reveals the high energy emission component – were it caused by excited state relaxation, one would expect negative amplitudes. Indeed, the existence of two MeLPPP chromophores oriented orthogonally to one another was concluded by Müller *et al.*[104]. Apart from this, the MeLPPP emission spectra are constant on the picosecond time

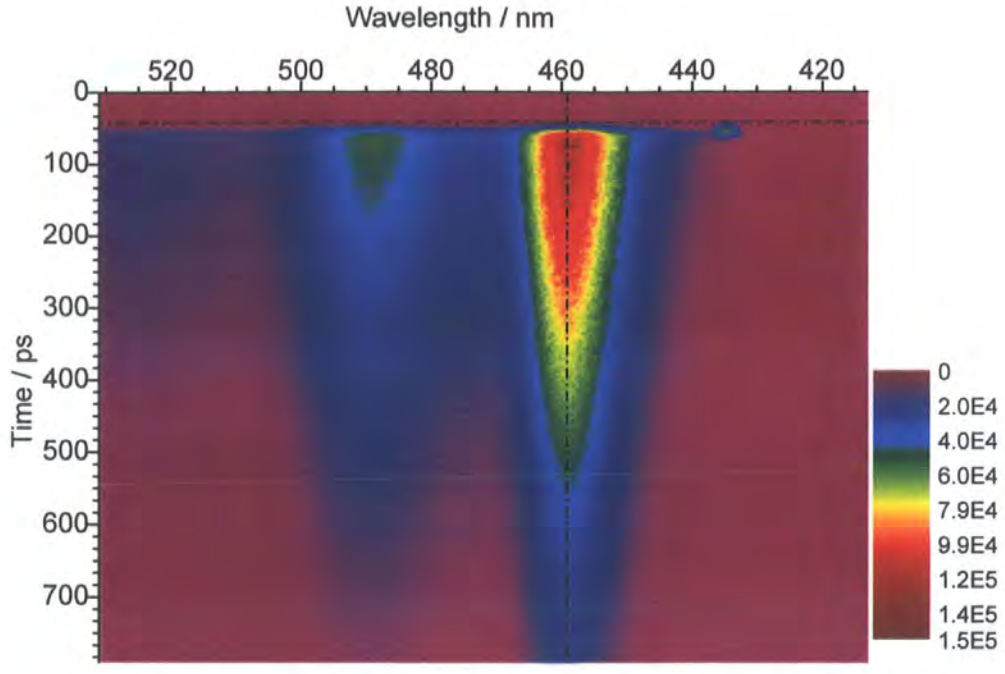

Figure 4-23 – Corrected streak camera image of the fluorescence of MeLPPP in a 10^{-5} wt./wt. decalin solution.

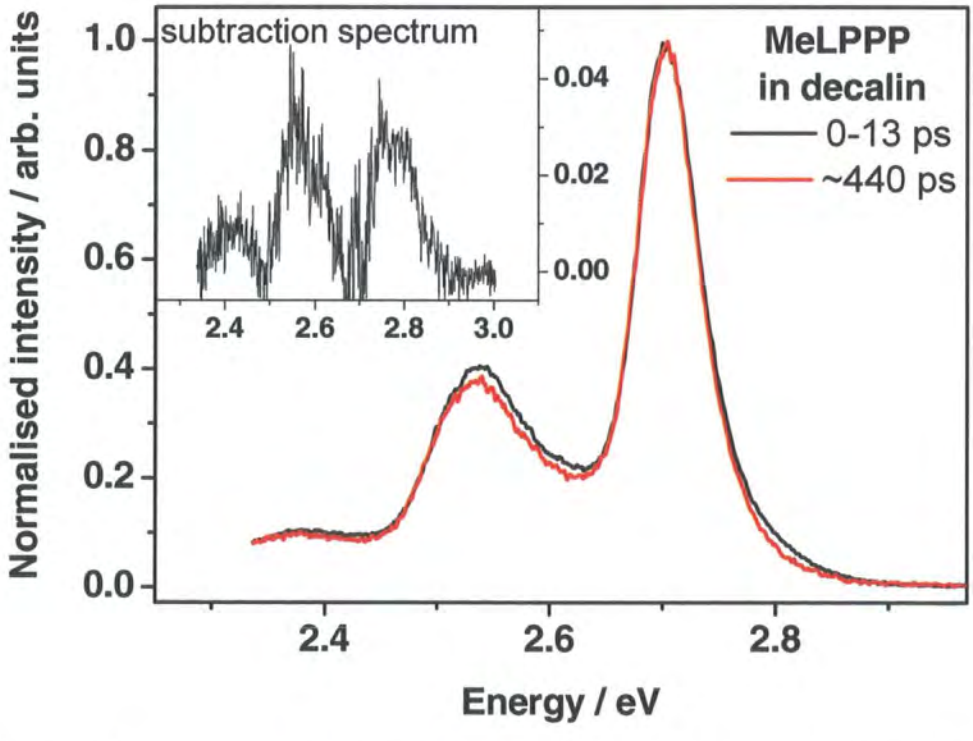

Figure 4-24 – Time integrated initial and final emission spectra of MeLPPP obtained from Figure 4-23. The inset shows the difference spectrum. Note, this is not negative as expected for a relaxation process but represents a decay off the blue emission side.

scale as expected for this microscopically rigid conjugated polymer. An MeLPPP/toluene solution was tested with the same result. In summary, the streak camera experiment detects a dynamic red-shift in PF2/6 but not in MeLPPP. This is an expression of the degree of excited state relaxation in these materials. The PF2/6 relaxation dynamics are exponential with increasing time constant for a solvent of higher viscosity, indicating a conformational relaxation component. A narrowing of vibronic modes as for oligofluorenes is also observed albeit weakly. However, it does not follow the exponential kinetics of the red-shift. Also, it persists beyond the monitored time window. These are deviations from the established picture of conformational relaxation in oligofluorenes. They can be interpreted as indications of the influence of exciton migration.

4.4.3. TCSPC measurements

More information about the PF2/6 system is gained via TCSPC: In analogy to the oligomer TCSPC experiments, PF2/6 was again studied in toluene and decalin solution. In line with previous measurements[16], the obtained TCSPC decay curves are adequately described using the decay/rise time framework found for the oligofluorenes, see above. A τ_3 of about 370 ps was observed at every collection wavelength, in agreement with the singlet lifetime in PF2/6[103]. In addition, one or two relaxation times, τ_1 and τ_2, were found depending on the solvent. Their corresponding amplitudes varied very similar to the behaviour shown for pentafluorene in decalin in Figure 4-14. The τ_1 and τ_2 relaxation times summarised in Figure 4-25 agree with those found in the streak camera experiments. The figure provides additional data for the relaxation of PF2/6 in MCH and decalin, taken from Dias *et al.*[16], which fit into the dependence of τ_1 and τ_2 on the solvent viscosity, η: As shown in Figure 4-25, the relaxation constants increase towards higher solvent viscosity. Surprisingly, τ_1 and τ_2 are faster than those seen in trifluorene (in toluene: 16 ps compared to 49 ps and in decalin: 6 and 69 ps compared to 18 and 93 ps). This clashes with the observed increase of relaxation times for a larger oligomer. This may again be explained by the presence of exciton migration, which is expected to add to the relaxation rate caused by conformational rearrangement.

It remains to validate the PF2/6 TCSPC results by comparison with the reference polymer MeLPPP. In line with the streak camera results, TCSPC experiments on the ladder polymer do not show the wavelength dependent decay/rise time behaviour associated with relaxational shifts. Instead, an overall biexponential decay with time constants of 40 and 286 ps is observed, in agreement with the literature[16]. These findings provide a reference case of zero conformational relaxation, which validates the experimental basis of all above observations.

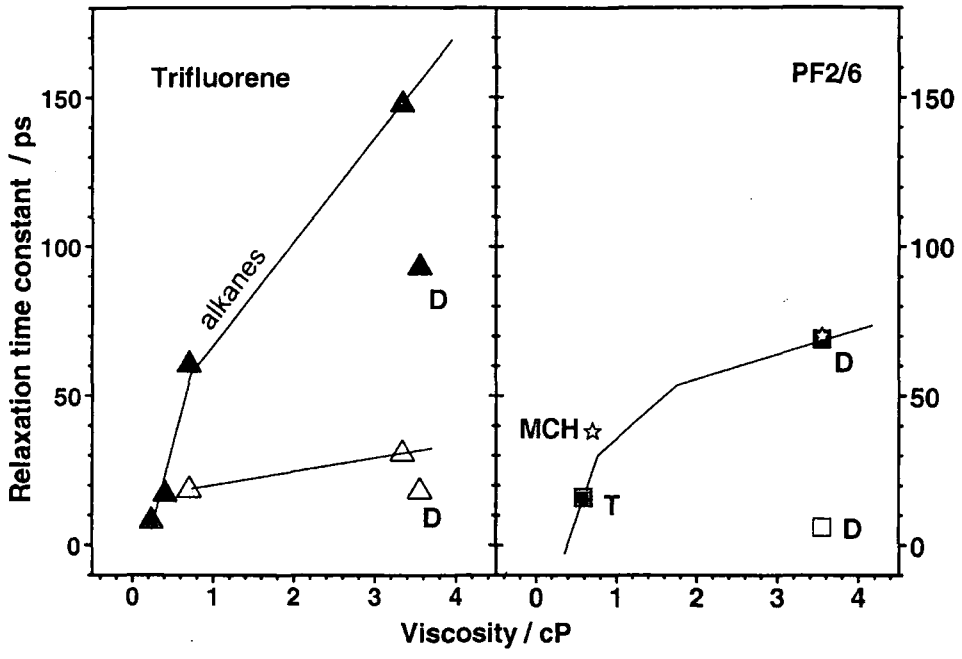

Figure 4-25 – The relaxation times of PF2/6 compared to those of tri(dihexyl-fluorene) are much faster. Only in decalin solution, a second relaxation component is found. MCH – methylcyclohexane; T – toluene; D – decalin. In analogy to Figure 4-15.

4.4.4. Excited state relaxation in a polyfluorene

Summary. Streak camera and TCSPC measurements have shown similarities between the excited state relaxation in poly- and oligofluorenes. Both, dynamic red-shift and mode narrowing are visible in the time-resolved emission spectra. The kinetics of the red-shift are exponential. The rate of these exponentials slows down when the viscosity of the solvent increases, indicative of conformational relaxation. Note, solvation effects have previously been ruled out for oligofluorenes and are considered very unlikely for a larger molecule of similar chemical build.

However, it was shown that PF2/6 relaxation occurs on a faster time scale than that of trifluorene in the same solvent. In contrast to this, pentafluorene relaxes significantly slower than trifluorene, consistent with its increased size. This contradiction indicates that the picosecond excited state relaxation of PF2/6 is not purely conformational. In agreement with this notion, the red-shift and mode narrowing dynamics are decoupled in the case of PF2/6. If both dynamics are caused by the same process, one expects coherence as is reliably observed for the purely conformational relaxation of oligofluorenes. These differences are attributed to the presence of a second relaxation process. Exciton migration is the only candidate for this as all other possible competitors can be excluded.

To which degree does torsional relaxation occur in PF2/6? To extract this information from the data available, the

dynamics of its competitor, exciton migration must be known. In solid state PF2/6, migrational relaxation occurs continuously on a time scale between 1 ps and 1 ns[26] after excitation. This overlaps with the time constants observed for long-lived conformational relaxation. However, excitation migration on isolated polymer chains in solution is less efficient than migration in solid state, which is dominated by interchain exciton jumps. Interchain contacts are ruled out for a PF2/6 of only 60 repeat units, in dilute solution. Despite their microscopic flexibility, polyfluorenes exhibit considerable macroscopic persistence preventing molecules from coiling back on themselves[53]. Therefore, excitation migration on isolated polymer chains in solution cannot be compared to that in solid state. Simulations of the anisotropy decay of a polythiophene by Grage *et al.*[80] suggest that an excitation does not even sample an entire polymer chain in solution. Here, the hopping time for a single migration jump was estimated to be ~ 10 ps. Thus, the dynamics of exciton migration and conformational relaxation overlap.

It remains to answer the question of how these processes compete. Considering the viscosity dependent relaxation times, it seems clear to attribute the initial spectral red-shift to a conformational process. In this scenario, the role of exciton migration is restricted to accelerating the overall rate of relaxation by means of quick downhill hopping. The contribution of conformational relaxation entirely accounts for the viscosity dependence of this rate. In summary, migration controls the rate but conformational relaxation the viscosity dependence. Clearly, this is only possible if their relative contributions are comparable. In this context, the conformational processes observed in oligofluorenes indeed span the range from 6 to 300 ps. In the competition with exciton migration, only the faster processes can contribute. The medium to long time regime is then dominated by migration. Thus, the viscosity dependent initial relaxation of PF2/6 is accelerated.

However, the above explanation has one significant flaw. During the competition in the initial time regime, the active conformational processes are selected in comparison with the rate of exciton migration, e.g. 10 ps[80]. Thus, the main decay contribution is dominated and rate limited by migration. In fact, the relaxation constants observed for PF2/6 via TCSPC are very similar to the above 10 ps. Here, it must be noted that, in decalin solution, the 6 ps component is significantly higher weighted than the 69 ps component. A further indication of dominating migration is the decoupling of shift and narrowing for PF2/6, which is an established characteristic of conformational relaxation in oligofluorenes. In conclusion, the combination of experimental results strongly suggests that conformational processes play only a minor role in the excited state relaxation of PF2/6, which is dominated by (intrachain) exciton migration.

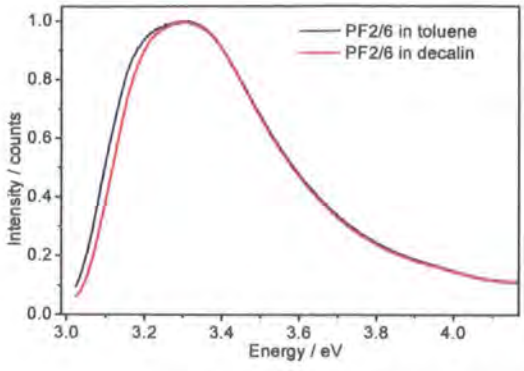

Figure 4-26 – Steady state photoexcitation spectra of 10^{-5}wt./wt. solutions of PF2/6 in toluene and decalin.

How can the solvent dependent relaxation rates be accounted for in a migration dominated scenario? In the following, the unusual implication of viscosity dependent exciton migration is considered. The rate and efficiency of exciton hopping depends on the ratio of uphill and downhill jumps in energy. For a given excitation energy above the localisation threshold, a wider global distribution of excited state energies (DOS) results in a faster initial migration. This agrees with the large Stokes shifts observed for highly disordered conjugated polymers[73] in the solid state.

When a solvent provides little frictional hindrance due to low viscosity, the average deviations of a chromophore from its conformational equilibrium will be larger than in a high viscosity solvent. As elaborated in detail in section 4.1.2., the local distribution of excited state energies is subject to thermal activation. In addition, a wider distribution of molecular conformations increases the disorder of the ensemble of molecules and, hence, the inhomogeneous broadening. In turn, this wider global DOS accelerates exciton migration. Note that one needs to consider the unrelaxed, i.e. ground state, DOS for such an argument. Indeed, the steady state excitation spectrum of PF2/6 in toluene is slightly wider than that of decalin[21], as shown in Figure 4-26. However, it cannot be said with certainty whether the observed small difference suffices to cause a change in the spectral dynamics of the above observed order. To resolve this, it is suggested to carry out a comparison of the temperature dependent behaviour of PF2/6 in toluene and decalin. Both solvents should converge to the same excited state dynamics at their freezing points. With this experiment, one is still unable to separate migrational and conformational components. Nevertheless, the presence of excited state relaxation of a polymer in a dilute frozen solution would underpin the notion of a dominating exciton migration.

To summarise the above, the initial and main component of the excited state relaxation in PF2/6 is found to be too fast to be explained by the long-lived type of conformational relaxation that has been observed in oligofluorenes. Instead, intrachain exciton migration is identified as the dominating process, in agreement with findings on MEHPPV[73]. A picture of viscosity dependent exciton migration is proposed to account for the observed viscosity dependent relaxation rates.

Note that conformational relaxation is not excluded but, as in oligofluorenes, immediately sets in with the excitation of a

chromophore. However, only those conformational components take effect, which can compete with the time scale of exciton migration. This includes in particular the femtosecond bond length adjustment[78] but also the fast fraction of the longer-lived components found in oligofluorenes.

In addition, the efficiency of conformational relaxation will be limited by exciton hopping as it is continuously restarted after each transfer to a new site. Therefore, as long as rapid downhill migration prevails, slow components such as planarisation cannot take effect. For these to occur, an exciton must be immobile, e.g. trapped at a local minimum of site energy. Nevertheless, intrachain migration is restricted by the limited number of chromophores, i.e. the local DOS, on an isolated polymer chain. Thus, even the lowest energy state of this local DOS may offer scope for conformational optimisation. Naturally, the energetic advantage of this process is small compared to the previous exciton migration. In this context, it does not surprise that no significant long-lived red-shift is found in the spectral dynamics of PF2/6. Furthermore, the relaxing chromophore is potentially a large conjugated chain segment. The associated time scale of the conformational optimisation is thus bound to be particularly slow, e.g. equivalent to the relaxation of a larger oligofluorene. In addition, the polymer fluorophores can be restricted at their boundaries, e.g. structural breaks on a chain[74], which may pose a further obstacle to the equilibration of the site geometry. For the future, the investigation of conformational relaxation in such a larger oligofluorene seems a worthwhile experiment in order to obtain an independent estimate of this type of relaxation in the polymer. For this, the oligomer chain length should allow the full accommodation of an exciton but still inhibit exciton migration, i.e. a molecule with 6 to 9 repeat units would be suitable.

Finally, the unusual dynamics of the PF2/6 mode narrowing are considered. For oligofluorenes, both shift and narrowing follow the same exponential decay, which is confirmed by TCSPC data. However, whereas for the polymer the red-shift still follows an exponential decay, whose rate is confirmed by TCSPC, the spectral narrowing evolves with non-exponential dynamics. Here, the width of the 0-0 vibronic only shows an insignificant initial decrease followed by a very long-lived narrowing which continues beyond the end of the red-shift dynamics. In the face of two (instead of one) excited state relaxation processes it can be expected that not all spectral characteristics evolve simultaneously. As to the small initial component shown in Figure 4-22, this is probably not fully resolved by the 13 ps integration window. This is suggested by an additional streak camera measurement in time range 1, where the component is larger

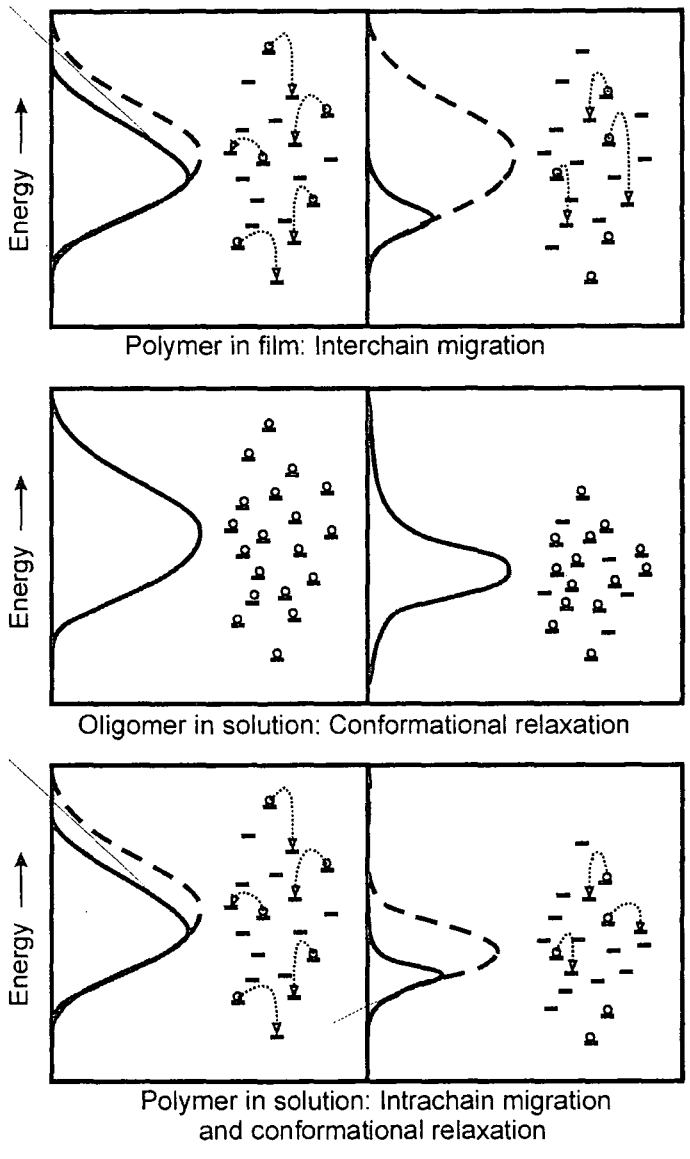

Figure 4-27 – Schematic of the different functions of excited state relaxation within the distribution of excited state energies (DOS) of an ensemble of conjugated polymer or oligomer molecules. The idea of this diagram is adapted from [105]. See text below for further details.

Dashed lines – global (inhomogeneously broadened) Gaussian DOS. Solid lines – distribution of populated sites within the global DOS. Left – initial DOS and population in the initial time regime. Right – DOS and population after relaxation. A selection of exciton sites corresponding to the respective DOS is depicted to the right of each DOS diagram. Bars represent excitons sites at their respective energy. Circles represent excitons, i.e. populated sites. Arrows represent exciton migration to another site.

Top: Exciton migration populates the lower energy states within a static DOS.

Middle: Conformational relaxation moves the entire DOS to a lower energy. The distribution of populated sites and the global distribution of excited state energies coincide.

Bottom: Competition of the individual processes in a polymer chain in solution.

by 50 % (not shown). An interpretation of the extremely fast time scale of these spectral dynamics again involves the increased efficiency of a combined migrational and (subpicosecond) conformational mechanism. Through these processes, the initially larger width of the DOS of PF2/6 in toluene is decreased below that of PF2/6 in decalin, in the fluorescence spectra shown in Figure 4-22. Here, the very slow mode narrowing observed after 100 ps is attributed to the extremely long-lived conformational relaxation described above, which sets in after exciton migration has equilibrated and continues until the final decay of the exciton to the ground state. It must be noted that the data shown in Figure 4-22 exhibit a large noise level. Naturally, TCSPC cannot be used in order to cross-check this finding as it is not sensitive to such subtle spectral changes. As a confirmation it must suffice that both, toluene and decalin solution show a similar behaviour, which is definitely not present in the oligofluorene data.

To summarise this discussion, the measurements confirm the previously found[16] viscosity dependent excited state relaxation of PF2/6 in dilute solution. However, the observed picosecond spectral dynamics differ qualitatively from those associated with the purely conformational relaxation in oligofluorenes. Consequently, the relaxation mechanism in PF2/6 must be understood in terms of an interplay between conformational processes and exciton migration, where the latter dominates and limits the overall relaxation rate. Dias *et al.*[16] argued that the migrational contribution can be distinguished by the absence of any viscosity dependence in its rate. However, from the present findings it follows that exciton migration on isolated molecules in dilute solution depends on the viscosity of the solvent. This is conclusively explained by the impact of solvent viscosity on the ground state disorder, which leads to a larger initial width of the excited state DOS in a low viscosity solvent (see Figure 4-26) and, thus, controls the rate of migration. In conclusion, this study shows that conformational and migration processes manifest themselves in very similar spectral dynamics with respect to shift, DOS narrowing and viscosity dependence.

However, these processes are very different in terms of their effect on the density of excited states, as illustrated in Figure 4-27. While exciton migration drives the exciton population to ever lower energy states in a static DOS, conformational relaxation relaxes the DOS itself, ideally leaving the exciton spatially confined. Clearly, an excited state must relax in order to stabilize itself. Nevertheless, the migrational pathway has the side effects of populating quenching sites and promoting bimolecular annihilation (see chapter 2.3). In order to improve the properties of a conjugated polymer in this respect, it is necessary to understand their separate photophysics, driving forces and time scales. As these materials are almost always influenced by both, exciton migration and conformational relaxation (see Figure 4-27), precise

estimates for the separate dynamics of both processes must be obtained from model systems that are similar to the polymer under investigation.

Apart from work on oligofluorenes, a study of pure intrachain exciton migration may be possible via imbedding polyfluorene into an inert matrix polymer, e.g. Zeonex. However, even at the extremely low concentrations used for single molecule spectroscopy, a complete isolation of the polymer chains is hard to achieve and aggregation or other interchain interactions may be present. As an example, Figure 4-28 shows the emission spectra of a sample of pentafluorene in a Zeonex matrix with a dilution comparable to the solution samples (10^{-5} pwt.) – interchain separation is clearly not achieved here as visible from the emission of oxidation defects. The latter are mainly populated via exciton migration[5].

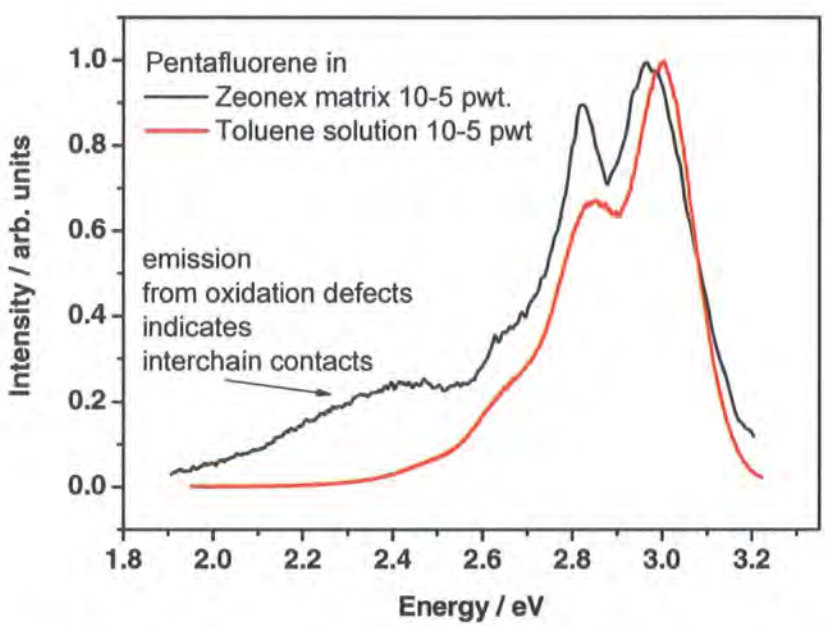

Figure 4-28 – Emission from oxidation defects is found in the fluorescence spectrum of pentafluorene in the matrix polymer Zeonex, indicating that interchain interactions are not inhibited.

4.5. Conclusions

What stands out from this study is the consistent observation of conformational relaxation dynamics in oligofluorenes. The streak camera and single photon counting measurements can resolve picosecond relaxation components. However, about 90 % of the overall Stokes shift eludes detection as it apparently occurs on the sub-picosecond scale. According to the literature, these fast relaxation processes involve solvation[64] as well as bond length changes within single repeat units[78].

On the picosecond time scale, spectral relaxation is entirely conformational: TCSPC decay curves of oligofluorene fluorescence were analysed by re-

convolution fitting and long-time relaxation constants between 6 and 300 ps, i.e. between the detection limit and the singlet lifetime, were extracted. These constants become slower with increasing oligomer size (by 10 to 50 %) and increasing solvent viscosity, in line with a process governed by geometry rearrangement of the emitting fluorophores. Relaxation also slows down at low temperature but this is rate limited by the simultaneous increase of solvent viscosity. Picosecond conformational reorganisation therefore depends on the frictional interactions between the molecule carrying the chromophore and its medium. From the dependence of the relaxation constants on molecular size and the longevity of these constants one concludes that large scale molecular motions dominate on the picosecond scale, involving all repeat units of the studied oligomers. The order of the relaxation constants agrees with what is expected from simulation for torsional reorganisation in polyfluorene[78]. This agrees with a planarisation of the excited fluorophores as proposed in the literature[67, 77]. However, considering its viscosity dependence, such large scale molecular rearrangement is generally irrelevant to excited state dynamics in the solid state.

An experimental study of the impact of conformational relaxation in polyfluorene, e.g. PF2/6, has been lacking for a long time. As oligofluorenes are a small scale model of this conjugated polymer, they close part of this gap. TCSPC data of the PF2/6 fluorescence show similar characteristics as observed for oligofluorenes, including viscosity dependent relaxation constants. In summary, previous findings[16] on excited state relaxation in PF2/6 were confirmed using better time resolution. However, compared to the pure conformational relaxation in oligofluorenes significant differences are observed. First, the relaxation constants in PF2/6 are shorter, e.g. maximal 69 ps in highly viscous decalin. Besides, the dynamics of spectral red-shift and mode narrowing no longer evolve simultaneously, which would be expected for a single relaxation mechanism. This must be attributed to the joint effects of conformational and migrational relaxation for the polymer. Due to their overlapping time scales, the relative contributions of these processes cannot be quantified. Nevertheless, it is clearly observed that exciton migration dominates the overall excited state relaxation and determines its time scale. Only after the equilibration of this process, very long-lived (> 100 ps) conformational components may occur.

As the main conclusion, it must be emphasised that the photophysics of oligofluorenes are not representative for those of polyfluorene as the different chain lengths result in qualitatively different excited state relaxation.

What can be concluded for the conformational relaxation in other conjugated polymers? Already a large variety of relaxation constants is observed if different solvents are used. Other materials not related to polyfluorene show different

degrees of rigidity, different equilibrium dihedral angles, different degrees of coiling and different side chains etc., all of which have an impact on the activity of excited state relaxation. As an extreme example, no excited state relaxation beyond 4 ps is found in the ladder-type MeLPPP, as a result of its rigid chemical structure.

5. The excited state behaviour of a polyspirobifluorene

5.1. Introduction and background

In this chapter, a polyspirobifluorene derivative is studied via time-resolved techniques. Its excited state decay is monitored via femtosecond photo-bleaching, single photon counting (TCSPC), and streak camera as a function of solvent. This study thus ties in closely with the chapter on conformational relaxation in oligo- and polyfluorenes.

5.1.1. Spiroconjugation

One obvious way to optimise the efficiency of polymer light emitting diodes (PLEDs) is the synthesis of new materials. Apart from a high quantum efficiency, important issues are morphological and chemical stability in order to avoid aggregation as well as defect formation such that the loss of excitation energy due to traps can be minimised. Long-time stability is of particular importance to any polymer given that most applications require a lifetime of thousands of hours. An example for the chemical degradation of polyfluorene derivatives involves the oxidation of the fluorene repeat unit into fluorenone, whereby oxygen replaces the two sidechains or hydrogen atoms, respectively, that are substituted at the centre 9-position of the fluorene repeat unit.[4, 106, 107] One successful attempt to increase the chemical stability of this 9-position involves the introduction of a spiro linkage.[6, 17, 18, 108-111] In addition to maintaining the high emission quantum yield of polyfluorenes in solution, spiro-linked side groups reduce aggregation in the solid state. This is due to the large steric hindrance that is generated by the orthogonal arrangement of backbone and side group. As a side effect, the glass transition temperature of spiro-substituted materials is raised rendering electroluminescent diodes made of such materials generally more stable and robust[6, 17].

Commonly, side groups are attached for the purpose of enhancing the solubility of a conjugated polymer and to prevent various kinds of aggregation. Due to a lack of conjugation, they do not interfere with the conjugated orbitals of the backbone, which determine the electronic properties of the material. However, the substitution of a pi-conjugated chemical unit through spiro linkage allows conjugation to spread off the backbone.[112] As in spirobifluorene polymers,[6, 18] such *spiroconjugation* may alter the electronic properties. As a result of the backbone coupling to the side groups, new molecular orbitals for ground and/or in the excited state may be formed, which did not exist at the unsubstituted backbone.[113]

As reported by Wu *et al.*,[6] this can have beneficial effects. Here, a spirobifluorene oligomer was found to exhibit a dramatically increased hole mobility in comparison to a similar fluorene-type oligomer.

5.1.2. Density functional theory and charge transport in polyspirobifluorene

Density functional theory (DFT) is a valuable tool to gain a deeper insight into the molecular orbitals. Via DFT, these complex many-body systems are modelled under the simplifying concept of electron density, which is evaluated via a density functional. The aim of each simulation is to minimise the total electronic energy of the molecular system as this situation corresponds to its equilibrated ground state. Then, the values of the electron density functional can be used to map the ground state wavefunctions of electron and hole, which correspond to the highest occupied molecular orbital (HOMO) and the lowest unoccupied molecular orbital (LUMO), respectively. With an additional variable molecular geometry, optimal conformations can be found in the course of energetic equilibration. Finally, time-dependent DFT is used to model excited states, such as excitons.

Clearly, a good electroluminescent polymer should facilitate good transport and injection properties simultaneously for both electrons and holes in order to achieve balanced charge transport and, thus, high emission quantum yields. In the case of Wu *et al.*,[6] DFT revealed the impact of spiroconjugation on the molecular orbitals. Based on these calculations, the authors concluded that spiroconjugation of the HOMO level facilitates intermolecular hole migration.

Generally, polyfluorenes are considered as hole transporting materials. However, the reverse is observed for the polyspirobifluorene investigated here: In device configuration, it performs better when copolymerised with a hole transporting unit. Therefore, the spiro-homopolymer appears to be an *electron transporting material.*.[114] When comparing the spirobifluorene derivative investigated in this chapter with the oligomer of Wu *et al.*,[6] apparently a minor chemical alteration of the spiro substituent results in a significant qualitative change of the physical properties. It is conceivable that the charge carrier transport of such materials could be optimised or tailored by chemical modifications of the orthogonally attached fluorene side groups. Clearly the combination of potentially tailored charge carrier mobilities, chemically stability, deep blue emission, and absence of aggregation makes polyspirobifluorene a promising material for PLED application. However, as a precondition, the underlying physical processes need to be understood in order to outline the route for further chemical optimization.

5.1.3. Excited state decay measurements

So far, the excited state decay of spiro-conjugated molecules is little investigated. However, it can provide crucial information about the molecular orbitals as shown by Milota *et al.*.[115] These authors investigated the fluorescence decay of a symmetric

molecule with two branches connected via a spiro linkage. Nearly mono-exponential decays were found, revealing little interaction between the two branches of the molecule.

To the best of my knowledge, this chapter presents the first time-resolved study of a spirobifluorene-type polymer. The excited state decay of dissolved polymer chains is measured in the nano- and picosecond domain as a function of solvent parameters such as polarity and viscosity. It is found that the fluorescence decay of polyspirobifluorene exhibits a surprising complexity when compared to common polyfluorene. This is explained by the existence of a wide distribution of the density of excited states (DOS) that is strongly influenced by the side fluorene groups in conjunction with a geometrical relaxation of the excited molecule. In order to support these conclusions, DFT calculations were performed by Dr. Stuart Clark of the University of Durham. These demonstrate that the orthogonally substituted side groups strongly participate in both, the HOMO and the exciton orbitals.

5.2. Experiments

5.2.1. Materials and sample fabrication

The chemical structure of the studied material is given in Figure 5-1. This blue-emitting polyspirobifluorene was synthesised by the Merck OLED GmbH and exhibits a remarkably high molecular weight of 770000 g/mol.[116, 117] The four branched alkoxy chains attached to the fluorene side groups are of particular interest, as will be shown. In the following, this polymer is referred to as M-PSBF.

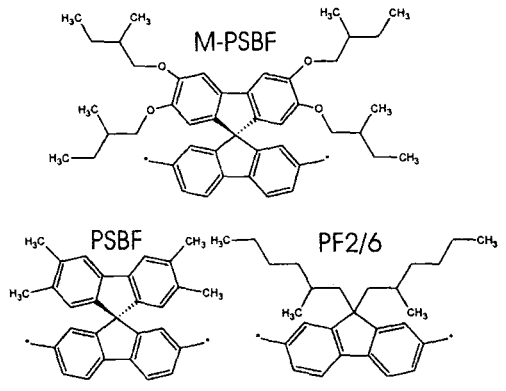

Figure 5-1 – Chemical structures of the investigated materials.

In order to investigate the influence played by the oxygen atoms, an additional, theoretical, version called PSBF is employed for DFT calculations only, where the ethylhexyloxy side chains are replaced by methyl groups. Some of the experimental results were also compared to the archetypical polyfluorene derivative PF2/6 (used here with M_W =160000 g/mol), whose chemical structure is shown in Figure 5-1.

The focus of this chapter lies on the excited state dynamics of M-PSBF in room temperature solutions. The polymer was dissolved in either chlorobenzene, toluene (both from ROMIL) or decalin (Riedel-deHaen). This combination of solvents spans a range in both, polarity and viscosity, that is sufficient to detect dependencies on these parameters. The high molecular weight of M-PSBF required

some care when preparing solutions. First, a master solution was stirred overnight at room temperature and then for another hour at a higher temperature. Information about this solvent specific temperature (up to 90 °C) was provided by the Merck OLED GmbH. Finally, the master solution was diluted to adjust the maximum optical density of the final sample to about 0.1. Toluene solutions of PF2/6 were fabricated to the same optical density stirring for 2 hours without heating. Note that the solutions were not degassed, i.e. oxygen was not removed, prior to any measurement. However, the timescale of the time-resolved experiments below 1 ns justifies this because exciton quenching by oxygen is rate limited by the diffusion of oxygen on the time scale of 1 μs.

In addition, thin films were produced by spin coating. For this, a master solution of 10 mg/mg M-PSBF in toluene was prepared as described above, and then spin coated onto quartz or sapphire discs at a rate of 2500 rpm to a thickness of ~50 nm.

5.2.2. Steady state characterisation

All samples were characterised as to their steady state photo-luminescence and – absorption spectra using a Fluorolog (Jobin Yvon) and a Lambda 19 (Perkin Elmer) spectrometer, respectively.

These steady state spectra were also used to determine the emission quantum yields (PLQY) of the solution samples. This was done using Rhodamine 6G as a standard with a known PLQY of 0.95 in ethanol solution:[118] All spectra are corrected for backgrounds resulting from scattered light and the solvent. Then, the photoluminescence spectrum of an M-PSBF solution is integrated and the integral, I_{MPSBF}, compared to the absorption of the sample at the excitation energy, a_{MPSBF}. This quotient is then set into relation to an analogous measurement on rhodamine 6G, which emits in a similar spectral region. From the known PLQY of the latter, φ_{R6G}, that of the polymer, φ_{MPSBF}, is inferred via

$$\varphi_{MPSBF} = \varphi_{R6G} \cdot \frac{I_{MPSBF}/a_{MPSBF}}{I_{R6G}/a_{R6G}}$$

[Equation 5-1]

The procedure is repeated for a second excitation energy in the main absorption band in order to estimate the experimental error. No significant difference was detected for the different excitation energies.

5.2.3. Picosecond spectroscopy

As in the previous chapter, both streak camera and time-correlated single photon counting (TCSPC) were employed as complementary techniques to monitor picosecond photoluminescence dynamics. The combined experimental setup is described in chapter 3 featuring a time resolution of ~ 1 ps for TCSPC (after re-convolution analysis, using 4096 MCP channels) and 12 ps (22 ps) for the streak camera experiment in time range 2 (4). The spectral resolution was 4 nm.

5.2.4. Pump-probe photobleaching

As will be shown later on, steady state and time-resolved fluorescence experiments did not suffice to explain the excited state behaviour of M-PSBF. This was resolved by comparison with additional pump-probe measurements of the samples' excited state recovery, which were carried out by S. M. King at the University of Durham. A detailed description of this so-called *photobleaching* setup is published in [65].

Briefly, a Mira 900-F Ti:sapphire oscillator (Coherent) and a RegA 9000 Ti-sapphire amplifier (Coherent) are used to generate laser pulses of 180 fs in width at a repetition rate of 100 kHz. The 780 nm output is frequency doubled to 390 nm and subsequently split into a pump and a probe beam. The probe pulse is optically delayed using a Newport IMS-600 delay stage. The excitation beam is reduced to a low dose of ~300 nJ cm^{-2}.[65] Upon excitation of a sample, the transmission, T, of the probe beam is monitored using a silicon photodiode and standard lock-in techniques. The very good signal to noise ratio allows detecting signals of $\Delta T/T$ down to 10^{-6}. A cut-off filter is used to prevent the detection of sample fluorescence. Using a small time increment, the time resolution of this setup is better than one picosecond. Limited only by the length of the delay stage, the time-dependence of the excited state density can be monitored from the subpicosecond to the nanosecond time scale.

5.2.5. DFT calculations

In support of the experimental data, electronic structure modelling of M-PSBF type and PSBF oligomers was carried out by Dr. Stewart Clark of the University of Durham.

For this, a first-principles DFT approach was employed based on the CASTEP algorithm. [119, 120] Electron exchange and correlation interactions were modelled within a generalized gradient approximation (GGA).[121] The method of Vanderbilt was applied to account for electron-ion interactions.[122] Thus, the excitonic state was simulated as well as the HOMO and LUMO orbitals.

In the CASTEP code, a plane wave basis set is employed for the expansion of the valence electron wavefunctions, here, with a cut-off kinetic energy of 450 eV. With this, differences in the total energy of a system can be converged with less than 0.0005 eV per atom. When calculating the electronic structure, the plane wave coefficients are varied as parameters. Finally, the equilibrium geometry of a molecule is approached by simulating the relaxation of the intramolecular forces (the Hellmann-Feynman forces) to less than 0.01eV/Å.

5.3. Results

The above experimental techniques are now employed to compare M-PSBF to the prototypical PF2/6 and, thus, to highlight the peculiarities of the polyspirobifluorene

derivative within the family of polyfluorenes.

5.3.1. Steady state spectra

To begin with, the ground state absorption and fluorescence spectra of both materials are examined for dilute toluene solution. As can be seen in Figure 5-2, the spectra of M-PSBF are red-shifted with respect to PF2/6 by ~ 10 nm. In addition, another absorption band is observed at around 3.7 eV, which is not present in PF2/6. It must be noted that the nature of this feature remains unclear. However, when the spiro polymer is excited at this peak, both, fluorescence spectrum and decay dynamics are unchanged. Therefore, it seems safe to ignore the feature. In summary, M-PSBF and PF2/6 show absorption and fluorescence spectra of similar shapes. Considering only these spectra, one would conclude that M-PSBF is yet another polyfluorene derivative. Compared to PF2/6, the slight red-shift only implies an extended conjugation in both, the ground and the excited state of the spiro polymer.

The next figure, Figure 5-3, focuses on the steady state photo-luminescence and -absorption of M-PSBF in the solvents decalin, toluene and chlorobenzene. As shown in Table 5-1, the former two are of low polarity but differ in their boiling point while the latter two exhibit low boiling points with different polarity. Thus, the effects of viscosity and polarity can be investigated in a qualitative manner. As shown in Figure 5-3 the absorption spectra are similar in all three solvents with only minor spectral shifts or alterations in shape. This implies that M-PSBF exhibits a similar ground state conformation in these solvents. Note that M-PSBF degrades to some degree

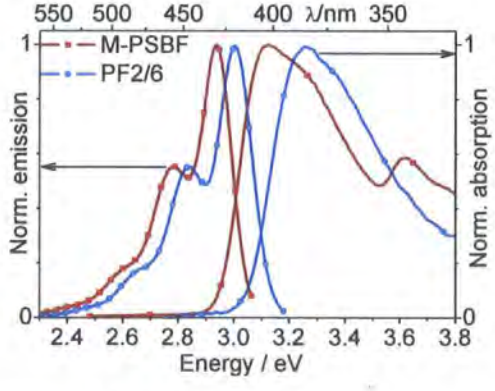

Figure 5-2 – Normalised steady state photo-luminescence and –absorption spectra of M-PSBF and PF2/6 in toluene solution.

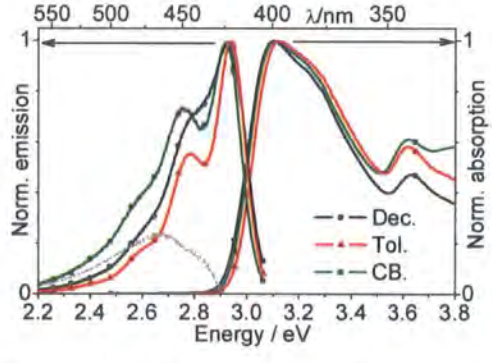

Figure 5-3 – Normalised steady state photo-luminescence and absorption spectra of M-PSBF in solutions of decalin, toluene and chlorobenzene. The grey curve is the difference spectrum between the CB. and Tol. emission. It represents a broad unstructured emission band, probably due to degradation, which contributes to the fluorescence in chlorobenzene.

medium	viscosity [cP]	polarity	decay kinetics [ps]	quantum yield
decalin	3.55	0.11	$t_{½} \sim 300$	0.85±0.04
toluene	0.60	0.017	(0.7) ~20 (0.3) 2300	0.80±0.04
chloro-benzene	0.8	0.14	(0.96) ~20 (0.04) 3000	0.44±0.04
thin film	∞		$t_{½} \sim 100$	0.31

Table 5-1 - Fluorescence lifetimes and emission quantum yields for M-PSBF as a function of solvent. The values in brackets indicate the normalised weighting of the decay components. The solvent viscosities and the polarity (in terms of the Lippert function) are given as well.

in chlorobenzene solution, which manifests itself in a structureless and broad luminescence band centred around 2.6 eV. In particular, the comparably low emission quantum yield in chlorobenzene, see Table 5-1, is attributed to degradation. Otherwise, no significant spectral differences are observed between the chlorobenzene and the toluene solution in spite of their enormous difference in polarity by one order of magnitude. Thus, any polarity induced effects on the excited state of M-PSBF are negligible. On the other hand, the viscosity of the solvent apparently induces spectral changes. In contrast to the low viscosity toluene, the fluorescence spectrum of the highly viscous decalin appears with poorly resolved vibronic modes. Temperature dependent measurements outside the scope of this chapter have shown that a reduced solution temperature affects the fluorescence spectrum in a very similar way.[123] Therefore, the observed spectral change is indeed caused by the change in solvent viscosity. With the knowledge acquired during the previous chapter, this influence of viscosity on the excited state conformation of M-PSBF is attributed to some kind of conformational effect which renders the excited state relaxation partly inhibited in highly viscous solvents. In the following, picosecond techniques are again employed to reveal this process in the fluorescence dynamics.

5.3.2. Excited state decay dynamics

Raw data. Figure 5-4, Figure 5-5, and Figure 5-6 present raw images of three streak camera measurements, one on M-PSBF in chlorobenzene, toluene and decalin, respectively. These images have undergone nothing but the standard background and shading correction (see chapter 3) and, yet, they reveal striking qualitative differences between the

fluorescence decays of the three samples. In the low viscosity solvents toluene and chlorobenzene, the dynamics can be divided into an initial and a long time regime. For toluene solution, the initial fluorescence decay occurs within 50 ps. After that, a pronounced long-lived component of > 1 ns dominates the dynamics. Note that a similar pattern is observed for chlorobenzene although here, the long-lived decay is of much weaker amplitude. However, as the extent and type of sample degradation in chlorobenzene is not known, these data will be ignored in the following analysis.

In obvious contrast to the previous, the fluorescence decay of M-PSBF in decalin appears much more homogeneous. Note, that the peak of the M-PSBF fluorescence is not the point of maximum intensity in the image of Figure 5-6 due to the increased scattering of excitation light. This scatter signal, however, is not attributed to the presence of aggregates as all spectra, decay curves and the quantum yield of M-PSBF / decalin solutions are stable with time.

Processing. Similar to the procedures in chapter 3, the above raw images are further processed. The spectral shift of the 0-0 fluorescence mode is extracted by calculating its centre of gravity, CG. For each time-resolved spectrum, a symmetrical region of the 0-0 mode was selected, from which CG(t) was calculated using an Excel routine. In comparison to the Gaussian fitting employed in chapter 3, this method has the advantage that more points in time can be evaluated. This is particularly important for a correct representation of the different *types* of decay kinetics in the three solvents. Furthermore, the fluorescence intensity is integrated over the entire

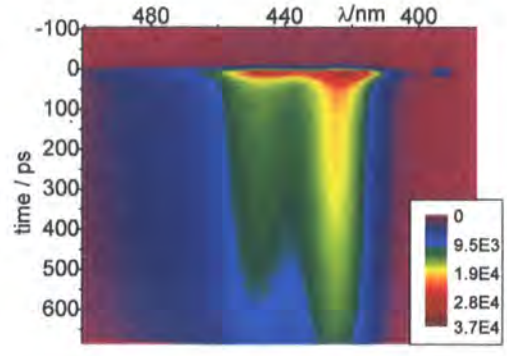

Figure 5-4 – Streak camera image of the fluorescence of M-PSBF in toluene solution. Note the excitation scatter at 390 nm/0 ps. The colour code represents the fluorescence intensity at each pixel.

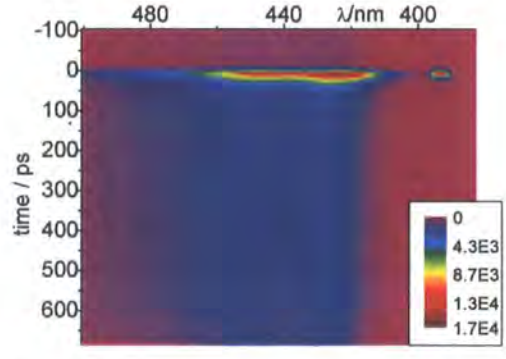

Figure 5-5 – Streak camera data of M-PSBF in chlorobenzene solution.

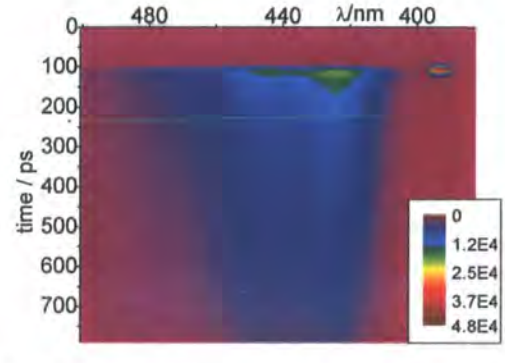

Figure 5-6 – Streak camera data of M-PSBF in decalin solution.

spectrum (excluding the excitation peak) and plotted as a function of time, I(t). Thus, CG(t) and I(t) are calculated for toluene and decalin solution.

Furthermore, as indicated in chapter 3, decay kinetics can be obtained via TCSPC with a higher signal to noise ratio. This renders the TCSPC data more suitable for re-convolution analysis, resulting in a better time resolution. However, one must always bear in mind that the deconvolution mode used here only allows to fit to a sum of exponential decays, which may be a rather crude approximation of the real decays. Such deconvoluted TCSPC fluorescence decays will be shown in the following for M-PSBF in the three solvents, on double logarithmic scales. These and the above streak camera data are recorded from the same samples.

In addition to the M-PSBF data of streak camera and TCSPC, analogous data were recorded from a toluene solution of the prototypical polyfluorene, PF2/6, under similar conditions. This is done in order to compare the different polyfluorene derivatives but also to validate the experimental methods.

Kinetics. As is widely known, PF2/6, like other polyfluorenes, exhibits a nearly mono-exponential decay of the spectrally integrated fluorescence with a time constant of ~380 ps,[106] and a decay pattern that only quantitatively depends on the solvent. Corresponding TCSPC and streak camera data are shown in Figure 5-7 as well as in Figure 5-9 further below. Note that all streak camera data in this thesis are not deconvoluted from the response of the laser scatter, which leads to a "bump" at ~50 ps.

In contrast to this, the fluorescence kinetics of M-PSBF are more complex and qualitatively depend on the solvent: The M-PSBF fluorescence in highly-viscous decalin solution decays significantly non-exponentially. No distinct time constants can be identified except for an estimated half-life of about 300 ps. In striking contrast to this, the low viscosity solvents chlorobenzene and toluene lead to a pronounced fast component of a few picoseconds, which the data fail to reproduce in its entirety in spite of deconvolution. This was found by a comparison of data obtained with a better raw time resolution < 7 ps (streak camera time range 1), where the weight of the short-lived component was significantly increased (not shown) compared to the

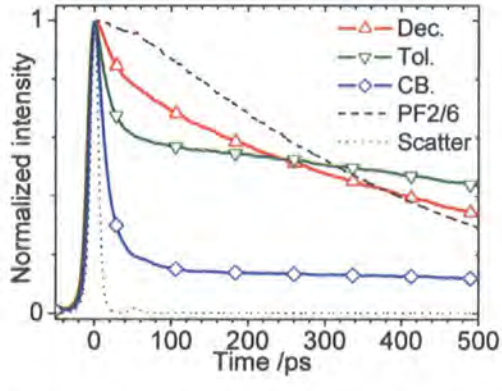

Figure 5-7 – Normalised fluorescence decay curves recorded via streak camera from M-PSBF in the three solvents and PF2/6 in toluene. The dotted line gives the typical scatter reference of the measurements. Data are extracted from Figure 5-4, Figure 5-5, and Figure 5-6 respectively.

TCSPC raw data. Otherwise, the experimental data of the different detection techniques agree very well.

In the TCSPC data shown further below, the fast component accounts for 70 % of the M-PSBF decay in toluene and 96 % in chlorobenzene solution. The remaining fluorescence is emitted at a much slower rate with a mono-exponential lifetime of more than 2000 ps, i.e. 2300 ps for toluene and 3000 ps for chlorobenzene. Note that another reason for employing the TCSPC experiment in the quantitative analysis of the decay kinetics was the large difference in the observed components. Whilst the initial decay touches the streak camera limits of time-resolution in time range 2, the long-lived decay slightly exceeds the maximum viewable time window of 2.1 ns in time range 4. The images taken in time range 2 therefore represent a compromise that allows a qualitative visualisation of the problem.

Quenching. Instinctively, one attributes the above fast component to excited state quenching, particularly thinking of degradation due to a chlorinated (and probably stabilised) solvent such as chlorobenzene. However, toluene is a standard inert solvent. To resolve this matter, the presence of a fast quenching process is investigated through the PLQY of a sample. Translated into the context of fluorescence kinetics, the long-lived component could be interpreted as the intrinsic, unquenched excited state lifetime of M-PSBF. The short component might represent a quenching process. If this was the case, then the weight of the long component should match the PLQY, i.e. values of less than 40 and 10 % are expected for toluene and chlorobenzene solution, respectively. The PLQY data measured for the three types of solution are given in Table 5-1. Even considering generous error margins, the PLQYs for toluene and chlorobenzene significantly exceed the expectations, i.e. the weight of the long-lived component. Clearly, the initial fast fluorescence decay cannot be attributed to excited state quenching.

Red-shift. Another important outcome of the above spectral analysis are the dynamics of the fluorescence red-shifts, CG(t), which are plotted in Figure 5-8 for the first vibronic mode. Apparently, CG(t) follows a pattern that is strongly correlated to the different decay regimes found above. For the low viscosity toluene solution, a rapid red-shift accompanies the initial fast

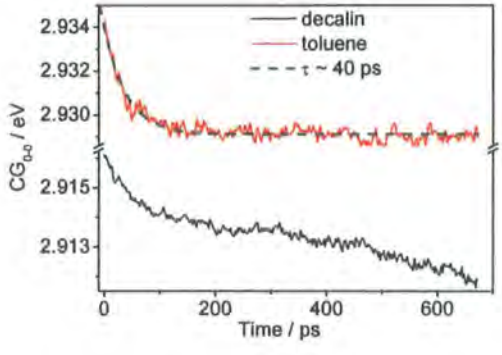

Figure 5-8 – Centre of gravity (CG) shift of the 0-0 fluorescence mode for M-PSBF in toluene and decalin solution extracted from the data in Figure 5-4, Figure 5-5, and Figure 5-6, respectively. The dashed line is a mono-exponential fit of 40 ps as a guide of the time scale. Note, the data are not deconvoluted from the system response.

fluorescence decay. Within the experimental errors, no further shift occurs during the long-lived monoexponential tail. However, the fluorescence spectrum of M-PSBF dissolved in decalin shifts continuously, which is again correlated to the absence of any distinct exponential decay regime.

5.3.3. Photobleaching results

Figure 5-9 displays the fluorescence decay of M-PSBF in toluene solution. The photobleaching data of an identical sample are also shown for comparison. Note that the fluorescence signal is proportional to the density of only the emissive singlet excitons, i.e. it represents the differential change of that proportion of excitations which decay radiatively. In contrast to this, the photobleaching signal is a measure of the overall density of excitations that have not yet decayed back to the ground state. Thus, with photobleaching one monitors the singlet exciton but additionally also all intermediate states, whether decaying radiatively or not. This includes, for example, triplet excitons and charge states. If the singlet exciton was the only excited state then any change of the singlet density would be equivalent to a change of the overall excitation density. Hence, the signals of fluorescence and photobleaching would show identical decay kinetics. This is the case for PF2/6 [65] and other common polyfluorenes, apart from a minor modification which arises from the formation of triplet excitons via intersystem crossing.

For the polyspirobifluorene derivative, the fluorescence signal decays clearly faster than the photobleaching, see Figure 5-9. This deviation implies that an additional metastable state is present apart from the singlet exciton. As both experiments excite M-PSBF in its main $S_0 \rightarrow S_n$ absorption band, one concludes that the singlet exciton transfers to this second state in addition to the common non-radiative and radiative transitions to the ground state. This may be accomplished either by Förster energy transfer or, alternatively, via some specific conformational relaxation of the chromophore.

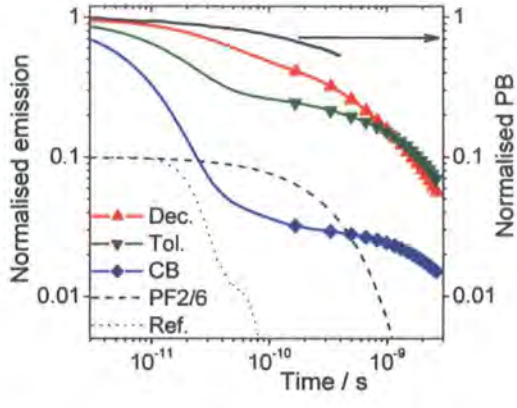

Figure 5-9 – Normalised M-PSBF fluorescence decays as observed by TCSPC in the three solvents on a double logarithmical scale. These are not raw data but the results of the re-convolution analysis. The dotted line represents the corresponding scatter reference and the typical fluorescence decay of PF2/6 in solution is included as a mono-exponential decay of 370 ps (both offset by a factor of 10). The photobleaching (PB) signal of M-PSBF in toluene solution is shown for comparison (black line).

In the latter special case, the relaxed conformation is associated with a decreased decay rate. In any case, the initial fast fluorescence decay has no analogue in the photobleaching. Hence, this component does not represent a decay to the ground state, but a transfer of excitations to a relaxed or an electronically different excited state of slower decay rate.

Note that the above conclusion can be drawn in spite of the imperfect temporal overlap between TCSPC and photobleaching data, see Figure 5-9, which arises from limitations of the femtosecond experiment. Nevertheless, the overlap is sufficient to cover the initial time regime, which is of interest here.

5.3.4. Solid state data

In addition to the above experiments on M-PSBF solutions, analogous measurements were carried out on thin M-PSBF films spun from toluene solution. One expects from the viscosity dependence of the solution data that the solid state acts like a decalin environment, being an extreme case of high viscosity.

Figure 5-10 shows a streak camera image of a film fluorescence decay under photo-excitation at 370 nm, in the main polyfluorene absorption band. The slight deviation from the 390 nm excitation in the solution experiment is of no importance as is lies still in the main absorption band. When comparing the above to the images recorded from the solutions, then obviously the film fluorescence decays much faster and entirely happens within the first 500 ps. For a more detailed analysis, fluorescence decay curves and time-resolved spectra are extracted from the shown data as well as the spectral dynamics of the first fluorescence mode. Note that for the latter the centre of gravity was calculated from Gaussian fits of the 0-0 mode. These provide a better accuracy compared to the previous method, which is required for the low signal intensity of the later spectra.

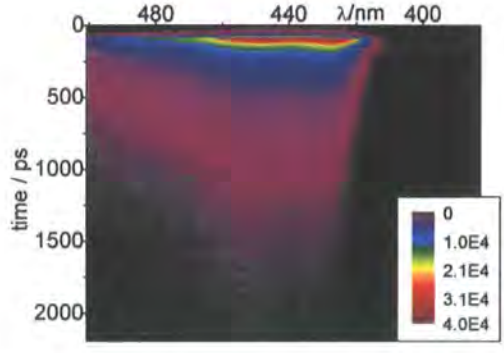

Figure 5-10 – Streak camera image of an M-PSBF film, excitation at 370 n. Collection in time range 4 with a resolution of 20 ps.

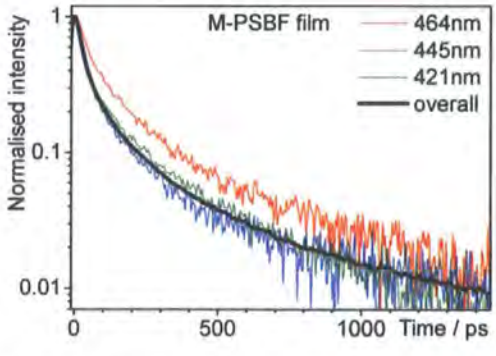

Figure 5-11 – Decay profiles extracted from Figure 5-10 on a logarithmical intensity scale; wavelengths are indicated. The black line is an integral over the entire spectral range. These data are not deconvoluted from the system response.

Figure 5-11 shows the raw fluorescence decays at various wavelengths as well as an integral over the entire spectrum. As can be expected from the complex solution data and additional interchain components in the solid state, these curves are not exponential, not even in the long-lived region (note the semi logarithmical presentation). For comparison, the fluorescence decay in a thin film of PF2/6 can still be fitted to a monoexponential decay with characteristic times of the order of <200 ps. Again, one can ask the question whether the accelerated and non-exponential decay of M-PSBF reflects some kind of non-radiative decay path. However, the PLQY of such thin films has been measured by the provider of the M-PSBF to be 0.31, which is very similar to that of PF2/6 films. Therefore, as in solution, one infers the population of an intrinsic excited state with lower decay rate, which is consistent with the photobleaching results presented below. Initially, excited states transfer to or relax into these sites and then decay radiatively at a slower rate. In this context, the long-time fluorescence kinetics of M-PSBF are still notably slower than the exponential decay of PF2/6 in solid state and even in solution.

Naturally, in the solid state this simple picture, which describes the solution environment, will be additionally complicated by the migration of excitons. In this context, Figure 5-12 shows the time-resolved spectra of the film fluorescence. Compared to the solution spectra they are red-shifted by several 10 meV. This

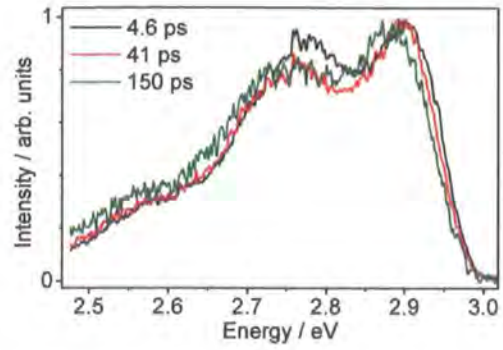

Figure 5-12 – Time-resolved spectra extracted from Figure 5-10. Note the spectral shift and change of Huang-Rhys parameter.

behaviour is observed for commonpolyfluorenes as well and is an expression of interchain contributions to the excited state relaxation, see chapter 3. Hence, these processes – essentially interchain exciton migration – proceed normally in M-PSBF films as compared to other polyfluorenes.

Besides, the time-resolved spectra of Figure 5-12 show a faster decay at the high energy side of the spectrum compared to the red tail. This indication of spectral dynamics is further confirmed in this figure as a red-shift of the centre of gravity of the first fluorescence mode. While such spectral relaxation is common in all polymers that exhibit a Stokes shift between absorption and emission energy, the previous experience with solution samples suggests that the red-shift is partially caused by an additional specific relaxation or a second excited state of lower energy. Unfortunately, due to the high error levels in Figure 5-13, one cannot tell whether or

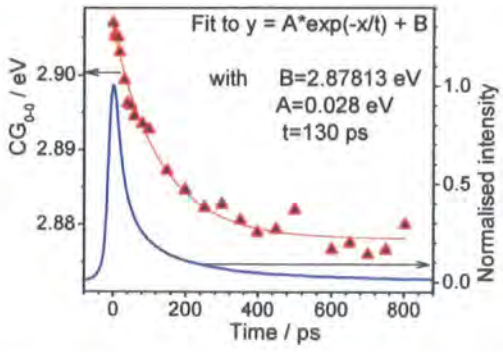

Figure 5-13 – The shift of the centre of gravity (CG) of the 0-0 vibronic of Figure 5-10 with an exponential fit (parameters shown in the legend). The integrated fluorescence decay is shown for comparison. These data are not deconvoluted from the system response.

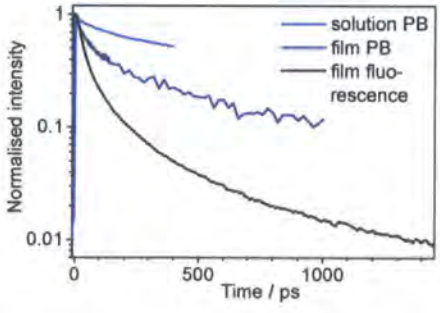

Figure 5-14 – A comparison of the integrated fluorescence decay of Figure 5-13 with the corresponding photobleaching (PB) data and PB data of a toluene solution of M-PSBF from Figure 5-9, all excited at 390 nm.

not the red-shift dynamics are exponential, i.e. whether they match the PF2/6 or the M-PSBF fluorescence decay. Note that the time scale of 130 ps given in Figure 5-13 overestimates the true time scale of the dynamics due to the use of raw data in the analysis. Furthermore, the actual amount of the shift (28 meV) is significantly larger than that observed for solutions (~7 meV) and this in spite of the fact that the streak camera experiment is unable to fully resolve the initial spectral dynamics in both cases. In fact, given the fast decay of the solid state fluorescence the overall red shift certainly is even larger than 28 meV. Again, this larger red shift is consistent with an additional migration activated relaxation towards low energy sites, which is not present to this extent in solution. This may also explain the noticeable reduced solid state quantum yields as compared to solution 0.31 versus 0.81, in terms of migration activated exciton quenching at impurity or chain defect sites. Due to this mutual relaxation by migration and other intrinsic processes, which are specific to this polyspirobifluorene, the information obtained from the solid state cannot be interpreted as straightforward as the solution data.

As above, the fluorescence decay is now compared with a corresponding photobleaching (PB) experiment. For purpose of comparison the solution photobleaching is shown as well. Compared to the corresponding thin solid film data, the latter dataset decays noticeably slower, which certainly reflects the increased emission quantum yield of the solution compared to the solid state. Again, the time resolutions and coverage of both measurements are different but their overlap suffices to make an important observation, i.e. the large deviation between both data sets. Considering that the intersystem crossing yield in this material is less than 0.1 in the solid state[65] this difference is not only due to triplet excitons but must also be explained by the presence

of another intermediate state (with a slower decay rate), which is populated from the initially excited state in analogy to the above argumentation for M-PSBF in toluene solution. Naturally, there will be differences between a film and a solution environment but, speaking of the same material, the type of the second or relaxed emissive state is bound to be the same in both cases.

5.3.5. Electronic structure calculations

As elaborated above, the chemical structure of a material obviously affects its electronic properties. To directly assess the impact of the alkoxy side groups on the photophysics of M-PSBF, DFT calculations of the exciton wavefunction have been performed by Dr. S. Clark.

For simplicity, the alkoxy groups are ignored to begin with and a chromophore-sized spirobifluorene oligomer of five PSBF repeat units is investigated, see Figure 5-1. This oligomer is identical to the material investigated by Wu *et al.*,[6] apart from its length, i.e. five instead of three repeat units. Of this molecule, the highest occupied (HOMO) and the lowest unoccupied (LUMO) molecular orbitals are calculated, starting from the optimised molecular conformation.

The results shown in the upper part of Figure 5-15 do not reveal any surprising features. The HOMO as well as the LUMO orbital of the PSBF pentamer are largely confined to the polymer backbone. This behaviour is also typical for any "normal" polyfluorene derivative such as PF2/6. The only, albeit weak, component of spiroconjugation can be seen in the LUMO orbital, which slightly extends into the orthogonally attached fluorene side groups. This effect was also observed by Wu *et al.* in their DFT study on the spirobifluorene trimer.[6]

As a next step, analogous calculations are performed on an M-PSBF pentamer in order to estimate the influence of the oxygen atoms in the side groups. Note that, for simplicity, the branched ethylhexoxy chains are truncated to methoxy groups. This truncation does not cause any significant alteration in the DFT results, since no electron donating or withdrawing but only saturated bonds are affected. Apparent from the middle part of Figure 5-15, the M-PSBF LUMO orbital again extends only slightly into the side groups. The HOMO orbital, on the other hand, displays an enormous impact of the inserted oxygen atoms. For M-PSBF, a significant part of it now extends into the fluorene side groups, giving a clear impression of spiroconjugation.[113] In conclusion, the strength of spiroconjugation depends sensitively on the precise molecular structure. Such large effects upon comparably small chemical modifications have been observed by Lee *et al.*[17] also for alkoxy substituted poly-spirobifluorenes. Furthermore, one can now set the

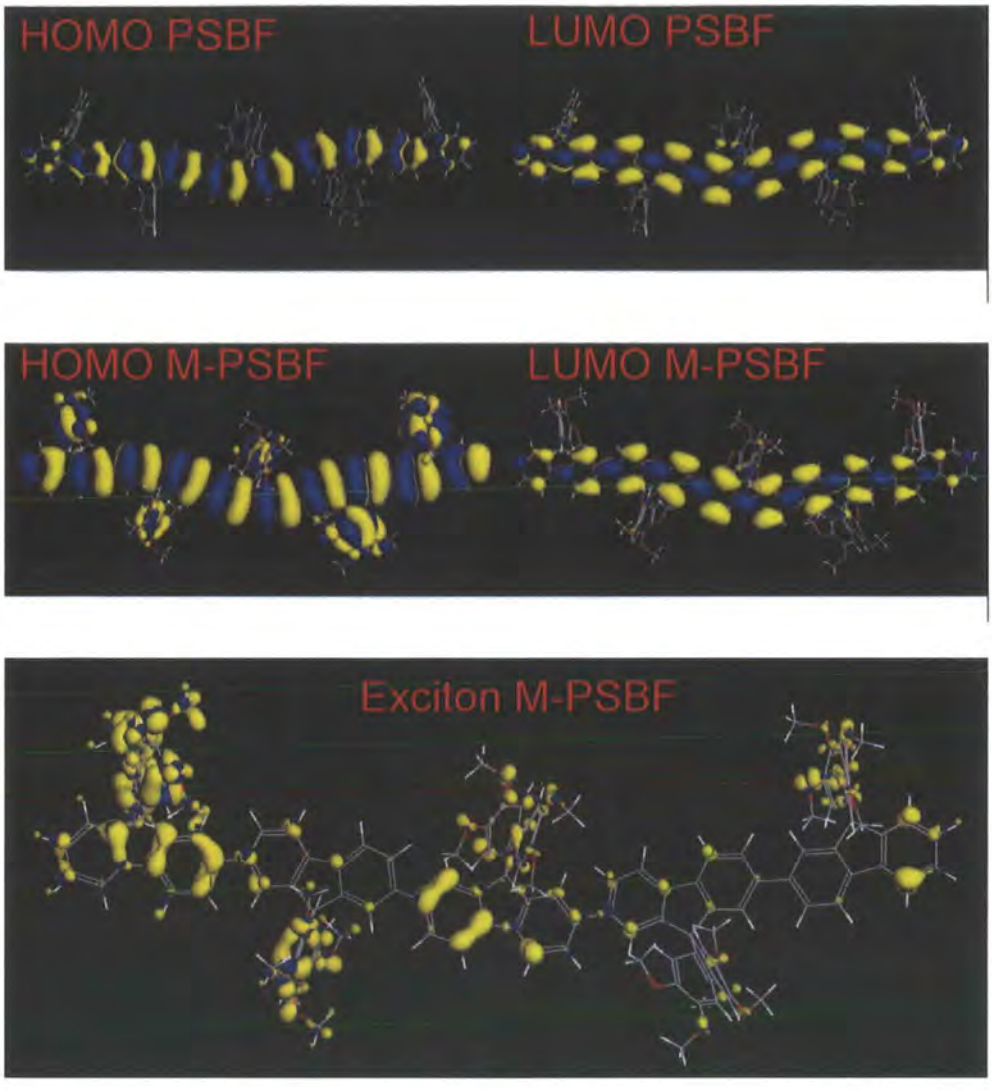

Figure 5-15 - Results of DFT calculations for PSBF (top) and M-PSBF (middle and bottom).

experimental data in context to the DFT results. Here, it seems plausible that the systematically extended conjugation of the ground state gives rise to the red-shifted spectra of M-PSBF when compared to PF2/6, as visualized in Figure 5-15.

As a final step, the excitonic state of M-PSBF is now considered, i.e. the situation that one electron is promoted from HOMO to LUMO orbital. DFT was then used to calculate the change in electron density resulting from this transition. This calculation is the most relevant for comparison to reality as the previous spectroscopy experiments do only probe the excited state of M-PSBF. In the lowest part of Figure 5-15, the computed electron density is shown to visualise the wavefunction of the exciton. Clearly, it has a component that extends into the fluorene side groups. In contrast to this, common polyfluorenes such as PF2/6 do not exhibit such a component simply due to the lack of conjugated side groups. Thus, the electronic structure of M-PSBF is qualitatively different in both, the ground and the excited state.

Note from Figure 5-15 that the exciton wavefunction of the M-PSBF pentamer is highly asymmetrical. This probably reflects the self-localisation of the excited state in terms of chapter 3: The electronic excitation and the molecular conformation are inseparable and react to each other's changes. As already inferred from the above experimental decays in different solvents, conformational relaxation seems to be operative in the excited state. Translated into DFT calculations, these yield the energetically lowest molecular configuration of the excited state. In can in principle be modeled similar to the ground state configuration by optimizing the positions of all atoms with respect to the overall energy of the system. Unfortunately, M-PSBF was too large to put this calculation into practice, which might have unveiled some geometrical distortion of the orthogonally attached fluorene-alkoxy groups in the relaxed excited states. Note, in this context, the data shown in Figure 5-15 (especially the exciton orbital) already consumed several hours of time on the powerful Durham University Parallel machine.

5.4. Discussion

5.4.1. Properties of the second excited state

To summarise the above, M-PSBF solutions exhibit clearly non-exponential fluorescence decays. This behaviour contradicts the decay kinetics of all other known polyfluorene derivatives, which are essentially monoexponential. Nevertheless, high emission quantum yields are obtained from M-PSBF. Therefore, the fluorescence dynamics cannot be attributed to a simple non-radiative quenching mechanism. The same conclusion is reached when comparing analogous data of M-PSBF and PF2/6 in their solid state.

Secondly, the deviation between the above fluorescence decays and corresponding photobleaching data clearly reveals the transfer of the initially excited singlet exciton into another metastable species, which is not simply the triplet exciton. A large fraction of the initially excited states transfer to this intermediate instead of decaying directly to the ground state. Thus, one infers that this second or relaxed metastable state must be of lower energy than the initial singlet exciton. It must also contribute to emission, as shown by the high emission yields in both film and solution. For this to occur, two possibilities are conceivable: back transfer from the intermediate to the original singlet exciton or direct radiative decay to the ground state. In the face of the fast transfer to or relaxation into the second state, the former seems unlikely, i.e. the transfer appears to be exothermic. In conclusion, the initially emitted fluorescence is attributed to the initially

excited singlet whereas any long-lived components correspond to the state of lower energy. This, in turn, implies that the energetic separation between the two states is rather small, i.e. some 10 meV, as is inferred from the modest dynamic spectral shifts in solution. Also, the spectral shapes are very similar, such that the energy shift must arise from a very minor modification of the chromophore. From this point of view, the observed phenomenon appears to be similar to the conformational relaxation of oligofluorenes in chapter 3. Consequently, explanation will be sought in the picture of relaxation rather than considering two entirely different excited states.

However, the pattern of the M-PSBF fluorescence kinetics is very different to the relaxation observed in common polyfluorene derivatives, with particular respect to the extremely long-lived component in toluene and chlorobenzene. The latter implies that despite its similar fluorescence spectrum, the second emissive state is much more stable once it is established.

In the following, two alternatives to the relaxation scenario are briefly discussed, which involve a true second excited state. However, these can safely be ruled out:

An intrachain charge transfer state. This type of excitation requires a polar chromophore. Polarity may be introduced by the oxygen atoms of the side groups. As shown by the DFT results, their electron affinity suffices to draw a part of the exciton wavefunction off the polymer backbone. Due to its polarity the emission spectrum and decay kinetics of a charge transfer state depend on the polarity of the medium. However, as no significant change is observed when comparing toluene and chlorobenzene solution, the presence of a charge transfer state in M-PSBF is excluded.

Excimer formation. This process depends on interchain interactions and is, thus, also rate limited by the solvent viscosity. However, the time scale for macromolecular diffusion is expected to be much slower than the initial fluorescence decay in low viscosity solvents. Moreover, excimer formation is a comparably irreversible process. Therefore, one would expect at least a very small long-lived decay component also in the highly viscous decalin, which is definitely not observed. Also, the interchain interactions leading to excimer formation are most likely mediated by the polarity of the side groups as these dominate the DFT results. Thus, one expects the process to depend on the polarity of the solvent, which is again not observed. Finally, any aggregation phenomena should be strongly pronounced in the solid state. Here, the very long-lived component (attributed to the stabilised aggregate state) would increase compared to solution, which is again at odds with the experimental observations.

Arguments in favour of conformational relaxation. In addition to the similar spectral shapes and small energetic shift between initial and final state, the viscosity dependence of the M-PSBF fluorescence dynamics indicates that structural relaxation is involved in the formation of the second metastable state. In this context, the M-PSBF exciton wavefunction of Figure 5-15 is calculated for the optimised ground state conformation only. This is by no means also the lowest energy geometry of the excited state, i.e. structural relaxation will almost certainly be operative. To be precise, this does not necessarily mean the type of torsional relaxation observed in chapter 3. Naturally, the latter process also occurs as is inferred from the nonzero Stokes shift and the flexible single bonds that join the repeat units. However, torsional relaxation may merely lead to the localisation of the exciton and cannot drastically alter the nature or lifetime of a state. In addition, chapter 3 has shown that the above macromolecular relaxation happens on a time scale of hundreds of picoseconds. In contrast to this, the observed few picosecond fluorescence decay intuitively corresponds to a process on a smaller spatial scale than the conformational rearrangement of several repeat units. At this point, it helps to draw parallels between the exceptional fluorescence dynamics of M-PSBF amongst other polyfluorenes and the pronounced spiroconjugation found by DFT calculation. The latter point out the significance of the alkoxy side groups, which implies that these constitute an important part of the relaxed state. In detail, their coupling to the exciton wavefunction might be modified via a specific type of conformational relaxation. Considering the invariable orthogonality between backbone and fluorene side group, most likely a scissor-like distortion of the spiro bridge will occur upon excitation. This was suggested by the manufacturing chemist at the University of Karlsruhe. As said above, unfortunately limitations in the calculation power prevent one from actually obtaining the relaxed excited state configuration using DFT.

5.4.2. Interpretation of the excited state dynamics in solution and solid state

A scenario of conformational relaxation, which consistently accounts for all experimental observations, is described in the following. Note that, throughout this thesis, the term DOS refers to the distribution of the excited state energies of an ensemble of chromophores. In an inhomogeneously broadened system such as a conjugated polymer, the DOS is a Gaussian.

M-PSBF is now pictured using two basic assumptions.

1. Compared to common polyfluorene derivatives, the width of the inhomogeneously broadened DOS of M-PSBF is larger due the spiro conjugation of the side fluorene groups that introduce a further distributed variable into the energy of the excited state via a scissor-like movement of the orthogonally attached side groups.

2. The decay rate of the excited states is a function of their corresponding energy, such that higher energetic excited states decay faster.

The general picture in mind is that, initially, the distance between side group and backbone is distributed randomly in the ensemble of ground states. Upon excitation, this translates into different degrees of spiroconjugation and, hence, in a wide distribution of excited state energies. A large distance renders any influence of the spiro linkage on the backbone electron density inefficient. In this decoupled case, the radiative decay rate should correspond to that of PF2/6, i.e. 350 ps. The other extreme situation involves the side fluorene groups in perfect geometric position for strong spiro conjugation, i.e. rather close to the backbone. Conjugation spreads into the side chains and the excited state is stabilised relative to a "common" backbone state, which is associated with a decreased energy and decay rate. Thus, initially, there will be excited states with high and low energy (and corresponding decay rates), which coexist in a wide DOS, as indicated in Figure 5-16.

In a high viscosity solvent, this DOS is static, since no or little geometric rearrangement of the atoms is possible within the lifetime of the excited state. As schematically depicted in the upper part of Figure 5-16, in this case the excited state density red shifts continuously as a function of time, as a consequence of the higher decay rate of the high energy tail of the DOS. This continuous shift is consistent with the experimental observations for decalin solution. Furthermore, in this scenario there will always be a mixture of

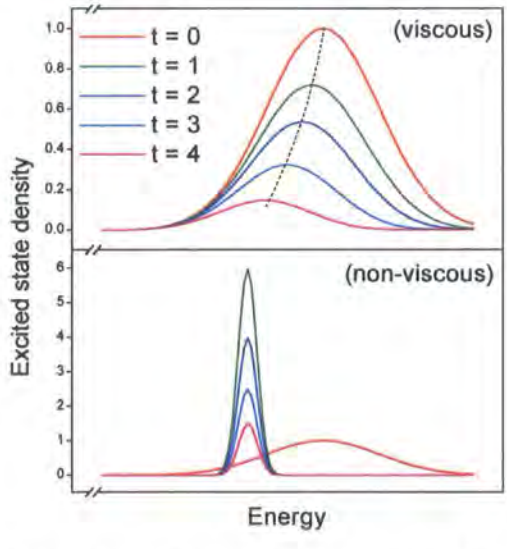

Figure 5-16 Schematic representation of the distribution of excited state energies (DOS) as a function of time for viscous and non-viscous solvents as indicated. The dashed line indicates the centre of the DOS, which is a measure of the red shift.

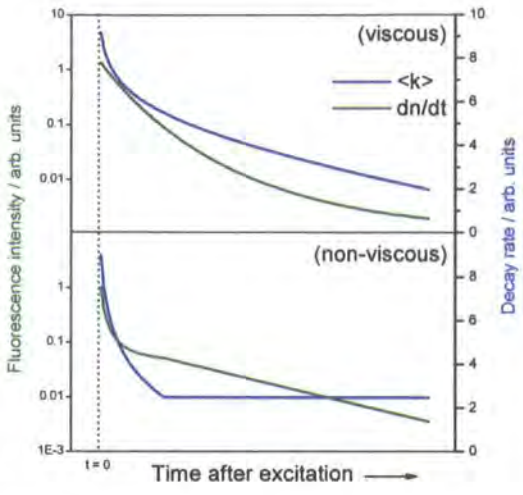

Figure 5-17 – Schematic of the average decay rate, <k>, and the semi logarithmical fluorescence decay as a function of time for viscous and non viscous solvents.

high and low energy – i.e. fast and slow decaying –excited states albeit the ratio of both changes towards the latter with increasing time. As a consequence, the decay rate is never constant but dispersive, and the observed fluorescence decay is non-exponential at all times, which is again consistent with experimental observations for decalin. The average decay rate and the fluorescence are schematically shown as a function of time in the upper part of Figure 5-17.

Geometric rearrangement, however, is allowed in non-viscous solvents. This may be achieved via a scissor-like movement of the spiro link. Thus, at low viscosity, the molecule quickly adopts the lowest energetic excited state configuration. Note that the rate and degree of this relaxation will not only depend on the viscosity of the solvent but also on the local environment of the chromophore. Therefore, although each individual excited state adopts its local minimum of energy, the macroscopic ensemble, which is probed by fluorescence spectroscopy, still exhibits some degree of inhomogeneous broadening, albeit less than the initially excited ensemble. As schematically shown in the lower part of Figure 5-16, this leads to a time dependent ensemble DOS that quickly narrows and shifts to the low energy tail of the original DOS at time zero. This narrow DOS is associated with a single - the lowest - excited state configuration, which also exhibits a single – slow - decay rate. Again, all of these assumptions are qualitatively reflected in the data for toluene and chlorobenzene. Here a spectral red shift only occurs during the initial phase. Furthermore, the fluorescence decays mono-exponentially with a slow rate after the fast relaxation. Schematically, the average decay rate and

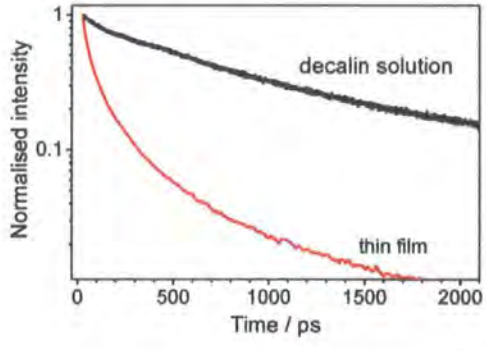

Figure 5-18 – Semi logarithmical presentation of the normalised fluorescence decays of a thin M-PSBF film (from streak camera, time resolution 22 ps) and of an M-PSBF/decalin solution (TCSPC, time res. 22 ps).

the fluorescence as a function of time are depicted in the lower part of Figure 5-17.

In a thin film, the DOS is static as in a high viscosity solvent and, therefore, one expects a similar behaviour of the fluorescence decay, which is, indeed, non-exponential. The observed spectral shift continues at least up to 500 ps, see Figure 5-13.

However, Figure 5-18 contrasts the fluorescence kinetics in thin film and decalin solution, where clearly the latter decays more slowly. This is understood when considering that, in the film, interchain interactions enable a further path of excited state relaxation. Although the DOS does not change with time, exciton migration aids the transfer of states to sites in the film that happen to be in a favourable low energy configuration. These sites then exhibit a higher time of residence while unrelaxed excitons in a high energy conformation tend to continue their migration until they have reached a site of lower energy and eventually get trapped. Qualitatively, the outcome is the same as in decalin solution. However, as thin film relaxation is caused by migration activated relaxation it is quantitatively much faster compared to the situation in solution.

5.5. Conclusions

In this chapter the photophysics of a polyspirobifluorene derivative, M-PSBF, are investigated in solution and solid state. As a chemical particularity, this material exhibits alkoxy groups attached to the fluorene side groups. The excited state dynamics of M-PSBF stand out amongst the family of polyfluorenes. Its fluorescence kinetics display a non-exponential pattern, which qualitatively depends on the viscosity of the medium, as do the fluorescence spectra. These unusual observations are explained by a specific excited state relaxation mechanism. M-PSBF exhibits a wider DOS than common polyfluorenes, which involves the side groups via spiro conjugation. The strength of the spiro conjugation, and, consequently, the energy of the excited state, is distributed by an angle or bend of the side groups relative to the backbone. And electric relaxation, if not prevented by highly viscous solvents, essentially drives this conformation into its optimum position.

Thus, this process, which is unknown in detail, works to increase the spiroconjugation, i.e. the coupling of the fluorene side groups. Its absolute strength is critically linked to the electron affinity of the alkoxy substituents, as confirmed by *ab initio* electronic structure calculations, which demonstrate that a significant spiroconjugation of the molecular orbitals only occurs when alkoxy substituents are

present in the side groups. Remarkably, the original function of these substituents was to enhance the solubility of the polymer. Apparently, very subtle chemical modifications can induce qualitatively different photophysics in a polyspirobifluorene. In the literature, similar effects are known for the attachment of hetero atoms to the fluorene side groups and alkoxy groups to the polymer backbone.[17, 18]

Thus, in the interest of PLED optimisation, it seems worthwhile to pursue a more detailed investigation of polyspirobifluorene derivatives. In particular, different substitution patterns with electron withdrawing or donating attachments to the fluorene side groups are of great interest. These could be used to tune and optimise the charge carrier mobilities of the polymer, thus adding another beneficial property to the morphological and chemical stability of polyspirobifluorene.

6. Investigation into the formation and excited state relaxation of the beta phase of polydioctylfluorene

6.1. Introduction and background

6.1.1. Spectroscopic evidence

During the last decade significant research efforts have been dedicated to polyfluorene-type conjugated polymers due to their bright blue emission in combination with high quantum yields[95, 96, 124-126]. Commonly, polyfluorene derivatives feature side chains, substituted at the 9-carbon position, to facilitate solubility. Within this family, polyfluorenes bearing linear alkyl side chains show a rich solid state morphology[127-129], which translates into exceptionally diverse photo physics. Clearly, the most prominent example is poly(dioctylfluorene) (PFO). Here, as early as 1999 Bradley, Grell and co-workers[130] discovered and investigated a new solid state morphology, which they dubbed β-phase of PFO and which shall be the topic of this chapter.

Like most conjugated polymers, solid state PFO is usually found in its amorphous phase, here also termed α-phase, which is a glass at room temperature. This is characterised by a wide density of states distribution (DOS) of excitons that translates into a broad, nearly featureless, absorption spectrum and an emission spectrum with poorly resolved vibronic progression. However, for particular samples, such as thin films that had undergone thermal cycling to low temperature or had been exposed to solvent vapours, new characteristic features are observed in the absorption and emission spectra: Both are red-shifted relative to the amorphous α phase and, for a conjugated polymer, show very well resolved vibronic progressions, as illustrated in Figure 6-1. Remarkably, these samples also exhibit an extremely small Stokes shift between absorption and emission, as shown below. The appearance of these spectral features is associated with the presence of the β-phase.

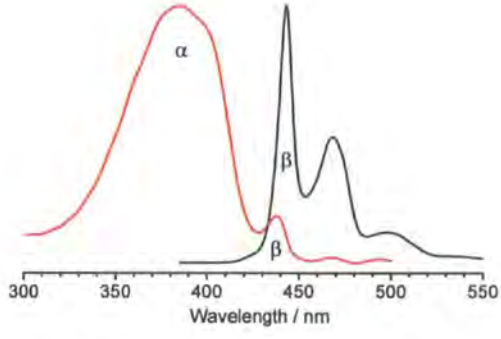

Figure 6-1 – Absorption and photoluminescence spectra of a mixed (α and β) phase PFO film. The emission is dominated by energy transfer to the β-phase

What is the β-phase? Clearly, with such distinct spectra, it differs qualitatively from other phenomena observed in conjugated polymers, such as "common" aggregates, excimers, oxidation defects and charge transfer states[5, 52, 57, 72, 131].

Given the similarities of its spectral features with those of ladder-type poly(paraphenylene) (LPPP) – a polymer that is chemically forced into a fully planar configuration – it was initially argued that the β-phase forms from a simple intrachain planarisation of the amorphous PFO backbone[130] leading to an extension of the

intrachain conjugation length. This conclusion was drawn from a study of PFO/polystyrene (PS) blends. However, the polymer concentration used did not suffice to isolate the polymer chains within the PS matrix but led to phase segregation[132]. Also, the fact that a minimum concentration of PFO is necessary to induce β-phase in solution[16, 130] speaks against an intrachain origin. Furthermore, both red shift and narrow line width of the β-phase spectra cannot be explained by a simple extrapolation of oligofluorene spectra to an infinite conjugation length[133]. In conclusion, although the adoption of a more planar chain conformation is associated with β-phase formation[133], its driving force is found in interchain interactions:

Most importantly, the β-phase spectral features grow in at fixed spectral positions at the expense of the amorphous phase spectra, as shown by in-situ experiments[130, 134, 135]. No gradual shift from α to β-phase is observed, as would be the case for an intrachain phenomenon. Instead, the β-phase emerges as a very well defined microscopic structure with its own spectral characteristics, which forms under very different sample treatment protocols[55, 130, 134, 136, 137]. These arguments support the notion that interchain processes drive the formation of the β-phase. These processes are mediated by the side chains; in particular they are inhibited for branched side chains, e.g. for poly(di-ethylhexyl-fluorene) (PF2/6)[134], but only observed with linear alkyl (especially octyl) groups as shown by experiments on polyfluorene derivatives substituted with a series of side chains[127, 134, 138].

Finally, it must be noted that in density functional theory (DFT) calculations[129], certain minimised energy conformations were identified for isolated PFO chains. The most planar of them with an inter-unit torsional angle of 160° was assigned to the β-phase on account of its high degree of intrachain order. However, although it implies an entirely conformational origin of the β-phase, this study cannot be applied to distinguish between inter- and intramolecular processes as it entirely neglects the latter.

6.1.2. Microscopic appearance

The β-phase renders polymer chains rigid when compared to those of the amorphous phase, which are rather floppy. In fact, intermolecular forces dominate the morphology of the β-phase leading to large scale ordering. As far as the solid state is concerned, not only phenomenological spectroscopic data are available for both, amorphous and β-phase. In particular, X-ray[55, 139] and electron diffraction[82] as well as X-ray and neutron scattering ([128] and references therein) experiments are powerful tools to reveal (ordered) structures on a few nanometer length scale. Naturally, these studies focus on the polymorphic crystalline phases of PFO. These form by quenching PFO thin films from the nematic phase, which exists at temperatures above 160°C [128, 129]. In contrast to these crystalline phases, the β-phase is found to be

mesomorphic[128], i.e. exhibiting a higher degree of supramolecular order (e.g. lamellar layers with ~1 nm spacing[55, 140]) than the amorphous phase but no defined crystalline structure. However, despite the wealth of studies[55, 139, 141, 142] the exact molecular arrangement of the β-phase remains vague. This is certainly caused by the large number of solid state phases and the complexity of the temperature dependent transitions between them, such that another morphology, which in this chapter is termed the γ-phase, can easily be mistaken for the β-phase, as will be shown later on.

Note, that in the above type of publications, the crystalline phases are termed α and α'. As in this chapter no crystalline structures are dealt with, a terminology of α for the primary, amorphous morphology can be used. In the following, β and γ will refer to other non-crystalline phases.

6.1.3. "β-phase" in solution

Independent of its actual molecular origin, the formation of the β-phase from the amorphous "background" is generally considered as a phase transition. It can easily be followed using temperature dependent photoluminescence spectroscopy, which was done here. The results presented above showed the metastability of the β-phase and its decomposition temperature of 353 K.

Further information can be gained from solution studies. When referring to a solution sample, the use of the term "phase" is not exact. However, both amorphous (α) and β-phase have their spectroscopic equivalents in PFO solutions[128]: Emission and absorption spectra similar to that of the amorphous phase are recovered when PFO is dissolved in a "good" solvent. Such a good solvent is identified as one which allows the solute polymer chains to maximise their interactions with the solvent molecules. On the other hand, these are minimised in poor solvents, where the polymer chains may form condensed structures[143]. For PFO, these structures bear spectroscopic signatures (in photo-absorption and emission) identical to that of the solid state β-phase. X-ray and neutron scattering experiments on highly concentrated solutions of PFO in methylcyclohexane (MCH) revealed the existence of 2-dimensional particles ("sheets"[128]) consisting of apparently 2 or 3 layers of polymer chains, 100 nm in diameter. Thus, a certain interchain order is present, which is different from common aggregation. Similar to its solid state pendants, α and β "phases" can coexist in solution but tend to separate at high PFO concentrations in a time frame of ~ 1 day[128]. The particles that grow during β-phase formation precipitate once they exceed a certain size[134], see Figure 6-2.

In solution, the thermo-dynamical parameters of β-"phase" formation have been studied by temperature dependent absorption spectroscopy of a dilute solution of PFO in a poor solvent (methylcyclohexane[134]). As expected, the

process is clearly exothermic and involves an entropy loss. Its driving force and time scale are temperature dependent and may reach up to several hours. On the other hand, if a PFO solution is exposed to a rapid temperature drop, spectral features of the β-phase develop almost instantly, as shown in Figure 6-2. The complexity of this "phase" transition is further indicated by the presence of a strong hysteresis with a dissociation point at 353 K[134] like in the solid state.

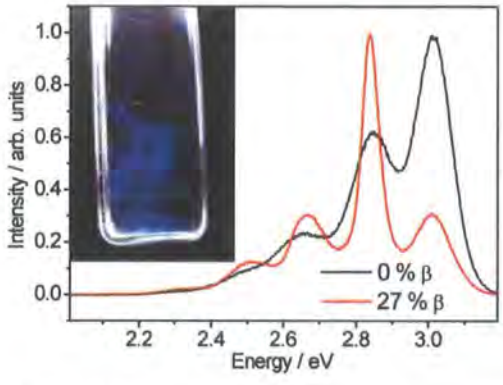

Figure 6-2 – Emission spectra of a PFO/xylene solution (10^{-3} wt./wt.) before and after β-phase induction (via cooling to 77 K). β-phase contents are given in the legend. Inset: Precipitation of the β-phase after cooling (27 % β sample under photoexcitation).

Solutions are not the application environment of conjugated polymers. However, all thin polymer films are drop or spin cast from a master solution. Hence, it is of great interest to see how the "phases" found in solution are transferred or modified in the casting step. It is known that samples cast from poor solvents tend to exhibit a higher fraction of β-phase[128, 144]. However, post-casting sample treatments[55, 130, 140] can significantly modify the β-phase. This study focuses particularly on the standard spin coating procedure and how its parameters can be modified to obtain a certain β-phase fraction.

6.1.4. Applications of the β-phase – energy transfer in a self-doped material

As in solution, phase segregation is also observed in thin films of PFO, where the β-phase forms "islands" imbedded in the amorphous bulk[144]. As shown for example by Rothe *et al.*[132], these act as efficient low energy traps for excitations from the surrounding amorphous α-phase. Therefore, an emission spectrum of a sample containing both α-and β-regions will show a β-phase contribution that is over-proportionally strong compared to the actual β-phase fraction, which is determined from β-contribution to the absorption spectrum. Given its narrow emission spectrum, the β-phase has the disposition for an extremely capable gain material for lasing[19, 145]. Hence, the trapping effect could be employed to transform the surrounding amorphous phase into a pump medium for a β-phase laser[145]. However, this application requires that (i) the size of the β-phase islands is sufficiently low and (ii) the overall number of these islands is large enough to overcome the loss threshold. To meet these requirements in quantity but also quality of the β-phase, one needs to precisely control its formation. As was elaborated above, this involves

controlling the state of the initial solution as well as the parameters which govern the deposition of the film. A repeatable fabrication protocol that allows obtaining a specified β-phase fraction and quality is highly desirable considering the large number of known and potential factors that are able to induce or decompose β-phase. Although this ultimate goal requires further study, a range of fabrication parameters and their influence on β-phase formation are identified in this chapter.

Additionally, two further issues are addressed here. The first is an investigation whether excitons are spatially confined at β-phase inclusions. In this case, they will not experience migration-activated quenching at the α-phase and, as a consequence, the average fluorescence lifetime will increase. Therefore, a study of the fluorescence decay behaviour is carried out via time-correlated single photon counting (TCSPC), as a function of β-phase fraction and temperature. Here, one must distinguish between photo-excitation in the absorption band of α- or β-phase. The former would result in fluorescence decays comprising a large number of components such as the radiative decays of α- and β-phase but also the energy transfer between the two and, at low concentrations of β-phase, its activation by exciton migration. Exciton migration within the β-phase and its relation to the size of β-phase inclusions are better studied by selectively exciting the β-phase and monitoring the dependence of any quenching, e.g. migrational, components of the fluorescence decay on the β-phase concentration and temperature. Besides, the knowledge of the fluorescence decay kinetics of the β- compared to the α-phase is still scarce[134, 144, 146] and was mainly obtained for solution.

The second issue is related to a potential quenching effect that metal electrodes may have on the excitations in the emissive material of a PLED[147]. Here, the dipole moment of the excitation induces a mirror dipole at an adjacent metal surface, which via dipole-dipole coupling eventually leads to the non-radiative decay of the excited state. This process is known as mirror quenching. Naturally, the coupling strength and, thus, the quenching efficiency depend on the alignment of the excitation dipole relative to the metal surface. In spin cast films of common conjugated polymers, such as the amorphous phase of PFO, the polymer chains and with them the excitation dipoles are predominantly oriented parallel to the film surface[148] and, as such, would be particularly susceptible to the above mirror quenching effect. On the other hand, the β-phase is an interchain structure with the potential for excitation dipoles oriented out of the surface plane. Hence, the importance of mirror quenching in polyfluorene LEDs may be evaluated by comparing the fluorescence decay kinetics of the polyfluorene α- and β-phases. While for the former, a reduction of the excited state lifetime is expected in the presence of a nearby metal electrode due to the additional non-radiative decay path, ideally no lifetime differences should occur in an analogous experiment on the β-phase.

6.2. Definition of the β-phase

6.2.1. Experiments

Steady state spectroscopy. A reliable measure of the β/α-phase fraction of a sample can only be obtained by steady state absorption spectroscopy, which was carried out using a Perkin-Elmer Lambda 19 spectrometer. In addition, the emission spectrum of each sample was characterised immediately after fabrication using a Jobin-Yvon spectro-fluorimeter (FLUOROMAX 3 or FLUOROLOG).

Temperature dependent spectroscopy. To study the α-β phase transition in thin film samples, steady state emission spectra were recorded as a function of temperature. To do this, a gated CCD camera experiment was employed, which is maintained by Dr. C. Rothe and normally used to detect time-resolved emission spectra in the range between 1 nanosecond and 1 second. With a wide temporal gate, the detected spectrum equals that of the steady state. The third harmonic of a pulsed Nd:YAG laser was used for photo-excitation at 355 nm, into the α-phase main absorption band, or for pumping a dye laser loaded with Coumarin 120, which then provided direct excitation of the β-phase. A closed-cycle temperature-controlled displex helium cryostat (Leybold) fitted into this setup provided sample cooling down to 11 K with an accuracy of 0.1 K.

Time-resolved measurements. The time-correlated single photon counting (TCSPC) experiment described in chapter 3 was used to obtain the fluorescence decay kinetics of film and solution samples. Here, photo-excitation was provided by a tunable Ti:Sapphire laser with a repetition rate of 76.3 MHz. The excitation wavelength was chosen either in the main absorption band of the α-phase (at 380 nm) or very close to the β-phase absorption peak (at 435 nm). The excitation power did not exceed 5 nW for a spot of 3 mm Ø, to prevent sample degradation. The final time resolution of the TCSPC experiment using 4096 time channels was $\Delta t \sim$ 1ps. Also, a JANIS liquid nitrogen cryostat was placed into the TCSPC setup in order to study the temperature dependence of the fluorescence decays of selectively excited β-phase in a thin film down to 77 K.

6.2.2. Sample preparation

Since the formation of β-phase is sensitively dependent on sample fabrication, it is useful to give an overview of the preparation methods tried and used in this study.

Poly(9,9-dioctylfluorene) (PFO) was provided by the research group of Prof. U. Scherf (Wuppertal) with exceptional purity, achieved by thorough purification of the monomer prior to polymerisation (Meijer method). Throughout the study, no PFO sample, including solution, thin film and annealed thin film, showed emission from oxidation defects[4, 5]. PFO was dissolved in a variety of organic solvents, such as tetra-hydrofurane (THF), chlorobenzene (CB),

chloroform (CF), toluene, methyl-cyclohexane (MCH) and xylene, as well as mixtures of xylene and THF. For solution samples, a concentration of typically 10^{-5} wt./wt. polymer per solvent was used, corresponding to a peak OD of below 0.3. Thin films were either drop cast (from MCH solution) or spin coated (other solvents) from master solutions of 5 mg/mg solvent and also from 15 mg/mg for one batch of xylene spun samples. Solvation was achieved by stirring the solutions at (60±2) °C for 10 to 15 minutes, according to the measurements shown in the following section and in line with preparation protocols used elsewhere[134]. Solvents with a low boiling point (CF and THF) were only heated to 55°C to prevent undue solvent evaporation. The completely transparent solutions were then immediately measured or processed into thin films. For spin coating, the spin speed was varied between 200 and 2700 rpm, as a further processing parameter. The film thicknesses were determined using a thin film analyser (FilmMetrics F20-UV). Thickness and OD varied according to solution concentration and spin speed, as shown in the following. For thin films, sapphire substrates (of 10 mm Ø) were used throughout to warrant an optimal thermal contact for temperature dependent spectroscopy.

Furthermore, a branched side chain poly(9,9-diethylhexylfluorene) (PF2/6) also synthesised by Prof. Scherf's group served as a reference material with zero β-phase fraction. The chemical structures of PFO and PF2/6 are shown in Figure 6-3. PF2/6 thin films were fabricated from toluene solutions via spin coating as described above.

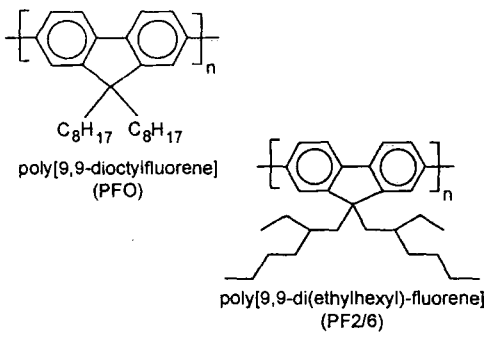

Figure 6-3 – Chemical structures of the materials used in this chapter.

6.2.3. Working hypothesis - the phases of PFO

In order to understand the experimental results presented in the following sections, it is essential to introduce a simplified classification of the different phases of PFO, which is an extension of the one published by Grell *et al.*[135] in accordance with newer findings by Chen *et al.*[55, 149]. In the course of this study, this hypothesis was found to consistently explain the steady state spectra for the large range of film and solution samples used.

First, the comparably simple solution environment is considered. Here, the appearance of PFO phases is governed by the phenomenological quality of the solvent. The two extremes of a "good" and a "poor" solvent (as described in section 6.1.3) may serve as a simplification to classify the phase behaviour of PFO in

solution: Solutions of PFO dissolved in a good solvent, using no or moderate heating at 60°C, exhibit absorption and emission spectra characteristic of the α-phase (see Figure 6-2), similar to those observed for PF2/6 in any suitable solvent. The single main absorption band is broad and the fluorescence spectrum appears with moderate vibronical resolution. The 0-0 mode appears subject to solvatochromism in the range between 410 and 425 nm[127]. Toluene, chlorobenzene (CB) and chloroform (CF) clearly belong to the group of good solvents, possibly also THF. However, when PFO is dissolved in a poor solvent, using the same heat treatment (60°C) such that solvation is apparently achieved and the solution is entirely transparent to the eye, the room temperature spectra show *additional* features associated with the β-phase, see Figure 6-1 and Figure 6-2 above: A comparably sharp absorption peak at 437 nm and a red-shifted and sharp emission spectrum with the first vibronic at about 444 nm. Poor solvents are MCH and xylene but also cyclo-pentanone and isodurene[144]. The solution equivalent to the β-phase, as shown by Dias *et al.*[134], is stable up to 353 K, i.e. above this temperature any solvent is good. However, for poor solvents, the β-phase re-forms with time at temperatures below 353 K.

Note, that the above describes two extremes. The real behaviour of a particular solvent is better understood in terms of its *ability* to dissolve β-phase or the solubility of PFO in this solvent. Apparently, the dry polymer material contains at least a fraction of β-phase prior to solvation. This is destroyed by the forces that act during solvation. Naturally, these forces depend on the solvent, i.e. they are enhanced for a solubility parameter, δ, around 9.3 $cal^{1/2}cm^{-3/2}$. However, as in any solution, the capacity of a solvent is limited when the temperature is reduced or the concentration is increased, and vice versa. In this context, a poor solvent is one that does not entirely dissolve β-phase at any temperature below its decomposition point of 353 K, even if the concentration of β-phase is very low. Knaapila *et al.* speak of "solvation at a colloidal level"[128]. In these cases, molecular solvation is not fully achieved and β-"nuclei" remain, visible in the absorption spectrum but (depending on concentration and temperature) not visible as particles. These nuclei subsequently lead to the condensation of β-phase, which may be aided by low temperature. Therefore, the age of a solution sample (and that of a thin film) determines the properties of its β-phase content. Eventually, large β-phase particles will form, which are visible to the eye and can be physically filtered out of the solution[134] as shown in Figure 6-2 above.

The above classification of solvents is valid for the large range of solution concentrations tested, from 10^{-5} up to 10^{+1} wt./wt.. Later on, the highly concentrated solutions were used for spin-coating thin films. Here, it was observed that the appearance of α- or β-phase in these films is correlated to the solvent quality of the master solution. It must be noted, however, that the deposition parameters also play a

decisive role[55, 140]. In this context, Khan *et al.*[144] were able to induce high β-phase fractions in films spun from isodurene (δ=9.3=δ_{PFO}) due to its high boiling point and slow evaporation. Further parameters are investigated later on. Typical absorption and photoemission spectra of thin films are shown in Figure 6-4 and Figure 6-5.

Besides the α- versus β-phase study, it was observed that certain thin film samples show spectral characteristics that resemble neither of these phases. Instead, their absorption spectra are extremely broad compared to those of the amorphous α-phase and exhibit a rather broad shoulder around 420 nm instead of a well defined peak at 437 nm, see Figure 6-4. The corresponding steady state emission is located between α- and β-spectra with respect to both, position (436 nm) and line width, see Figure 6-5. Such spectra can be induced by annealing *any* PFO thin film sample above 353 K. Therefore, as a working hypothesis, they are attributed to another phase of PFO, which will be termed γ-phase in the following. Notably, the same spectral characteristics have been observed by Chen *et al.*[55, 149] in thin films, which were slowly cooled down from the nematic phase that exists above 430 K. The authors identified this phase as being metastable but crystalline, exhibiting an X-ray diffraction pattern very similar to that of the main crystalline phase of PFO. These data give evidence for the *existence* of some phase with the above spectral characteristics although it is not clear how a crystalline

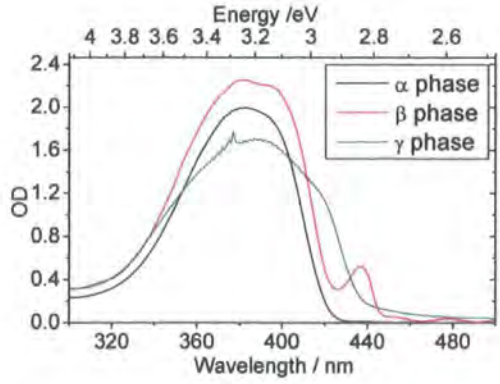

Figure 6-4 – Absorption spectra of three typical thin film PFO samples containing (black) only α-phase, (red) both α- and β-phase, (green) α- and γ-phase.

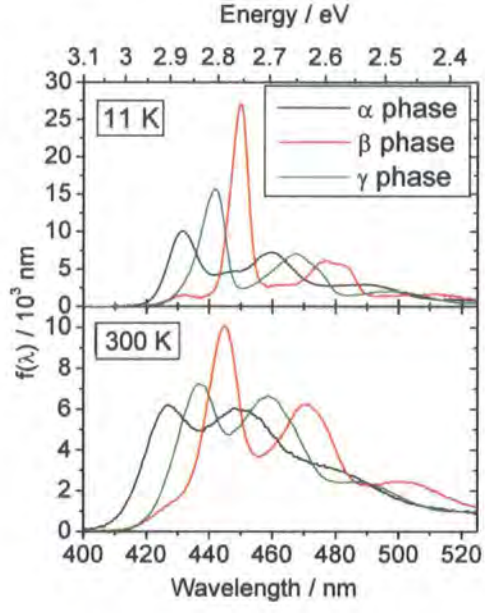

Figure 6-5 – Photoluminescence spectra of the samples in Figure 6-4 at low and room temperature.

phase can form from heating above just 353 K or 80°C. Possibly, the order-disorder transition at 79.3 °C[128] observed in calorimetric measurements suffices to induce partial crystalline ordering. In agreement, this temperature was identified with the onset of crystallisation by

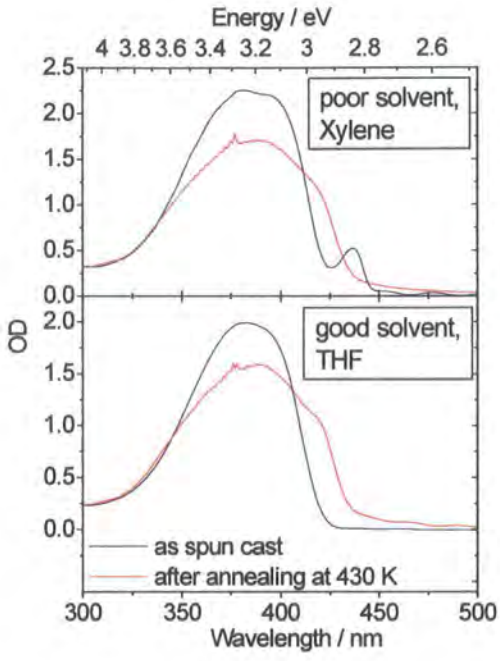

Figure 6-6 – Absorption spectra of two PFO thin films before and after heating to 430 K. Top – spun from xylene solution (initially with α- and β-phase); bottom – spun from THF solution (initially only α-phase). γ-phase is induced and β-phase destroyed above 353 K.

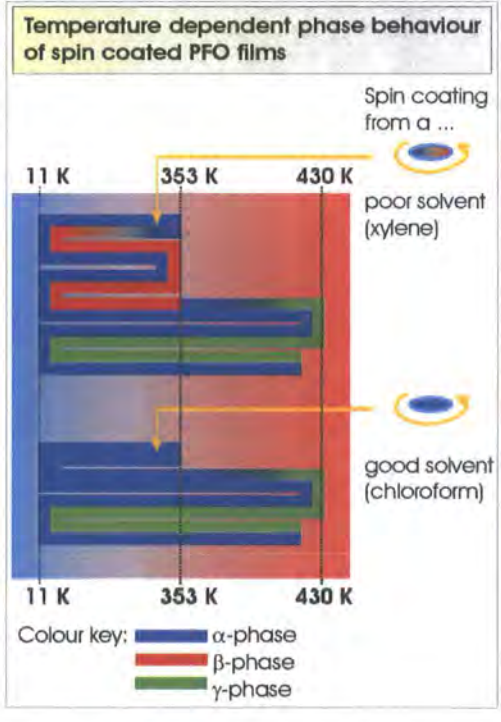

Figure 6-7 – Temperature dependence and transitions of the low temperature phases of PFO for thin films spin-coated from two types of solvent.

ellipsometry measurements[150]. However, any assumption about the microscopic appearance of this γ-phase is beyond the possibilities of this study.

In summary, heating above 80°C irreversibly eliminates any β-phase in films spun from poor solvents similar to its complete decomposition in solution. For films spun from *any* solvent, it irreversibly induces the γ-phase, in the temperature range studied. Corresponding absorption spectra are shown in Figure 6-6. This suggests a competition between the two metastable phases. While β-phase formation is favoured in the presence of its nuclei, the γ-phase appears to be a more stable morphology of solid state PFO as it prevails at higher temperatures. According to Chen *et al.*[55], it involves a larger degree of structural ordering and, therefore, requires a larger chain mobility and some activation energy for formation.

Figure 6-7 gives an overview of the solid state phase transition behaviour of PFO, which was obtained from temperature dependent photoluminescence spectroscopy covering the range of 11 K to 370 K. The steady state emission spectra of thin PFO films spun from either CF or xylene served to identify the different regimes and the transition temperature. Note that the β-phase formation shows a hysteresis also for thin films, with the same transition temperatures as in solution[134]. The fact that β-phase is only grown during the first cooling cycle demonstrates its stability at temperatures below 353 K and supports the concept of small condensation nuclei which

solvent	Used here	Solubility parameter δ / $cal^{1/2} cm^{-3/2}$	Boiling point /°C
chloroform	Y	9.3	61
toluene	Y	9.21	110
chloro-benzene	Y	9.2	131
tetrahydro-furan	Y	9.1	66
xylene	Y	8.91	138
methyl-cyclohexane	(Y)[a]	7.84	101
isodurene	N[b]	9.3	198
cyclo-pentanone	N[b]	10.4	130

Table 6-1 – Properties of the solvents used for film fabrication. [a] from [134] / [b] from [144].

remain intact if the film is not heated above 353 K. However, these nuclei and any β-phase are irreversibly destroyed when the film temperature exceeds this value. These results agree with and take further previous measurements by Khan *et al.*[144].

6.3. β-phase in as spin coated films

Having provided a general classification of the phases of PFO, the attention is now turned to their formation and how it is affected by sample preparation.

As a prerequisite, a measure of the β-phase relative to the α-phase content of each sample was obtained from its absorption spectrum, i.e. the value at 437 nm. For this, the spectrum was normalised to the peak of the α-absorption band. Any residual contribution of the α-band was estimated by interpolation and subtracted from the value at 437 nm. However, this method cannot be used to determine exact β-phase fractions, which would require an area normalisation of the absorption spectra and integration over the β-phase peak. However, this resulted in even higher error levels than the above method, in particular for samples containing little β-phase. In addition, one assumes that α- and β-phase excitation have the same oscillator strength, which may not be true. Therefore, the first method was used, which allowed the comparison of samples prepared under different conditions with respect to their β-phase fraction.

6.3.1. Solvent dependence

As shown above, the interactions between solvent molecules and PFO chains play a key role in the formation of β-phase. In order to investigate which parameters of sample preparation can be used to modify these interactions, a standard spin coating procedure was used to fabricate thin films.

Here, the most obvious parameter to vary is the solvent of the master solution. A range of organic solvents with various solubility parameters, δ, in the solubility window of PFO, were therefore employed. These included THF, CB, CF and xylene, see Table 6-1. The use of MCH for spin coating was inhibited because the maximum PFO concentration achievable with temperature-aided solvation (at 60°C) did not suffice to produce a satisfactory film thickness. Similarly, for xylene solutions a

concentration of 15 mg/mg was an upper limit above which gel formation was observed.

The occurrence of β-phase in the spin coated films essentially followed the distinction between good and poor solvents, i.e. between complete and partial solvation of PFO, which can be expressed by the similarity of the solubility (or Hildebrand) parameter of the solvent with that of PFO (~9.3), see Table 6-1. According to their δ, different degrees of solvation are observed within both groups, as shown by the failure to spin coat films from MCH. Nevertheless, PFO films could be drop cast from MCH solution, resulting in a higher β-phase content than the films spin coated from xylene.

6.3.2. Fabrication parameters

From the poor solvent group, only xylene remained for a study of further processing parameters. The advantages of cyclopentanone and isodurene[144] were not known at the time of the experiments, leaving plenty of scope for future investigation.

To start with, the experiments involved investigating a number of inconspicuous factors: As an example, it was found that, for wetting the substrate prior to spinning, the pipette must be changed after each sample to prevent the residual solution trapped in the tip end from evaporating and forming β-phase during the time between spin coating 2 sample. Furthermore, each master solution was kept agitated at all times to warrant its homogeneity. Next, serious fabrication parameters could be targeted, such as the temperature at which the master solution is dissolved, the concentration of the master solution and the spin speed.

The former appeared hard to control as the permitted temperature range was limited by the onset of solvation in xylene, at ~55°C, and the complete break-up of the β-phase above ~80°C. Thus, to avoid partial β-solvation by possible inhomogeneous heating (in a water bath on a heater plate), which might arise despite sample agitation, the temperature was kept as low as possible, at 60°C, with relatively large deviations of ±2°C.

Furthermore, two polymer concentrations, 5 and 15 mg per mg xylene, were used for master solutions. Studies on both dilute[134] and highly concentrated[128] solution suggested no dependence of the β-phase fraction on polymer concentration. However, here the more concentrated master solution yielded β-phase fractions in thin films that were higher by a factor of ~2. This is attributed to the increase in solution viscosity and its influence on the spin coating process: A larger amount of solution remains on the substrate requiring a longer time to evaporate and, therefore, allowing more β-phase to assemble[130, 144, 151].

Notably, the formation of β-phase is also affected by the speed at which the thin film

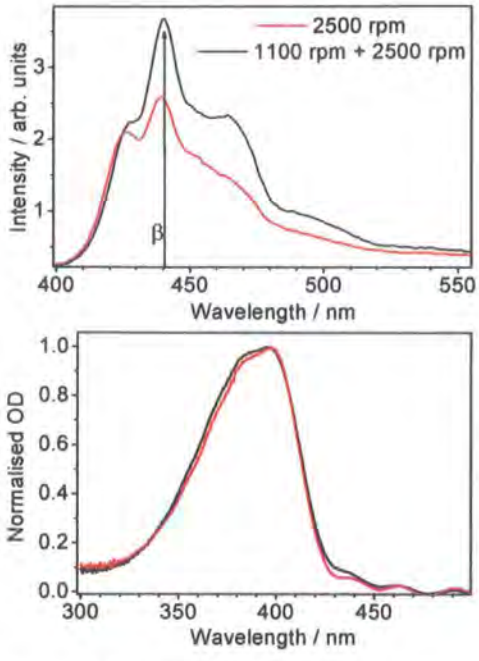

Figure 6-8 – Photoluminescence and absorption spectra of two thin films of PFO spin coated from 5 mg/ml xylene solution at different spin speeds.

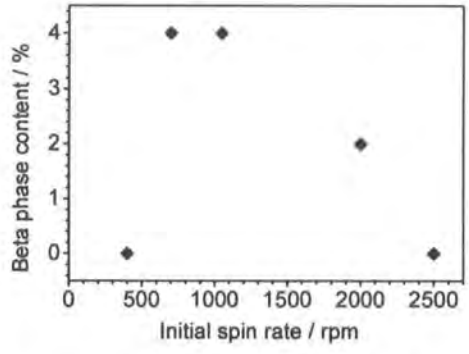

Figure 6-9 – The β-phase fraction of thin film samples spin coated from a 5 mg/mg xylene solution of PFO depends on the spin speed.

is spun. Therefore, thin films were spun from xylene solution for 60 s at various spin rates between 200 and 2500 rpm. To ensure that the final sample was dry and finished, 30 s at 2500 rpm completed each procedure, 2700 rpm being a standard speed for spin coating. A maximum of β-phase fraction was found for initial spin speeds that were comparably slow but still sufficiently high to sweep excess solution off the circular substrate. Figure 6-8 shows corresponding spectral data for a master solution of 5 mg PFO per mg xylene.

Clearly, the reason for this rate dependence is found in the crucial role of solvent evaporation on the formation of β-phase. If this is allowed to proceed slowly[130, 144, 151], then the polymer chains are able to respond to the physical stress imposed due to the gradual lack of solvation and a slow ordering towards the β-phase occurs. Naturally, these conditions are ideally fulfilled in a drop casting process, which required ~ 1 day to complete for the MCH films mentioned in section 6.3.1 above. Hence, the β-phase content and quality is not simply transferred 1:1 from master solution to thin film but during film fabrication further growth and rearrangement take place if the fabrication conditions allow this.

Furthermore, the β-phase fraction of spin coated films is subject to other parameters such as the time taken between wetting the substrate and starting the spin stage (usually a few seconds). This type of parameter could not be precisely controlled as these steps were carried out manually, resulting in a significant variation between different samples of the same batch, as shown later in this chapter.

Hence, the goal of this part of the study, to precisely determine the conditions required for a certain β-phase fraction, was not reached. Instead, a wide range of

parameters were found that require more precise control. Mostly, these are related to the rate of evaporation of the solvent. The insufficient β-phase control is probably due to the relatively low β-phase fraction in xylene samples (maximum 4 % as shown in Figure 6-9) compared to other solvents and its tendency to form a gel at high concentration. Meanwhile, higher β-phase fractions of 20 and 25 % have been published for isodurene and cyclopentanone[144], respectively. For future experiments, these solvents will have to be used instead of xylene.

6.3.3. γ-phase in as spin coated films

Due to availability, the majority of solvents tried in thin film fabrication dissolved PFO well and significantly inhibited β-phase formation. This section reviews the emission and absorption spectra and analyses the fabrication dependences of thin films spun from THF, CB and CF. These samples generally display α-phase characteristics. However, this is a simplified view as here also a dependence on fabrication conditions is observed with respect to the partial appearance of γ-phase. This dependence is not unlike that described above for the β-phase in xylene samples: When a slower spin speed is used, spectral features typical for the γ-phase may be observed without the need to anneal the thin film above 80°C. The spectral features, however, are identical to those of annealed films. As shown in Figure 6-10, the degree of γ-phase formation at a fixed spin speed depends on the solvent.

In this context, the low boiling point and fast evaporation of chloroform largely inhibit γ-phase formation. However, despite its equally low boiling point (see Table 6-1), γ-phase is almost always induced when spin coating from THF solutions. Typically, when spin coating from THF immediate crystallisation was observed already in the pipette, possibly caused by a particular way in which THF escapes from the solution.

In summary, γ-phase can form in thin films already at room temperature provided that no β-phase nuclei are present in the master solution. This suggests that the importance of the order-disorder transition of PFO at 79.3°C lies in the decomposition and solvation of all β-nuclei rather than in a thermal activation of γ-phase formation. Apparently, β- and γ-phase formation compete with each other during solvent evaporation. Besides, the emission spectra show that α-phase is present in each sample, coexisting with either β- or γ-phase inclusions.

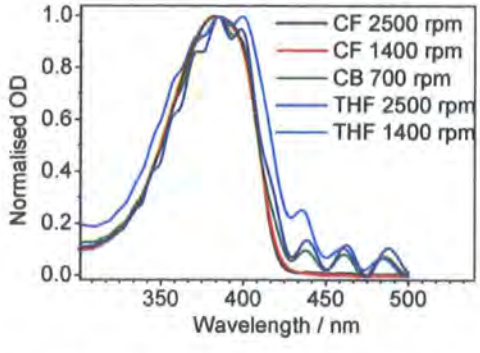

Figure 6-10 – Absorption spectra of thin PFO films. Spin coating speed and solvents are indicated in the legend.

6.3.4. Summary

The formation of ordered phases in PFO thin films mainly depends on two factors, in line with [144]: First, the solubility of PFO in the solvent of the master solution determines whether β-nuclei are present or only fully dissolved polymer chains, see Table 6-1. These nuclei may grow into large particles which then precipitate. Second, upon spin coating, the solvent evaporates, thereby inducing a stress on the dissolved molecules. Fast evaporation caused by high spin speeds or a low solvent boiling point "freezes" the conformations and intermolecular order of the polymer chains. Slow evaporation due to a high boiling point or low spin speed allows the molecules to react to the stress and rearrange. Here, β-phase formation is favoured in the presence of β-nuclei but, otherwise, γ-phase is formed. Each of them coexists with the amorphous α-phase background.

6.4. Mobility of β-phase excitons

6.4.1. Introduction

The previous chapter about a polyspirobifluorene has shown how the relaxation of excited states is affected when their DOS includes intrinsic trap states. As soon as a trap is populated, the exciton is "pinned down" and immobile. While in the above case, the situation arose from intrachain conformational relaxation, the here investigated β-phase forms via interchain interactions and phase segregates into island-like regions within the amorphous background phase[152]. Nevertheless, the population of these β-phase regions via exciton migration from the α-phase is efficient.

The present chapter investigates the excited state relaxation that occurs within the β-phase. Commonly, in amorphous solid state PFO the probability of quenching due to non-radiative decay channels (such as defect quenching)[5] is increased when an excitation is able to migrate. In other words, a reduced mobility results in a longer exciton lifetime. Considering a mixed phase PFO sample, excitons will eventually be trapped within the β-phase. If the β-phase region is sufficiently small, then the exciton will be spatially confined and immobile. Otherwise, it can migrate within the β-phase. From the increased level of inter- and intrachain order of the β-phase, it can be inferred that this migration will be nearly barrier free compared to the disordered amorphous phase – similar to MeLPPP. Any quenching site, or defect, within a β-phase island will be immediately found. As the probability of a β-phase defect scales with the island size, the exciton lifetime should decrease for a larger average size, i.e. at a larger β-phase fraction. On the other hand, small inclusions, which supposedly occur at low β-phase fractions, should render an exciton effectively confined. To test this hypothesis, in the following the excited state dynamics of β-phase excitons will be investigated as to their dependence on the size of β-phase inclusions, i.e. on

sample fabrication. Here, one expects an increase of the β-phase fluorescence lifetime towards lower β-fractions, which should finally converge to the intrinsic β-phase exciton lifetime at a threshold island size. In this context, a confinement of excitations with minimal quenching losses is of crucial importance to the application of a β-phase laser pumped by excitations residing on the surrounding amorphous phase. Therefore, the confinement threshold marks the ideal fabrication conditions for such a lasing material.

The following section presents a variety of measurements of the excited state relaxation in PFO thin film samples spin coated from xylene solution with the aim to confirm exciton confinement and, if possible, identify the corresponding fabrication conditions.

6.4.2. Measurements and samples

The fluorescence decay kinetics of the thin films introduced in section 6.3, namely those spin coated from xylene solution, were studied via time-correlated single photon counting (TCSPC). Here, one must distinguish between photo-exciting in the main absorption band of the α-phase and selective excitation of the β-phase. The former involves α-β energy transfer, which was observed with 15 ps in dilute MCH solution[134] and with 3 ps[96, 144] in the solid state, both at comparably high β-phase fractions between 15 and 25 %. The latter is very close to the time resolution of the TCSPC experiment (~1 ps), so that the energy transfer in thin films is hard to resolve. Only if the fraction of β-phase is very low, the activation of energy transfer by exciton migration from the amorphous phase might be recorded. However, in order to reveal an effect of exciton migration *within* the β-phase, all contributions to the fluorescence decay curves must be excluded which are related to the α-β energy transfer. This is done via selective photo-excitation at 435 nm using a pulsed tunable Ti:sapphire laser.

Thin films were spin coated from a 15 mg/mg xylene solution of PFO at various spin speeds to induce different, detectable degrees of β-phase. In analogy to section 6.3, each spin cycle was finished with a standard fast spin of 2500 rpm. Note that these samples are an early stage batch fabricated from a highly concentrated master solution. As a side effect of the high solution viscosity, the film thicknesses and maximum OD are higher, reaching up to 250 nm and 2.2, respectively, at 700 rpm, see figures 11 and 13.

Nevertheless, the occurrence of β-phase in these films is at least partly caused by solvent evaporation upon spin coating because the spin speed dependence of the β-phase fraction is similar to that presented in section 6.3 for films spun from 5 mg/mg xylene solution and peaks at 760 rpm with 10 %, see Figure 6-12.

Note, both 15 and 5mg/mg solution underwent the same heat treatment (solvation at 60°C) and were transparent prior to spin coating. The comparably high

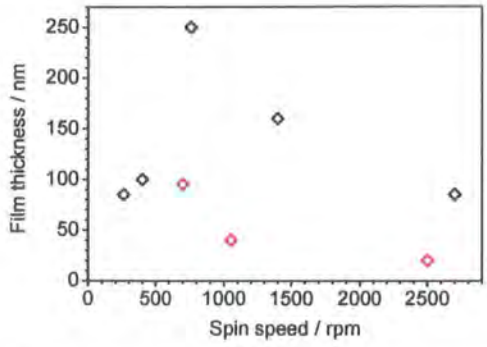

Figure 6-11 - Film thicknesses of samples spun from (red) 5 and (black) 15 mg/mg xylene solution of PFO.

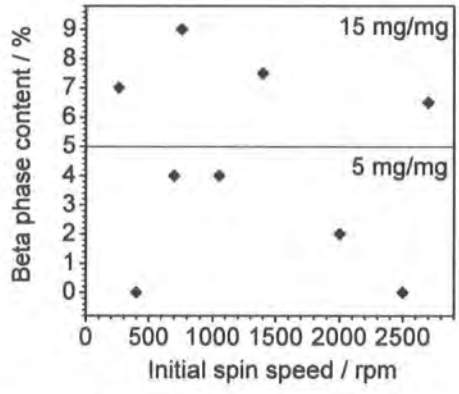

Figure 6-12 - Dependence of the β-phase fraction on the initial spin speed for films spun from 15 and 5 mg/mg xylene solutions of PFO. Accuracy is 0.5 %, reference is the absorption spectrum of an "α-phase only" sample spun from chloroform at 2500 rpm.

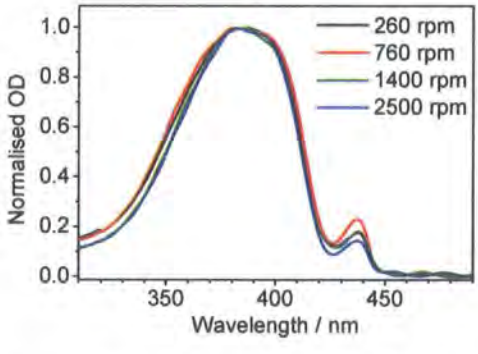

Figure 6-13 – Absorption spectra of thin films spun from a 15 mg/mg xylene solution of PFO at an initial spin speed as indicated. Note the grow-in of the β-phase absorption peak.

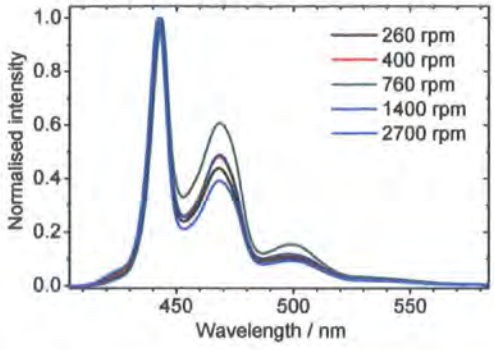

Figure 6-14 – Photoluminescence spectra corresponding to figure 13, excitation at 390 nm. Note the relative decrease of the β-phase 0-0 mode due to reabsorption, for a spin speed of 760 rpm.

β-phase fraction of the 15 mg/mg samples provided an OD at 435 nm that was sufficient for selective excitation of the β-phase, ranging from 0.12 (at 6 % β-phase fraction) to 0.5 (at 10 %), see Figure 6-13.

Immediately after sample fabrication, absorption and emission spectra as well as fluorescence decays were recorded. The emission spectra (photo-excitation at 425 nm) of all samples show almost exclusively β-phase emission, see Figure 6-14. A β-phase (and γ-phase) free thin film spun from chloroform at 700 rpm served as a reference.

6.4.3. Fluorescence decay kinetics

The TCSPC fluorescence decays with photo-excitation at 435 nm were collected at 442 nm through a cut-off filter, which in addition to the double monochromator blocked any scattered excitation light. Re-

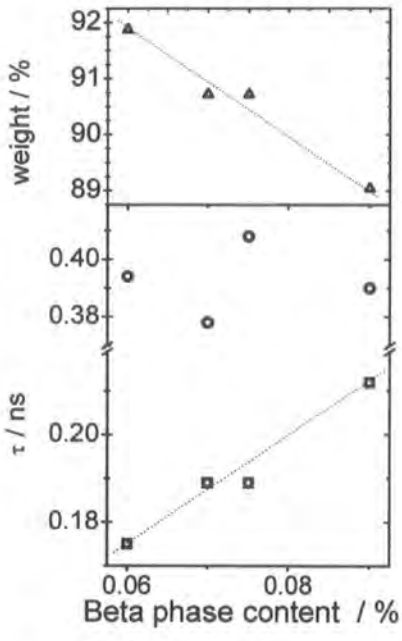

Figure 6-15 – Results of analysed TCSPC data (re-convolution fitting) of the samples in Figure 6-13, dependent on their β-phase fraction. Top: Relative amplitude A_2 (corresponding to τ_2) Bottom: τ_1 (circles) and τ_2 (squares). The lines are guides to the eye.

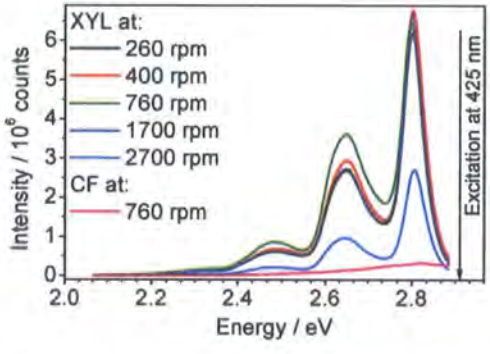

Figure 6-16 – True intensity steady state fluorescence spectra of thin PFO films spun at indicated spin speeds from xylene and CF. Photo-excitation at 425 nm.

convolution fitting was employed for analysis, requiring a sum of two exponentials for the PFO films spun from xylene: The first component, $\tau_1 \sim 400$ ps, accounted for 10 % of each decay curve. The importance of τ_1 grew with increasing β-phase fraction, as shown in Figure 6-15. The value of τ_1 showed a wide random variation, probably due to its low weight. Note, the same decay time, including the large variation, was found before by Ariu *et al.*[96] for thin films spun from chloroform solution, which were swelled by toluene vapour to induce 13 % of β-phase. No other component was mentioned in this publication. However, for the xylene films used here, a main component of $\tau_2 \sim 200$ ps accounted for 90 % of the decay, its importance slightly decreasing with increasing β-phase fraction. τ_2 itself increased with β-phase fraction, see Figure 6-15.

For comparison, the fluorescence decay of a β-phase free film (spun from chloroform, photo-excitation at 435 nm) was governed by a 220 ps lifetime without any longer-lived contribution, in agreement with the literature[47]. In this context, it must be emphasised that only a negligibly small amount of α-phase emission could have been collected from the samples containing β-phase because of their high β-phase fractions and its selective excitation at 435 nm, see Figure 6-16. Therefore, τ_2 and the above α-phase fluorescence decay time are not the same. Both, τ_1 and τ_2 are associated with β-phase excitons.

6.4.4. Discussion and conclusions

An average decay time was calculated for each sample according to

$$\tau_{average} = \frac{A_1 \cdot \tau_1 + A_2 \cdot \tau_2}{A_1 + A_2}$$

[Equation 6-1]

A_i denoting the amplitudes of the decay components. As shown in Figure 6-17, $\tau_{average}$ *increases* at higher β-phase fractions, which mainly reflects a rise of τ_2 but also the slight increase of the weight of the long-lived component τ_1.

The opposite is expected for a migration controlled excited state decay. Therefore, first, this unexpected result sheds some doubt on the intuitive assumption that β-phase inclusions will be smaller at lower β-phase fraction. However, unless verified by X-ray (or related) experiments there is no evidence of the contrary. Second, one may question whether the rule-of-thumb that all quenching processes are activated by exciton migration applies to excitons residing within a minority phase. It is conceivable that a small size of β-phase inclusions renders an exciton more susceptible to external disturbances from which a large inclusion size may provide greater protection. Then, the fluorescence decay kinetics no longer provide a measure of the exciton mobility and the evaluation of exciton confinement is not possible.

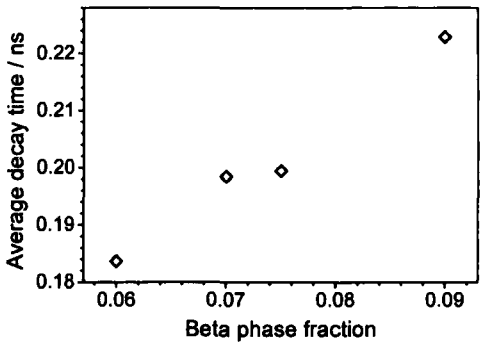

Figure 6-17 – Average TCSPC fluorescence decay time corresponding to figure 15.

Third, the origin of the second decay component requires investigation: In this context, it must be noted that no emission spectrum, including characteristics of oxidation defects[4], other than that of the β-phase was detected when exciting at 435 nm. Hence, the shorter lived contribution represents either a non-radiative decay channel or a type of excited state from within the β-phase. The former is unlikely due to the films being very emissive. Exact quantum yields could not be measured due to the high OD values, which led to reabsorption, see Figure 6-14. When tried, quantum yields of 0.2 were recovered for excitation at 425 nm compared to values of 0.33 for thin amorphous films of polyfluorene that were free of reabsorption. Hence, a very significant part of the shorter lived component leads to emission.

Therefore, one might conclude that the quality of β-phase in the thick xylene films used here is different from that of the swelled films used by Ariu *et al.*[96] due to the very different solvent environments and time scales of β-phase formation, in line with a recent publication[153]. It must be

noted that all relevant samples studied in this section stem from the same batch. The experimental results may not represent the average β-phase sample. Therefore, for a more detailed interpretation, a larger variety of samples needs to be studied, which must include films spin coated from isodurene and cyclopentanone[144] to provide a sufficiently high β-phase fraction. In addition, the TCSPC and emission study of these samples must be accompanied by X-ray or neutron diffraction experiments or any other technique that allows conclusions about the internal structure, ordering and "grain size" within a thin film sample and preferably, about the size of the β-phase inclusions. Then, fluorescence decay kinetics can be directly related to structural properties and any assumptions about correlations between film fabrication and β-phase formation will be backed up by solid experimental facts.

6.4.5. Additional experiments - room temperature anisotropy

The aim of the previous experiment was to prove the immobilisation of β-phase excitons. As this issue could not be resolved via TCSPC, attention is now turned to a steady state fluorescence anisotropy measurement. The anisotropy, r(λ), is calculated as[52]

$$r(\lambda) = \frac{C(\lambda) - 1}{C(\lambda) + 2}$$

$$C(\lambda) = \frac{I_{VV}(\lambda) \cdot I_{HH}(\lambda)}{I_{VH}(\lambda) \cdot I_{HV}(\lambda)}$$

[Equation 6-2]

$I_{AB}(\lambda)$ referring to the fluorescence intensity spectrum. Indexes A and B refer to excitation and emission polarisation, respectively, and can be horizontal (H) or vertical (V). In a sample comprised of fluorophores that are oriented randomly with respect to the possible directions of polarisation, r(λ) has an upper limit of 0.4[52], which is reached only when the dipole moments of excited and emitting states are collinear. Processes that involve a change in the orientation of the excited state dipole moment therefore reduce the photoluminescence anisotropy. These include molecular rotation (in solution) and excitation migration. Hence, a restriction of migration results in an increase in r(λ).

Here, the room temperature anisotropy of two thin film samples was determined according to [Equation 2-1 from steady state emission spectra using a Jobin Yvon Fluorolog spectrometer. The first sample was spun from a 15 mg/mg PFO/xylene

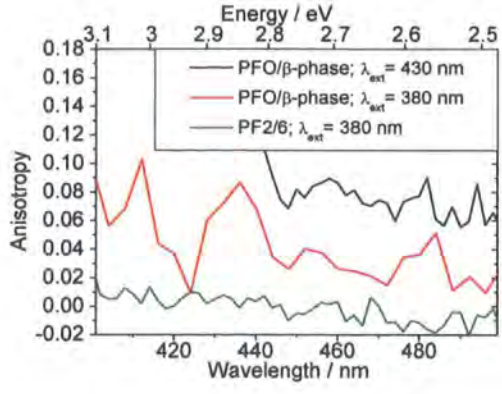

Figure 6-18 – Steady state fluorescence anisotropy of a PFO/β-phase film (excitation at 430 and 380 nm) and an amorphous PF2/6 film (excited at 380 nm).

solution at 2500 rpm, yielding a β-phase fraction of 6.5 %. Due to its thickness of 80 nm and moderate OD values, see Figure 6-13 reabsorption effects were small, see Figure 6-14. If these affected the measurement at all, they led to an underestimation of r(λ). A comparative anisotropy measurement of a β-phase free PF2/6 film (thickness 50 nm) was also carried out.

The results are shown in Figure 6-18. Apparently, the fluorescence anisotropy of the PF2/6 film (excitation at 380 nm) is about zero across its entire emission spectrum. In contrast, when exciting the PFO film at 380 nm, r(λ) is significantly higher (averaging to about 0.03) despite the increased noise level. Note the steep drop to 0.01 near the 0-0 mode of the α-emission and the rise to 0.07 at the 0-0 mode of the β-phase spectrum. On one side, the above data can be interpreted as evidence of a reduced mobility of excitons trapped at β-phase inclusions, which are small compared to their diffusion length. On the other, they may hint at some macroscopic interchain order of the β-phase. In any case, excitons are efficiently confined at β-phase inclusions.

To obtain selective information about β-phase excitons, the PFO sample was also excited at 430 nm. Note that this wavelength does not exactly match the 437 nm required for selective excitation of the β-phase but still leads to a significant reduction of the α/β ratio of excited chromophores. Once again, the anisotropy is higher that for 380 nm excitation, averaging at 0.07. Thus, the confinement of excitons on the β-phase is confirmed. Note that all of the anisotropy measurements were carried out using a sample with a rather high β-phase fraction. Hence, the results obtained will also apply to samples with comparable or less β-phase, i.e. all of the thin films investigated here.

6.4.6. Additional experiments - temperature dependence of spectra and kinetics

Background. An important parameter in the study of exciton migration is temperature. As lined out in chapter 4, one distinguishes between temperature independent downhill jumps and Boltzmann-weighted uphill jumps to sites of higher excited state energy. Initially after photo-excitation, most jumps are downhill and excitons migrate at the same rate at all temperatures, T, provided that their density of states (DOS) and the excitation energy are constant. After a certain time, τ(T), uphill and downhill jumps become equally probable. Due to the Boltzmann-weighting of the former, τ(T) occurs earlier at a higher temperature and, here, also the average excited state energy $E_{av}(\tau, T)$ of this equilibrium is higher. Therefore, effectively more potential exciton sites participate in the migration process at a higher temperature, the average distance between these sites is comparably small and, thus, the overall rate of migration is higher. At low temperature, the migrational equilibrium occurs later, $E_{av}(\tau, T)$ is lower –

which corresponds to a red-shift of the average emission intensity – and exciton migration slows down. In turn, less migration reduces the probability of an exciton to encounter quenching sites, which should increase the average fluorescence lifetime at low temperature. This applies only if the system is dominated by excitation migration. As shown by the anisotropy and TCSPC measurements, this is not the case. Therefore, it is interesting to study the temperature dependence of fluorescence spectra and selectively excited decay kinetics for a sample containing β-phase.

Decay kinetics. In this section, one sample, a thin film spun at 2500 rpm from a 15 mg/mg PFO/xylene solution is studied via TCSPC. Note that these measurements were carried out 4 days after sample preparation such that the microscopic appearance of the β-phase may have developed towards a larger inclusion size. Using a nitrogen flow cryostat, the temperature dependence of the fluorescence decay kinetics is investigated, exciting the β-phase selectively at 435 nm and collecting its emission at 442 nm.

When comparing this experiment to the previous room temperature measurements, the results are qualitatively reproduced. The fluorescence decays obtained from re-convolution analysis are biexponential with a short-lived component of (140 ± 5) ps accounting for 60-80 % of the signal and an additional highly variable long-lived decay of (300 ± 20) ps. The variation in brackets is the one observed across the temperature range investigated. Notably, both contributions are faster compared to section to the room temperature experiment above, the only differences between them being the sample age, which may have led to some kind of maturing of the β-phase, and its positioning in a cryostat. While the latter may incur adverse effects like uncorrelated scattering of the excitation light, it was found that the scatter reference responses obtained at each temperature were identical such that any relative changes detected by the experiment can be trusted.

From the above decay components, an average fluorescence lifetime, $\tau_{average}$, was calculated according to [Equation 6-1]. As shown in Figure 6-19, $\tau_{average}$ *decreases* towards low temperature and increases to its old value when reheating the sample. This behaviour contradicts the one expected for a migration dominated system. It does not so much reflect a temperature dependence of the individual lifetimes but rather a (reversible) increase of the weight of the faster component at low temperature. For reassurance, one can compare the raw

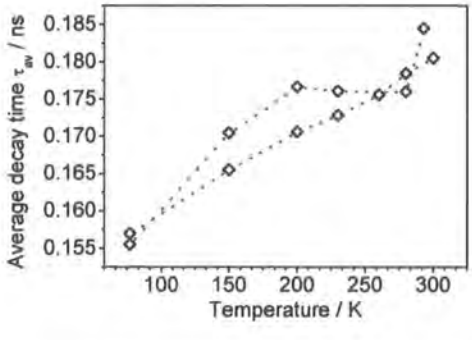

Figure 6-19 – Average decay times of the temperature dependent TCSPC measurements on a PFO/β-phase film (both, cooling and heating run).

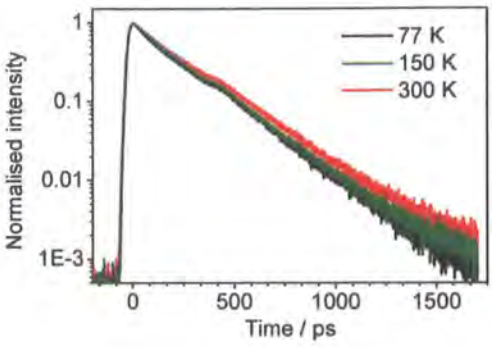

Figure 6-20 – TCSPC raw decay curves corresponding to Figure 19; excitation at 435 nm; collection at 442 nm.

data, which are shown in Figure 6-20: Clearly, the fluorescence decay accelerates at low temperature. From the temperature independent scatter profiles it is concluded that the decrease of $\tau_{average}$ is not an artefact of re-convolution analysis. This is further confirmed by the reversibility of the dependence. The gap between the cooling and the heating run in Figure 6-19 are attributed to insufficient thermal equilibration of the sample in the course of the measurement.

Investigating the origin of the unexpected T dependence of $\tau_{average}$, one may argue that inhomogeneities of the sample dominate the data: Due to the contraction of the cryostat cold finger at low temperature, the position (but not the size) of the excitation spot on the sample shifted with temperature by 3 mm in total – but it remained constant with respect to the collection optics of the TCSPC. However, any influence of sample inhomogeneities on the fluorescence decay is unlikely due to the size of the collection area (diameter 3 mm) which is large compared to the expected lateral sizes of β-phase inclusions (< 100 μm[152]).

Hence, the observed effect is representative of the entire sample. One may further ask whether it is related to some kind of β-phase formation at low temperature. However, in this case, the dependence would not be reversible as at all times the temperature was kept far from the dissociation point of the β-phase at 80°C. Instead, as expected due to the high sample age, the β-phase fraction and the size of the inclusions are saturated and stable. Therefore, two conclusions may be drawn: First, (in this sample) the temperature dependence of the fluorescence kinetics is *not* dominated by excitation migration. This entirely agrees with the high steady state anisotropy found above in a similar sample.

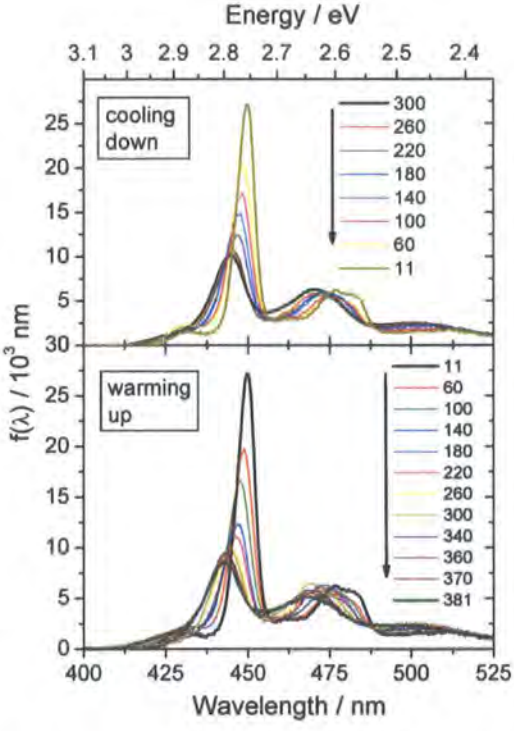

Figure 6-21 – Temperature dependent photoluminescence spectra of a PFO/β-phase film recorded via CCD camera. Temperature in K is indicated in the legend. Excitation at 355 nm.

However, even if migration is completely suppressed the excited state lifetime is expected to be *constant* with T. Therefore, the accelerated low temperature fluorescence decay can only be explained by some change in the nature of the excited states – a temperature dependent *reversible* change in the microscopic quality of the β-phase.

Emission spectra. Additional information is obtained from temperature dependent steady state emission spectra. The sample used previously for anisotropy measurements was placed in a closed cycle helium cryostat, photo-excited at 355 nm and its emission detected via CCD camera as described above. As the β-phase fraction of this sample is saturated and rather high, the α-β energy transfer proceeds quickly such that the steady state emission spectra show almost no contribution of the α-phase.

The spectra shown in Figure 6-21 were recorded when cooling down from room temperature to 11 K and slowly heating back to 300 K and beyond. At low temperature, the α-phase emission partly grows back due to the freezing out of migration activated energy transfer. Note that the growing α-phase emission remains at an almost constant spectral position while, simultaneously, the β-phase emission shows a notable red-shift at -0.0186 nm/K as shown in Figure 6-22. Further spectral changes include an increase of the emission intensity, a simultaneous decrease of the Huang-Rhys parameter and a narrowing of the vibronic modes. All of these changes are fully reversible when heating the sample.

This behaviour is observed in many common amorphous conjugated polymers, where they are explained by an increase of intrachain conjugation in the absence of thermally activated phonons at low temperature. This narrows and red-shifts the DOS of excited states. The reduction of exciton migration adds to this effect such that the emission originates from a smaller part of the altered DOS. However, in an amorphous material the intrachain conjugation cannot be extended infinitely. Instead, it is restricted by the imperfection

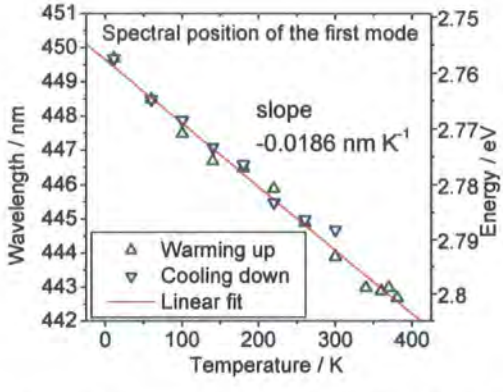

Figure 6-22 – Spectral shift of the 0-0 mode of the β-phase fluorescence spectra of Figure 6-21.

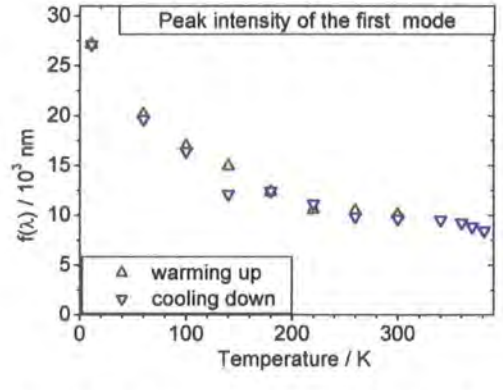

Figure 6-23 – Intensity of the 0-0 mode of the β-phase fluorescence spectra of figure 21.

of the compositions and conformations of solid state polymer chains. Secondly, at some finite temperature the excited state relaxation due to migration is limited by the decay of the excitations[154]. This is the case for amorphous PF2/6 films at 15 K, where migration continues beyond 1 ns, as shown by Meskers *et al.*[154], and the red-shift saturates at 50 K[155]. Note that migration within a narrower, more homogeneous DOS is less temperature dependent. Consistent with the small width of the β-phase DOS, Ariu *et al.*[96] have observed a rather fast relaxation time of 25 ps for thin films containing the β-phase, at 5 K. In MeLPPP, which has a comparably narrow DOS and supposedly a similar chain conformation as the β-phase, energy migration in a thin film at 1.5 K was recently measured on the 30 ps scale[156]. Note that exciton migration is a dispersive process with a time- and wavelength-dependent rate so that the above time scales can only be a guideline. Hence, despite the striking difference between spectral relaxation in α- and β-phase, the latter still displays the "normal" behaviour of an amorphous conjugated polymer bearing in mind its extremely narrow DOS. Seemingly, this is also true for the increase of the emission yield at low temperature. This is mainly carried by the 0-0 vibronic mode of the emission as shown in Figure 6-23, resulting in a decrease of the Huang-Rhys parameter at temperatures below 160 K.

S was calculated from the above spectra according to *[Equation 4-2]*, see Figure 6-24. Hence, the ground state geometry approaches that of the excited state at low temperature. This may be interpreted in terms of either an extended conjugation, due to an increase of ground state planarity at low temperature, or as an inhibited geometry relaxation due to intermolecular interactions. Speaking of a solid state sample, the latter refers to that type of conformational relaxation which involves femtosecond bond length adjustment, see chapter 4. In both cases, the behaviour of S is evidence of an increasing molecular restriction and closer packing of polymer chains at low temperature.

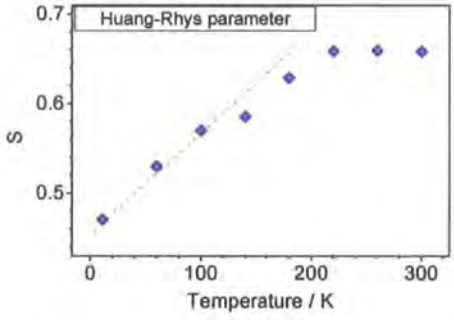

Figure 6-24 – Huang-Rhys parameter calculated from spectra in figure 21 (cooling run only). The line is a guide to the eye.

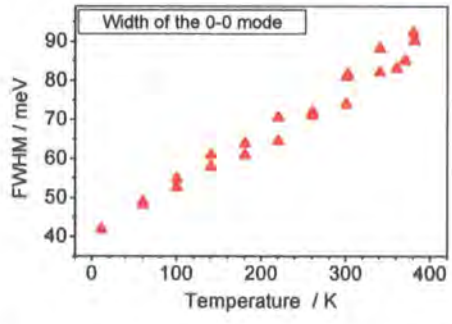

Figure 6-25 – FWHM of the 0-0 mode of the fluorescence spectra in figure 21, determined manually without peak fitting.

However, the comparison with amorphous polyfluorene does not hold in detail. The temperature dependent spectra by Guha *et al.*[155] suggest that the decrease of S should level off at a finite temperature, which is ~ 110 K for amorphous polyfluorene and ~ 60 K for MeLPPP. Strikingly, no saturation is observed in Figure 6-24 for the β-phase, which indicates that the relevant phonon modes are still stiffening at this low temperature. Similarly, the narrowing of the 0-0 fluorescence mode is still linear at 11 K (see Figure 6-25), again in contrast to measurements on MeLPPP and PF2/6 by Guha *et al.*[155].

This behaviour deviates from that of amorphous conjugated polymers and implies a decrease of inhomogeneous broadening beyond the possibilities of even the rigid-rod polymer MeLPPP. Effectively, this indicates an extension of conjugation between different polymer chains. Indeed, interchain interactions are associated with β-phase formation. Hence, it seems plausible that exciton delocalisation may spread across several polymer chains at least at low temperature. In x-ray and related studies[55, 128, 140] the β-phase was shown to be mesomorphic, i.e. not possessing the perfect order of a crystal but still a higher degree of interchain order than amorphous materials. At room temperature, the intermolecular forces leading to this imperfect order may be disturbed due to the macromolecular nature of the material. It is conceivable that, at low temperature, when these disturbances are significantly reduced the average intermolecular distance decreases to allow conjugation to spread across several polymer chains. Naturally, the structural imperfections of the large polymer chains inhibit crystallisation via this gradual process. The static spatial distribution of polymer chains retains a basic level of inhomogeneous broadening, which is obvious from the still almost Gaussian shape of the 11 K luminescence spectra. Nevertheless, with increasing two-dimensional exciton delocalisation the β-phase approaches the behaviour of a crystal thereby reducing the width of the exciton DOS and the importance of inhomogeneous broadening to the emission spectrum.

Thus, the nature of the excited state is gradually changed with temperature towards a multidimensional delocalisation. Then, the reduction of the excited state lifetime, τ, at low temperature should be understood as a further expression of this anomaly.

6.4.7. Summary

Section 6.4 documents that, within the β-phase, excitations are limited in their mobility. Therefore, their lifetime is not governed by migration activated quenching. In agreement with this, the β-phase fluorescence decay time decreases at low temperature, which is interpreted as an appearance of interchain conjugation.

The validity of these conclusions for a wider range of β-phase samples still needs to be verified by analogous measurements on thin films spin coated from solvents

other than xylene[141]. In addition, photoluminescence spectroscopy and lifetime experiments must be compared to some measure of the microscopic structure of the samples, which can now only be speculated on.

6.5. The influence of electrodes on β-phase films

6.5.1. Motivation

In the view of the sophisticated efforts dedicated to increasing device performance[8, 9, 89], the use of an intrinsic material property to reduce excited state quenching is highly desirable. As outlined above, Becker *et al.*[147] have proposed that an excitation in the polymer layer of an LED can be quenched due to a mirror effect in the vicinity of an electrode. It is the aim of this section to evaluate the importance of mirror quenching in amorphous polyfluorene films and investigate its effect on samples that contain the β-phase. In contrast to the amorphous phase[148], the excitation dipole moment of a β-phase exciton may be oriented out of the surface plane, thereby reducing the strength of coupling to the electrode. Therefore, thin films containing the β-phase may be less susceptible to mirror quenching. To verify or invalidate this expectation, the excited state quenching in different layered electrode-polymer structures is compared. Reference samples are fabricated from PF2/6, which only contains amorphous material[127, 134]. These are then contrasted to analogous samples spun from 5 mg/mg xylene solutions of PFO at 2500 rpm, containing ~ 1% β-phase. Compared to the samples studied in the previous section, this β-phase fraction is rather low. Only a maximum of one third of all excitons reside within the β-phase, as shown by emission spectra, see section 6.5.4 below. However, the high spin speed responsible for this was necessary to obtain a very thin film of < 25 nm thickness and, hence, to expose as much of the polymer layer to the electrode interface as possible. At the time, xylene was the only choice of solvent which produced β-phase. For future experiments, isodurene or cyclopentanone are better suited[144] to obtain a high β-phase fraction at the spin speed and solution concentration required.

6.5.2. Sample structures and experiments

Five different electrode-polymer structures were investigated:

GP. A thin polymer film (PFO or PF2/6) on a glass substrate. Using the GP structure, any effects arising from the exposure of one polymer interface to the air and the protection of the other by the glass substrate could be assessed.

GIP. A glass substrate covered with a layer of indium tin oxide (ITO) onto which a polymer film was spin coated (see GP structure). Here, ITO is studied on its own

as the standard cathode in common PLED structures.

GAP. A glass substrate onto which a 100 nm thick layer of aluminium was evaporated. A thin polymer film was then spin coated onto the aluminium in an air atmosphere after less than 30 min. exposure to air. Aluminium is studied here as a pure metal electrode with high conductivity. Mirror quenching, if present, should be pronounced in the GAP structure.

GPA. Here, the first step is spin coating the polymer film onto glass. Then, a 100 nm layer of aluminium is evaporated onto the polymer. With respect to mirror quenching this structure is identical to GAP. However, the effect of the evaporation process on the quality of the metal-polymer interface can be studied in GPA.

GPBA. Similar to GPA but with a 5 nm thick layer of barium evaporated onto the polymer. 100 nm of aluminium wasevaporated onto the barium. This structure is used to compare the quenching effect of different metals. A GABP structure could not be fabricated as barium would immediately oxidise in the air atmosphere used for spin coating.

To monitor the overall intensity quenching, steady state excitation and emission spectra were recorded, from which a property proportional to the quantum yield was obtained. Equally important, also the photo-excited fluorescence decays were compared. Mirror quenching in a thin polymer film is expected to lead to lifetime

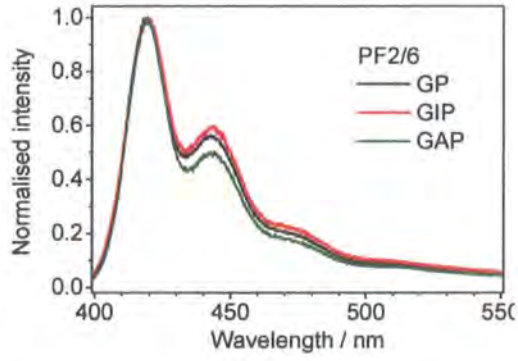

Figure 6-26 – Normalised steady state emission spectra of PF2/6-electrode structures. Excitation and collection were carried out at/from the polymer-air surface.

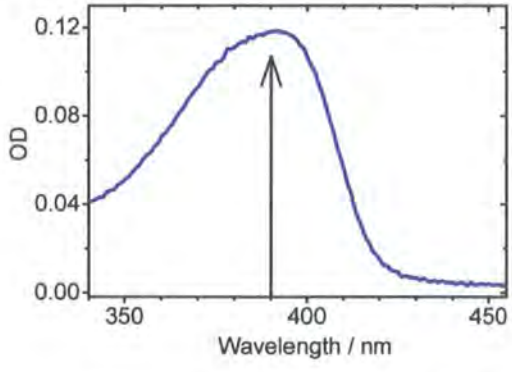

Figure 6-27 – Photoabsorption spectrum of the PF2/6 GP structure. The arrow indicates the excitation wavelength used in this study.

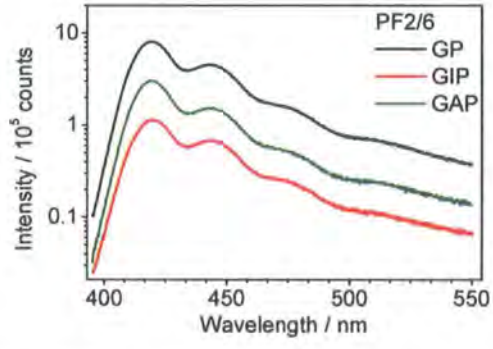

Figure 6-28 – True intensity photoluminescence spectra corresponding to figure 26.

quenching. Thus, an accelerated fluorescence decay should be observed caused by the presence of an additional non-radiative decay path.

6.5.3. Results and discussion – PF2/6

Figure 6-26 shows the steady state emission spectra of PF2/6 structures (GP, GAP and GIP) photo-excited in the main polyfluorene absorption band at 390 nm. All polymer films were fabricated from the same 5 mg/mg toluene solution of PF2/6. They exhibit thicknesses below 25 nm (not measurable) and comparable OD values at 390 nm of 0.13±0.02, see Figure 6-27. As expected, their emission spectra only display features characteristic of amorphous PF2/6.

Apparent from Figure 6-26, the presence of an electrode has only a small effect on the spectral shape of the emission. However, the overall intensity and, hence, the quantum yield decrease by a factor of 3 in the presence of the aluminium interface and by a factor of 9 in the presence of ITO, see Figure 6-28. Unexpected from the conductivities of aluminium (σ_{Al} = 38*10^4 S/cm) and ITO (σ_{ITO} = 1 S/cm), which clearly suggest a larger mirror effect for aluminium, the ITO substrate quenches the luminescence stronger. This is rather interpreted as an effect of chemical interactions at the ITO-polymer interface and the diffusion of electrode material into the polymer[157]. Similarly, aluminium atoms may diffuse into the boundary polymer layer and cause impurity quenching. However, from this experiment no conclusions can be made about the presence or absence of mirror quenching.

Figure 6-29 shows the corresponding fluorescence decay curves, obtained via single photon counting (TCSPC) with photo-excitation at 391 nm and collection at the 0-0 mode of the emission, at 423 nm.

Using deconvolution fitting, the main (>90 %) decay components were determined as 155 ps (GP), 130 ps (GIP) and 125 ps (GAP). Hence, a slight acceleration is observed for structures involving an electrode. However, considering the thickness of the polymer layer of only 25 nm, a more significant effect[147], i.e. lifetimes inversely proportional to the quantum yield, would be expected if mirror quenching is present, particularly for the GAP samples. In conclusion, the quenching observed in the steady state spectra is not induced by an additional non-radiative decay channel that affects the entire surface of the thin polymer film. Rather, local defects near the aluminium and ITO surfaces lead to the observed efficient quenching. In this context, the fluorescence decay curves of a GP sample with photo-excitation and collection either through the glass or from the polymer side were compared. It was found that a polymer surface exposed to the air gives rise to accelerated fluorescence decays (from 180 to 155 ps). The coincidence of oxygen and UV radiation promote the formation of oxidation defects at the surface[5]. Therefore, a more careful study should use an Argon or vacuum environment during

measurements. Nevertheless, the oxidation effect quickly saturates as all decay kinetics were reproducible after the first measurement. No significant change, i.e. no green defect emission band, was found in emission spectra recorded after TCSPC measurements. In this study, due to restrictions by the opaque aluminium layer photo-excitation was facilitated from the polymer-air side for GP, GIP and GAP; GPA and GPBA were excited from the glass side. Therefore, the above fluorescence decays are already accelerated, which may conceal further (mirror) quenching effects. However, the emission spectra *are* significantly quenched for GAP and GIP – without an equivalent lifetime quenching. Moreover, the fluorescence decays obtained from GIP samples for front and back excitation are identical, i.e. the quenching due to ITO dominates here.

It must be noted that Becker *et al.*[147] also used excitation at a polymer side exposed to air. With this setup, they varied the thickness of the polymer film to demonstrate mirror quenching for thin films (down to 15 nm) using the steady state fluorescence yield. However, the same intensity-thickness dependence will be obtained from any other surface based quenching mechanism. The latter includes any defects, e.g. oxidation, and or impurities that are introduced in the proximity of an electrode or other surface.

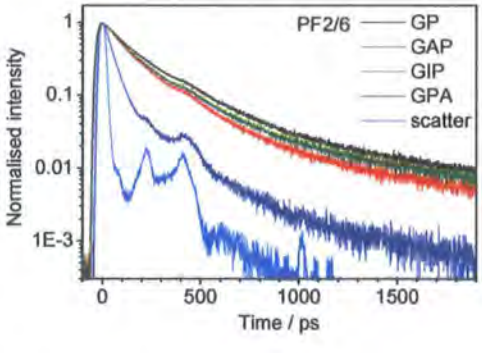

Figure 6-29 – TCSPC raw decay curves of PF2/6-electrode configurations; excitation at 390 nm; collection at 423 nm; a representative scatter is also shown.

Apparently, defect and mirror quenching have rather moderate influences on the fluorescence lifetime of PF2/6. Strikingly, the decay of the PF2/6 GPA structure is considerably accelerated with a main component of only 40 ps. This is interpreted as a non-radiative decay rate consistent with the low PLQY of the GPA samples compared to GAP, see Figure 6-28 above. In comparison to GAP, this indicates the impact of the evaporation conditions on the polymer film. It is conceivable that during evaporation the metal atoms enter the polymer material. Therefore, the quenching will affect areas deeper in the polymer film, i.e. the bulk, which explains the observed lifetime quenching. In contrast, for GAP and GIP, a much smaller fraction of excitons is directly exposed to defects slowly diffusing into the polymer layer. The decay kinetics then consist of a distribution of lifetimes dominated by the unquenched bulk. In summary, the quality and definition of the polymer-electrode interface is drastically reduced as a result of metal evaporation.

6.5.4. Results and discussion – PFO

Analogous measurements were carried out on PFO structures of the types GP, GIP, GAP, GPA and GPBA. Again, polymer films for all samples were spin coated in one run from the same 5 mg/mg xylene solution, yielding thicknesses of ~ 25 nm and OD values at 390 nm of 0.22±0.02, compare Figure 6-30.

The steady state emission and excitation spectra of these samples were measured 4 hours after fabrication. The contribution of β-phase fluorescence was always visible, as shown in Figure 6-31. The same dependence of the emission yield is observed as for PF2/6: With respect to the GP structure, the fluorescence intensity of the GAP sample is decreased by a factor of 3 and by a factor of 7 for GIP, see Figure 6-32. This is expected considering the low β-phase fraction of the PFO samples.

Furthermore, in the case of α- and β-phase being differently affected by the quenching one would expect their emission contributions to change systematically. This, however, is not the case, as shown in Figure 6-32 above. Besides, the same figure

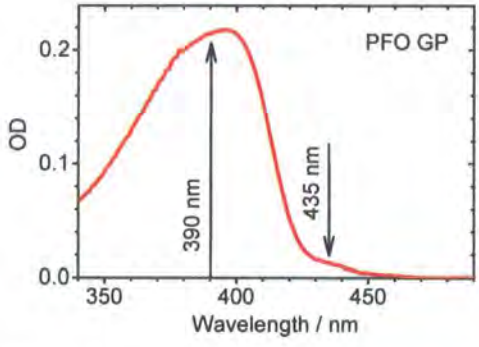

Figure 6-30 – Absorption spectrum of a PFO GP structure. The arrows indicate the excitation wavelengths used here.

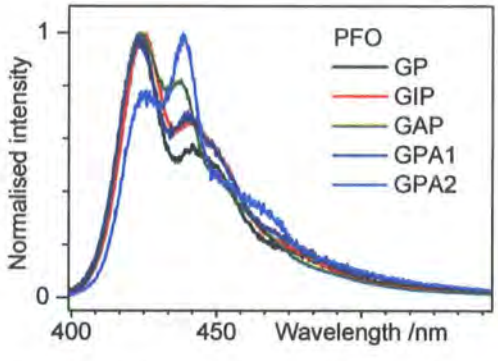

Figure 6-31 – Normalised steady state photoluminescence spectra of several PFO-electrode configurations (excitation at 390 nm). Note the variation of the β-phase contribution of the GPA structures.

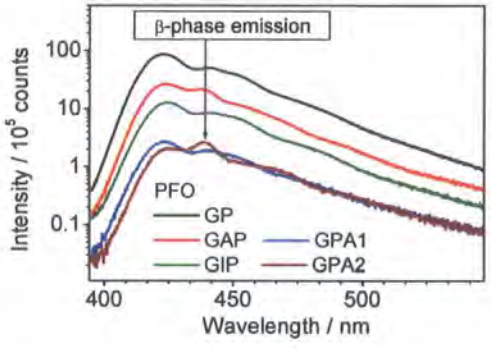

Figure 6-32 – True intensity photoluminescence spectra corresponding to Figure 6-31.

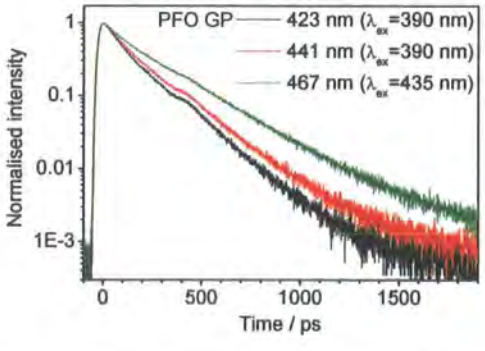

Figure 6-33 – TCSPC raw decays of PFO-GP structures under excitation at 390 and 435 nm with collection wavelengths indicated.

shows that the β-phase contribution in the fluorescence spectrum of all structure types was subject to a significant inter-sample variation. Therefore, one cannot draw conclusions about selective α- or β-phase fluorescence quenching in the presence of a certain electrode. It must be concluded that both phases are affected to the same degree, within the experimental limits. Note that the above inter-sample variation of the fluorescence spectra was not reflected in the photo-absorption spectra – it is known that only a small change in β-phase concentration is required to enhance the energy transfer from the amorphous phase.

Next, fluorescence decays of GP, GIP and GAP were studied. For excitation at 390 nm these are biexponential: For GP, lifetimes of (70 ± 10) and (150 ± 20) ps were determined by reconvolution fitting. When collecting the emission further to the red (at 441 nm), thereby sampling more of the β-phase fluorescence, another, weaker component of 300 ±30 ps becomes visible, as illustrated in Figure 6-33. Consistently, selective excitation of the β-phase at 438 nm and collection at 467 nm yielded a similar lifetime, which is attributed to the β-phase fraction of the emission.

GAP and GIP samples exhibit similar fluorescence decay behaviour, albeit slightly accelerated than for GP, as shown in Figure 6-34. Here, lifetimes of (55 ± 10) and (130 ± 15) ps were found. The longer lived component at 441 collection was present as well but also faster, (230 ± 30) ps, compared to GP samples. Its relative amplitude matches the expectation for a β-phase component and confirmation via selective β-phase excitation was obtained. In conclusion, the fluorescence decay kinetics of PFO, including the β-phase component, show the same qualitative dependence on sample structure like PF2/6. Therefore, in analogy to the findings on PF2/6, the significance of mirror quenching is found to be low. Instead, quenching is again attributed to impurities which diffuse into the polymer layer and quench both α- and β-phase excitations near the surface.

Figure 6-32 also showed the emission spectra of two GPA samples. Their intensity is decreased by a factor of 30 compared to the reference GP, indicating a dominant quenching process as found for PF2/6. Note, these samples were photo-excited and monitored through the glass substrate, which however had an OD of only 0.03 at the emission wavelengths.

The corresponding GPA fluorescence decay curves, see Figure 6-35, consistently show a pronounced lifetime quenching with two components, one of (50 ± 5) ps and a dominant one in the region of the TCSPC time resolution, i.e. 2 to 6 ps. The detection of scattered excitation light is ruled out due to the use of a cut-off filter. In summary, the lifetime in GPA samples of 50 ps is significantly accelerated compared to the other sample types, which is interpreted as a quenching effect related to the impact of evaporation on the polymer layer, similar to PF2/6. A comparable degree of fluorescence quenching is found when barium is evaporated onto PFO and capped by aluminium (GPBA).

Besides, in Figure 6-31 and Figure 6-32 the two GPA emission spectra are shown with strikingly different β-phase contributions. Can decay kinetics be employed to reveal the origin of this inter-sample variation? For instance, the spatial distribution of β-phase within a sample, e.g. its distance to the polymer-electrode interface, is bound to bias a surface based quenching process. Therefore, the β-phase of the GPA2 sample may have formed further away from the aluminium interface than in GPA1. In accordance, the 50 ps decay component at 441 nm collection is significantly slower for GPA2 (~ 57 ps) compared to GPA1 (~ 46 ps), with an error level of ±3 ps also visible from the raw decay curves of Figure 6-35. This difference may be due to a small hidden contribution of a longer lived lifetime originating from unquenched β-phase regions. Indeed, via selective excitation at 438 nm, a separate β-phase lifetime of ~ 250 ps was confirmed in GPA2, see again Figure 6-35.

Finally, it must be noted that both GPA samples were fabricated and measured identically, down to minute details, so that the origin of the differences cannot be explained here.

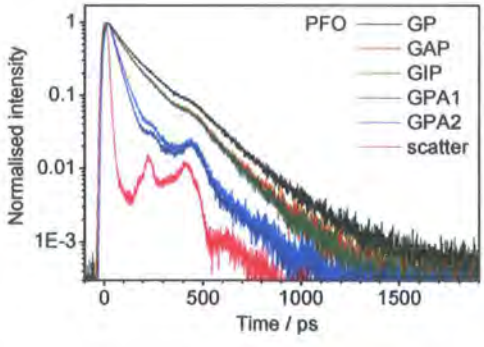

Figure 6-34 – TCSPC raw decays of PFO-electrode structures under excitation at 390 nm, collection at 423 nm. The scatter reference signal is representative for Figure 6-33Figure 6-35.

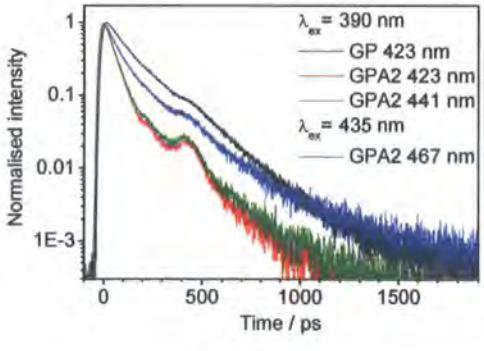

Figure 6-35 – TCSPC raw decays of a PFO GP and the PFO GPA2 sample. Collection and excitation wavelengths are indicated.

6.5.5. Summary

In summary, both PF2/6 and PFO thin films show signs of considerable fluorescence quenching in the presence of an electrode. According to Becker *et al.*[147], their thickness of up to 25 nm should render them highly susceptible to mirror quenching. However, this implies that a non-radiative decay channel affects the majority of excitations in the thin polymer layer. This is clearly not the case as the corresponding fluorescence decay kinetics change only moderately. Rather, surface-based point defects cause efficient quenching within a short radius. This quenching proceeds faster than the time resolution of the TCSPC experiment (~ 1 ps). Such defects may arise from electrode material which has diffused into the adjacent part of the polymer layer[157].

Interestingly, quenching by ITO is more effective than by aluminium in spite of ozone cleaning of the ITO surface prior to spin coating. However, it cannot be said from the present data whether this is due to the oxygen content of ITO or because of its surface roughness and tendency to form dendrites. Also, a polymer-air interface gives rise to accelerated fluorescence decays arising from oxidation defects. Therefore, it is advisable to study thin films in an inert (nitrogen) atmosphere, which was used neither here nor by Becker *et al.*[147]. It is concluded that the thickness dependence of the fluorescence intensity of polymer films observed in the above study could have rather been caused by another surface based quenching mechanism than the mirror effect.

Another process certainly is of greater importance. The most drastic excited state quenching is observed when the electrode metal is evaporated onto the polymer. Here, no significant difference is found between evaporation of barium or aluminium. Naturally, the evaporation process transports metal atoms deeper into the polymer film than room temperature diffusion, possibly deep enough to affect the entire film thickness. Accordingly, a major lifetime quenching is observed. It is expected that also the impact of metal evaporation decreases when thicker polymer films are used.

6.6. Final remarks

This chapter presented results on the solid state room temperature phases of PFO. In addition to the known amorphous (α) and β phases a third (γ) phase was spectroscopically characterised and identified as the crystalline α' phase[140, 149]. For spin coated films, their appearance depends on the solvent of the master solution. A poor solvent, e.g. xylene, cannot entirely dissolve the β-phase content of the dry polymer material. The remaining β-nuclei are transferred to the spin cast film. A slow solvent evaporation, e.g. for slow spin speeds or high viscosity, aids further intermolecular organisation at these nuclei. The film then contains the amorphous phase with some fraction of β-phase. This fraction saturates with time and is accelerated by low temperature.

A similar dependence was observed for the γ-phase in films spun from good solvents. The γ-phase is also obtained by heating any thin film above 80 °C. This is the temperature at which β-phase is destroyed.

For films spun from xylene solution, the exciton mobility was investigated using room temperature steady state anisotropy, sample and temperature dependent fluorescence decays. All measurements consistently indicate that the migration of β-phase excitons is restricted. However, in the future more reliable and comprehensive results can be obtained using isodurene and cyclopentanone as solvents.

Furthermore, temperature dependent fluorescence spectra have revealed the

uniqueness of the β-phase within the class of conjugated polymers. The spectral characteristics as well as a reduced excited state lifetime at low temperature suggest a strengthening of interchain interactions at low temperature that eventually allows interchain conjugation.

Finally, the effect of mirror quenching due to nearby electrodes was found to be negligible for α- and β-phase alike. A much stronger quenching is induced by the evaporation of the metal cathode onto the polymer.

In general, the experimental results obtained with xylene spun films show poor reproducibility, e.g. for fluorescence decays, and high inter-sample variation, as shown earlier in this chapter. While this might be due to the sensitivity of β-phase formation and its evolution with time, xylene is clearly not the most suitable solvent to induce β-phase. Here, fractions are comparably low and the tendency of the solvent to form a gel may also play a role. Therefore, a further confirmation of the results with a wider range of β-phase samples is necessary.

7. Conclusions

During the last decade polyfluorene-type conjugated polymers have attracted significant research interest given their saturated blue emission in combination with a generally good chemical stability. Their applicability to polymer light emitting diodes (PLEDs) is constantly being improved via the synthesis of new derivatives. This thesis investigates the interdependence between the chemical structure and excited state relaxation of several polyfluorene derivatives from a variety of angles.

The starting point is a systematic study of the intrinsic conformational relaxation of oligo-and polyfluorenes in dilute solution. Photo-excitation sets these molecules into vibration and also leads to imbalanced structural forces. The activation of these phonon modes relaxes the molecule into its optimum excited state conformation. As a rule of thumb, the time of structural relaxation scales with its spatial size. A comparison with the picosecond resolution of the streak camera and TCSPC experiments yields that only long-lived components can be detected, which are identified as torsional relaxation towards a more planar configuration of the chromophore[16]. In detail, this is observed as a dynamic red shift of the emission or a pattern of fast decay at the blue side of the fluorescence and build-up at the red spectral end. Unsurprisingly, within this torsional component, relaxation times increase with the spatial extent of the exciton wavefunction, as found by the comparison of small oligofluorenes. In polyfluorene chains, conformational relaxation lasts up to hundreds of picoseconds, which is extremely long compared to the lifetime of the singlet exciton of 370 ps. On a shorter time scale, the excited state relaxation of these isolated molecules is dominated by intrachain exciton migration. The importance of this

process is often played down, as it is far less efficient than its interchain equivalent. However, it is still more efficient than large scale molecular rearrangement. The fact that the above polyfluorene chains are only about 60 repeat units long, accommodating ~10 potential exciton sites, suggests that also larger oligofluorenes of above 10 repeat units (or at least two exciton sites) are subject to migration.

In some cases, a material is chemically modified under the naïve assumption that minor chemical modifications do not substantially alter the photophysics of the original molecule. This is not always true as is established in the study of a polyspirobifluorene (chapter 5), which exhibits alkoxy groups attached to the fluorene side groups. The original purpose of this substitution was to enhance the steric hindrance of the polymer. However, as a side effect the alkoxy groups lead to a specific type of conformational relaxation, which invalidates the dominance of migration found in common polyfluorenes. The key phenomenon revealed by electronic structure calculations is spiroconjugation, i.e. the involvement of the orthogonally attached fluorene side groups in the excited state wavefunction, which is amplified considerably in the presence of alkoxy groups. Along with this, the electron mobility is dramatically increased, providing strong evidence that even side chains can add electronic functionality to a conjugated polymer[6]. The excited state dynamics in this material are non-exponential and, thus, contradict all previous observations in "common" polyfluorenes. A *qualitative* dependence on the solvent viscosity is observed not to be mistaken for the quantitative dependence arising from the backbone relaxation studied above. The findings are interpreted within a picture of two excited states, one extending over the backbone and the second of slightly lower energy due to an additional side group contribution. The conversion between them is accomplished via side group rotation: At low viscosity, this enables a quick trapping in the second state, represented by a fast fluorescence decay and spectral red-shift whilst simultaneously the ground state population does not recover. At high viscosity, the conversion remains incomplete leading to an energetic distribution within the spiroconjugated states. This manifests itself in a continuously red-shifting fluorescence spectrum. From the point of view of excited state relaxation, the population of the second state renders the excitations localised at a single spiro centre, where they cease to be prone to migration activated quenching. In a thin film, the trapping process is only accelerated due to interchain migration. Thus, using a particularly suitable example, this study demonstrates and investigates in detail how sensitively the electronic properties of a conjugated polymer can depend on chemical modification. With this knowledge, the synthesis of further polyspirobifluorene derivatives offers an interesting, feasible path to controlling polymer photophysics and, important for

PLED application, to tailoring charge carrier mobilities.

Finally, polymer synthesis can also influence the ground state morphology in the solid state, the most prominent example being the β-phase of poly(dioctylfluorene) (PFO), which is investigated in the last chapter. Linear alkyl chains are often attached to the repeat units to aid solubility and prevent solid-state interchain interactions such as aggregation. However, these – and in particular octyl side chains – promote the formation of a low energy subsystem within the amorphous solid state polyfluorene matrix – the β-phase. Also, a β-phase precursor is known to exist in solution parallel to the dissolved isolated polymer chains. Thereby, a two level system is formed already in the ground state, where both states are subject to disorder and exhibit an inhomogeneously broadened DOS. The energy transfer to the β-phase is widely studied and eludes detection by TCSPC and streak camera due to its time scale. The focus of the present study rather concerned the excited state relaxation within the β-phase and to which extent migration activated quenching is inhibited due to the trap effect. Both of these issues are of prime importance if one wants to employ the unique properties the beta phase for an electrically driven organic laser as has recently been proposed[19]. In one solid state sample, a restriction of exciton migration is observed as a decreasing fluorescence lifetime at low temperature. The effect is further confirmed by the high steady state fluorescence anisotropy of the solid state β-phase. This is attributed to a conjunction of spatial confinement arising from phase segregation and the very narrow DOS of the β-phase singlet. Consistent with a very low Stokes shift between absorption and emission, conformational relaxation is not expected in the β-phase due to its interchain character, which is confirmed in a fundamental characterisation of the phase transitions of PFO using temperature dependent steady state fluorescence spectra. Solvents which dissolve PFO on the molecular level inhibit β-phase growth in solution. Otherwise, the β-phase exists in rigid sheets of several molecules[128]. These sheets function as nuclei for the condensation of β-phase in solution and solid state, which takes place at a temperature dependent rate. The attempt to optimise β-phase formation in the solid state via controlled sample fabrication has shown how extremely sensitive these interactions depend on the ambient conditions, most crucially the solvent evaporation rate. Thus, the β-phase evolves and matures even in an apparently dry solid film sample. Finally, temperature dependent emission spectra verified the presence of a third supposedly crystalline phase in the existence region of the β-phase, i.e. below 353 K. Hence, a range of improvements are suggested for sample fabrication, which will provide the basis for further investigation towards the application of the β-phase as an intrinsic organic laser.

In summary, this work is a contribution to the understanding of the excited state relaxation of polyfluorenes. It has provided an insight into the fundamental properties of isolated molecules as well as specific excited and ground state effects arising from side chain substitution. While these were mainly revealed by picosecond time-resolved spectroscopy, supplementary time-resolved and steady state techniques were often needed to complete the picture. Thus, it was shown how the versatility of organic chemistry translates into a diversity of photophysics, from which eventually arises a specific material for every conceivable application.

8. Publications

Publications resulting from this thesis:

S. I. Hintschich, F. B. Dias and A. P. Monkman, *Dynamics of conformational relaxation in photoexcited oligofluorenes and polyfluorene*, PHYSICAL REVIEW B 74 (4): Art. No. 045210 JUL 2006

S. I. Hintschich, S. M. King, S. J. Clark, C. Rothe and A. P. Monkman, *The complex excited state behaviour of a polyspirobifluorene derivative*, submitted to Advanced Materials

S. M. King, S. I. Hintschich, D. Dai, C. Rothe, S. J. Clarke, A. P. Monkman, *Excited State Dynamics of a Polyspirobifluorene Derivative in the Solid State*, submitted to Advanced Materials

S. I.Hintschich, C.Rothe, and A.P. Monkman, *Exciton confinement in the beta-phase of polydioctylfluorene and its application for a polymer laser*, in preparation

Other publications of the author:

A. K. Shaw, R. Sarkar, D. Banerjee, S. Hintschich, A. Monkman and S. K. Pal, *Direct observation of protein residue solvation dynamics*, JOURNAL OF PHOTOCHEMISTRY AND PHOTOBIOLOGY A: CHEMISTRY, Volume 185, Issue 1, 1 January 2007, Pages 76-85

C. Rothe, S. I. Hintschich and A. P. Monkman, *Violation of the exponential-decay law at long times*, PHYSICAL REVIEW LETTERS 96 (16): Art. No. 163601 APR 28 2006

H. D. Burrows, V. M. M. Lobo, J. Pina, M. L. Ramos, J. S. de Melo, A. J. M. Valente, M. J. Tapia, S. Pradhan, U. Scherf, S. I. Hintschich, C. Rothe and A. P. Monkman, *Interactions between surfactants and {1,4-phenylene-[9,9-bis(4-phenoxy-butylsulfonate)]fluorene-2,7-diyl}*,

COLLOIDS AND SURFACES A-PHYSICOCHEMICAL AND ENGINEERING ASPECTS 270: 61-66 DEC 1 2005

F. B. Dias, M. Maiti, S. I. Hintschich and A. P. Monkman, *Intramolecular fluorescence quenching in luminescent copolymers containing fluorenone and fluorene units: A direct measurement of intrachain exciton hopping rate*, JOURNAL OF CHEMICAL PHYSICS 122 (5): Art. No. 054904 FEB 1 2005

S. I. Hintschich, C. Rothe, S. Sinha, A. P. Monkman, P. S. De Freitas and U. Scherf, *Population and decay of keto states in conjugated polymers*, JOURNAL OF CHEMICAL PHYSICS 119 (22): 12017-12022 DEC 8 2003

S. I. Hintschich, C. Rothe and A. P. Monkman, *Temperature dependence of long-lived photoexcitations in a polythiophene*, SYNTHETIC METALS 135 (1-3): 365-366 Part 1 Sp. Iss. SI APR 4 2003

C. Rothe, S. I. Hintschich, L.-O. Palsson and A. P. Monkman, *Pressure dependent radiative quantum yields of the prompt and delayed luminescence of polyfluorene films*, (erratum on vol 360, pg 111, 2002), CHEMICAL PHYSICS LETTERS 373 (5-6): 646-647 MAY 28 2003

C. Rothe, S. I. Hintschich, L.-O. Palsson and A. P. Monkman, *Pressure dependent radiative quantum yields of the prompt and delayed luminescence of polyfluorene films*, CHEMICAL PHYSICS LETTERS 360 (1-2): 111-116 JUL 3 2002

C. Rothe, S. Hintschich, A. P. Monkman, M. Svensson and M. R. Anderson, *Spectroscopic investigation of the different long-lived photoexcitations in a polythiophene*, JOURNAL OF CHEMICAL PHYSICS 116 (23): 10503-10507 JUN 15 2002

9. References

1 J. H. Burroughes, D. D. C. Bradley, A. R. Brown, R. N. Marks, K. Mackay, R. H. Friend, P. L. Burns, and A. B. Holmes, Nature **347**, 539 (1990).

2 Innovationmagazine, http://www.innovationmagazine.com/innovation/volumes/v4n3/features3.shtml.

3 isuppli, http://www.isuppli.com/catalog/detail.asp?id=8203.

4 E. J. W. List, R. Guentner, P. S. de Freitas, and U. Scherf, Advanced Materials **14**, 374 (2002).

5 S. I. Hintschich, C. Rothe, S. Sinha, A. P. Monkman, P. S. de Freitas, and U. Scherf, Journal of Chemical Physics **119**, 12017 (2003).

6 C. C. Wu, W. G. Liu, W. Y. Hung, T. L. Liu, Y. T. Lin, H. W. Lin, K. T. Wong, Y. Y. Chien, R. T. Chen, T. H. Hung, T. C. Chao, and Y. M. Chen, Applied Physics Letters **87** (2005).

7 CDT, http://www.cdtltd.co.uk.

8 A. van Dijken, J. Bastiaansen, N. M. M. Kiggen, B. M. W. Langeveld, C. Rothe, A. Monkman, I. Bach, P. Stossel, and K. Brunner, Journal of the American Chemical Society **126**, 7718 (2004).

9 C. F. Shu, R. Dodda, F. I. Wu, M. S. Liu, and A. K. Y. Jen, Macromolecules **36**, 6698 (2003).

10 Novaled, http://www.novaled.com.

11 H. D. Burrows, V. M. M. Lobo, J. Pina, M. L. Ramos, J. S. de Melo, A. J. M. Valente, M. J. Tapia, S. Pradhan, U. Scherf, S. I. Hintschich, C. Rothe, and A. P. Monkman, Colloids and Surfaces a-Physicochemical and Engineering Aspects **270**, 61 (2005).

12 U. Scherf and E. J. W. List, Advanced Materials **14**, 477 (2002).

13 M. Grell, W. Knoll, D. Lupo, A. Meisel, T. Miteva, D. Neher, H. G. Nothofer, U. Scherf, and A. Yasuda, Advanced Materials **11**, 671 (1999).

14 R. D. Xia, G. Heliotis, and D. D. C. Bradley, Synthetic Metals **140**, 117 (2004).

15 A. J. Sandee, C. K. Williams, N. R. Evans, J. E. Davies, C. E. Boothby, A. Kohler, R. H. Friend, and A. B. Holmes, Journal of the American Chemical Society **126**, 7041 (2004).

16 F. B. Dias, A. L. Macanita, J. S. de Melo, H. D. Burrows, R. Guntner, U. Scherf, and A. P. Monkman, Journal of Chemical Physics **118**, 7119 (2003).

17 K. S. Lee, Y. H. Kim, Y. Lee, J. Jang, and S. K. Kwon, Journal of Polymer Science Part a-Polymer Chemistry **43**, 2316 (2005).

[18] D. Vak, S. J. Shin, J. H. Yum, S. S. Kim, and D. Y. Kim, Journal of Luminescence **115**, 109 (2005).

[19] C. Rothe, F. Galbrecht, U. Scherf, and A. Monkman, Advanced Materials **18**, 2137 (2006).

[20] M. Pope and C. E. Swenberg, *Electronic Processes in Organic Crystals and Polymers* (Oxford University Press, Oxford, 1999).

[21] S. I. Hintschich, D. F. B., and M. A.P., Physical Review B **74** (2006).

[22] D. Wasserberg, S. P. Dudek, S. C. J. Meskers, and R. A. J. Janssen, Chemical Physics Letters **411**, 273 (2005).

[23] S. Tretiak, A. Saxena, R. L. Martin, and A. R. Bishop, Physical Review Letters **89** (2002).

[24] A. J. Heeger, S. Kivelson, J. R. Schrieffer, and W. P. Su, Reviews of Modern Physics **60**, 781 (1988).

[25] R. Richert and H. Bassler, Journal of Chemical Physics **84**, 3567 (1986).

[26] S. C. J. Meskers, J. Hubner, M. Oestreich, and H. Bassler, Chemical Physics Letters **339**, 223 (2001).

[27] B. Movaghar, M. Grunewald, B. Ries, H. Bassler, and D. Wurtz, Physical Review B **33**, 5545 (1986).

[28] M. Deussen, M. Scheidler, and H. Bassler, Synthetic Metals **73**, 123 (1995).

[29] H. S. Nalwa, Wiley. **(Chichester ; New York), p. 4 v** (1997).

[30] D. Hertel, Y. V. Romanovskii, B. Schweitzer, U. Scherf, and H. Bassler, Synthetic Metals **116**, 139 (2001).

[31] C. Rothe and A. Monkman, Journal of Chemical Physics **123** (2005).

[32] P. W. Atkins, *Molecular Quantum Mechanics*, 1983).

[33] M. G. Harrison, S. Moller, G. Weiser, G. Urbasch, R. F. Mahrt, H. Bassler, and U. Scherf, Physical Review B **60**, 8650 (1999).

[34] A. P. Monkman, H. D. Burrows, I. Hamblett, S. Navarathnam, M. Svensson, and M. R. Andersson, Journal of Chemical Physics **115**, 9046 (2001).

[35] R. Kersting, U. Lemmer, R. F. Mahrt, K. Leo, H. Kurz, H. Bassler, and E. O. Gobel, Physical Review Letters **70**, 3820 (1993).

[36] T. H. Forster, in *10th Spiers Memorial Lecture*, 1959), p. 7.

[37] C. H. J. Wells, *Introduction to Molecular Photochemistry*, 1972).

[38] E. F. H. Brittain, W. O. George, and C. H. J. Wells, *Introduction to molecular spectroscopy; theory and experiment* (Academic Press, London, New York,, 1970).

[39] H. D. Burrows, J. S. de Melo, C. Serpa, L. G. Arnaut, A. P. Monkman, I. Hamblett, and S. Navaratnam, Journal of Chemical Physics **115**, 9601 (2001).

[40] C. Rothe, R. Guentner, U. Scherf, and A. P. Monkman, Journal of Chemical Physics **115**, 9557 (2001).

[41] Y. V. Romanovskii, A. Gerhard, B. Schweitzer, U. Scherf, R. I. Personov, and H. Bassler, Physical Review Letters **84**, 1027 (2000).

[42] J. F. Rabek, *Photodegradation of Polymers* (Springer, 1996).

[43] G. Cerullo, S. Stagira, M. Zavelani-Rossi, S. De Silvestri, T. Virgili, D. G. Lidzey, and D. D. C. Bradley, Chemical Physics Letters **335**, 27 (2001).

[44] D. L. Dexter, Journal of Chemical Physics **21**, 836 (1953).

[45] M. A. Baldo, S. Lamansky, P. E. Burrows, M. E. Thompson, and S. R. Forrest, Applied Physics Letters **75**, 4 (1999).

[46] M. A. Baldo, D. F. O'Brien, Y. You, A. Shoustikov, S. Sibley, M. E. Thompson, and S. R. Forrest, Nature **395**, 151 (1998).

[47] B. P. Lyons, K. S. Wong, and A. P. Monkman, Journal of Chemical Physics **118**, 4707 (2003).

[48] S. A. Bagnich and A. V. Konash, Chemical Physics **263**, 101 (2001).

[49] A. P. Monkman, H. D. Burrows, I. Hamblett, and S. Navaratnam, Chemical Physics Letters **340**, 467 (2001).

[50] R. W. T. Higgins, A. P. Monkman, H. G. Nothofer, and U. Scherf, Applied Physics Letters **79**, 857 (2001).

[51] A. R. Buckley, M. D. Rahn, J. Hill, J. Cabanillas-Gonzalez, A. M. Fox, and D. D. C. Bradley, Chemical Physics Letters **339**, 331 (2001).

[52] J. R. Lakowicz, *Principles of fluorescence spectroscopy* (Kluwer Academic/Plenum, New York, 1999).

[53] M. Knaapila, R. Stepanyan, B. P. Lyons, M. Torkkeli, and A. P. Monkman, Advanced Functional Materials **16**, 599 (2006).

[54] S. H. Chen, H. L. Chou, A. C. Su, and S. A. Chen, Macromolecules **37**, 6833 (2004).

[55] S. H. Chen, A. C. Su, and S. A. Chen, Journal of Physical Chemistry B **109**, 10067 (2005).

[56] F. Schindler, J. Jacob, A. C. Grimsdale, U. Scherf, K. Mullen, J. M. Lupton, and J. Feldmann, Angewandte Chemie-International Edition **44**, 1520 (2005).

[57] T. Q. Nguyen, V. Doan, and B. J. Schwartz, Journal of Chemical Physics **110**, 4068 (1999).

[58] S. Kishino, Y. Ueno, K. Ochiai, M. Rikukawa, K. Sanui, T. Kobayashi, H. Kunugita, and K. Ema, Physical Review B **58**, R13430 (1998).

[59] Castech, in *http://www.castech-us.com/casbbo.htm*.

[60] W. Becker, *Advanced Time-Correlated Single-Photon Counting Techniques* (Springer, 2005).

[61] Globals, in http://www.lfd.uci.edu/globals/.

[62] Hamamatsu, Photonics Deutschland, HPDTA User Manual ver. 6.4/02 (2003).

[63] A. K. Shaw, R. Sarkar, D. Banerjee, S. Hintschich, A. Monkman, and S. K. Pal, Journal of Photochemistry and Photobiology A: Chemistry **185**, 76 (2007).

[64] M. Glasbeek and H. Zhang, Chemical Reviews **104**, 1929 (2004).

[65] S. King, C. Rothe, and A. P. Monkman, Journal of Chemical Physics **124**, 234903 (2006).

[66] T. Gustavsson, G. Baldacchino, J.-C. Mialocq, and S. Pommeret, Chemical Physics Letters **236**, 587 (1995).

[67] J. Cornil, D. Beljonne, C. M. Heller, I. H. Campbell, B. K. Laurich, D. L. Smith, D. D. C. Bradley, K. Mullen, and J. L. Bredas, Chemical Physics Letters **278**, 139 (1997).

[68] S. Karabunarliev, M. Baumgarten, E. R. Bittner, and K. Mullen, Journal of Chemical Physics **113**, 11372 (2000).

[69] S. Karabunarliev, E. R. Bittner, and M. Baumgarten, Journal of Chemical Physics **114**, 5863 (2001).

[70] M. L. Horng, J. A. Gardecki, A. Papazyan, and M. Maroncelli, Journal of Physical Chemistry **99**, 17311 (1995).

[71] D. R. Lide, *Handbook of organic solvents* (CRC, Boca Raton, 1995).

[72] T. G. Bjorklund, S. H. Lim, and C. J. Bardeen, Journal of Physical Chemistry B **105**, 11970 (2001).

[73] G. D. Scholes, D. S. Larsen, G. R. Fleming, G. Rumbles, and P. L. Burn, Physical Review B **61**, 13670 (2000).

[74] S. N. Yaliraki and R. J. Silbey, Journal of Chemical Physics **104**, 1245 (1996).

[75] M. M. L. Grage, P. W. Wood, A. Ruseckas, T. Pullerits, W. Mitchell, P. L. Burn, I. D. W. Samuel, and V. Sundstrom, Journal of Chemical Physics **118**, 7644 (2003).

[76] N. DiCesare, M. Belletete, C. Marrano, M. Leclerc, and G. Durocher, Journal of Physical Chemistry:A **103**, 795 (1999).

[77] M. I. Sluch, A. Godt, U. H. F. Bunz, and M. A. Berg, Journal of the American Chemical Society **123**, 6447 (2001).

[78] I. Franco and S. Tretiak, Journal of the American Chemical Society **126**, 12130 (2004).

[79] J. G. Muller, M. Anni, U. Scherf, J. M. Lupton, and J. Feldmann, Physical Review B **70**, art. no. (2004).

[80] M. M. L. Grage, T. Pullerits, A. Ruseckas, M. Theander, O. Inganas, and V. Sundstrom, Chemical Physics Letters **339**, 96 (2001).

[81] B. Schweitzer and H. Bassler, Synthetic Metals **109**, 1 (2000).

82 G. Lieser, M. Oda, T. Miteva, A. Meisel, H. G. Nothofer, U. Scherf, and D. Neher, Macromolecules **33**, 4490 (2000).

83 R. Richert and H. Bassler, Chemical Physics Letters **118**, 235 (1985).

84 E. J. W. List, U. Scherf, K. Mullen, W. Graupner, C. H. Kim, and J. Shinar, Physical Review B **66** (2002).

85 C. Rothe and A. P. Monkman, Physical Review B **68**, art. no. (2003).

86 R. C. Kwong, S. Sibley, T. Dubovoy, M. Baldo, S. R. Forrest, and M. E. Thompson, Chemistry of Materials **11**, 3709 (1999).

87 V. Cleave, G. Yahioglu, P. Le Barny, R. H. Friend, and N. Tessler, Advanced Materials **11**, 285 (1999).

88 U. Scherf, S. Riechel, U. Lemmer, and R. F. Mahrt, Current Opinion in Solid State & Materials Science **5**, 143 (2001).

89 C. Y. Jiang, W. Yang, J. B. Peng, S. Xiao, and Y. Cao, Advanced Materials **16**, 537 (2004).

90 J. Morgado, F. Cacialli, R. Iqbal, S. C. Moratti, A. B. Holmes, G. Yahioglu, L. R. Milgrom, and R. H. Friend, Journal of Materials Chemistry **11**, 278 (2001).

91 S. Westenhoff, C. Daniel, R. H. Friend, C. Silva, V. Sundstrom, and A. Yartsev, Journal of Chemical Physics **122**, art. no. (2005).

92 D. Beljonne, G. Pourtois, Z. Shuai, E. Hennebicq, G. D. Scholes, and J. L. Bredas, Synthetic Metals **137**, 1369 (2003).

93 G. Fytas, H. G. Nothofer, U. Scherf, D. Vlassopoulos, and G. Meier, Macromolecules **35**, 481 (2002).

94 H. Meier, U. Stalmach, and H. Kolshorn, Acta Polymerica **48**, 379 (1997).

95 T. Miteva, A. Meisel, W. Knoll, H. G. Nothofer, U. Scherf, D. C. Muller, K. Meerholz, A. Yasuda, and D. Neher, Advanced Materials **13**, 565 (2001).

96 M. Ariu, M. Sims, M. D. Rahn, J. Hill, A. M. Fox, D. G. Lidzey, M. Oda, J. Cabanillas-Gonzalez, and D. D. C. Bradley, Physical Review B **67** (2003).

97 M. Tavasli, S. Bettington, M. R. Bryce, A. P. Monkman, H. A. Al Attar, F. B. Dias, and S. King, Abstracts of Papers of the American Chemical Society **229**, U966 (2005).

98 T. Yamamoto, Progress in Polymer Science **17**, 1153 (1992).

99 U. Scherf, Journal of Materials Chemistry **9**, 1853 (1999).

100 Y. Jiang and G. J. Blanchard, Journal of Physical Chemistry **99**, 7904 (1995).

101 K. Dahl, R. Biswas, and M. Maroncelli, Journal of Physical Chemistry B **107**, 7838 (2003).

102 C. K. Zeberg-Mikkelsen, A. Baylaucq, M. Barrouhou, and C. Boned, Physical Chemistry Chemical Physics **5**, 1547 (2003).

[103] i. T. s. lifetime of the PF2/6 fluorescence measured in the laboratories at Durham University.

[104] J. G. Muller, J. M. Lupton, J. Feldmann, U. Lemmer, and U. Scherf, Applied Physics Letters **84**, 1183 (2004).

[105] C. Rothe, *M.Sc. Thesis* (University of Durham, 2002).

[106] F. B. Diaz, M. Maiti, S. Hintschich, and A. P. Monkman, Journal of Chemical Physics **122**, 054904 (2005).

[107] S. Hintschich, C. Rothe, S. Sinha, and A. P. Monkman, Journal of Chemical Physics **119**, 519346 (2003).

[108] D. Vak, C. Chun, C. L. Lee, J. J. Kim, and D. Y. Kim, Journal of Materials Chemistry **14**, 1342 (2004).

[109] R. Zhu, G. A. Wen, J. C. Feng, R. F. Chen, L. Zhao, H. P. Yao, Q. L. Fan, W. Wei, B. Peng, and W. Huang, Macromolecular Rapid Communications **26**, 1729 (2005).

[110] N. Johansson, D. A. dosSantos, S. Guo, J. Cornil, M. Fahlman, J. Salbeck, H. Schenk, H. Arwin, J. L. Bredas, and W. R. Salanek, Journal of Chemical Physics **107**, 2542 (1997).

[111] B. Schartel, T. Damerau, and M. Hennecke, Physical Chemistry Chemical Physics **2**, 4690 (2000).

[112] F. Steuber, J. Staudigel, M. Stossel, J. Simmerer, A. Winnacker, H. Spreitzer, F. Weissortel, and J. Salbeck, Advanced Materials **12**, 130 (2000).

[113] H. E. Simmons and T. Fukunaga, Journal of the American Chemical Society **89**, 5208 (1967).

[114] F. Laquai, G. Wegner, C. Im, H. Bassler, and S. Heun, Journal of Applied Physics **99** (2006).

[115] F. Milota, C. Warmuth, A. Tortschanoff, J. Sperling, T. Fuhrmann, J. Salbeck, and H. F. Kauffmann, Synthetic Metals **121**, 1497 (2001).

[116] H. Becker, S. Heun, K. Treacher, A. Büsing, and A. Falcou, in *Digest of Technical Papers*, (2002), Vol. 33, p. 780.

[117] H. Becker, A. Bursing, A. Falcou, S. Heun, E. Kluge, A. Parham, P. Stößel, H. Spreitzer, K. Treacher, and H. Vestweber, Proceedings of SPIE - The International Society for Optical Engineering **4464** (2001).

[118] D. Magde, R. Wong, and P. G. Seybold, Photochemistry and Photobiology **75**, 327 (2002).

[119] S. J. Clark, M. D. Segall, C. J. Pickard, P. J. Hasnip, M. J. Probert, K. Refson, and M. C. Payne, Zeitschrift Fur Kristallographie **220**, 567 (2005).

[120] M. D. Segall, P. J. D. Lindan, M. J. Probert, C. J. Pickard, P. J. Hasnip, S. J. Clark, and M. C. Payne, Journal of Physics-Condensed Matter **14**, 2717 (2002).

[121] J. P. Perdew and Y. Wang, Physical Review B **45**, 13244 (1992).

[122] D. Vanderbilt, Physical Review B **41**, 7892 (1990).

[123] S. King, C. Rothe, S. Hintschich, D. Dai, and A. Monkman, (submitted).

[124] M. Gross, D. C. Muller, H. G. Nothofer, U. Scherf, D. Neher, C. Brauchle, and K. Meerholz, Nature **405**, 661 (2000).

[125] G. Klaerner and R. D. Miller, Macromolecules **31**, 2007 (1998).

[126] K. S. Whitehead, M. Grell, D. D. C. Bradley, M. Jandke, and P. Strohriegl, Applied Physics Letters **76**, 2946 (2000).

[127] J. Teetsov and M. A. Fox, Journal of Materials Chemistry **9**, 2117 (1999).

[128] M. Knaapila, V. M. Garamus, F. B. Dias, L. Almasy, F. Galbrecht, A. Charas, J. Morgado, H. D. Burrows, U. Scherf, and M. A.P., Macromolecules **39**, 6505 (2006).

[129] W. Chunwaschirasiri, B. Tanto, D. L. Huber, and M. J. Winokur, Physical Review Letters **94** (2005).

[130] M. Grell, D. D. C. Bradley, G. Ungar, J. Hill, and K. S. Whitehead, Macromolecules **32**, 5810 (1999).

[131] C. Rothe, S. Hintschich, A. P. Monkman, M. Svensson, and M. R. Anderson, Journal of Chemical Physics **116**, 10503 (2002).

[132] C. Rothe, S. M. King, F. Dias, and A. P. Monkman, Physical Review B **70** (2004).

[133] M. J. Winokur, J. Slinker, and D. L. Huber, Physical Review B **67** (2003).

[134] F. B. Dias, A. L. Macanita, J. Morgado, H. D. Burrows, and A. P. Monkman, (submitted).

[135] M. Grell, D. D. C. Bradley, X. Long, T. Chamberlain, M. Inbasekaran, E. P. Woo, and M. Soliman, Acta Polymerica **49**, 439 (1998).

[136] A. J. Cadby, P. A. Lane, H. Mellor, S. J. Martin, M. Grell, C. Giebeler, D. D. C. Bradley, M. Wohlgenannt, C. An, and Z. V. Vardeny, Physical Review B **62**, 15604 (2000).

[137] O. Worsfold, J. Hill, S. Y. Heriot, A. M. Fox, D. D. C. Bradley, and T. H. Richardson, Materials Science & Engineering C-Biomimetic and Supramolecular Systems **23**, 541 (2003).

[138] P. Blondin, J. Bouchard, S. Beaupre, M. Belletete, G. Durocher, and M. Leclerc, Macromolecules **33**, 5874 (2000).

[139] S. Kawana, M. Durrell, J. Lu, J. E. Macdonald, M. Grell, D. D. C. Bradley, P. C. Jukes, R. A. L. Jones, and S. L. Bennett, Polymer **43**, 1907 (2002).

[140] S. H. Chen, A. C. Su, C. H. Su, and S. A. Chen, Journal of Physical Chemistry B **110**, 4007 (2006).

[141] M. Knaapila, R. Stepanyan, M. Torkkeli, B. P. Lyons, T. P. Ikonen, L. Almasy, J. P. Foreman, R. Serimaa, R. Guentner, U. Scherf, and A. P. Monkman, Physical Review B **71** (2005).

[142] M. Misaki, Y. Ueda, S. Nagamatsu, Y. Yoshida, N. Tanigaki, and K. Yase, Macromolecules **37**, 6926 (2004).

[143] A. Y. Grosberg and A. R. Khokhlov, *Statistical Physics of Macromolecules* (American Institute of Physics - Woodbury, New York, 1994).

[144] A. L. T. Khan, P. Sreearunothai, L. M. Herz, M. J. Banach, and A. Kohler, Physical Review B **69** (2004).

[145] M. N. Shkunov, R. Osterbacka, A. Fujii, K. Yoshino, and Z. V. Vardeny, Applied Physics Letters **74**, 1648 (1999).

[146] H. Y. Byun, I. J. Chung, H. K. Shim, and C. Y. Kim, Macromolecules **37**, 6945 (2004).

[147] H. Becker, S. E. Burns, and R. H. Friend, Physical Review B-Condensed Matter **56**, 1893 (1997).

[148] M. Tammer, R. W. T. Higgins, and A. P. Monkman, Journal of Applied Physics **91**, 4010 (2002).

[149] S. H. Chen, A. C. Su, C. H. Su, and S. A. Chen, Macromolecules **38**, 379 (2005).

[150] M. Campoy-Quiles, P. G. Etchegoin, and D. D. C. Bradley, Synthetic Metals **155**, 279 (2005).

[151] A. L. T. Khan, M. J. Banach, and A. Kohler, Synthetic Metals **139**, 905 (2003).

[152] M. Anni, M. E. Caruso, S. Lattante, and R. Cingolani, Journal of Chemical Physics **124** (2006).

[153] M. E. Caruso, S. Lattante, R. Cingolani, and M. Anni, Applied Physics Letters **88** (2006).

[154] S. C. J. Meskers, J. Hubner, M. Oestreich, and H. Bassler, Journal of Physical Chemistry B **105**, 9139 (2001).

[155] S. Guha, J. D. Rice, Y. T. Yau, C. M. Martin, M. Chandrasekhar, H. R. Chandrasekhar, R. Guentner, P. S. de Freitas, and U. Scherf, Physical Review B **67** (2003).

[156] R. Hildner, U. Lemmer, U. Scherf, and J. Kohler, Chemical Physics Letters **429**, 103 (2006).

[157] M. P. de Jong, D. P. L. Simons, M. A. Reijme, L. J. van Ijzendoorn, A. W. D. van der Gon, M. J. A. de Voigt, H. H. Brongersma, and R. W. Gymer, Synthetic Metals **110**, 1 (2000).